THE UNIVERSITY OF CHICAGO

IDENTIFICATION AND CHARACTERIZATION OF A NOVEL STRESS RESPONSE PATHWAY IN *ACINETOBACTER BAUMANNII*

A DISSERTATION SUBMITTED TO

THE FACULTY OF THE DIVISION OF THE BIOLOGICAL SCIENCES

AND THE PRITZKER SCHOOL OF MEDICINE

IN CANDIDACY FOR THE DEGREE OF

DOCTOR OF PHILOSOPHY

COMMITTEE ON MICROBIOLOGY

BY

MICHAEL JOHN GEBHARDT

CHICAGO, ILLINOIS

JUNE 2017

TABLE OF CONTENTS

LIST OF FIGURES

LIST OF TABLES

ACKNOWLEDGEMENTS

Throughout my entire life, I have been blessed with the great fortune of having a supporting cast of people who were willing and able to provide me with assistance whenever needed. I also quickly realized that success was very rarely achieved by one's own self without the helping hands of others. While I cannot possibly recount the many instances and examples of how people have helped guide me towards becoming the scientist I am today, I can point out a few key people that have been particularly instrumental.

From a scientific standpoint, it should be made very obvious that the works contained herein would not have been possible without the excellent guidance and mentorship provided to me by my advisor, Dr. Howard Shuman. I most certainly would not be the scientist I am today without his help and will be forever grateful for the time and care he took to help me complete the works described below. I also owe a great deal of gratitude to the members of my advisory committee, Drs. Lucia Rotheman-Denes, Sean Crosson, Lance Peterson and Olaf Schneewind, who not only helped shape the direction of my research project, but also directly influenced my intellectual development and my approach to scientific inquiry. I also would like to acknowledge previous mentors, including Susanne Flaker-Johnson and Drs. Marc Rott, William Schwann, Joseph Toce and Sheila Shurtleff, all of whom recognized my potential and encouraged me to pursue science as a career.

I also would like to thank both the past and present members of the Shuman lab for their many years of support, critical discussions and even supplying some much-needed distractions. Particularly, I would like to acknowledge Dr. Kierstyn Schwartz for helping me navigate many aspects of graduate life at the University of Chicago and Dr. Paco Amaro for providing endless technical advice (as well as constant reminders that life is hard). Additionally, I am very grateful

to Dr. Joelle Gabay, who was always ready to discuss the intricacies of experimental approaches. I also benefitted greatly from Dr. Stefan Pukatzki, who's excitement for new ideas, experiments and the Packers made the lab a brighter place. Finally, I would be remiss not to mention Rachael Jacobson and Brian Goldspiel, not only for taking part in the most epic dot game ever, but also for their friendship and unrelenting support over the years; which means much more to me than I can say.

I was also fortunate enough to develop many close friendships with other graduate students during my time at the University of Chicago. Every summer, many a Friday evening were spent on the diamond with the Sterile Technique softball team, which wouldn't have been possible without the hard work of Dr. Bryan Berube and Ryan Ohr, two of the best captains I've had the pleasure of playing sports with. While the softball team was a great way to get people out of the lab for some exercise and beer, perhaps more important were the friendships borne through these activities. Additionally, I'll always remember Aaron Hecht for our riveting discussions – he challenged me to become a better scientist and I'm grateful for that. In addition, I was lucky enough to live near and often walked home together with Danny Chan– the many conversations about we had about life, society and science were often the highlight of my day.

To my friends and family, I cannot say enough about how much your unyielding support has meant to me over the years. To my mom, Jacqueline Lehto, there aren't enough words to acutely describe just how much her love and support has helped me become the person I am today. She always seems to know when I need a few words of encouragement. To my dad, Mark, and brother, Peter, thank you for all of the fishing trips – I don't think people appreciate the therapeutic value of sitting on a lake in the middle of nowhere – even in snowstorms! To my wife's parents, John and Julie Bomkamp, I cannot thank you enough for how much you've

helped Joanna and I over the years. Also, I would like to acknowledge the best running partner I've ever had – my dog Baxter.

Finally, to my wife, Dr. Joanna Gebhardt, I know full well that I would not have made it this far without her by my side. She has always been willing to listen to my ideas and offer a different perspective on many of the challenges I was faced. Her strength, sense of humor, intelligence and creativity are unmatched. I'm grateful for all the adventures that we've already shared and I look forward to those yet to come.

ABSTRACT

Bacterial pathogenesis requires an invading bacterium to sense and adapt to the harsh environments encountered inside the human host. This is especially true for opportunistic pathogens, such as *Acinetobacter baumannii,* an organism that is rapidly emerging as a serious source of hospital acquired infections, in part due to the high levels of antibiotic resistance harbored by contemporary clinical isolates. A key limitation to combatting *A. baumannii* is that a thorough understanding of the molecular mechanisms that underlie *A. baumannii* pathogenesis is lacking.

In order to identify potential virulence determinants harbored by *A. baumannii*, I employed a large-scale forward genetic screen known as transposon insertion sequencing, or TnSeq, with *A. baumannii* strain AB5075, a contemporary isolate that exhibits both enhanced virulence and resistance to multiple classes of antibiotics. The TnSeq screen identified 300 genes that are specifically required for the survival and/or growth of *A. baumannii* inside *Galleria mellonella* larvae, an established insect infection model for studying microbial pathogenesis. Importantly, the genes identified in the screen encompassed many of the previously characterized virulence determinants of *A. baumannii* and, more importantly, also uncovered several novel genes that are critical for *A. baumannii* pathogenesis.

My follow-up studies focus on genes involved with transcriptional regulation and reveal that several of the transcription factors required for growth inside the *Galleria* larvae, which are given the name '*gig'* (for Growth in *Galleria*), are also required for resistance to antibiotics and environmental stress. Using a combination of genetic and biochemical approaches, I demonstrate that GigA and GigB comprise a previously undiscovered signal transduction pathway required for not only virulence in the *G. mellonella* model, but also for resistance to environmental stress

and antibiotic exposure. Additionally, I provide evidence that GigA/GigB are required for establishing an appropriate transcriptional response to antibiotic exposure. My studies also uncover a direct link between GigA/GigB and the nitrogen phosphotransferase system (PTS^{Ntr}), a well-conserved metabolic sensing pathway. These findings suggest that GigA/GigB are master regulators of a global stress response and the coupling of the GigA/GigB signaling axis to the PTS^{Ntr} allows *A. baumannii* to integrate cellular metabolic status with environmental cues.

CHAPTER I

Introduction

A Brief History of *Acinetobacter baumannii*

Over the last several decades, the gram-negative coccobacillus, *Acinetobacter baumannii*, has emerged as a significant human pathogen. The chief concern for *A. baumannii*, which is largely considered an opportunistic human pathogen, is the rapid emergence of antibiotic resistance amongst contemporary clinical isolates. The earliest reports that defined the *Acinetobacter* genus occurred in the 1950's and 1960's in the works of Brisou and Prevot (Brisou and Prevot 1954). Shortly thereafter, seminal experiments performed by Paul Baumann and Elliot Juni provided evidence that many non-motile, oxidase-negative bacterial isolates originally classified in the genera *Moraxella, Herellea, Mima, Bacterium, Achromobacter,* or *Acinetobacter* should all be grouped within the *Acinetobacter* genus (Baumann, Doudoroff, and Stanier 1968, Henriksen 1973, Juni 1972). These studies were primarily conducted using genetic transformation experiments and were supported by the robust metabolic capacity harbored by members of *Acinetobacter*. Indeed, early studies of *Acinetobacter* largely focused on the ability of these organisms to assimilate a wide variety of carbon sources, including aromatic compounds such as protocatechuate, vanillic acid, and other benzoic acid derivatives. Additional studies from the lab of Nicholas Ornston furthered the understanding of the metabolic pathways for many of these compounds, as well as exploring the natural competence for DNA uptake in *A. baylyi*, an oft-studied *Acinetobacter* (D'Argenio et al. 1999).

Even as a nascent genus, the pathogenicity of *A. baumannii* and other closely related *Acinetobacter* species was a subject of debate. Many early reports claimed that *A. calcoaceticus*, one of the first *Acinetobacter* species defined, was the causative agent for a wide variety of infections. However, other research showed that in many cases, the isolation of *A. calcoaceticus* was potentially due to specimen contamination during collection. Despite these discrepancies, two factors were clear very early on. First, it was realized that particular patient populations appeared to be at a greater risk of acquiring an *Acinetobacter* infection. These groups included patients with compromised immunity, such as neonates and the elderly, as well as post-surgical patients. Second, many of the isolates expressed resistance to several antimicrobials (Henriksen 1973).

Presently, it is appreciated that only a small number of *Acinetobacter* species are routinely isolated as a cause of human infection; the majority of which are classified in the *Acinetobacter baumannii*/*calcoaceticus* complex (Antunes, Visca, and Towner 2014). This complex is comprised of *A. baumannii, A. calcoaceticus, A. nosocomialis* and *A. pittii*; and of these*, A. baumannii* is by far the most common, and potentially severe, cause of human disease. As mentioned above, the prevailing hypothesis regarding *A. baumannii* is that this organism represents an opportunistic pathogen infecting immunocompromised individuals, although recent reports now suggest that many *A. baumannii* infections result from a breach of anatomical barriers, such as mechanical ventilation, surgical sites and placement of indwelling devices, such as catheters (Pour et al. 2011, Wroblewska et al. 2008, Enoch et al. 2008). In addition to these nosocomial infections, there are increasing reports of community associated *Acinetobacter* infections (Wong et al. 2017).

In addition to the ability of *Acinetobacter baumannii* to cause disease following breaks in the anatomical barrier, a major concern with this pathogen is the development of antibiotic resistance. Furthermore, *A. baumannii* is generally considered to be resistant to many environmental stressors, including desiccation and the routine decontamination practices employed in the clinical setting. This resistance likely underlies the ability of *A. baumannii* to readily colonize the clinical environment (La Forgia et al. 2010, Kawamura-Sato et al. 2010, Roca et al. 2012). Compounding this issue is the fact that *A. baumannii* is adept at the acquisition and/or development of antibiotic resistance. Given these two characteristics, namely, the ability to colonize the clinical setting and development/emergence of strains harboring multiple antibiotic resistances, the Centers for Disease Control and Prevention (CDC) currently classifies *A. baumannii* as a serious threat, the second highest level of concern regarding antibiotic resistance among bacterial pathogens (Centers for Disease Control and Prevention 2016).

Genetic Diversity of *Acinetobacter baumannii*

As discussed above, the initial characterization of bacterial species that would become the *Acinetobacter* genus were formally grouped following natural transformation experiments with one particular *Acinetobacter* strain (now known to be *A. baylyi*). These studies were successful largely because the strain being tested possessed the ability to take up DNA from its environment through a process called natural competence (Juni 1972). This early finding of natural competence for DNA uptake foreshadowed one of the major factors at play in the clinical setting today where the seemingly promiscuous nature of *A. baumannii* has allowed for the rapid acquisition of antibiotic resistance determinants.

In the clinical microbiology laboratory setting, efforts to categorize and differentiate *Acinetobacter* isolates by routine biochemical testing does not allow for a species level identification. Using these routine-testing procedures, clinical diagnostic laboratories are, at best, able to classify a particular isolate as a member of the *Acinetobacter baumannii-calcoaceticus* complex. For species-level identification, molecular diagnostic tests, such as PCR-based assays, are required. The use of multi-locus-sequence-typing (MLST) is largely considered the gold standard and early efforts to classify *A. baumannii* isolates identified the existence of three international clonal lineages (ICL's) (Antunes, Visca, and Towner 2014). More recently, however, with the advent of rapid sequencing technologies, it has become apparent that there are presently 6 ICLs circulating globally, and these groups contain well over 400 MLST types.

Interestingly, a recent report surveyed the genetic diversity of ~180 *Acinetobacter* genomes and concluded that the *A. baumannii* species is actually quite distinct from other *Acinetobacter* species, including the non-*baumannii* species also found within the *A. baumannii*/*calcoaceticus* complex (Diancourt et al. 2010). One possible interpretation of this finding is that *A. baumannii* recently emerged as a species upon developing the ability to colonize a new niche and the population encountered a significant genetic bottleneck associated with colonizing said niche. Despite the long-held belief that *A. baumannii* is a soil-dwelling organism like many of the other *Acinetobacter* spp., recent environmental surveys have found evidence that this may not be the case. These studies further suggest that *A. baumannii* is actually found most commonly in the hospital environment. Given the notion that views *A. baumannii* as a specialized hospital-colonizing organism, the ability to survive in the harsh environment of the medical clinical may, in fact, represent the environmental niche leading to the genetic bottleneck that initiated the *A. baumannii* speciation event (Antunes, Visca, and Towner 2014).

In addition to the apparent genetic isolation of *A. baumannii* as a species, there is also an appreciable amount of variation within the species. As mentioned above, recent studies have identified ~400 MLST clones of *A. baumannii* clinical isolates. Coupled with the isolation of *A. baumannii* from other *Acinetobacter* species, the apparently high intra-species diversity supports a model where *A. baumannii* recently emerged from an environmental bottleneck and the current genetic diversity represents a radial expansion into sequence space following the aforementioned speciation of *A. baumannii* (Diancourt et al. 2010).

Imperi and colleagues analyzed 12 sequenced *A. baumannii* genomes from strains varying both in antibiotic resistance profile and the corresponding sites of isolation. The results of this analysis suggested that *A. baumannii* harbors a relatively small core-genome (i.e. the genes shared by all *A. baumannii* isolates), consisting of approximately 1,400 genes out of the ~8800 genes predicted across the 12 genomes, or approximately 16% of the genome. Interestingly, when two of the 12 genomes (one from a non-pathogenic *A. baumannii* isolate and another isolated in the 1950's) were excluded from the analysis, the predicted core genome size increased to ~65% of a given genome, suggesting that these two strains are quite distinct from the remaining isolates, which were all contemporary clinical strains (Imperi et al. 2011). For comparison, a similar study performed on 17 sequenced *E. coli* genomes, which also included both pathogenic and non-pathogenic isolates, estimated the *E. coli* core genome to consist of approximately 45% of a given genome (Rasko et al. 2008). Again, these findings support a model where *A. baumannii* has recently emerged from a genetic bottleneck, with the relatively high conservation maintained by contemporary clinical isolates providing further support for the recent divergence of *A. baumannii* from other *Acinetobacter* species.

Acinetobacter baumannii as a human pathogen

As mentioned above, the infections caused by *A. baumannii* most typically present as opportunistic or nosocomial in nature. Common sites of infection for *A. baumannii* generally result from the introduction of *A. baumannii* into what should be a normally protected site. The infections quite often occur following a breach in an anatomical barrier, either from an indwelling medical device, such as tubing for mechanical ventilation or from catheterization, and lead to infections such as pneumonia and sepsis, respectively. Indeed, in these two common infections, *A. baumannii* is afforded access to a host environment that is normally well protected by anatomical defenses. Many of the infections associated with indwelling devices are attributed to the ability of *A. baumannii* to colonize the surfaces of devices that are introduced into the host (Wong et al. 2017).

In addition to infections resulting from indwelling devices, *A. baumannii* infections frequently result from traumatic injuries that allow entry of *A. baumannii* into host tissues, such as the colonization and subsequent infection of surgical wounds. The propensity to cause deep tissue infections also became readily apparent during the recent wars in Iraq and Afghanistan. During these military operations, many wounded soldiers acquired *A. baumannii* infections during transit through the medical evacuation route. These infections were often caused by strains of *A. baumannii* harboring multiple drug resistances and were observed so frequently that the organism was given the moniker of 'Iraqibacter' (Scott et al. 2007).

Based on the common sites of *A. baumannii* infection described above, it can be appreciated that one significant requirement for *A. baumannii* to cause disease is that this organism has to be adept at colonizing the clinical setting. Indeed, there are many reports demonstrating the ability of *A. baumannii* to survive on surfaces. This survival is mediated by an

ability to resist not only desiccation (Jawad et al. 1998), but also the routine decontamination practices employed by hospitals (Antonios Markogiannakis et al. 2008, Kawamura-Sato et al. 2010). A further complication to colonization of health-care facilities is the fact that eradication of the organism can be quite difficult and costly, both in terms of the direct costs associated with disinfection strategies and also the cost on human health, as contamination of health care facilities often leads to a series of infections arising from the contaminating *A. baumannii* strains (La Forgia et al. 2010).

In addition to being an increasingly common cause of hospital-acquired infections, it has recently been appreciated that *A. baumannii* is also a cause of community-acquired infections, particularly in tropical regions with humid climates, such as Southeast Asia and Australia. Interestingly, in many of these cases, patients that present with community-acquired *A. baumannii* infections typically also suffer from significant comorbidities, such as diabetes, cancer, alcoholism and pulmonary diseases (Falagas et al. 2007). This correlation further supports the classification of *A. baumannii* as an opportunistic pathogen, and suggests that the organism is not well adapted to infect healthy individuals.

Antibiotic Resistance of *Acinetobacter baumannii*

Arguably one of the greatest advances in the history of mankind has been the development of antibiotics as a means to treat bacterial infections. Since the advent of the therapeutic deployment of antibiotics for the treatment of bacterial infections, countless lives have been saved. Despite the successes of antibiotics as therapeutic agents, bacterial pathogens have not been defeated, and moreover, have developed resistance to nearly every therapeutically useful antibiotic. In fact, even before the clinical use of penicillin, researchers had isolated

strains of bacteria that expressed resistance to these newly discovered molecules (Abraham and Chain 1940). Presently, the continued and expanding emergence of bacterial pathogens harboring multiple antibiotic resistances (i.e. the 'MDR' phenotype) represents a serious threat to effective health care (Hwang and Gums 2016). *A. baumannii* is no different, and there are now several reports citing the isolation of pan-resistant strains (Leite et al. 2016, Gottig et al. 2014, Huttner et al. 2013).

Over the last several years, there have been numerous publications regarding the dissemination of *A. baumannii* strains harboring multiple antibiotic resistances. Many of these reports identify a particular antibiotic resistance determinant, such as novel ß-lactamase enzyme or aminoglycoside-modifying enzyme, and identify the responsible genetic element responsible for the spread of these agents. Several recent reviews provide a summary of many of these findings (Wong et al. 2017, Dijkshoorn, Nemec, and Seifert 2007, Peleg et al. 2012). Of all the antibiotic resistance mechanisms described for *A. baumannii,* perhaps the most concerning are those reporting the isolation of strains harboring carbapenem resistance. The carbapenem antibiotics, including meropenem, imipenem and ertapenem, are generally considered as last line drugs due to their broad spectrum of activity towards both gram-negative and gram-positive species. Carbapenem resistance amongst *A. baumannii* isolates has been attributed to several varieties of β-lactamase enzymes, including metallo-β-lactamases like the New Dehli β-lactamase (NDM). Furthermore, certain oxacillinase (OXA) family members found in *A. baumannii* isolates are capable of hydrolyzing carbapenems (Da Silva and Domingues 2016).

In addition to the acquired antibiotic resistance mechanisms described above, *A. baumannii* also harbors a high level of intrinsic antibiotic resistance. There are several factors that likely account for the relatively high innate levels of antibiotic resistance amongst *A.*

baumannii strains. For example, many *A. baumannii* genomes directly encode antibiotic resistance genes, such as the *ampC* β-lactamase and *cat*, a chloramphenicol modifying enzyme (Roca et al. 2012). In order for these genes to confer clinically relevant antibiotic resistance, however, often requires increased expression of the gene, which most often occurs when insertion sequences, such as the ISAba1 element, insert upstream of a particular antibiotic resistance gene (Da Silva and Domingues 2016).

In addition to chromosomally encoded resistance genes, low outer membrane permeability also contributes to the intrinsic antibiotic resistance of *A. baumannii*. For example, work from the Nikaido group has demonstrated that the major porin protein found in the outer membrane, named outer membrane protein A (OmpA), is a relatively poor channel for antibiotics and, as such, limits the entry of antibiotics into the cell (Sugawara and Nikaido 2012). Additionally, many MDR strains of *A. baumannii* harbor mutations that reduce or eliminate the expression of other porins, such as the CarO channel. The CarO porin has been shown to allow for entry of carbapenem antibiotics (Catel-Ferreira et al. 2011) and eliminating or decreasing the expression of this protein drastically increases the minimum inhibitory concentration required to prevent the growth of these *A. baumannii* strains.

A third mechanism of intrinsic antibiotic resistance harbored by *A. baumannii* includes antibiotic efflux pumps. *A. baumannii* genomes typically encode for a variety of efflux pumps. The most well studied and versatile efflux pumps harbored by *A. baumannii* include the Resistance-Nodulation-Cell Division (RND) family of transporters. Of the several RND-family pumps found in *A. baumannii*, the best-characterized is the AdeABC efflux system, which has been experimentally shown to efflux a wide variety of toxic molecules from the cell, including several categories of antibiotics (Yoon et al. 2015). In addition to RND family exporters, many

A. baumannii isolates also encode pumps of different families, including the Major Facilitator Superfamily (MFS) and the Proteobacterial Antimicrobial Compound Efflux, or PACE, family (Hassan et al. 2015). Much like the RND family of transporters, these other classes of efflux proteins are also capable of exporting a variety antimicrobial compounds, as well as disinfectant molecules like chlorhexidine. Similar to what is seen with the CarO outer membrane porin, many antibiotic resistant strains of *A. baumannii* modulate the expression of efflux pumps. In contrast to the case described above for the CarO porin; however, the mutations that modulate expression of efflux pumps to increase antibiotic resistance generally result in increased efflux pump expression relative to drug sensitive strains (Nowak et al. 2016, Yoon, Courvalin, and Grillot-Courvalin 2013).

Virulence factors harbored by *A. baumannii*

Despite the relative abundance of information pertaining to the development and acquisition of antibiotic resistance determinants amongst contemporary clinical *A. baumannii* isolates, one significant shortcoming in our understanding of *A. baumannii* as a pathogen is the paucity of information regarding the molecular mechanisms that lead to pathogenesis in the host. Indeed, very few virulence factors have been identified and well characterized for *A. baumannii*.

One of the most widely studied virulence factors harbored by *A. baumannii* is the aforementioned OmpA protein. Aside from its function as an outer membrane porin, OmpA has also been shown to induce apoptosis in mammalian tissue culture cells and is reported to possess immunomodulatory functions, although these studies were performed using outer membrane vesicles and were likely contaminated with lipopolysaccharides (LPS), which would likely impact immune signaling (Jin et al. 2011). Other reports demonstrate that OmpA mediates

adhesion of *A. baumannii* to eukaryotic cell surfaces and mutant strains lacking OmpA were attenuated for virulence in a murine pneumonia model (Choi et al. 2008). In addition to OmpA, other reported virulence factors harbored by *A. baumannii* include phospholipase enzymes, LPS, and siderophores, which are iron-scavenging molecules (Fiester et al. 2016, Erridge et al. 2007, Gaddy et al. 2012).

Along with the aforementioned secreted virulence factors, several surface structures have also been classified as *A. baumannii* virulence factors. For instance, a chaperone/usher pilus, CsuAB, has been shown to be important for adherence of *A. baumannii* cells to both host cells and also abiotic surfaces, which as described above, is a critical component of the *A. baumannii* lifestyle as a means of surface colonization in the clinical setting (Tomaras et al. 2003). Additionally, while not an exactly considered as virulence factors, many *A. baumannii* isolated elaborate Type IV pili that are involved in both twitching motility and DNA uptake, and as such are an important aspect of horizontal gene transfer (Wilharm et al. 2013).

As well as the pili described above, many *A. baumannii* also encode genes that appear to comprise a Type II secretion system (T2SS). In many gram-negative bacteria, the T2SS, also known as the general secretion pathway, is utilized to secrete degradative enzymes to break down large macromolecules, such as starches, into smaller molecules that can then be easily transported into the bacterial cell (Korotkov, Sandkvist, and Hol 2012). Many pathogens also secrete proteins via the T2SS during the infection process as well. Recent reports have identified a role for the T2SS harbored by *A. baumannii* and have shown that a lipase enzyme, LipA, which digests long-chain fatty acids, also plays a role in virulence, as strains harboring mutations in either T2SS structural genes or the *lipA* gene itself were less fit in a mouse model of infection (Johnson et al. 2016).

In addition to the T2SS, there has been at least one report of a Type IV Secretion System (T4SS) in *A. baumannii* isolates (Smith et al. 2007). Indeed, inspection of *A. baumannii* genomes does identify genes bearing an *icm* annotation, in reference to the *icm/dot*-like T4SS found in *Legionella pneumophila* (Segal, Purcell, and Shuman 1998, Vogel et al. 1998). However, a more parsimonious explanation for the presence of these *icm* genes is that they encode components of a Type IV Secretion System involved with DNA conjugation machinery are commonly found on plasmids.

While not necessarily a virulence factor per se, one of the most critical factors of *A. baummannii*'s ability to cause disease is the elaboration of a polysaccharide capsule. The importance of the capsule for *A. baumannii* is highlighted in a recent report that assessed the genetic variation across several *A. baumannii* genomes. The authors find high variability across the genetic content of the capsule biosynthetic locus present in various *A. baumannii* isolates, suggesting that the capsule locus is under positive selection, potentially as a means of escaping recognition by the human immune system (Kenyon and Hall 2013). It is important to note, however, that evolutionary pressures to diversify the capsule locus can arise from sources other than recognition by a host's immune system. Indeed, a recent report demonstrates that bacteriophage of *A. baumannii* may use the capsule as a receptor (Regeimbal et al. 2016). Despite the possibility of alternative pressures driving diversity of the capsule locus among *A. baumannii*, the role of the capsular polysaccharide production as a requirement for virulence has been well documented, both in our laboratory and others (Gebhardt et al. 2015, Geisinger and Isberg 2015, Russo et al. 2010). In addition to the major polysaccharide capsule encoded by the K locus of *A. baumannii*, many isolates also encode for a second capsular polysaccharide, poly-

N-acetyl-glucosamine, which has not been shown to be required for virulence, but has been demonstrated to play a role in biofilm formation (Choi et al. 2009).

The preceding paragraphs provide a brief review of the reported virulence factors harbored by *A. baumannii*, and as can be deduced from this information, *A. baumannii* appears to lack any major virulence factor or factors that are often associated with pathogens. As a means to rationalize this information with the emergence of *A. baumannii*, perhaps the apparent lack of *bona fide* virulence factors demonstrates that *A. baumannii* has not evolved specifically as a human pathogen. Indeed, many bacterial pathogens possess specific virulence factors for eliciting direct damage to the host organism, such as the multiple toxins harbored by *Staphylococcus aureus*, or for the colonization of specific host tissues, such as the Type I pili utilized by uropathogenic *Esherichia coli* strains in order to colonize the human urinary tract (reviewed in Sampedro et al. 2014 and Schwartz et al.2013). Additionally, bacterial pathogens often possess elaborate secretion systems that are designed to translocate toxins and other proteins that modulate host cell physiology. In many cases, these secretion systems transport the effector proteins directly into host cells in order to alter intracellular physiology as a means to either evade the host immune response or to establish a replicative niche for the pathogen (Dietsche et al. 2016). However, a concerning trend among recent publications are reports describing the isolation of *A. baumannii* strains with enhanced virulence properties (Harris et al. 2013, Jacobs, Thompson, Black, et al. 2014, Jones et al. 2015) In light of these reports, it is interesting to speculate that these strains may represent the future of the *A. baumannii* species. Indeed, one provocative interpretation of these observations is that the trend towards greater virulence represents the evolution of *A. baumannii* away from being an opportunistic pathogen into a human-adapted pathogen.

Model systems used to study *A. baumannii* disease

The virulence factors descried above were identified and characterized through the use of a variety of *in vitro* and *in vivo* model systems. Published systems used to study the pathogenesis of *A. baumannii* have ranged from *in vitro* infections of eukaryotic cells grown in tissue culture to infection of invertebrates, such as the amoeba *Dictyostelium discoideum* and the nematode *Caenorhabditis elegans*, to mammalian model systems including mice and rats (Smith et al. 2007, Jacobs, Thompson, Black, et al. 2014, Harris et al. 2013, van Faassen et al. 2007). Not surprisingly, these models range in complexity and the specifics of each model varies from lab to lab, which confounds the ability to correlation results from one model with those of another. However, the various model systems used to study *A. baumannii* virulence have both strengths and weaknesses, as discussed in greater detail below.

The simplest models used to study *A. baumannii* include those involving invertebrates. Several organisms have been utilized as a tool for uncovering virulence properties of *A. baumannii*. These include the well-studied model organisms *D. discoideum* and *C. elegans*, which have been used primarily to assess the ability of *A. baumannii* to resist phagocytosis and also impact the fitness of the host. These models were first reported for *A. baumannii* in papers that identified and described an ethanol-stimulated virulence phenotype, in which *A. baumannii* was found to resist grazing by *D. discoideum* and decrease *C. elegans* reproductive fitness specifically in the presence of ethanol. Several genes responsible for this phenotype, given the name ethanol-stimulated virulence genes (*esv*), were found by screening a transposon library for clones that were no longer able to resist protist grazing in the presence of ethanol (Smith et al. 2007, Smith, Des Etages, and Snyder 2004). Interestingly, as shown in Chapter II, the ethanol phenotype is not an *A. baumannii* specific trait and also extends to the non-pathogenic *A. baylyi*.

Another invertebrate model used to study *A. baumannii* pathogenesis that has been widely adapted is the use of larvae of the wax moth *Galleria mellonella*. This insect has been used extensively as a tool for studying host-pathogen interactions, both for use of specific host-pathogen studies with pathogens specific to insects, such as the gram-positive bacterium *Bacillus thuringiensis* and nematodes, and also for the study of many human pathogens. Importantly, there has been a positive correlation in the genetic elements required for causing disease in the *Galleria* model with the findings in more complex (and presumably more realistic) mammalian models, suggesting that the *Galleria* model is a suitable surrogate for the study of bacterial pathogenesis (Puza and Mracek 2009, Grizanova et al. 2014, Jander, Rahme, and Ausubel 2000, Harding et al. 2012). Some additional strengths of the *G. mellonella* model are that the larvae are commercially available and inexpensive; the larvae survive well at 37 ˚C and are easy to manipulate. Another important feature of this model is that the insect immune systems are evolutionarily similar to the innate immune system found in mammalian hosts and include phagocytic cells, the production of antimicrobial peptides and an oxidative burst. Many of the pathogen detection and signal transduction pathways are also conserved between insects and mammals (Fuchs et al. 2010).

As far as mammalian models are concerned, most reports detail experiments resulting from the infection of either mice or rats. The most common route of infection in these models is pulmonary infection, which matches the most common clinical presentation observed in humans – ventilator associated pneumonia. Other models include subcutaneous inoculation of bacteria to model skin infections, direct injection of bacteria into surgical sites, and also intraperitoneal injections to simulate sepsis (Jacobs, Thompson, Black, et al. 2014, Hraiech et al. 2013). The utility of these models varies with both the strain of *A. baumannii* and the breed of mouse/rat.

Indeed, some *A. baumannii* isolates are relatively avirulent in these models without direct immune suppression of the animals by cyclophosphamide injection (Jones et al. 2015). Additionally, some strains of inbred mice, including the A/J strain, demonstrate enhanced sensitivity to *A. baumannii* infection and do not require additional immune suppression to observe pathogenesis (Qiu et al. 2009). The report from Qiu and colleagues demonstrate that neutrophil recruitment is a major component of the increased sensitivity of A/J mice to *A. baumannii* infection, suggesting that the early recruitment of immune cells to the site of infection may be a critical factor for clearance of this particular pathogen.

Gene regulation in *A. baumannii*

Another area of need in the *Acinetobacter* field is the identification of transcriptional regulatory networks that underlie the expression of virulence determinants. Such an understanding has been beneficial for many other pathogens. For example, virulence gene expression in *S. aureus* is controlled in part by the *agr* system, a quorum sensing system used to monitor staphylococcal population density signaling, and recent efforts have focused on generating novel therapeutic strategies that antagonize this system as a means to combat infections caused by *S. aureus* (Khan et al. 2015). Also, extensive research investigating expression of the genes required for disease in other pathogens, such as *Listeria monocytogenes* and *Salmonella* spp., has provided excellent models of how these bacteria regulate expression of specific virulence pathways for survival inside the host (Xayarath and Freitag 2012, Erhardt and Dersch 2015). In *A. baumannii*, however, a small number of regulatory pathways underlying the expression of the genes required for pathogenesis have been characterized and these will be discussed below.

A commonly utilized mechanism of gene regulation in bacteria is through signal transduction modules known as two-component systems (TCS). These signaling systems typically consist of a sensor kinase protein (SK), which is activated by particular environmental cues and, following an autophosphorylation event, transmits this detected change in environmental conditions to a partner protein called a response regulator (RR). Typically, RR proteins have a DNA-binding domain and activation of the RR by SK activity results in gene expression changes that are specific for adapting to the particular environmental condition sensed by the SK (reviewed in Zschiedrich, Keidel, and Szurmant 2016). For *A. baumannii,* several TCS systems have been characterized for the regulation of a variety of processes, ranging from biofilm formation to controlling expression of key drug efflux pumps.

One of the earliest two component systems to be discovered and characterized in *A. baumannii* is the BfmRS system, which has been shown to play a critical role in biofilm formation. These two proteins are well conserved, with BfmS comprising the sensor kinase protein and BfmR serving as the response regulator. Work from the lab of Luis Actis initially discovered that disruption of the *bfmRS* genes led to decreased biofilm formation and follow-up studies determined that this TCS was required for expression of the CsuAB pilus described above (Tomaras et al. 2003, Tomaras et al. 2008, Thompson et al. 2012). Additional work from both the Shuman lab and other groups has expanded the role of the BfmRS TCS to extend beyond biofilm formation and pilus expression. Indeed, these recent reports have shown that the BfmRS TCS is required for *A. baumannii* virulence, as determined with both *in vitro* model systems (Liou et al. 2013) and *in vivo* models (see Chapter II and Gebhardt et al. 2015). Finally, the *bfmRS* genes were recently identified as playing a role in the regulation of capsule formation of *A. baumannii* (Geisinger and Isberg 2015).

As discussed above, many *A. baumannii* clinical isolates that demonstrate an MDR phenotype over express the AdeABC multi-drug efflux pump. In several cases, the mechanism driving the increased expression of this efflux pump has been determined to be mutations to the AdeRS and/or BaeRS two-component systems. These two TCS systems appear to have at least a partially overlapping regulon, as both have been shown to control expression of the *adeABC* genes. The BaeRS TCS likely lies upstream of the AdeRS TCS, as the BaeR protein did not bind to the promoter regions of genes found to be differentially expressed in the absence of the *baeR* gene, suggesting that the BaeRS-mediated control of these genes is indirect and possibly mediated by the AdeRS TCS. Additionally, strains deleted for the BaeRS TCS demonstrate sensitivity to a greater range of disinfectant molecules relative to isogenic wild type strains (Lin et al. 2014, Lin, Lin, and Lan 2015, Nowak et al. 2016).

While the previously mentioned TCS systems appear to be unique to *A. baumannii* and closely related organisms, several groups have studied other two-component systems that are widely conserved across many gram-negative bacterial species. These other TCS systems include the PmrAB, OmpR/EnvZ and GacA/GacS two-component systems. The PmrAB TCS has been shown, both in *A. baumannii* and other gram-negative organisms, to respond specifically to polymyxin-like antibiotics, including colistin and other anti-microbial peptides. Much like the case in other bacteria, signaling through PmrAB leads to expression of modified LPS species with decreased affinity for the amphipathic nature of colistin and similar anti-microbial agents (Beceiro et al. 2011). In addition to PmrAB, the OmpR/EnvZ TCS, which is also well conserved in other gram-negative species, has recently been shown to mediate osmotic stress resistance and is also required for virulence (Tipton and Rather 2016). Finally, the GacA/GacS two component system has been shown to be required for stress resistance and secondary metabolite biosynthesis

in several gram-negative bacterial species (Heeb and Haas 2001). Recent work from the lab of Anton Peleg has determined that the GacS sensor kinase functions as a global regulator required for several aspects of *A. baumannii* physiology, including biofilm formation and virulence. Additionally, GacS also is required for the expression of a set of genes required for phenylacetic acid catabolic pathway that is required for virulence in a murine infection model (Cerqueira et al. 2014).

In addition to the aforementioned two component systems, other researchers have examined the transcriptional response of *A. baumannii* under various environmental conditions, including antibiotic exposure, as well as growth in the presence of ethanol, which, as mentioned above, stimulates virulence in *A. baumannii*. Analysis of the transcriptome of *A. baumannii* exposed to the antibiotic tigecycline showed decreased expression of genes involved with the citric acid cycle and an increased expression of genes involved with benzoic acid metabolism, suggesting that when faced with antibiotic pressure, *A. baumannii* relies on alternative carbon sources for metabolic purposes (Liu et al. 2016). This study also found that many efflux pumps had increased expression following antibiotic exposure. Henry and colleagues also report the effects of exposure to colistin, an antibiotic that disrupts the outer membrane of gram-negative bacteria (Henry et al. 2015). Colistin exposure led to the increased expression of genes involved in the maintenance of the outer membrane and fatty acid metabolism, consistent with the disruption of the outer membrane that results from exposure to anti-microbial peptides such as colistin. In response to ethanol exposure, two major categories of genes demonstrate increased expression; genes involved with ethanol metabolism and stress response genes (Camarena et al. 2010). These findings are not overly surprising as *A. baumannii* is able to utilize ethanol as a

carbon source and, given that ethanol is a toxic molecule, the induction of stress response genes is a logical outcome.

One final transcriptional regulatory network that has been well characterized in *A. baumannii* is the transcriptional regulator Zur, which controls a suite of genes required for the acquisition of the important micronutrient zinc. The Zur regulator controls the expression of the high-affinity Zn^{2+} transport system, ZnuABC. In addition to regulating the expression of the *znuABC* genes, work from Eric Skaar's group has determined the regulon of the Zur protein, which includes genes involved in metal acquisition, stress responses, transcriptional regulation, amino acid biosynthesis and virulence (Mortensen et al. 2014, Hood et al. 2012).

The bulk of my dissertation has focused on conducting experiments aimed at answering some of the questions raised above. Specifically, I sought to uncover the genetic determinants harbored by *A. baumannii* that endow this organism with the ability to cause human disease. In light of the relatively poor characterization of gene expression networks in *A. baumannii*, I placed particular emphasis on the regulatory mechanisms that mediate control of virulence gene expression. Additionally, I wished to enhance our understanding of how *A. baumannii* incorporates environmental signals into generating the appropriate response to survive the harsh environments encountered during colonization of clinical environments and within a human host. Ultimately, the results of these endeavors offer new insight into the emerging pathogenesis of *A. baumannii* by providing a framework for understanding the evolution of *A. baumannii* from a hardy, soil dwelling organism into a successful human pathogen. In the forthcoming chapters, I describe the identification and characterization of regulatory networks that connect three key aspects of *A. baumannii* pathogenesis in the contemporary clinical setting: antibiotic resistance, persistence under environmental stress and nutritional versatility.

CHAPTER II

Using TnSeq to identify virulence regulatory networks in *Acinetobacter baumannii*

This chapter is adapted from the published manuscript 'Joint transcriptional control of virulence and resistance to antibiotic and environmental stress in *Acinetobacter baumannii'*. The authors on this manuscript are as follows: Michael J Gebhardt, Larry A Gallagher, Rachael K Jacobson, Elena A Usacheva, Lance R Peterson, Daniel V Zurawski, Howard A Shuman. M.J.G. performed all experiments alone with the exception of the preparation of the Transposon Sequencing library and mapping of the data to the AB5075 genome (L.A.G.) and E.A.U. performed the antimicrobial susceptibility testing shown in Table 2.4.

INTRODUCTION

Acinetobacter baumannii is rapidly emerging as a significant human pathogen (Visca, Seifert, and Towner 2011). Current estimates predict that of the approximately 45,000 *A. baumannii* infections per year in the United States (and roughly one million annual infections world-wide); half of these infections (~ 23,000) result from strains resistant to carbapenem antibiotics, and lead to a mortality rate approaching 20% (Spellberg and Rex 2013). Indeed, many of the currently circulating strains of this opportunistic pathogen exhibit a multidrug-resistant (MDR) phenotype and even pan-resistant strains have been reported (Gottig et al. 2014). For *A. baumannii*, the MDR phenotype can be attributed to a combination of intrinsic and acquired traits (Peleg et al. 2012). While work to identify and characterize the repertoire of *A.*

baumannii virulence determinants has begun, additional studies are required to understand the genetic basis of virulence and to translate how these determinants impact human disease (Antunes, Visca, and Towner 2014).

Bacterial genetics represents an extremely powerful tool for identification of virulence factors (Cox et al. 1999, Slauch and Camilli 2000), and, as genetic technology has advanced, so too has the scale of genetic screens (Gallagher, Shendure, and Manoil 2011, van Opijnen, Bodi, and Camilli 2009, van Opijnen and Camilli 2013, Wang et al. 2014). Early techniques to identify bacterial genes required for a given phenotypic trait relied heavily on direct mutation of DNA using DNA damaging chemicals or exposure to ultraviolet radiation, followed by screening of surviving bacterial clones for the desired phenotype. As the molecular age began in the late 1970's and into the 1980's, the first reports of using transposons as a means to conduct forward genetic screens appeared in the literature (Shaw and Berg 1979). Much like the physical mutagenesis approaches, the founding experiments using transposon mutagenesis typically relied on the screening of individual colonies for a desired phenotype. Further genetic analyses were then required to identify underlying genetic cause of the phenotype in question.

As time progressed, the complexity and diversity of transposon mutagenesis screens increased, both in size and scope. Several experimental approaches were developed that began to allow researchers study larger numbers of transposon mutants within a single experiment. One such experiment, signature-tagged mutagenesis or STM, was employed in a study of *Mycobacterium tuberculosis* and led to the identification of a critical *M. tuberculosis* virulence factor, chord factor (Cox et al. 1999). This experimental approach relied on the incorporation of known DNA sequences in the transposon (i.e. a 'signature' tagged strain for each transposon insertion mutant). The STM experiments allowed for the experiments to assay a pool of 10's to

100's of transposon mutants, which represented a significant advance over previous screens where mutants were tested in isolation.

Additional experimental approaches, such as IVET (*in vivo* expression technology) relied not on transposon mutagenesis, but rather on the transcriptional activation of promoters in a given environment, such as during an infection, as a means to identify genes. A typical IVET experiment utilizes an attenuated pathogenic strain harboring a genetic mutation known to reduce virulence of that particular organism. This strain is then provided a copy of the complementing gene in which the native promoter for the gene in question has been replaced with a random library of DNA fragments. The rationale here is that, during the infection, only those library fragments containing promoters for genes normally expressed within the host environment will drive expression of the complementing gene. Thus, IVET experiments enrich for genes that are specifically expressed inside of the host during the infection process, allowing for the identification of virulence factors (Slauch and Camilli 2000). The significance of the IVET experimental approach was again that a large number of bacteria could be screened as a population.

The most recent advance in terms of genetic screens followed closely behind the advent of next generation sequencing technologies (NGS), such as the Illumina sequencing platforms. At present, NGS platforms are capable of performing several hundred million sequencing reactions simultaneously. This depth of sequencing, when coupled with a transposon mutagenesis experiment, can essentially be used to finely map transposon insertion sites across a given bacterial genome at very fine-scale resolution. Collectively, these experiments have been termed Transposon Insertion Sequencing, or TnSeq. Several different versions of TnSeq experiments, with variations in the transposons used, molecular biology processing steps and the

data analysis pipelines, have been developed and employed across many different bacterial species during exposure to a wide range of environmental conditions (van Opijnen, Bodi, and Camilli 2009, Gallagher, Shendure, and Manoil 2011, Wang et al. 2014). The power of these experiments lies in the number of mutants that can be assessed in a single experiment, with the numbers approaching 10^6 unique transposon mutants being assayed in some experiments (Langridge et al. 2009).

In the following sections, I describe the results of such an experiment conducted to uncover genes required for *A. baumannii* virulence using strain AB5075, a contemporary MDR isolate that represents currently circulating isolates of *A. baumannii* (Gallagher et al. 2015, Jacobs, Thompson, Black, et al. 2014, Zurawski et al. 2012). Using TnSeq, we identified 300 genes required for survival and/or growth within *Galleria mellonella* larvae, an established insect model system for a variety of human microbial diseases (Peleg et al. 2009). In addition to several known virulence factors, the screen reported herein also identified many novel genes, including several transcriptional regulators that control both virulence-related genes and those required for antibiotic resistance.

As *A. baumannii* clinical isolates are increasingly resistant to antibiotic therapy (Boucher et al. 2009), we hypothesized that environmental virulence factors may be associated with resistance to antimicrobial compounds. Thus, we assessed antibiotic sensitivity of a subset of the mutants. We found that several mutants defective for growth in *G. mellonella* larvae also exhibited increased susceptibility to antibiotics and other environmental stress conditions. These results highlight the existence of a link between virulence, antibiotic resistance and environmental stress resistance in *A. baumannii* (Wright et al. 2014, Geisinger and Isberg 2015,

Roux et al. 2015) and further suggest that selection for increased environmental stress resistance may also inadvertently select for strains with enhanced virulence.

RESULTS

Initial Characterization of *Acinetobacter baumannii* strain AB5075

The majority of the studies described in this chapter and those the follow were performed using *Acinetobacter baumannii* strain AB5075, a contemporary multi-drug resistant clinical strain that was isolated as the causative agent of either a blood stream infection or osteomyelitis infection of a soldier wounded in the Iraq/Afghan wars (Zurawski et al. 2012). Other researchers have demonstrated that this strain was more virulent in several infection models and, more importantly, this particular strain is genetically tractable, allowing for the construction of strains with targeted genetic mutations strains (Jacobs, Thompson, Black, et al. 2014, Jacobs, Thompson, Gebhardt, et al. 2014). Upon receipt of this strain from collaborators, I first sought to confirm that the strain expressed the characteristic multi-drug phenotype. Compared to the commonly used laboratory strain, ATCC 17978, strain AB5075 was found to be more resistant to several additional antibiotics (Table 2.1), confirming the MDR phenotype of this strain. Importantly, the AB5075 strain retains sensitivity to several antibiotics, including tetracycline, hygromycin and apramycin, allowing for the use of these antibiotics as selective markers for plasmid maintenance and/or construction of mutant strains.

Dictyostelium discoideum as a model for *A. baumannii* infection

Previous reports have used the environmental amoeba, *Dictyostelium discoideum*, as a model system to assess the virulence potential of microbial pathogens (Pukatzki, Kessin, and

Mekalanos 2002). A commonly used method to assess bacterial pathogenesis with the *Dictyostelium* is to measure the ability of the amoebae to form a plaque, or zone of clearing, on a lawn of bacterial growth on an agar surface. Essentially, this model tells the researcher whether or not the bacteria in question are able to resist phagocytosis, or grazing, by the *D. discoideum* predator. As discussed in the previous chapter, *A. baumannii* has been used in this model and the ethanol stimulated virulence phenotype was demonstrated using this experiment (Smith et al. 2007).

In order to determine the utility of the *D. discoideum* model for studying the virulence potential and to confirm the ethanol stimulated virulence phenotype of *A. baumannii* strains, I conducted *Dictyostelium* Plate Test (DPT) assays in which a bacterial suspension is mixed with *Dictyostelium* trophozoites and plated onto low nutrient agar plates (SM/5 plates). The low nutrient concentration of this media allows for bacterial growth but lacks adequate nutrient sources for the *Dictyostelium*. As such, the amoebae turn to consumption of the bacteria as a food source. As shown in Figure 2.2 and consistent with previous reports, both *A. baumannii* strains, AB5075 and ATCC 17978 resist grazing by *Dictyostelium* when ethanol is added to the medium. More telling than this observation, perhaps, was that the well-characterized, non-pathogenic *Acintoebacter baylyi* strain ADP1 also resists grazing when ethanol is added to the medium. Finally, as an additional non-pathogenic control, *E. coli* strain MC4100 was included in the experiment as well. Interestingly, on the plates containing ethanol, MC4100 bacteria and the amoebae suggest that the ethanol stimulated virulence response may not be a strictly bacterial phenomenon, as the size of plaques on the SM/5 + ethanol plates containing the lawn of MC4100 are remarkably smaller than those on the SM/5 plates without ethanol (Figure 2.2). This observation suggests that in addition to the enhanced growth of *Acinetobacter* in the presence of

ethanol, the growth and/or health of the *Dictyostelium* cells is likely reduced in the presence of ethanol.

The decreased fitness of the *Dictyostelium* amoebae in the presence of ethanol and the observation that the non-pathogenic *A. baylyi* also exhibits increased 'virulence' in the presence of ethanol, leads to several conclusions regarding the DPT as a model. First, the DPT model is likely an inappropriate method for studying the pathogenicity of *Acinetobacter* isolates, as *A. baylyi*, a non-pathogenic *Acinetobacter* species, exhibits 'virulence' in the presence of ethanol. Also, the inclusion of a laboratory-adapted *E. coli* as a control strain identified that inclusion of ethanol in the growth medium likely decreases the fitness of the amoebae. As such, my interpretation of the DPT assay as a means to study pathogenesis of *A. baumannii* is that this model is inadequate for identifying specific virulence factors harbored by this organism.

Validation of the *Galleria mellonella* infection model

Because the *Dictyostelium* model does not adequately differentiate between pathogenic and non-pathogenic *Acinetobacter* species, we employed the *Galleria mellonella* infection model (Peleg et al. 2009, Fuchs et al. 2010, Kavanagh and Reeves 2004). Previous work with several microbial pathogens has demonstrated a positive correlation between the *Galleria* model and mammalian disease models (Jander, Rahme, and Ausubel 2000, Lionakis 2011, Mukherjee et al. 2010). Infection of *Galleria* larvae with various *Acinetobacter* strains showed that the model easily distinguishes non-pathogenic from pathogenic *Acinetobacter* spp. In contrast to the results obtained with the DPT experiments described above, Figure 2.2 shows that *A. baylyi* does not survive during 4 hours within larvae, whereas the human pathogenic isolates ATCC 17978 and AB5075 survive and grow within the larvae during the same time period. Furthermore, larvae

infected with these strains displayed dramatic differences in survival, with strain AB5075 leading to rapid mortality, *A. baylyi* ADP1 causing minimal larval killing over the course of the experiment and ATCC 17978 leading to intermediate levels of killing (Fig. 2.2). The enhanced growth within larvae and the rapid larval killing kinetics are consistent with previous reports that AB5075 is more virulent than the ATCC 17978 strain and supports a correlation between growth in *G. mellonella* larvae with the previously reported virulence of specific *A. baumannii* strains in mammalian models (Jacobs, Thompson, Black, et al. 2014).

Assessment of *Acinetobacter* Clinical Isolates using the *Galleria mellonella* Infection Model

Through a collaboration with a clinical investigator at a local hospital (NorthShore University Health System, Evanston, IL), we obtained a series of clinical *Acinetobacter* isolates (Table 2.2). The goal behind this collaboration was to address the question of whether non-*A. baumannii* members of the *A. baumannii*/*calcoaceticus* complex of organisms, which are at present largely indistinguishable from each other using routine clinical microbiology techniques, can be differentiated using the *Galleria mellonella* infection model. Towards this end, I tested 12 clinical *Acinetobacter* isolates for virulence in the *G. mellonella* model. The isolates, which have been identified to the species level, included both drug sensitive and multi-drug resistant strains of *A. baumannii* and three strains of the closely related *Acinetobacter pittii*. Virulence was assessed in these strains by monitoring survival of larvae infected with the various strains. As shown in Figure 2.3, the *A. pittii* strains (ACI strains 10, 11, 12) were less virulent to *G. mellonella* larvae than those of the *A. baumannii*. Additionally, strains of a single clonal origin (ACI 1-3, 13) were equally as virulent as AB5075. These strains were collected during an outbreak of infections stemming from the Intensive Care Unit of the NorthShore University

Hospital and the outbreak strain proved particularly recalcitrant to decontamination practices (La Forgia et al. 2010). A general trend amongst the clinical isolates was that the strains harboring an MDR phenotype were generally more virulent as measured by the *G. mellonella* assay, although a larger sample size would be required to confirm this finding.

TnSeq of *A. baumannii* in *Galleria mellonella* larvae

Given that the *G. mellonella* infection model readily differentiates pathogenic from non-pathogenic *Acinetobacter spp.*, as well as between more- and less-virulent *A. baumannii* strains, we sought to identify the genetic elements of *A. baumannii* strain AB5075 that are required for growth and/or survival within *G. mellonella* larvae. Towards this end, we performed a TnSeq experiment using the TnSeq Circle method with a previously described library of transposon mutants (Gallagher, Shendure, and Manoil 2011, Gallagher et al. 2015). Aliquots of the transposon library were inoculated into either a rich laboratory medium (LB) or *G. mellonella* larvae, incubated for 4 hours at 37 ˚C and processed as described in the Materials and Methods chapter. A diagrammatic representation of the TnSeq experiment is depicted in Figure 2.4. Quantification of the bacterial growth in the LB control sample and the recovery from the *G. mellonella* larvae showed that the bulk population grew at a similar rate under both conditions. This finding suggests that the immune response of *G. mellonella* has a minimal ability to control the growth of *A. baumannii* AB5075.

The DNA collected from the *G. mellonella* and LB passaged pools were used to generate Illumina sequencing libraries and transposon insertions were mapped and quantified as described elsewhere (Gallagher, Shendure, and Manoil 2011). In order to identify mutants that were underrepresented following growth in *G. mellonella*, a read ratio (RR) was determined for each

gene between the *G.mellonella* and LB samples. Using a 10-fold reduction (RR ≤ 0.10) as a significance cut-off, 300 genes were defined as essential for growth of AB5075 within *G. mellonella* larvae (Fig. 2.5). The subset of genes identified by TnSeq discussed herein is listed in Table 2.3; the complete listing of the 300 genes can be found in Table 2.5. We anticipated that the *G. mellonella* TnSeq screen would identify three main categories of genes: (i) genes required for nutrient acquisition within *G. mellonella*, (ii) genes required for resisting the *G. mellonella* immune responses, and (iii) genes performing an as yet unknown role during infection.

Nutrient Acquisition/Metabolic Functions

A recently described concept of innate immune defense to bacterial infection is "nutritional immunity", or the ability of the host to restrict access of essential nutrients (Hood and Skaar 2012). The TnSeq screen identified several genes involved in acquisition systems for two essential micronutrients, zinc and iron (Table 2.3). Many genes required for the acinetobactin siderophore system were found to be required for growth in *G. mellonella* (Gaddy et al. 2012, Zimbler et al. 2009) as well as ABUW_2074, a Fur family transcriptional regulator (RR_{fur} = 0.050), which potentially plays a role in the regulating expression of genes required for iron uptake. Additionally, mutants with insertions in each of the three structural genes of the *znuABC* zinc uptake system and the transcriptional regulator controlling the expression of these genes (*zur*) exhibited very low RR. Zinc acquisition has been previously demonstrated as an important virulence determinant for *A. baumannii* disease in a murine lung infection model (Hood et al. 2012). Consistent with previous reports, a *znuB* mutant showed decreased survival after 4 hours of infection, confirming the requirement for zinc acquisition in the *Galleria* model (Figure 2.6) (Mortensen et al. 2014, Hood et al. 2012). Recently, transcriptome data obtained

from a *zur* mutant strain of *A. baumannii* was published and comparison of the *zur*-controlled genes with our TnSeq dataset identified eight genes that were both differentially expressed in the *zur* mutant and required for growth in *G. mellonella* (Mortensen et al. 2014). These genes include *znuA*, a TetR family regulator (ABUW_1692), *otsB* (ABUW_3122), an isochorismatase hydrolase (ABUW_2374), and four genes of unknown function (ABUW_2145, ABUW_2439, ABUW_2442 and ABUW_2679). Identification of these well-known metal ion acquisition systems provides proof of principle that the *Galleria* model imposes nutrient-limitation stresses similar to those in mammalian infection models.

Another pathway required for growth in the larvae is cysteine metabolism/sulfur assimilation (Table 2.3), which is well conserved and has been characterized in many bacterial species (Campanini et al. 2015, van der Ploeg, Eichhorn, and Leisinger 2001). One explanation for the requirement of these genes is that *G. mellonella* limits free cysteine as a pathogen restriction strategy, as shown previously (Wyatt, Loughheed, and Wyatt 1956). An alternative hypothesis for the cysteine requirement in the *Galleria* model is that cysteine serves as a protectant from oxidative and/or nitrosative stresses, which are widely conserved antimicrobial defense strategies. Indeed, *cys* genes have been linked to increased susceptibility to oxidative stress in several other bacterial species (Alvarez et al. 2015, Turnbull and Surette 2010, Shatalin et al. 2011). Additional studies pertaining to cysteine metabolism and the requirement of *cys* genes in the *G. mellonella* model are discussed in greater detail in Chapter IV.

Eight genes predicted to play a role in the catabolism of aromatic compounds were identified as required for growth in *G. mellonella* (Table 2.3). This could indicate that the *Galleria* hemolymph contains aromatic hydrocarbons as carbon sources for *Acinetobacter*. Mutants predicted to be defective in the metabolism of various aromatic compounds, including

benzoic acid and protocatechuate, were reduced following growth in *Galleria*, indicating a link between aromatic compound catabolism and the ability to grow in the larvae. Additionally, two of the identified genes, *paaI* and *paaY*, predicted to be involved with phenylacetic acid catabolism, have previously been implicated in virulence (Cerqueira et al. 2014).

Capsule, cell envelope, and membrane biogenesis

Transposon insertions within several genes required for capsule, cell wall and outer-membrane biogenesis reduced the ability of *A. baumannii* to survive and grow within *Galleria* larvae (Table 2.3). This result is not surprising, as many of the immune defense mechanisms employed by the larvae will first encounter the bacterial outer membrane/cell envelope. Indeed, mutants with transposon insertions in several genes required for capsule biosynthesis were completely absent from the output DNA pool after growth in *Galleria* (Fig. 2.7). Also, strains harboring insertions in the *pbpG* gene, encoding a D-alanyl-D-alanine endopeptidase required for modification of peptidoglycan, were unable to grow in the larvae ($RR_{pbpG} = 0$). This gene was previously shown to be required for growth of *A. baumannii* in human serum, a murine pneumonia model and a rat pneumonia model (Russo et al. 2009, Wang et al. 2014). In addition to the capsule operon and *pbpG*, transposon insertion in several other genes involved with lipopolysaccharide (LPS) biosynthesis, including *lptE, lpxL* and *lpsB*, were undetected or underrepresented in the larval samples (RRs of 0, 0, and 0.025, respectively). In many gram-negative bacteria, like *E. coli*, LptE is an essential protein required for proper insertion of LPS into the outer membrane (reviewed in (May et al. 2015)). In some gram-negative organisms, however, such as *Neisseria meningitidis,* LptE is not essential for transport of LPS (Bos and Tommassen 2011). Analysis of a previously published list of candidate essential genes in *A.*

baumannii AB5075 indicates that other LPS transport genes (*lptA, lptB, lptC,* and *lptD*) are essential, whereas *lptE* is not required for growth in rich medium (Gallagher et al. 2015). The requirement of *lptE* in the *Galleria* model suggests that there may be environments where LptE is required for proper assembly of LPS.

To validate these findings and to establish a protective role for capsule production in the *G. mellonella* disease model, as has been shown in other disease models (Russo et al. 2010), we constructed a strain with an in-frame deletion of the *ptk* gene. Ptk is a structural component of the capsular polysaccharide export machinery along with Wza and Ptp. Recovery of mutants in all three genes was significantly reduced in the *G. mellonella* larval output pool ($RR_{wza} = 0.013$, $RR_{ptp} = 0$, $RR_{ptk} = 0$). When we infected *G. mellonella* larvae with the *ptk* mutant, larval killing and bacterial growth were dramatically reduced compared to wild type AB5075 (Fig. 2.7) and was restored by expression of the wild-type *ptk* gene *in trans*, confirming the importance of capsule as a virulence factor in *A. baumannii*.

Stress Response Genes

Sixteen genes required for growth within *G. mellonella* are predicted to mediate stress resistance. These genes include those involved in the general stress response, including *cinA, csp*, *typA* and *uspA*; DNA repair, *uvrD*; membrane/envelope stress, ABUW_1447 (HptX homolog) and *rseP*; oxidative induced stress, *pqiA* (paraquat) and *arsC* (arsenate); and osmotic stress resistance, ABUW_2237 (cation transport), *otsB, kef*, *kefF, mscS*, *trkA*, and *trkH* (Table 2.3). These results suggest that the ability of *A. baumannii* to grow and/or survive in *G. mellonella* may be dependent upon the organism's ability to cope with the environmental stresses imposed by the innate immune response to infection. As the *G. mellonella* larva contains

hemocytes, phagocytic cells that, much like human neutrophils, generate an oxidative burst and produce antimicrobial peptides, which can mimic osmotic shock, (Kavanagh and Reeves 2004, Krishnan, Hyrsl, and Simek 2006, Lionakis 2011, Peleg et al. 2009, Kim et al. 2010), we infer that these stress response genes may also play a role in human disease.

To confirm the phenotypes of the stress response genes identified in the TnSeq screen, we constructed mutants containing in-frame, unmarked deletions of several of the hits and tested these strains for virulence defects in the *G. mellonella* model. In the few instances where attempts to generate in-frame deletions were unsuccessful, we used strains harboring a transposon insertion in the gene of interest. Deletion strains showing defective survival and/or growth within *G. mellonella* include both genes with known/predicted functions, including *ptk, bfmS*, a two component system (TCS) sensor kinase (described in further detail below), *znuB,* stress response genes, *rseP*, *typA*, *uspA*; and genes with uncharacterized functions (Figure 2.6).

As several of the stress response genes identified in the TnSeq screen are predicted to mediate osmotic stress resistance, we conducted additional experiments to demonstrate a role for osmotic stress resistance in the *G. mellonella* model. The osmotic stress gene mutants used in Figure 2.8 were defective for growth in freshly collected larval hemolymph, consistent with the results obtained by the TnSeq experiment. Decreased killing of larvae by several strains harboring deletions of osmotic stress genes also was also observed (Figure 2.8).

Furthermore, I performed additional complementation experiments on a subset of genes (*rseP*, *typA*, and *uspA*) predicted to be involved in both sensing and surviving stress. In other proteobacteria, the *rseP* gene encodes an intramembrane protease that transmits outer membrane stress via RpoE/σ^E (Makinoshima and Glickman 2006), while *typA* and *uspA* are predicted to be involved in the general stress response and have previously been shown to play a role in

virulence (Micklinghoff et al. 2010, Neidig et al. 2013, Kvint et al. 2003). I confirmed the initial TnSeq results by assessing the ability of these mutants to grow within and kill *G. mellonella*. Strains defective for these genes displayed a *Galleria* growth defect, which was restored to near wild-type levels by complementation with wild type copies of the genes expressed *in trans* (Figure 2.9).

Antibiotic Resistance Genes

All strains of *A. baumannii* harbor efflux pumps associated with removal of toxic compounds from bacterial cells (Yoon et al. 2015). The TnSeq screen identified genes belonging to three different types of efflux systems; *adeI, adeJ* and *adeK* (RR's of 0.0247*,* 0.0233*,* and 0, respectively), which encode the resistance-nodulation-cell division pump, AdeIJK (Damier-Piolle et al. 2008); four different genes containing EamA-like transporter domains of the metabolite/drug transporter family (ABUW_1156, RR = 0.044; ABUW_1499, RR= 0.062; ABUW_1520, RR = 0.064 and ABUW_2550, RR = 0.058) and a member of the Proteobacterial Antimicrobial Compound Efflux family, ABUW_1673 (RR = 0) (Hassan et al. 2015) (Table 2.3). Decreased recovery of strains harboring interruptions of these genes following growth in *Galleria* larvae relative to rich medium suggests that *Galleria* produces toxic compounds during infection that *A. baumannii* must export for survival. In addition to these drug efflux systems, recovery of strains harboring insertions within two genes, ABUW_1851 and ABUW_2123, encoding a putative aminoglycoside phosphotransferase and a beta-lactamase family protein were also reduced following *G. mellonella* growth. Although annotated as encoding potential antibiotic resistance mechanisms, I hypothesize that the proteins produced by these genes may

perform other functions, as *G. mellonella* larvae likely do not produce either aminoglycosides or β-lactams.

Transcriptional Regulators

Other than genes of unknown function, the largest single category of hits from the TnSeq screen includes genes annotated as having signal transduction or transcriptional regulation functions (Table 2.3). Among the 32 genes in this group, only a few have previously recognized functions; *arsR* (arsenic resistance), *alkR* (alkane metabolism), *bfmS*, (biofilm formation), and *soxR* (redox homeostasis) (Liou et al. 2013, Tomaras et al. 2008, Ratajczak, Geissdorfer, and Hillen 1998, Kobayashi, Fujikawa, and Kozawa 2014). An insufficient number of transposon insertions mapped to the *bfmR* (the cognate response regulator for *bfmS*) in either the LB sample to be included in the TnSeq analysis. Several other putative transcriptional regulatory genes were found; two TCS response regulators, seven LysR – family regulators, five TetR - family regulators, four AraC – family regulators, two AsnC/Lrp family regulators, a MarR family regulator and several others. One of the TetR family regulators, ABUW_1692, and one of the AsnC/Lrp regulators (ABUW_1755, described below), were reported to be differentially expressed in the *zur* mutant (Mortensen et al. 2014) as well as during biofilm growth (Rumbo-Feal et al. 2013). Coupled with the *bfmS* requirement for growth in *G. mellonella*, this finding suggests similar genetic pathways are required for biofilm formation and growth/survival in *G. mellonella*.

Follow up studies identified a subset of genes that are required for both growth within and killing of *G. mellonella* larvae. We term these genes '*gig*', for Growth-in-*Galleria*. While many additional genes listed in Table 2.5 could be considered to have the '*gig'* phenotype, we

formally classify only a small subset as *'gig'* genes because loss of these particular genes leads to a robust defect for both growing within and killing *Galleria* larvae. The *gig* genes include ABUW_3260, a predicted TCS response regulator with a PP2C protein phosphatase domain (*gigA*); ABUW_3261, a putative anti-anti-sigma factor (*gigB*); ABUW_3161, a LysR family regulator (*gigC*); and ABUW_1755, an AsnC/Lrp family regulator (*gigD*) (Figure 2.10). Expression of the *gigB, gigC* and *gigD* genes *in trans* restored the *Galleria* growth defect of these strains (Figure 2.10). Attempts to complement the *gigA* mutant for growth in *Galleria* yielded ambiguous results.

Deletions of the *bfmS* gene reveal differences between AB5075 and 17978

As mentioned previously, one of the better-characterized two component regulatory systems that has been characterized in *A. baumannii* includes the sensor kinase BfmS and the response regulator BfmR. The genes encoding these proteins, *bfmRS*, are oriented sequentially in the *A. baumannii* chromosome and were previously shown to be required for biofilm formation in strain 17978, with mutant strains lacking the *bfmS* gene showing defective biofilm formation (Liou et al. 2013). Interestingly, other researchers have reported that the *bfmS* gene was not required for biofilm production in another *A. baumannii* isolate, ATCC 19606 (Tomaras et al. 2008). In order to confirm the role of the BfmS sensor kinase in strain AB5075, I measured biofilm formation using the crystal violet staining method (Djordjevic, Wiedmann, and McLandsborough 2002). Deletion of the *bfmS* gene in the AB5075 strain background leads to a ~3-fold increase in biofilm formation, whereas the same deletion in the 17978 strain background (i.e. 17978 Δ*bfmS*) leads to a ~50% reduction in biofilm formation (Figure 2.11). As discussed above, deletion of *bfmR* in the AB5075 strain background appears to impart a significant fitness

cost (as assessed by the lack of Tn-insertions mapping to the *bfmR* gene in the TnSeq dataset), so I was unable to assess the biofilm formation in a *bfmR* deficient AB5075 strain. The discrepant results pertaining to the role of the *bfmS* gene suggests that the BfmRS two component regulatory system has evolved different functions as these strains have diverged from their common ancestor.

Mutations in *gig* Genes Show Decreased Antibiotic Resistance

As discussed above, several genes required for growth in *G. mellonella* appeared to be involved with resistance to either environmental stress and/or antibiotics (Table 2.3). We therefore tested the hypothesis that genes required for virulence may also have an important role in resisting environmental stress(es), such as exposure to antibiotics. In order to test this hypothesis, we performed antibiotic susceptibility testing according to the Clinical Laboratory Standards Institute (CLSI) guidelines and discovered that several genes that exhibited a RR < 0.10 in the *G. mellonella* model also mediate resistance to antibiotics. For example, strains deleted for either *gigA* or *gigB* show increased sensitivity to several antibiotics, including meropenem, aminoglycosides and tigecycline (Table 2.4, Figure 2.12). The Δ*ptk* strain showed enhanced susceptibility to several antibiotic categories, suggesting that capsular polysaccharides also serve to protect *A. baumannii* from antibiotic killing. In addition, deletion of a LysR family regulator (ABUW_1966) or *zur* led to increased susceptibility to peptidoglycan targeting antibiotics, including penicillins and meropenem. The strain harboring a transposon insertion in *typA* also exhibited sensitivity to several antibiotics. The finding that these genes are also required for growth within and/or killing of *G. mellonella* larvae supports the hypothesis that there is a link between virulence and the ability to resist environmental and/or antibiotic stresses.

DISCUSSION

Acinetobacter baumannii has emerged as a serious health risk due to its rapid acquisition of antimicrobial resistance and the species' inherent ability to survive in the clinical environment by resisting decontamination practices employed in health care facilities (Kawamura-Sato et al. 2010), thus providing the potential for spread to susceptible patients. Despite the increasing prevalence of MDR isolates, however; the molecular mechanisms underlying the pathogenesis of *A. baumannii* remain poorly defined. In this chapter, I confirmed that many of the known virulence genes harbored by *A. baumannii* are required for growth and/or survival within *G. mellonella* larvae, a well-established invertebrate model. Additionally, this work also identified a large number of previously uncharacterized genes that contribute to *A. baumannii* virulence.

Recently, Geisinger and Isberg published the results of experiments investigating the capsule synthetic genes of *A. baumannii* (Geisinger and Isberg 2015). Other work indicates that the capsule locus is quite variable across the sequenced genomes of *A. baumannii* isolates, suggesting that this important surface structure is under positive selection by environmental stresses and, perhaps, immune recognition (Scott et al. 2014). Indeed, our data suggest that the presence of capsule is protective during antibiotic stress (Table 2.4). Furthermore, the literature appears to be in agreement that production of exopolysaccharide capsule is a critical component for *A. baumannii* virulence in all models of infection that have been tested, including the *Galleria* model used for the studies described here (Geisinger and Isberg 2015, Russo et al. 2010). In accordance with this, we confirmed the requirement for capsule synthesis in AB5075 by showing that deletion of *ptk*, a gene required for capsule export, impaired growth within the larval cavity and attenuated larval killing (Figure 2.7). Geisinger and colleagues reported difficulty in generating *ptk* mutant strains using strain ATCC 17978 and found that strains with

ptk mutation had acquired suppressor mutations in the *bfmRS* locus (Geisinger and Isberg 2015). We readily obtained *ptk* null mutants in the AB5075 strain and sequencing of the *bfmRS* locus in four independent *ptk* deletion strains did not reveal any changes from the wild type *bfmRS* sequence, although we cannot exclude that these strains have not acquired other suppressor mutations. Additional observations from both the Shuman lab and others demonstrate that *A. baumannii* strains harboring deletions of the BfmS sensor kinase generate excess polysaccharides (data not shown and Geisinger and Isberg 2015), suggests that the BfmRS two component system may modulate capsule production. Based on this observation, we speculate that BfmS may act as a phosphatase for BfmR, and loss of BfmS leads to increased BfmR-P, which in turn activates capsule production.

As capsular polysaccharides are commonly associated with protection from host defenses and antibiotics, and because *G. mellonella* produces antimicrobial peptides in response to bacterial infection, we originally hypothesized that the increased capsule production in the *bfmS* mutant may confer protection from the insect defenses. On the contrary, we observed that *bfmS* null strains were defective for growth/persistence in *G. mellonella* (Figure 2.6). An additional interesting finding is presented in Figure 2.11, where I demonstrated that loss of *bfmS* in the AB5075 background led to increased biofilm production. This finding is in contrast to the situation observed in the 17978 strain background where loss of *bfmS* decreases biofilm formation, a finding consistent with previous reports for the 17978 strain (Liou et al. 2013). For the cognate response regulator, *bfmR*, we were unsuccessful in obtaining a deletion strain in the AB5075 background and strains harboring a transposon insertion in this gene appear to have a growth defect. In light of these observations, I propose that the *bfmRS* two component system functions in a broader role, beyond only mediating biofilm formation. I also propose that the

BfmRS regulon does not fully overlap in terms of the genes under control of this TCS across different *A. baumannii* strains, as evidenced by the differential requirement of the *bfmR* gene for strain viability (essential in AB5075, dispensable in 17978) and also the discordant consequences resulting from loss of *bfmS* in regards to biofilm formation.

Wang, *et al*. recently published results investigating the genetic requirements of *A. baumannii* to persist in a murine pneumonia model (Wang et al. 2014). Despite the use of different strains (Wang and colleagues used strain ATCC 17978) and model systems, the two studies did identify many of the same genes. For instance, both experiments identified known virulence factors for *A. baumannii*, including zinc and iron acquisition systems, capsule and LPS biosynthesis genes, amino acid metabolism and acquisition genes, and the *bfmRS* two-component system (Wang et al. 2014). The correlation between the present study and the Wang study, which used a mammalian infection model, demonstrates the utility of the *G. mellonella* system for studying *A. baumannii* infection. Beyond these similarities, however, the work described herein, as discussed below, identified additional virulence genes that were not previously identified.

When we looked more closely at the genes involved with amino acid biosynthesis, we observed that many genes involved with the cysteine metabolism/sulfur assimilation pathway were required for *A. baumannii* to grow in *Galleria.* This pathway is well conserved across bacterial species (Kessler 2006) and aside from generating cysteine for protein synthesis, the sulfur assimilation pathway appears to prevent damage due to oxidative stress, possibly by maintaining a reducing environment inside the cell (Turnbull and Surette 2010). As oxidative stress is a widely conserved pathogen restriction factor, we hypothesize this pathway may be involved in oxidative stress resistance of *A. baumannii*. Interestingly, when we interrogated the data from Wang and colleagues, we observed that several genes in the cysteine/sulfur

assimilation were also required for persistence in the murine pneumonia model, even though the authors did not comment on these genes (Wang et al. 2014). The correlation between the two studies further emphasizes the importance of the cysteine/sulfur pathway for *A. baumannii* virulence. As the sulfur assimilation pathway has recently attracted renewed interest as a target for novel antimicrobial therapeutics (reviewed in Campanini et al. 2015), it will be important to investigate whether pharmacologic perturbation of this pathway represents a viable strategy to treat *A. baumannii* infection.

Our experiment also identified many genes involved with transcriptional regulation (n = 32), which is significant because one of the key differences distinguishing *A. baumannii* from the closely related but non-pathogenic *A. baylyi* is the presence of transcription regulatory genes. Indeed, Adams and colleagues recently found that one major difference between *A. baylyi* and *A. baumannii* is the presence of substantially more transcriptional regulators in *A. baumannii* (~10% of the pan-*A. baumannii* genes) (Adams et al. 2008). The authors of this study concluded that these transcriptional regulators may control genes allowing *A. baumannii* to be a human pathogen. Of the 32 regulator genes identified in this study, half of the genes do not have an ortholog in *A. baylyi*, supporting the conclusions of the aforementioned study. Future studies to define genes controlled by the transcriptional regulators identified in our screen will likely highlight the key regulatory networks involved with how *A. baumannii* senses and responds to the host environment.

Interestingly, several of the genes required for growth in *Galleria* identified in our screen also show a defect for growth in sub-inhibitory concentrations of various antibiotics (Figure 2.12, Table 2.4). The functions of genes required for surviving both within *Galleria* and during environmental and/or antibiotic stress encompass signal transduction, transcriptional regulation

and genes predicted to play a role in stress survival. We thus conclude that the stresses imposed upon *A. baumannii* during infection overlap with those faced by bacteria during exposure to antibiotics and other environmental stressors. Antibiotics mediate cell killing through a variety of mechanisms. We have also demonstrated that strains harboring deletions of specific transcriptional regulators required for virulence in the *Galleria* display increased antibiotic sensitivity. As such, we infer that these regulators may also control genes required for detoxification of stress or for alteration of cell/envelope permeability - a property that could impact sensitivity to both antimicrobial peptides and antibiotics. We further propose that selection for increased survival to environmental stresses, such as clinical disinfectant strategies, antimicrobial compounds, etc., inadvertently selects for strains displaying a hyper-virulent phenotype and may in fact select for MDR in clinical settings. This hypothesis is supported by work from Geisinger & Isberg, where they observe increased virulence after exposure to sub-lethal levels of antibiotics (Geisinger and Isberg 2015), and Roux, et al., who recently reported loss of virulence in antibiotic-sensitive bacterial mutants (Roux et al. 2015). The coming chapters will focus on further characterization of several transcriptional regulators described herein.

CHAPTER III

Characterization of GigA and GigB. Master Regulators of a Global Stress Response in *Acinetobacter baumannii*

This chapter is adapted from a version of the forthcoming manuscript 'GigA and GigB are Master Regulators of Antibiotic Resistance, Stress Responses and Virulence in *Acinetobacter baumannii*' which has been submitted for publication. The authors on this manuscript are Michael J. Gebhardt and Howard A. Shuman. M.J.G. performed all experiments presented in this chapter.

INTRODUCTION

Many opportunistic pathogens arise as nutritionally versatile soil organisms that are environmentally resilient. Two examples of such opportunistic pathogens include the phylogenetically related gram-negative organisms *Pseudomonas aeruginosa* and *Acinetobacter baumannii*, both of which can utilize a variety of carbon and nitrogen sources and survive harsh environmental conditions, including the clinical healthcare setting and the hostile environment encountered inside a human host (Antunes, Visca, and Towner 2014, Gellatly and Hancock 2013). Environmental resistance itself can be broken down into the ability to survive a variety of physical and chemical insults, such as changes in pH, temperature and osmolarity. As soil organisms, these bacteria must also compete for limited nutritional resources and survive exposure to antibiotics produced by other soil microbes. This competition has likely shaped the

evolution of *A. baumannii* and *P. aeruginosa* such that both organisms are nutritionally versatile and resistant to environmental challenges.

However, unlike other pathogens, such as *Staphylococcus aureus*, which possesses a large collection of host-adapted virulence factors that promote both colonization of human skin and serious invasive disease, or *Salmonella* species, which elaborate secretion systems dedicated to the delivery of toxins and other effector proteins directly into host cells, *A. baumannii* lacks well conserved host-specific virulence factors (Becker and Bubeck Wardenburg 2015, Dietsche et al. 2016). Indeed, many virulence factors harbored by *A. baumannii* can be viewed as survival factors as opposed to *bona fide* host-adapted virulence factors. For example, the polysaccharide capsule, one of the most important virulence factors expressed by *A. baumannii*, likely serves as a means of protection from environmental insults (Geisinger and Isberg 2015, Gibson et al. 2006, Wu et al. 2014, Withman et al. 2013), including protection from protist grazing, which is not dissimilar from avoiding phagocytosis by human immune cells. Other virulence factors, such as the acinetobactin siderophore and the ZnuABC zinc acquisition system, are required for virulence in infection models and are also likely to be important for acquiring nutrients in soil to compete for limited resources (Hood et al. 2012, Mihara et al. 2004).

While antibiotic therapy for bacterial infections represents one of the greatest medical advances in the history of mankind, bacterial pathogens have not disappeared, and moreover, many have acquired resistance to nearly every therapeutically useful antibiotic (Boucher et al. 2009). The continued and expanding emergence of bacterial pathogens harboring multiple antibiotic resistances (i.e. the 'MDR' phenotype) represents a serious threat to effective health care (Hwang and Gums 2016). *A. baumannii* is no different, as many clinical isolates now present with the MDR phenotype (Huttner et al. 2013). While considerable effort has been

directed towards understanding the nature of horizontally acquired resistance mechanisms (reviewed in Wong et al. 2017), perhaps a less appreciated factor is the intrinsic antibiotic resistance harbored by *A. baumannii*. Intrinsic antibiotic resistance can be defined as the sum of those mechanisms that are not acquired via recent horizontal gene transfer events. As mentioned in previous chapters, one contributor to intrinsic antibiotic resistance includes the presence of chromosomally encoded antibiotic resistance genes, such as genes conferring resistance to β-lactam antibiotics (*ampC*) and chloramphenicol (*cat*), which are present in many *A. baumannii* genomes (Rodriguez-Martinez, Poirel, and Nordmann 2010). Additionally, *A. baumannii* harbors a large number of antimicrobial efflux pumps and exhibit low outer membrane permeability, both of which contribute to decreased antibiotic sensitivity (Damier-Piolle et al. 2008, Yoon, Courvalin, and Grillot-Courvalin 2013, Sugawara and Nikaido 2012). Given the relative poor characterization of transcriptional regulatory networks in *A. baumannii*, it is also not surprising that the mechanisms for coordinating the intrinsic antibiotic resistance phenotype remain poorly understood and are likely complex.

In the preceding chapter, I described the results of a Transposon Insertion Sequencing (TnSeq) experiment that led to the discovery of 300 genes required for the growth and/or survival of *Acinetobacter baumannii* within the larval cavity of the wax moth, *Galleria mellonella*. Follow up studies on a subset of these genes identified a previously unappreciated link between virulence in the *Galleria* model and antibiotic resistance. These findings served as the basis for the work described below, where I present results from experiments focused on the characterization of two of the genes identified in the TnSeq experiment. An in depth characterization of these two genes, *gigA* and *gigB* (for Growth in *Galleria*), revealed that, in addition to being required for virulence in the *Galleria* model and the characteristic multi-drug

resistant (MDR) phenotype of a contemporary *A. baumannii* isolate, AB5075, strains lacking *gigA* and/or *gigB* also display decreased resistance to several *in vitro* stress conditions.

The genetic context of and protein domains encoded by the *gigA* and *gigB* genes suggest that they comprise upstream components of a novel signal transduction pathway. I show that GigA, a non-canonical two-component system (TCS) response regulator (RR) harboring a PP2C protein phosphatase domain, dephosphorylates phospho-GigB, a predicted anti-sigma factor antagonist protein. Additional genetic experiments establish a link between GigA/GigB and the Nitrogen Phosphotransferase system (PTS^{Ntr}). In other organisms, the PTS^{Ntr} has long been considered a system that monitors intracellular nitrogen levels and coordinately regulates metabolism in conjunction with the carbohydrate PTS system (Jahn et al. 2013, Pfluger and de Lorenzo 2008, Goodwin and Gage 2014). However, recent work by others implies expanding roles for the PTS^{Ntr} outside of central metabolism; these include the regulation of biofilm formation in *Pseudomonas* and stress responses in *E. coli* (Lee et al. 2015, Cabeen, Leiman, and Losick 2016, Godino, Príncipe, and Fischer 2016). I report here that loss of the PTS^{Ntr} components in *A. baumannii* suppresses all of the known phenotypes associated with the *gigA* and *gigB* mutant strains. Interestingly, it appears that all species within the *Acinetobacter* genus harbor an incomplete PTS^{Ntr}, lacking an Enzyme IIA ($EIIA^{Ntr}$) homolog, the usual terminal phospho-acceptor protein. These results suggest that the PTS^{Ntr} in *Acinetobacter* has been repurposed to participate in this newly described stress response and I present *in vitro* evidence for direct phosphate transfer from phosphoenolpyruvate (PEP) to GigB via the PTS^{Ntr}. Based on these data, I propose that the small phospho-carrier protein, NPr, functions as an anti-sigma factor to regulate the sigma factor RpoE (σ^E).

Taken together, the data presented below are consistent with a model in which stress signals transmitted through GigA/GigB inactivate NPr, thus relieving the inhibition of a sigma factor, RpoE (σ^E), and ultimately lead to the transcription of a large number of stress response genes. I propose that integration of signaling through GigA and GigB with the metabolic surveillance mediated by the PTS^{Ntr} allows *A. baumannii* to modulate the transcriptional landscape under a wide range of environmental conditions. This work highlights how GigA and GigB function as a signal transduction module across a variety of environmental conditions and confers *A. baumannii* with two emergent properties that are essential for its success as a human pathogen; virulence and intrinsic antibiotic resistance.

RESULTS

As discussed in the previous chapter, the *gigA* and *gigB* genes (locus tags ABUW_3260 and ABUW_3261, respectively) are required for both virulence and antibiotic resistance of *A. baumannii* (Gebhardt et al. 2015). The two genes are found sequentially on the *A. baumannii* AB5075 chromosome (Figure 3.1) and demonstrate high sequence conservation across *A. baumannii* isolates (Figure 3.2). The GigA protein contains an N-terminal TCS Receiver domain and, unlike canonical TCS Response Regulators, harbors a PP2C protein phosphatase domain in the C-terminus. The GigB protein contains a Sulfate Transport and Anti-Sigma Factor Antagonist (STAS) domain. In several other bacterial species, TCS response regulators (TCS-RR) harboring PP2C phosphatase domains and STAS domain-containing anti-anti-sigma factors function together to regulate the activity of anti-sigma factors, effectively functioning to activate alternative sigma factors (Yang et al. 1996, Sharma, Rigby, and Alper 2011, Thompson et al. 2015, Morris and Visick 2013, Bouillet et al. 2016). The *Bacillus subtilis* Sigma B (σ^B)

regulatory system represents a well-characterized example of such a signal transduction pathway. In this system, the anti-sigma factor RsbW binds to and inactivates σ^B. During periods of stress, signals are transmitted to and activate RsbU, a TCS-RR harboring a PP2C domain. Upon activation, RsbU dephosphorylates RsbV, a STAS domain protein. Unphosphorylated RsbV performs a partner-switch with RsbW and σ^B. This sequesters RsbW, allowing σ^B to transcribe stress response genes. To reset the system, RsbW possesses kinase activity towards RsbV, eliminating the RsbV-RsbW interaction, which allows RsbW to bind and inhibit σ^B (Kuo et al. 2004). In contrast to these systems, I was unable to identify proteins sharing homology with RsbW in *A. baumannii*, suggesting a novel interaction partner for the GigA/GigB signaling axis and a different mechanism of regulation.

GigA and GigB are required for *in vitro* stress resistance

In order to understand how the GigA and GigB proteins contribute to intrinsic antibiotic resistance and virulence in *A. baumannii*, I subjected strains harboring in-frame deletions of the *gigA* and *gigB* genes to a variety of *in vitro* stress conditions. Consistent with previous observations, strains lacking GigA (Δ*gigA*) or GigB (Δ*gigB*), or both GigA and GigB (Δ*gigAB*), show sensitivity to aminoglycoside antibiotics, including kanamycin and gentamicin (Figure 3.3 A). The wild-type AB5075 strain is kanamycin resistant and exhibits an efficiency of plating of 0.1-0.5 on LB agar plates containing 500 μg/ml kanamycin. In contrast, the *gig* mutant strains exhibit plating efficiencies of 100 to 1000-fold lower than the wild type strain. In addition to the direct plating defect on solid medium containing added aminoglycosides, the sensitivity of *gig* mutants to aminoglycosides is also observed as an increased lag time (see Grosser et al. 2016) relative to wild type AB5075 when grown in LB containing added kanamycin (Figure 3.3 B, C).

Further testing revealed that the eventual growth the Δ*gigA* and Δ*gigB* mutants seen in Figure 3.3 panel B in the presence of kanamycin results from the emergence of strains harboring suppressing mutations, as colonies grown from these cultures no longer displayed an increased lag time (Figure 3.4).

In addition to aminoglycoside sensitivity, I also observed decreased plating efficiency when the Δ*gigA* or Δ*gigB* strains are cultured on media adjusted to pH 5.5 or at pH 7.0 containing the added heavy metal ion zinc (Zn^{2+}, supplied as 1.25 mM $ZnCl_2$) (Figure 3.3 A). Further, *gig* mutants show a pronounced small-colony phenotype when grown at 50 ˚C on LB agar plates compared to WT AB5075, although a loss of colony forming units under this growth condition is not observed (Figure 3.3 D). Similar *in vitro* phenotypes were observed in the strain lacking both *gigA* and *gigB* (Δ*gigAB*). Complementation studies reveal that in the Δ*gigAB* mutant, expression of either *gigA* or *gigB* alone fails to restore wild type resistance to kanamycin, while concurrent expression of both *gigA* and *gigB* restores the strain to wild type kanamycin resistance (Figure 3.3 E).

GigA is a non-canonical Two Component Response Regulator

To gain insight into the function of GigA, I searched for similar proteins from related bacteria. *Pseudomonas aeruginosa* encodes one of the most closely related, non-*Acinetobacter* homologs to the *gigA* gene. This *P. aeruginosa* gene, PA2798, is also annotated as a TCS-RR harboring a C-terminal PP2C domain. In order to compare GigA to the PA2798 protein, I performed a protein alignment (Figure 3.5) using the Clustal Omega program (Sievers and Higgins 2014) and also used the Phyre2 server (Figure 3.6), which generates a three dimensional structural model based on similar proteins with known structures (Kelley et al. 2015). Comparing

the amino acid sequence and predicted domain organization of PA2798 with that of GigA identifies a few distinct differences. In the three dimensional structure of PA2798 (3EQ2, www.pdb.org), a coiled-coil region connects the N-terminal REC domain with the C-terminal PP2C domain spanning 57 residues from Leucine-111 to Leucine-167 (Figure 3.5). The corresponding GigA region encompasses only 37 amino acids, spanning from Asparagine-83 to Leucine-119. The alignment also reveals that the GigA REC domain, at 78 amino acids in length, is shorter than the REC domain of PA2798, which contains 111 residues. Despite the apparent truncation in the GigA REC domain, the predicted phospho-accepting aspartic acid residue (Asp-56 in PA27978; Asp-32 in GigA) appears to be conserved in GigA (Figures 3.5, 3.6). Aside from these differences, the PA27978 structure shows three residues, Asp-210, Gly-213 and Asp-382, as coordinating an Mg^{2+} ion, which are conserved in the GigA sequence and correspond to residues Asp-162, Gly-165, and Asp-311 in GigA (Figures 3.5, 3.6).

As shown in Figures 3.5 and 3.6, the GigA-REC domain appears truncated. In light of this observation, I wanted to determine if the predicted phosphoryl-accepting aspartic acid residue in the GigA-REC domain (Asp-32) is required for GigA activity. To do so, I generated alleles of GigA with mutations predicted to mimic the phosphorylated (Aspartic acid-32 to Glutamic acid, D32E) and non-phosphorylated (Aspartic acid-32 to Alanine, D32A) states. Studies comparing the kanamycin plating efficiency of the Δ*gigA* strain expressing wild type *gigA*, $GigA^{D32E}$ or $GigA^{D32A}$ *in trans*, showed that all three GigA alleles restored kanamycin resistance (Figure 3.7), suggesting that Asp-32 is not critical for GigA functionality. This finding also suggests that the GigA-REC domain does not require phosphorylation for its activity. As such, it is possible that the REC domain serves only a structural role, rather than regulating GigA phosphatase activity. Such a scenario has been reported for the SprE/RssB protein in *E. coli*,

where mutation of the phosphoryl-accepting aspartate residue (Asp-58) does not alter protein activity (Peterson, Ruiz, and Silhavy 2004). Another potential explanation is that the predicted GigA residue (Asp-32) is not the phosphoryl-accepting residue. Indeed, alignment of GigA with PA2798 reveals that several additional aspartate residues (residues 29, 30 and 35) are in close proximity - in terms of the primary GigA sequence - to Asp-32 (Figure 3.5).

Determination of the GigB Translation Start Site

The annotated gene sequence for the *gigB* gene predicts that the start codon is a GTG codon, which can be used by bacteria as an alternative to the more commonly used ATG codon. As an example, the first publication describing the genome sequence for *Esherichia coli* reported that about 15% of *E. coli* genes were initiated with a GTG start codon instead of the ATG codon (Blattner et al. 1997). Inspection of the AB5075 genome revealed that GTG is predicted to serve as the start codon for ~5.5% of the annotated genes. In regards to translation efficiency, Reddy and colleagues reported, again for *E. coli*, the translation efficiency varies based on the initiating codon, with GTG being approximately one half to one third as efficient as the ATG codon (Reddy, Peterkofsky, and McKenney 1985). Close inspection of the *gigB* gene sequence revealed the presence of a second potential start codon, ATG, 39 nucleotides downstream from the annotated start codon. An alignment of the *A. baumannii* AB5075 *gigB* with a homologous gene found in *P. aeruginosa* strain PAO1 (locus tag PA2797) shows better alignment using the downstream translation initiation site (Figure 3.5). Comparison of the *gigB* orthologs in other *A. baumannii* genomes reveals that several genomes predict that the start codon is downstream ATG, rather than the GTG annotated in the AB5075 genome assembly. Of note, however, is that

both codons are conserved across several *A. baumannii* genomes, raising the question of which start codon is used by *A. baumannii* to initiate translation of the GigB protein.

In order to determine which start codon is used to initiate translation of the GigB protein, I generated GigB-LacZ translational fusions in the vector pMJG129. This vector is derived from the translational fusion vector pGS-lac-02 (Gal-Mor, Zusman, and Segal 2002). The plasmid harbors a derivative of the *lacZ* gene that lacks a promoter to drive transcription of the gene, a ribosomal binding site for protein translation (Shine-Dalgarno Sequence) and also lacks a suitable start codon. By cloning DNA of interest into a BamHI restriction endonuclease restriction site located 5' to this promoter-less *lacZ* gene, both transcription and translation initiation can be assessed. I generated four constructs to analyze the GigB translation start site. Each test plasmid contained the final 343 nucleotides of the *gigA* gene, which ends 63 nucleotides upstream of the GTG start codon. The 3' end of each of construct varied, but upon ligation into the pMJG129 plasmid, all four constructs generate an in frame translational fusion with the *lacZ* gene. A map of plasmid pMJG129 and depictions of the various constructs used to assess GigB translation initiation are depicted in Figure 3.8. The $GigB_{GTG}$ construct includes the *gigB* promoter region and the fusion to *lacZ* occurs immediately following the annotated GTG start codon. The second pair of constructs are designed to assess translation initiation from the downstream ATG, with one construct containing the WT *gigB* sequence up to the ATG codon ($GigB_{GTG\text{-}ATG}$), while the other construct contains a T to A mutation of the GTG codon (resulting in GAG) in addition to the second ATG sequence ($GigB_{GAG\text{-}ATG}$). Finally, a fourth construct contains an extended translation product, encoding the first 53 amino acids (starting from the GTG codon) before the fusion to *lacZ* ($GigB_{1\text{-}53}$). Translation initiation from these various plasmids was assessed in wild type AB5075 using the Miller Assay for measuring β-

galactosidase (β-Gal) activity (Miller 1972). As shown in Figure 3.8, strain AB5075 harboring the empty vector, pMJG129, did not produce measurable β-Gal activity. Additionally, AB5075 harboring the $GigB_{GTG}$ construct also produced undetectable levels of β-Gal. The three other constructs gave rise to significantly higher levels of β-Gal. The $GigB_{GAG-ATG}$ construct consistently generated higher levels of β-Gal than the $GigB_{GTG-ATG}$ construct, while the $GigB_{1-53}$ construct produced roughly 10-fold less β-Gal activity than strains harboring $GigB_{GTG-ATG}$ (Figure 3.8).

Taken together, these data suggest that the GTG codon is not used as a translation start site, at least under the growth conditions examined (i.e. cells growing exponentially in LB medium. An important additional construct required to strengthen these conclusions includes testing a reporter construct where the GTG start codon is present, but the downstream ATG codon is mutated such that it no longer encodes for methionine. For example, the ATG codon could be changed to ATT, which would encode an isoleucine residue. Assuming that the GTG is not used as a translation initiation codon, this construct would be predicted to yield little to no β-Gal activity. One interesting observation obtained from these studies was that the $GigB_{1-53}$ construct produced less activity measured relative to the GTG-ATG construct (Figure 3.8). This finding suggests that there could be additional regulation of the transcription and/or translation of the *gigB* gene.

Interestingly, as discussed below, the GigB protein is undetectable during exponential growth via western blot (Figure 3.11). This finding does not correlate with the high levels of β-Gal measured from $GigB_{GTG-ATG}$ construct, which produces very high levels of β-Gal activity (Figure 3.8). One interpretation of these disparate observations is that post-transcriptional or post-translational regulatory events maintain low levels of GigB during exponential growth. For

example, the GigB protein could have an inherently short half-life that is mediated by sequences downstream of the ATG codon. Alternatively it is possible that the translation initiation codon could vary based on changes in the environment, which has been described before for an alternative sigma factor (σ^R) in *Streptomyces coelicolor* (Kim et al. 2009). In light of these possibilities, additional studies using the pMJG129 constructs should be assessed under a variety of environmental and physiological conditions.

GigB Is Phosphorylated *in vivo*

The *gigB* gene also has a closely related homolog in *Pseudomas aeruginosa*. The PA2797 gene encodes a STAS domain protein sharing 38% identity with the *A. baumannii gigB* gene (Figure 3.5). In other bacterial species, STAS domain proteins are regulated by phosphorylation of a serine residue within a characteristic 'DSSG' motif, with the first serine residue being the site of phosphorylation (Thompson and Visick 2015). In GigB, this motif is D_{58}-S_{59}-T_{60}-V_{61} (using the ATG codon as residue 1), and Mass Spectroscopic analysis of a functional GigB variant harboring a C-terminal 6X-Histidine tag identified peptide fragments consistent with both phosphorylated and non-phosphorylated serine residues at residue 59 (Figure 3.9). To confirm the presence of both phosphorylated GigB (GigB–P) and non-phosphorylated GigB, I utilized the Phos-tag™ gel system, which allows for detection of non-phosphorylated and phosphorylated forms of a given protein based on decreased migration of the phosphorylated species (Kinoshita et al. 2006). Western blot analysis of whole cell lysates separated by Phos-tag™ SDS-PAGE revealed the presence of two discrete bands recognized by anti-GigB antibodies, consistent with the presence of both GigB and GigB–P *in vivo* (Figure 3.9). The higher mobility band at ~18 kDa migrates near the predicted molecular weight of GigB (~18.4 kDa), while the lower mobility

band migrates near 25 kDa. Interestingly, I also observe a similar migration pattern following purification of recombinant 6X-His-GigB from *E. coli.* The recombinant GigB protein migrates as a single band when separated by standard SDS-PAGE; however, two distinct bands are visible when the sample is electrophoresed through SDS-PAGE containing Phos-tag^{TM} acrylamide (Figure 3.10). Western blot analysis further revealed that both bands visible by Coomassie Blue staining were also recognized by GigB antibodies (Figure 3.10). This finding suggests that GigB is phosphorylated when expressed in *E. coli*. Further evidence supporting the phosphorylation of Ser-59 is that the lower mobility GigB species, *i.e.* GigB–P, is not observed upon mutation of Serine 59 to either an alanine or an aspartic acid (Figure 3.9).

To assess the requirement of phosphorylation at Serine-59 for GigB function, I generated a series of complementing plasmids harboring variants of the *gigB* gene that are either predicted to mimic the phosphorylated state (Serine-59 to Aspartic Acid) or encodes a form that cannot be phosphorylated (Serine-59 to Alanine). As shown in Figure 3.7, complementation experiments using either mutant allele revealed that neither restored the kanamycin resistance of a Δ*gigB* strain to wild type levels. These results suggest that turnover of serine-phosphorylation is required for proper GigB function. An alternative explanation is that the mutated alleles are unstable or not expressed. While I cannot fully eliminate this possibility, western blot analysis suggests the mutant GigB proteins are produced at levels indistinguishable from the wild type protein (Figure 3.9).

GigA Functions as a GigB Phosphatase

As mentioned above, STAS domain anti-anti-sigma factors are typically regulated by PP2C-domain containing protein phosphatases (Pane-Farre, Lewis, and Stulke 2005). Attempts

to visualize GigB via western blot analysis in whole cell lysates prepared from wild type AB5075 were unsuccessful in the absence of expression of GigB *in trans* on a multi-copy plasmid (see the left-most lane in Figure 3.11 Panel A). Interestingly, in strain backgrounds lacking the *gigA* gene, GigB–P is readily detected and reintroduction of the *gigA* gene at the Tn7 locus eliminates the appearance of the GigB–P (Figure 3.11 Panel B). From these results, I conclude that GigA acts as a phosphatase of GigB–P. As a means of testing whether the GigB/GigB–P ratio changes during an imposed stress, I also exposed wild type AB5075, Δ*gigA* and the Δ*gigA*-complemented strains to 500 μg/mL kanamycin. This concentration of kanamycin decreases the growth rate, but does not completely inhibit growth (Figure 3.11 D). Analysis of the kanamycin-exposed samples via Phos-tag™ SDS-PAGE and western blotting did not reveal changes in the ratio of GigB/GigB–P (Figure 3.11). One potential explanation for this result is that the GigB/GigB–P switch mediated by GigA could be a transient phenomenon and thus not observable at the time point used for these experiments (30 minutes post kanamycin exposure).

As several attempts to purify recombinant GigA from *E. coli* were unsuccessful, I have been unable to directly assess GigA phosphatase activity *in vitro*. As an alternative approach, I hypothesized that GigA phosphatase activity could be assessed by co-expression of both GigA and GigB in a heterologous host. To do so, I transformed *E. coli* BL21(DE) with a plasmid harboring an allele of *gigA* with a C-terminal Strep-tag (WSHPQFEK) and a second, compatible plasmid containing a C-terminal 6xHistidine tag of either wild-type *gigB* or the Serine to Alanine (S59A) allele of *gigB*. Western blot analysis of whole cell lysates from these strains demonstrated that in the presence of GigA, GigB–P was not observed (Figure 3.11 Panel C). These results suggest that GigA is either constitutively active or is activated by an additional

factor(s) present inside *E. coli* and support the conclusion that GigB–P is directly targeted by GigA.

Mutations in Nitrogen Phosphotransferase genes suppress the phenotypes of *gigA* and *gigB* mutants

In order to identify additional components of the GigA/GigB signaling axis, I sought suppressors that restore kanamycin resistance in the Δ*gigB* strain. Suppressor mutations in the Δ*gigB* strain background were isolated by plating overnight cultures of a Δ*gigB* strain onto LB plates containing 500 μg/mL kanamycin. Following purification of kanamycin resistant (Km^R) colonies on non-selective LB agar plates, I isolated 7 clones that demonstrated a restored resistance to kanamycin (Figure 3.12). Whole-genome sequencing of these seven Km^R clones revealed that six of the seven strains harbored mutations in the *ptsP* gene (locus tag ABUW_3468), which is predicted to encode the Enzyme I component (EI^{Ntr}) of the Nitrogen Phosphotransferase system (PTS^{Ntr}). Deletion of the entire *ptsP*/ABUW_3468 open reading frame in the Δ*gigB* background also restored kanamycin resistance to wild-type levels, confirming that loss of *ptsP* is sufficient for the Km^R phenotype observed in the suppressing clones (Figure 3.13). An alternative explanation for the Km^R phenotype in the Δ*gigB ptsP*-null background is that loss of *ptsP* functions as a by-pass mutation; leading to kanamycin resistance independently of *gigB*. If loss of *ptsP* does in fact function as a by-pass mutation, one would predict that the other 'Gig'-related phenotypes would persist in the Δ*gigB* Δ*ptsP* strain. However, when I examined additional Gig phenotypes, the Δ*gigB* Δ*ptsP* strain also demonstrates wild type levels of resistance to acidic pH, exposure to exogenous zinc, and colony size at 50 ˚C (Figure 3.13). Taken together, these results make it unlikely that loss of the *ptsP* gene bypasses the

requirement of *gigB* for kanamycin resistance and support the idea that EI^{Ntr}, or a related protein, participates in opposing the activity of GigA/B.

To further explore the role of *ptsP* in the GigA/GigB pathway, I also created strains harboring in-frame deletions of the *ptsP* coding sequence in both wild-type AB5075 and the Δ*gigA* strain. These experiments also revealed that loss of *ptsP* in the Δ*gigA* background suppressed the Gig phenotypes to near wild type levels, while a nominal effect was observed in the wild type strain background harboring the Δ*ptsP* deletion alone (Figure 3.13). Furthermore, loss of the *ptsP* gene in either the Δ*gigA* or Δ*gigB* strain backgrounds restored growth in *Galleria* larvae (Figure 3.13).

The PTS^{Ntr} system acts negatively downstream of GigA and GigB

Because loss of EI^{Ntr} resulted in suppression of *gig* mutant phenotypes, I further examined the AB5075 genome for additional phosphotransferase system (PTS) components. Interrogation of several databases, including STRING (www.string-db.org), KEGG (http://www.genome.jp/kegg) and BIOCYC (https://biocyc.org), identified only 4 genes predicted to encode PTS proteins (Table 3.1). These genes include *fruA* and *fruB*, which together encode a carbohydrate-specific PTS system; the aforementioned *ptsP* gene, encoding the EI^{Ntr} protein; and *ptsO*, encoding the small phospho-carrier protein NPr, the second component of the Nitrogen PTS (PTS^{Ntr}). In many other bacterial species, the PTS^{Ntr} contains a third protein, Enzyme IIA ($EIIA^{Ntr}$), encoded by the *ptsN* gene. A clear homolog for *ptsN*/$EIIA^{Ntr}$ is lacking in *A. baumannii*. Expanding the analysis to closely related organisms revealed that a *ptsN*-related gene is not only absent from *Acinetobacter baumannii*, but is absent from the entire *Moraxellaceae* family (Figure 3.14).

Due to the absence of the *ptsN* gene in *A. baumannii*, I hypothesized that the PTS^{Ntr} has been repurposed in this organism and considered other potential functions for the PTS^{Ntr}. First, I sought to determine if suppression of Gig phenotypes by removal of EI^{Ntr} was a direct result of missing the EI^{Ntr} protein in particular, or if suppression was due to a loss of phosphoryl transfer to the NPr protein. To assess the role played by the *ptsO* gene product, NPr, in suppressing the phenotype of the *gigA* and *gigB* mutants, I first constructed an in-frame deletion of the *ptsO* coding sequence in wild-type AB5075, Δ*gigA* and Δ*gigB*. The *ptsO* gene (locus tag ABUW_3293) appears to be part of a poly-cistronic message, as the stop codon of the gene immediately 5' to *ptsO* (ABUW_3294) overlaps with the initiating ATG codon of the *ptsO* coding sequence and the start codon for the gene immediately 3' to *ptsO* (ABUW_3292) lies only two nucleotides downstream of the *ptsO* stop codon. In order to construct a Δ*ptsO* strain, we designed a deletion cassette, which, after removal through homologous recombination, leaves behind a small, 27 nucleotide open reading frame comprising the first and last four codons and stop codon of the *ptsO* coding sequence (Figure 3.14). This architecture should maintain the open reading frames for the genes immediately upstream and downstream of *ptsO*.

Upon testing the *ptsO* deletion strains, I observed restoration of the Gig phenotypes to wild type levels in either the Δ*gigA* or Δ*gigB* backgrounds, with no change in the kanamycin phenotype for strain AB5075 Δ*ptsO* (Figure 3.13). Interestingly, when grown at 50˚C, the AB5075 Δ*ptsO* strain exhibited an approximate 100-fold reduction in colony forming units relative to wild-type AB5075 (Figure 3.13). Similarly, a ~10-fold plating defect is observed when plating the AB5075 Δ*ptsO* strain on LB agar containing 1.25 mM $ZnCl_2$ (Figure 3.13). Finally, loss of the PTS^{Ntr} proteins in either the *gigA* or *gigB* null background restores growth in *G. mellonella* while the corresponding mutations (Δ*ptsP* or Δ*ptsO*) in the wild-type AB5075

background have little effect on the ability of the bacteria to grow within the insect larvae (Figure 3.13). From these data, I conclude that the suppressing phenotype of losing the PTS^{Ntr} in the Δ*gigA*/Δ*gigB* backgrounds is consistent with the hypothesis that NPr acts in a negative fashion and downstream of GigA and GigB.

A. baumannii PTS^{Ntr} Proteins Mediate Phospho-Transfer to GigB

In other bacterial species, the PTS^{Ntr} proteins mediate phosphate transfer from phosphoenolpyruvate (PEP) to $EIIA^{Ntr}$ via a two-step transfer between EI^{Ntr} and NPr (Rabus et al. 1999, Powell et al. 1995). Given the genetic connection between GigA/GigB and the absence of an $EIIA^{Ntr}$ homolog in *A. baumannii,* I hypothesized that phosphorylated NPr (NPr–P) may instead transfer a phosphate group to GigB. In order to assess phospho-transfer from NPr–P to GigB, I purified recombinant forms of the *A. baumannii* AB5075 EI^{Ntr} and NPr proteins from *E. coli* and performed *in vitro* phospho-transfer assays. To visualize the phosphorylation states of the various proteins, I utilized the Phos-tag™ gel system. As shown in Figure 3.15, I was able to recapitulate phospho-transfer from PEP to NPr through EI^{Ntr} *in vitro* with purified components. When recombinant GigB protein (purified from *E. coli* cells co-expressing GigA to eliminate GigB–P, see Figure 3.11) was included in the PEP/PTS^{Ntr} phospho-transfer reaction, I observed the formation of GigB–P bands only when PEP is included in the reaction containing EI^{Ntr}, NPr and GigB (Figure 3.15). Additionally, I observed that GigB–P formed across a wide range of PEP concentrations. Importantly, GigB–P did not form in the absence of any single component. From this observation, I conclude that NPr–P mediates phosphate transfer to GigB.

Over-expression of NPr induces a 'Gig' phenotype

Given the genetic and biochemical interactions described above, I propose that GigA and GigB act positively and functionally oppose the PTS^{Ntr} proteins, as evidenced by the requirement of GigA and GigB for stress resistance. The evidence presented above further indicates that EI^{Ntr} and NPr antagonize the activity of the GigA/GigB axis such that in the absence of GigA/GigB, concurrent loss of either PTS^{Ntr} protein restores stress resistance. A strong prediction of this model is that increased expression of the PTS^{Ntr} components will induce a Gig phenotype in an otherwise wild type genetic background. To test this prediction, I compared the response of wild type AB5075 harboring the empty vector, pMJG120, to bacteria containing a plasmid-borne copy of the *ptsO* gene controlled by an IPTG-inducible promoter (pMJG120.*ptsO*), under *in vitro* stress conditions (exposure to 500 µg/mL kanamycin) in the presence and absence of IPTG. As shown in Figure 3.16, over expression of *ptsO* in wild type AB5075 leads to decreased plating efficiency on LB agar containing kanamycin and also confers an increased lag time when grown in liquid media containing kanamycin. These results are consistent with the hypothesis that over-expression of *ptsO* leads to a Gig phenotype in wild type AB5075 and supports the hypothesis that NPr acts negatively in the GigA/B signaling axis.

Having established that over-expression of *ptsO*/NPr induces a Gig phenotype in wild type AB5075, I screened a genomic fragment library (pRK75, see the Materials and Methods Chapter) for clones that suppress the *ptsO*/NPr-induced Gig phenotype (Figure 3.17). When I cultured wild-type AB5075 harboring plasmid pMJG120.*ptsO* and the pRK75 library on LB plates containing kanamycin and IPTG, conditions that inhibit growth of AB5075 pMJG120.*ptsO*, I recovered several kanamycin-resistant colonies. The initial prediction was that this experimental approach would identify at least two mechanisms for restoring kanamycin

resistance; one of which would be the isolation of plasmids harboring kanamycin resistance determinants. Another scenario I predicted is that the suppressing clones would contain plasmids harboring genetic elements that antagonize the effects of NPr, including *gigA*/*B*. Indeed, upon purification and sequencing of the plasmids from 16 independent kanamycin resistant clones, I recovered 3 clones harboring a plasmid containing genetic material mapping to plasmid pAB5075-1 containing an IS element, ISAba125, which includes an aminoglycoside phosphotransferase (ABUW_4087, *aphA6*). Interestingly, this particular aminoglycoside modifying gene, *aphA6*, was first described in 1988 (Martin, Jullien, and Courvalin 1988). The 13 remaining kanamycin resistant clones contained DNA fragments mapping to the *gigA*/*gigB* locus (Figure 3.17). Of these 13 plasmids mapping to the *gigA*/*gigB* region, there were two unique clones. Importantly, these results provide strong evidence for the GigA/B – PTS^{Ntr} interaction and further suggest a stoichiometric relationship between GigA/B and NPr, as kanamycin sensitivity returns on media containing increasing concentrations of IPTG (Figure 3.17 panel A), which further raises the NPr levels.

While all of the 16 sequenced clones (n = 16) from this experiment contained either the *gigAB* region or an aminoglycoside resistance determinant, I was unable to exclude the possibility that additional components of the pathway remain undiscovered. Indeed, this approach is limiting in that each kanamycin resistant clone needs to be purified and then sequenced individually. Additionally, as the majority of the clones (13/16) harbored plasmids containing the *gigAB* locus, the recovery of lower-frequency plasmids would be challenging using this experimental approach. In order to circumvent these limitations, I also performed a larger scale sequencing experiment by using Illumina Next Generation Sequencing technology to sequence approximately 100,000 kanamycin resistant clones containing pRK75 library plasmids

that restore growth upon kanamycin in the presence of NPr over expression. This number of colonies represents an approximate 12-fold over-representation of the pRK75 library, which contained ~8,000 clones. As a control, I also sequenced plasmid DNA from an equivalent number of colonies harvested from bacteria grown in the absence of kanamycin and IPTG. This control sample serves as the 'input' DNA to assess the enrichment of particular gDNA fragments.

Results of this sequencing project are shown in Figures 3.18 and 3.19. In total, 1.8 million reads mapped to the AB5075 genome and plasmids from the input pool and 3.0 million reads mapped following kanamycin selection. Consistent with the results obtained by sequencing isolated colonies, the only regions showing enrichment following kanamycin selection included the *gigAB* locus (Figure 3.18) and the locus containing the *aphA6* genes (Figure 3.19). The *ptsO* gene was also over-represented in both sequencing libraries due to the fact that the experiment was conducted with a strain harboring pMJG120.*ptsO*, the *ptsO*-expression plasmid (Figure 3.18). There were additional regions of enrichment (the asterisks in Figure 3.18), but these likely represent sequencing artifacts, as close inspection of the read-mapping revealed it was only due to a single mapped read. If these regions were truly enriched, a larger region of enrichment would have been expected, as the plasmid insert sizes for the pRK75 library ranged from 5 – 10 kb in length.

Loss of *gigA* or *gigB* leads to significant transcriptome changes

The domain structure and functions of similar proteins in other bacterial species suggest that the GigA and GigB proteins may function to activate an alternative sigma factor in response to environmental stressors. This hypothesis is also consistent with a model where trains lacking

either *gigA* or *gigB* will have an altered RNA expression profile, or transcriptome, relative to wild type AB5075. In order to test this hypothesis and assess the transcriptional consequence of the Δ*gigA* / Δ*gigB* mutations, I performed RNASeq analysis on RNA samples collected from exponentially growing cultures of wild type AB5075 and the Δ*gigA* and Δ*gigB* mutant strains. In addition to analyzing the RNA collected from exponentially growing cultures of these three strains, I also assessed the transcriptional responses of each of the three strains following a 30-minute exposure to kanamycin (500 μg/mL). Using stringent analysis parameters (false discovery rate/*q* value of ≤ 0.01 and $\log_2$ fold changes greater than +/- 2), 1390 and 1443 genes were differentially expressed during exponential growth in the Δ*gigA* and Δ*gigB* mutant strains, respectively, relative to wild type AB5075 (Figure 3.20). Importantly, the vast majority of the differentially expressed genes (n = 1253) were common to both the Δ*gigA* and Δ*gigB* samples, suggesting a significant overlap in the transcriptional landscape of these two strains.

In response to kanamycin exposure, 275 genes were differentially expressed (199 genes with increased expression and 76 genes with decreased expression) in wild type AB5075 (Figure 3.20). Interestingly, the response to kanamycin in the Δ*gigA* or Δ*gigB* mutant backgrounds was impaired. Of the 199 genes showing increased expression following kanamycin exposure in wild type, very few genes showing increased expression in response to kanamycin were also up regulated in either Δ*gigA* or Δ*gigB* (n = 24 and n = 26, respectively). A similar situation was observed for the genes exhibiting decreased expression in response to kanamycin exposure; with only 6 (Δ*gigA*) or 7 (Δ*gigB*) genes overlapping with the 76 genes exhibiting decreased expression in response to kanamycin exposure in wild type AB5075 (Figure 3.20 panels B and C). Taken together, the RNASeq data suggest that GigA and GigB are not only required for maintenance of the transcriptional landscape during growth of *A. baumannii* in rich media, but

are also required for generating the appropriate transcriptional changes necessary for survival during acute exposure to antibiotics.

Increased expression of the *mla* operon correlates with enhanced SDS Resistance of *gigAB* mutant strains

Analysis of the RNASeq experiment described above revealed an interesting finding. The *mla* operon, which has been characterized as an ABC-type (ATPase Binding Cassette) transport system for maintenance of lipid asymmetry in the gram-negative outer membrane (Malinverni and Silhavy 2009), was over expressed in strains lacking either *gigA* or *gigB* (Figure 3.21). The expression of this operon was not increased in the wild type background in response to kanamycin. Much of the work exploring regarding the function of the Mla transport system has been performed in the model organism, *E. coli* (Malinverni and Silhavy 2009, Thong et al. 2016) and a key phenotype of *E. coli* strains lacking the *mla* system is an increased sensitivity to outer membrane stress, which is frequently experimentally mediated by the combination of chelation of divalent cations via ethylenediaminetetraacetic acid (EDTA) and exposure to detergents, such as the anionic detergent, sodium dodecyl sulfate (SDS). Given the higher expression levels of several *mla* genes in the *gig* mutant backgrounds I assessed the sensitivity to EDTA and SDS for wild type AB5075 and the Δ*gigA*, Δ*gigB* and Δ*gigAB* mutants. As shown in Figure 3.21, strains lacking the *gig* genes show a slight, but reproducible, increase in SDS resistance compared to wild type AB5075. Interestingly, all four strains displayed sensitivity to the combination of 0.5% SDS and 100 μM EDTA, suggesting that the ability of the *gig* mutant strains to resist SDS mediated killing requires the presence of divalent cations (Figure 3.21).

Genetic evidence for RpoE (σ^E) as the regulated sigma factor

The finding that strains lacking either *gigA* or *gigB* demonstrate a significantly altered transcriptome supports the aforementioned hypothesis that GigA/GigB and the PTS^{Ntr} coordinately regulate a sigma factor. As such, I performed experiments aimed at identification of the sigma factor involved in the GigA/B signaling axis. The genome of *A. baumannii* AB5075 encodes 5 sigma factors (Table 3.2). I was able to obtain or construct interruption/deletion mutants for three sigma factor genes, *rpoE, fecI* and *rpoN*, while the two remaining sigma factors (*rpoD*, *rpoH*) appear essential for growth of strain AB5075 (Gallagher et al. 2015). Initially, I hypothesized that *rpoN* may be the sigma factor regulated by the GigA/B signaling axis, due to the potential functional overlap between the PTS^{Ntr} and nitrogen regulation performed by σ^{54} in other organisms (Powell et al. 1995, Pfluger and de Lorenzo 2008). However, when I subjected the sigma factor null strains to various *in vitro* stress conditions, strains harboring interruptions of either *fecI* or *rpoN* behaved similarly to wild-type AB5075 (Figure 3.22). Interestingly, the strain lacking *rpoE* was phenotypically similar to Δ*gigA*/Δ*gigB* strains, with increased sensitivity to acid pH, aminoglycosides and zinc. Additionally, much like the *gig* mutant strains, the Δ*rpoE* strain shows an increased resistance to SDS-mediated killing. The *rpoN* disruption strain (*rpoN*::Tn) also displayed increased SDS-resistance relative to wild type AB5075 (Figure 3.22).

Despite the Δ*rpoE* strain phenotypically resembling the Gig phenotype, I am cautious about concluding that RpoE is part of the GigA/B axis for several reasons. First, in other gram-negative species, RpoE is primarily regulated by targeted proteolysis of the RpoE anti-sigma factor, RseA (Alba and Gross 2004). While there is not a predicted RseA homolog in the *A. baumannii* genome, homologs of the proteases responsible for RseA cleavage, DegS and RseP, are present in the *A. baumannii* genome, suggesting that a similar regulatory mechanism may be

conserved in *A. baumannii*. Additionally, in the case of *E. coli*, expression of the heat shock sigma factor, RpoH / σ^{32}, is known to be controlled, at least in part, by RpoE (reviewed in Noor 2015). Given these findings, and that the RpoH homolog in *A. baumannii* is essential for the viability of strain AB5075, more definitive studies are required to confirm that RpoE is regulated by the GigA/B signaling axis.

Current working model for the GigA/B Axis

Taken together, the data presented above are consistent with the model depicted in Figure 3.23. In this model, stress is either perceived directly by, or transmitted to, GigA through an as yet unknown mechanism. Upon activation, GigA functions as a phosphatase, removing the phosphate group on the Ser-59 residue of GigB. Non-phosphorylated GigB then functions as an anti-anti-sigma factor. The genetic linkage between GigA/B and the PTS^{Ntr} supports the hypothesis that NPr functions as an anti-sigma factor for an alternative sigma factor, likely RpoE (σ^{E}). This model further predicts that NPr–P is required for the anti-sigma factor activity and is generated by PO_4^- - transfer from PEP via EI^{Ntr}. When GigB is un-phosphorylated, it can sequester NPr–P from the sigma factor, allowing for the expression of the appropriate stress response genes. Additionally, the phosphate group from NPr–P is transferred to GigB as a consequence of their interaction, which leads to the inactivation of GigB. NPr is then released and can be converted back to NPr–P via phosphate flux through the PTS^{Ntr}.

An alternative interpretation of the data presented above can lead a slightly different model for regulation of signaling output. In this model, GigA is constitutively active (see Figure 3.11) and does not require activation by a canonical TCS-Sensor Kinase protein. This second model, where GigA is not regulated, requires that another step in the signaling axis be the site of

regulation. There are several points where this regulation could be mediated. For example, as shown in Figures 3.16 and 3.17, changes in the NPr concentration directly alter the stress-resistance phenotype, suggesting that levels of NPr and/or NPr–P play an important role in mediating the output of the GigA/B signaling axis. Additionally, as GigB is undetectable in wild type AB5075 via western blot, the intracellular concentration of GigB and or GigB–P could also mediate control of the system.

DISCUSSION

In this chapter, I sought to enhance our understanding of two previously identified virulence related genes of *A. baumannii*. These two genes, *gigA* and *gigB*, were initially discovered due to their requirement for survival and growth within the *G. mellonella* infection model and were subsequently demonstrated to be required for the intrinsic antibiotic resistance phenotype of an MDR *A. baumannii* isolate, AB5075 (discussed in Chapter II and Gebhardt et al. 2015). Herein, I provide evidence that GigA and GigB are also required for wild type resistance to a variety of *in vitro* stress conditions, including acidic pH, exposure to the heavy metal ion Zn^{2+}, and growth at elevated temperature (Figure 3.3). Interestingly, two *Pseudomonas aeruginosa* genes that are closely related to *gigA* and *gigB*, PA2798 and PA2797, respectively, are also required for intrinsic aminoglycoside resistance (Krahn et al. 2012), suggesting that the signaling axis reported here may be broadly conserved.

The GigA and GigB proteins harbor domains found in proteins that form signal transduction pathways in other bacterial species, such as the well characterized regulatory cascade controlling the activity of σ^B in *B. subtilis* and signaling modules described for *Vibrio fisheri* and *Shewanella oneidensis* (Yang et al. 1996, Bouillet et al. 2016, Morris and Visick

2013). In contrast to these systems, which typically include an anti-sigma factor protein (such as RsbW in the *B. subtilis* σ^B regulatory cascade), *A. baumannii* lacks proteins with the RsbW domain, suggesting a novel mechanism for GigA/GigB function. Indeed, I identified a connection between the GigA/GigB proteins with the nitrogen phosphotransferase system (PTS^{Ntr}) and show that NPr-P phosphorylates GigB *in vitro* (Figure 3.15). Additionally, I demonstrate that GigA/GigB and the PTS^{Ntr} – function in opposition, where GigA/GigB activity promotes stress survival, while the PTS^{Ntr} negatively regulates this response. Given these findings and the fact that *A. baumannii* lacks the third and final protein of the PTS^{Ntr}, $EIIA^{Ntr}$, I propose the model depicted in Figure 3.23, where GigA/GigB converge with the PTS^{Ntr} as a means to regulate σ^E.

Consistent with this model of σ^E regulation, transcriptome analysis of strains lacking either *gigA* or *gigB* showed significant variation from wild type AB5075, with well over 1,000 genes being differentially expressed in the mutant backgrounds (Figure 3.20). Importantly, there was considerable overlap between the Δ*gigA* and Δ*gigB* mutant transcriptomes, a finding consistent with the similar *in vitro* phenotypes shared by the two strains. Additionally, exposure to kanamycin altered the expression of 275 genes in wild type AB5075 (Figure 3.20). When comparing the kanamycin response between wild type AB5075 and the Δ*gigA* or Δ*gigB* mutant strains, however, I observed that most of these genes were not affected by kanamycin in the *gig* mutant backgrounds, indicating that the appropriate transcriptional response is not executed in the Δ*gigA*/Δ*gigB* strains.

The significant differences observed at the transcriptome level in the Δ*gigA*/Δ*gigB* mutant strains support a model where GigA and GigB act as master regulators of a global stress response pathway and suggests that this pathway is a crucial regulatory component for

maintaining homeostasis in *A. baumannii*. While it is possible that the loss of signaling through GigA/GigB directly leads to all of the transcriptional changes observed, it is also conceivable that the loss of GigA/GigB causes compensatory activation of other stress response pathways. This situation has been reported in *E. coli*, where survival of strains lacking RpoE requires the acquisition of suppressing mutations that dampen other, RpoE-independent stress response pathways (Button, Silhavy, and Ruiz 2007).

While the data presented herein support the model depicted in Figure 3.23, alternative models should also be considered. One such alternative model is similar to the Rsb pathway of *Chlamydia trachomatis*, which regulates the availability of the primary/housekeeping sigma factor, σ^{66} (Thompson et al. 2015). This model is attractive given a previous report that in *E. coli*, HPr - the carbohydrate specific ortholog of NPr - interacts with Rsd, a small protein that binds to and mediates the availability of the primary sigma factor, σ^{D} (Park et al. 2013, Park et al. 2015). It is conceivable that a similar situation may be occurring in *A. baumannii*, however searching the AB5075 genome for proteins containing the Rsd domain did not identify any potential matches.

Another less likely possibility is that GigA/GigB and the PTS^{Ntr} do not regulate the availability of a sigma factor, but rather converge upon an additional protein or proteins that remain unidentified. I find this unlikely based on the results of the NPr over expression screen, in which only two types of suppressors were identified: clones harboring plasmids containing the *gigAB* region and those harboring an aminoglycoside-modifying enzyme (Figures 3.16, 17, 18, and 19). These findings of this experiment confirm the NPr – GigA/B interaction, although I cannot formally exclude the existence of additional components in the signaling axis that were not recovered by the screen.

To conclude, I view the interplay between the GigA/GigB axis and the PTS^{Ntr} as a means to maintain homeostasis under diverse environmental conditions. Bacterial fitness, particularly during an infection, is impacted by several factors, including exposure to antibiotics; nutrient deprivation, either from the host's restriction of nutrients as part of the immune response or as bacteria colonizing a surface in the clinical settings; and the harsh conditions imposed upon bacteria by the host's immune response to an invading pathogen. The multivariate nature of the Gig phenotype supports this idea of bacterial fitness in that cells lacking *gigA*/*gigB* do present sensitivity to a variety of stress conditions, including exposure to antibiotics, virulence and environmental stress. I thus propose that connecting a global stress response pathway, such as the GigA/GigB axis, with a central metabolic sensing pathway, the PTS^{Ntr}, allows *A. baumannii* to maintain cellular homeostasis in multiple environments, and ultimately enables the organism to coordinately regulate gene expression in response to the changing environmental conditions encountered during various aspects of the infectious process.

CHAPTER IV

GigC – a Transcriptional Regulator Controlling Cysteine Biosynthesis

INTRODUCTION

A major facet of the human innate immune response is the sequestration of essential metabolites and other factors required for growth of bacteria. This process encompasses a variety of pathways and strategies. For example, nutritional immunity is a recently defined term that describes mechanisms employed by host organisms that aim to sequester essential micronutrients, including many essential heavy metal ions like iron, zinc and manganese, from invading pathogens (Hood and Skaar 2012). The success of this strategy is reflected in the wide range of eukaryotic hosts, ranging from mammals to insects and plants, that employ pathogen-restriction strategies involved with limiting access to certain nutrients (Kavanagh and Reeves 2004). One unsurprising consequence of the host's efforts to limit access to key nutrients to invading organism is that pathogens have developed strategies to counteract these defense mechanisms. Indeed, many nutrient scavenging systems have evolved among bacterial pathogens that afford access to sequestered nutrients, such as siderophores for iron-acquisition.

In addition to sequestration of micronutrients like the trace heavy metal ions required as enzyme cofactors and within the active sites of metalloproteins, many hosts also limit the availability of certain amino acids. For example, the hemolymph (circulatory fluid) of the *Galleria mellonella* larvae was found to lack detectable levels of the amino acid cysteine (Wyatt, Loughheed, and Wyatt 1956). In addition to nutritional limitation, sequestration of cysteine in the *Galleria* hemolymph is likely an important requirement for the generation of reactive oxygen

species in response to infection. This is because cysteine is a powerful reducing agent and its presence in the hemolymph would likely hinder the development of the oxidative burst.

Not surprisingly, however, many bacterial pathogens are able to synthesize the amino acid cysteine through the action of several distinct enzymes. This pathway is known as the reductive sulfur assimilation pathway and begins with a sulfate ion (SO_4^-), which is subsequently reduced to hydrogen sulfide is then combined with an activated form of serine, O-acetyl serine, to form cysteine. The sulfur assimilation pathway is generally well conserved across bacteria, and many of the proteins found in this pathway are also present in *A. baumannii* (Figure 4.1). Aside from being one of the essential amino acids required for protein biosynthesis, cysteine, and the sulfur atom therein, is required for synthesis of many other important biomolecules, such as the amino acid methionine, reducing compounds such as glutathione, and cofactors such as coenzyme A, lipoic acid, molybdopterin, and Fe–S clusters (Campanini et al. 2015).

Given the wide range of roles played by both cysteine and the other sulfur-containing biomolecules, researchers have sought to identify and characterize the mechanisms that regulate the expression of the genes involved in the sulfur assimilation and cysteine biosynthetic pathways (i.e. the *cys* genes). Much of our understanding about the regulatory networks controlling expression of the *cys* genes results from studies in the gram-negative species *Escherichia coli* and *Salmonella typhimurium* and the gram-positive organism *Bacillus subtilis*. In *E. coli* and *Salmonella*, *cys* gene expression is largely mediated by a LysR family transcriptional regulator protein, CysB (Hryniewicz and Kredich 1991). CysB functions as a transcriptional activator and mutant strains lacking the *cysB* gene demonstrate decreased *cys* gene expression. Additional studies have identified a potential inducing substrate, O-acetyl-serine, which is the product of CysE enzymatic activity and is combined with H_2S to generate

cysteine through the action of cysteine synthase enzymes, CysK and CysM (Kredich 1992). In addition to CysB, a second protein, Cbl (for CysB-like), is responsible for the expression of genes involved with acquisition of sulfur from non-sulfate sources, such as alkanesulfonates (van der Ploeg et al. 1997). In *Bacillus subtilis,* the CysL protein has been shown to control the expression of several *cys* genes, including those encoding sulfite reductase, *cysI* and *cysJ*. The CysL protein bears similarity to the CysB protein found in *E. coli* and other proteobacteria (Guillouard et al. 2002). Interestingly, both of the major *cys* gene regulators, *E. coli* CysB and *B. subtilis* CysL, were shown to negatively regulate their own expression, a trait common to many LysR-family transcriptional regulators (Maddocks and Oyston 2008).

Researchers studying the expression of the *cysJIH* operon in *Salmonella* also examined the ability of hydrogen sulfide (H_2S) to provide protection from oxidative stress (Alvarez et al. 2015). The authors found that expression of the *cysJIH* operon increased in response to oxidative stress and concluded that the increased expression of proteins involved with the sulfur assimilation pathway resulted in an increased intracellular thiol pool, which may be critical to preventing damage resulting from exposure to oxidative conditions. Similarly, another group has demonstrated that inhibition of H_2S production resulted in an increased sensitivity to a variety of antibiotics for several bacterial pathogens, including *E. coli, Bacillus anthracis, Staphylococcus aureus* and *Pseudomonas aeruginosa* - a close relative of *A. baumannii* (Shatalin et al. 2011). Taken together, these reports highlight the importance of H_2S for maintenance of the thiol pool under oxidative stress, and also suggest that the sulfur assimilation and cysteine biosynthetic pathways represent a viable therapeutic target for controlling bacterial infections.

Due to the continuing emergence of antibiotic resistance amongst bacterial pathogens, an active area of research is focused on the identification of novel targets for new antimicrobial

drugs. One key necessity of such an antibacterial drug target is that a similar target is not found in the host. For example, many current antibiotics target the bacterial cell wall, a structural feature that not found in the human host. The bacterial sulfur assimilation/cysteine biosynthetic pathway represents another attractive therapeutic target. Indeed, in mammals do not generate cysteine *de novo* from sulfate, but rather cysteine is produced from methionine via a process known as the reverse transsulfuration pathway (Griffith 1987). In this pathway, methionine serves as the sulfur source while the amino acid serine provides the requisite carbon and nitrogen. This pathway is distinct from the mechanisms used to produce cysteine in bacteria, where cysteine is synthesized by combing O-acetyl serine with hydrogen sulfide (H_2S). Furthermore, mammals also lack the reductive sulfur assimilation pathway described above. As such, the cysteine biosynthetic pathway, and more specifically, the enzymes involved with the reductive sulfur assimilation pathway, represent an attractive therapeutic target for bacterial infections.

In the past few years, several enzymes of the sulfur assimilation pathway have been the subject of studies looking for inhibitors. For example, several studies have searched for inhibitors of the CysH protein, which encodes an adenosine phosphosulfate (APS) reductase that functions to reduce sulfate to sulfite. These studies have primarily focused on the *Mycobacterium tuberculosis* CysH protein and have included the use of non-hydrolyzable analogs of the native CysH ligands and also molecular docking simulations to identify potential ligands from pre-existing small molecule libraries (Cosconati et al. 2008, Hong, Bhave, and Carroll 2009). Additional examples of sulfur assimilation/cysteine biosynthetic proteins that have received attention as novel therapeutic targets include CysE (serine acetyl transferase) and the cysteine synthase enzyme CysK (Salsi et al. 2010, Agarwal et al. 2008). Given the apparently high

conservation of the enzymes of the sulfur assimilation/cysteine biosynthetic pathway, these studies provide a good starting point for further investigation and also may also be directly applied to other pathogenic organisms.

In this chapter, I describe the experiments aimed a characterizing the GigC protein – a transcriptional regulator that bears homology with known regulators of *cys* gene expression found in other bacterial species. This line of investigation was initiated as a result of finding that several *cys* genes were found to be required for growth of *A. baumannii* in the *Galleria mellonella* infection as described in Chapter II. In addition to determining that a strain lacking the *gigC* gene is auxotrophic for the amino acid cysteine, I present data showing that the GigC protein is also required for the appropriate expression of several *cys* genes. Further experiments demonstrate direct binding of GigC to the *cysI* promoter. Finally, I performed a biochemical and biophysical characterization of the GigC protein and identify potential ligands of the GigC protein and also determine that the GigC protein likely exists as a tetramer in solution. Taken together, the experiments described below provide a solid foundation for future studies and serve as a platform for understanding how *A. baumannii* regulates the expression of genes involved in sulfur assimilation and cysteine biosynthesis.

RESULTS

Cysteine/Sulfur Assimilation Genes Identified by Transposon Sequencing

One of the largest groups of genes identified by the Transposon Sequencing experiments presented in Chapter II fall into the category of amino acid metabolism and transport, with nearly 10% of the hits (25 of the 300 genes) bearing annotations of this nature. Among these 25 genes, nine genes are annotated as having involvement in the sulfur assimilation pathway, the major

bacterial pathway for cysteine biosynthesis (Campanini et al. 2015). Of these nine genes (listed in Table 4.1), six are predicted to encode proteins required of the sulfur assimilation pathway (Figure 4.1), two encode predicted transport proteins (ABUW_1760 and ABUW_1941) and a gene annotated as *cysG* (ABUW_0853), which encodes a predicted siroheme synthase protein. Siroheme is an essential cofactor required for the final reduction of sulfite to sulfide carried out by the CysI protein, one of the required sulfur assimilation proteins (Spencer et al. 1993), identifying *cysG* as another critical component of the sulfur assimilation pathway.

Loss of GigC, a LysR-family Transcriptional Regulator, Confers a Cysteine Auxotrophy

One prediction that arises from the identification of genes involved with sulfur assimilation and cysteine biosynthesis (i.e. the *cys* genes) is that another hit from the TnSeq screen may be a transcriptional regulator that controls the expression of the *cys* genes. To test the hypothesis that one of the transcriptional regulators identified in the TnSeq screen controls cysteine biosynthesis, I tested strains lacking individual transcriptional regulators for the ability to grow on minimal medium plates with 10 mM succinate (M63S). In this growth medium, the only available nitrogen source is ammonium sulfate, $(NH4)_2SO_4$, and the only sulfur available in the medium is supplied from ammonium sulfate and ferrous sulfate ($FeSO_4$). As such, growth on this medium requires the ability to synthesize all of the amino acids *de novo*, including cysteine. Of the transcriptional regulators tested, only the strain lacking *gigC* (AB5075 annotation ABUW_3161), a LysR family transcriptional regulator, failed to grow on M63S (Figure 4.2). This finding suggests that the Δ*gigC* strain lacks the ability to synthesize an essential metabolite. Interestingly, the strain was able to grow when cysteine (20 μg/mL) was added to the medium, suggesting that the Δ*gigC* mutant strain is a cysteine auxotroph. The requirement for added

cysteine was abrogated by re-introduction of the *gigC* coding sequence at the Tn7 attachment site, confirming that the phenotype resulted directly from loss of the *gigC* gene as opposed to a secondary mutation (Figure 4.2).

As described previously in Chapter II, the gene encoded by ABUW_3161 has been given the name *gigC* and is one of the transcriptional regulators required for growth of *A. baumannii* in the *Galleria mellonella* model. The results presented in Chapter II showed that the TnSeq Read Ratio for transposon insertions within the *gigC* coding sequence was 0.0007, well below the significance threshold of 0.10. Consistent with these results, our validation studies using a strain harboring a deletion of the *gigC* gene confirmed the growth defect in the *Galleria* model, which was complemented by insertion of the *gigC* gene at the Tn7 locus (Figures 2.6 and 2.10).

GigC is required for resistance to the alkyl-depleting agent N-Ethyl Maleimide.

As discussed above, in addition to its requirement for the *de novo* biosynthesis of cysteine, the sulfur assimilation pathway also been shown to play an important role in oxidative stress resistance (Turnbull and Surette 2010). As such, I hypothesized that, in addition to the cysteine auxotrophy, strains lacking the GigC protein may also demonstrate increased sensitivity towards stressors that confer oxidative stress upon bacteria. To test this hypothesis, I exposed the Δ*gigC* deletion strain to agents that generate oxidative stress, including the quaternary amine compound paraquat and the alkyl-depleting agent N-Ethyl Maleimide (NEM). As shown in Figure 4.2, the Δ*gigC* strain exhibits a modest increase in sensitivity to paraquat relative to wild type AB5075, but the difference did not reach statistical significance. However, following a two-hour incubation with 5 μg/mL NEM, I observed that CFU recovery from a strain lacking *gigC*

was reduced approximately 100 fold, where as both wild type AB5075 and the complemented Δ*gigC* strain (Δ*gigC*::*gigC*$^{+}$) demonstrated nearly 100% survival (Figure 4.2).

GigC Regulates the Expression of *cys* Genes

Given that strains lacking the *gigC* gene demonstrate a cysteine auxotrophy (Figure 4.2), I hypothesized that the GigC protein, a transcriptional regulator, may control the expression of one or more of the *cys* genes identified in the TnSeq Screen (Figure 4.1, Table 4.1). In order to test this hypothesis, the promoter regions of several of the genes listed Table 4.1 were cloned in to the vector pMJG126. Plasmid pMJG126 contains a promoterless *lacZ* gene, and, introduction of promoter regions upstream of *lacZ* generates a transcriptional reporter for testing the activity of that particular promoter (for a map of plasmid pMJG126, see Figure 6.2). The standard Miller assay (Miller 1972) was performed in order to assess levels of β-galactosidase, which serves as a means to assess promoter activity, in wild-type, Δ*gigC* , and complemented Δ*gigC* strains harboring various pMJG126 derivatives. As shown in Figure 4.3, the promoters of the *cysI, cysDN* (as these two genes appear to be co-transcribed, a single promoter construct was used to assess their transcriptional activity) require the presence of GigC for expression. Interestingly, the *cysH* promoter construct was found to be more active in the Δ*gigC* background, suggesting that GigC normally represses expression of this gene. The additional promoters tested, including those for the *cysQ* gene, the *gigC* gene and ABUW_1760, a predicted sulfate permease, were not affected by the absence of *gigC* (Figure 4.3).

As a mean to further understand the regulatory events underlying *cys* gene expression in terms of GigC activity, I also conducted promoter expression analyses to test the activity of the *cysI* promoter following growth under different medium conditions. In contrast to the

experiments described above which were conducted with the freely replicating plasmid pMJG126, these experiments were conducted in a strain harboring an integrated plasmid, pMJG118.*cysI*. The plasmid pMJG118 harbors the ColE1 origin of replication, which does not replicate in *A. baumannii* and can thus be used as an integration vector (Figure 6.1). The other salient feature of pMJG118 is that the plasmid contains the same promoterless *lacZ* construct as plasmid pMJG126 and by introducing DNA sequences bearing homology to regions of the *A. baumannii* chromosome, the plasmid can be used to construct strains harboring a chromosomally encoded *lacZ* gene under control of a given promoter. Integration of plasmid pMJG118.*cysI* into the *cysI* region of both wild type AB5075 and its isogenic Δ*gigC* derivative resulted in strains MG626 (wild type) and MG627 (Δ*gigC*). Miller assays using these strains showed similar results for *cysI* promoter activity as observed for strains harboring pMJG126.*cysI* in that the strain lacking *gigC* shows less activity from the *cysI* promoter (Figure 4.3). A lower level of *PcysI* promoter activity was observed during growth in LB for strain MG626 (wild type AB5075 harboring the integrated pMJG118.*cysI* vector) relative to the strain bearing the pMJG126.*PcsyI* plasmid. This discrepancy can likely be attributed to to copy number differences, as strain MG626 harbors only a single copy of *lacZ* and the *PcysI-lacZ* fusion is likely present in multiple copies when incorporated into the freely replicating pMJG126-derived plasmid (Figure 4.3). One additional difference between the *lacZ* reporter constructs was that strain MG627 (Δ*gigC*::pMJG118.*cysI*) produces a measurable amount of ß-galactosidase while the pMJG126.*cysI* construct does not, suggesting that there is basal *cysI* promoter activity from the chromosomal locus even in the absence of *gigC*. One potential explanation for this observation is that the promoter construct used to generate pMJG126.*cysI* does not include all of the potential promoters driving *cysI* expression.

The results from the *cysI* promoter activity experiments also demonstrate that *gigC* is required for increasing *cysI* expression in response to the source of sulfur present in the growth medium. As shown in Figure 4.3, strain MG626 shows increased *cysI* promoter activity in response to decreasing sulfur availability. Comparison of *cysI* promoter activity across different nutrient and sulfur sources reveals that expression of *cysI* is increased about 3 fold in a minimal growth medium with sulfate as the sole source of sulfur (M63 Succinate medium) compared to the promoter activity in a cysteine-replete rich medium (LB). Additionally, *cysI* expression decreases when cysteine is present in the medium, either when supplied as casamino acids, which contains small amounts of cysteine (Nolan 1971), or when 20 µg/mL L-cysteine is included in the growth medium (Figure 4.3). Taken together, these data demonstrate that *cysI* expression is regulated in part by the concentration of cysteine present in the growth medium and that GigC is required for mediating this response.

Recombinant GigC Exists as a Tetramer in Solution

In order to further explore the functions of the GigC protein, I generated a plasmid for the recombinant expression and purification of a C-terminal 6X-Histidine tagged version of GigC (GigC-6XHis). Using the *E. coli* expression strain BL21(DE), I purified the recombinant GigC-6XHis using nickel-affinity chromatography as described in the Materials and Methods Chapter. As shown in Figure 4.4 panel A, the majority of recombinant protein eluted from the column in the presence of 100 mM imidazole, although there was abundant GigC-6XHis protein in several of the elution fractions. Fractions containing recombinant protein were pooled, concentrated and stored for future use.

In order to determine the size of GigC-6XHis protein in solution, size exclusion chromatograph (SEC) was performed using an AKTA Fast Performance Liquid Chromatography (FPLC) instrument. The SEC column was calibrated by assessing the elution volume of a mixture of proteins on known molecular weight (Figure 4.4). Based on the elution volume of GigC-6XHis of 11.17 mL, the apparent molecular weight of the GigC-6XHis protein was calculated to be approximately 122 kDa. Since a monomer of GigC-6XHis protein is predicted to have a molecular weight of 34 kDA, the SEC data suggests that GigC-6XHis may exists as a tetramer in solution, as the calculated molecular weight of GigC-6XHis (121 kDa) is close to the theoretical weight of 136 kDa for a tetramer of GigC-6XHis. This finding is consistent with the results from three-dimensional structures of other LysR-family transcriptional regulators that were found to be tetramers, including CbnR, a LysR regulator from *Ralstonia eutropha* that controls expression of genes involved with 3-chlorobenzoate metabolism and the AhpB regulator found in *Vibrio cholerae*, which regulates expression of a key virulence factor, the toxin-coregulated pilus, in response to changes in oxygen tension and pH (Muraoka, Okumura, Uragami, et al. 2003, Taylor et al. 2012).

Evidence for Direct Binding of GigC to the *cysI* Promoter

Having established that strains lacking the *gigC* gene demonstrate reduced expression of the *cysI* gene, I next wished to assess the ability of the GigC protein to interact with promoter of this gene. The *cysI* gene was chosen in part due to the finding in *Bacillus subtilis* that the CysL protein, a LysR family transcriptional regulator known to be involved with cysteine metabolism, harbors a similar domain structure to the GigC protein (Figure 4.2), including an N-Terminal helix-turn helix domain, HTH-1, and a C-Terminal Periplasmic Binding Protein Domain (PBP2).

Additionally, the *B. subtilis* CysL protein has been shown to regulate expression of the *cysJI* operon (Guillouard et al. 2002).

In order to assess binding of GigC to the promoter region of the *cysI* gene, I used an electrophoretic mobility shift assay (EMSA). I designed oligonucleotide primers to amplify a 208-nucleotide product containing the predicted promoter region of the *cysI* gene (Figure 4.5). The primers used for amplification, MJG896 and MJG897 contain the infrared dye, IRDye 700, conjugated to the 5' terminus of each primer to allow for visualization of the PCR product using a LiCor Odyssey InfraRed detection device **(**excitation/emission maxima of 684 nm and 702 nm, respectively**)**. The resulting PCR product was combined with recombinant GigC protein and incubated at room temperature for 30 minutes prior to the addition of 10X loading buffer (see Materials and Methods). The reaction mixtures were resolved through a 4% Tris-Acetate-EDTA buffered polyacrylamide gel and imaged using a LiCor Odyssey® CLx imaging system. Results of a typical experiment are shown in Figure 4.5 and demonstrate that migration of *cysI* promoter DNA is decreased in the presence of GigC protein. This result is consistent with the direct binding of GigC to the *cysI* promoter. Interestingly, when the probe DNA (i.e. *cysI* promoter) was resolved through the gel in the absence of GigC, two discrete bands were observed (Figure 4.5). Further investigation of the DNA sequence of the probe revealed the presence of an inverted repeat, which has the potential to form a hairpin structure (Figure 4.5). If this hairpin structure had formed in the EMSA probe preparation, it would likely explain the presence of two different mobility species that are observed following electrophoresis, as hairpin structures alter the shape of DNA molecules and can impact their migration through polyacrylamide gels (Xodo et al. 1991).

Identification of Potential GigC Ligands

LysR family regulators typically harbor an N-terminal DNA binding domain and a C-terminal substrate binding domain which are connected by a linker region (Maddocks and Oyston 2008). In GigC, these domains are an HTH-1 DNA binding domain that spans residues 5 to 64, and PBP2-CysL-Like substrate binding domain spanning from residue 93 to 290 (Figure 4.2).

In order to identify potential ligands that may serve as activators of the GigC protein, I employed a technique known as differential scanning fluorimetry (Vivoli et al. 2014). Differential scanning fluorimetry (DSF) is an experimental approach that provides information about the inherent stability of a protein by monitoring protein denaturation due to increasing temperature. The readout of this experimental technique is measured as the changing fluorescence emission from a dye, SYPRO Orange. This dye preferentially binds to the hydrophobic residues of proteins, which are typically sequestered from the surface of a soluble protein, and as such, upon denaturation of the protein, an increased fluorescence signal can be detected (Simpson 2010). By taking the first derivative of SYPRO Orange emission over a thermal denaturation curve, the melting temperature for a given protein can be determined by identifying the temperature at which dye binding reaches maximal intensity. Using DSF, the GigC melting temperature was determined to be 64.9 ˚C (Figure 4.6).

While the melting temperature of a particular protein is of general interest, the DSF technique is particularly useful for identifying potential ligands. The rationale for using DSF as a tool to identify protein ligands is that ligand binding typically increases the protein's thermal stability relative to the unbound state. In order to screen potential GigC ligands, I performed DSF experiments in which the GigC protein was combined with several small molecules and

determined the melting temperature. The small molecules used for this assay include several potential ligands that are either products or intermediates of the sulfur assimilation pathway, including sulfate and sulfite ions, glutathione, cysteine and two serine derivatives, O-acetyl serine and N-acetyl serine. Of these ligands, only the addition of sulfate (Tm = 66.1 ˚C) and cysteine (T_m = 68.2 ˚C) produced an appreciable increase in the thermal stability of GigC (Tm 64.9 ˚C) (Figure 4.6).

DISCUSSION

Like most free-living bacteria, *Acinetobacter baumannii* possesses the genetic capacity to grow under severe nutritional limitations. Indeed, as a prototroph, *A. baumannii* can synthesize all essential amino acids and biosynthetic precursors from a single carbon and nitrogen source, such as the succinate and ammonium sulfate found in the M63 medium. This property likely serves the *A. baumannii* well, especially as a hospital-colonizing agent, where the environment is likely nutrient poor (Roca et al. 2012). In addition to surviving on surfaces in a clinical environment, *A. baumannii* also encounters nutrient-poor conditions during the process of infection as well. As discussed above, one of the mammalian innate immune defenses - nutritional immunity - is based on the sequestration of key micronutrients, such as zinc, iron and other biologically active metal cations, from pathogens. Additionally, the recent development of high-throughput transposon sequencing experiments in infection models allows for the identification of other metabolic pathways that are required by pathogens during an infection. Indeed, several of the recently published TnSeq screens using *A. baumannii* infection models have highlighted the importance of various metabolic pathways in the disease process, including

those for the transport and/or biosynthesis of several amino acids (Wang et al. 2014, Subashchandrabose et al. 2016).

In this chapter, I described the discovery and characterization of GigC, a transcriptional regulator required for the expression of genes involved in the sulfur assimilation/cysteine biosynthetic pathways. Much of the experimentation presented above resulted from testing the hypothesis that one of the transcriptional regulators identified in the TnSeq experiment discovered in Chapter II might control the expression of genes required for the sulfur activation/assimilation pathway, an illustration of which is shown in Figure 4.1.

For *A. baumannii*, the sulfur assimilation pathway begins with sulfate, which possesses an oxidation state of +6, and, following a series of reductive steps, generates hydrogen sulfide, where the sulfur atom has an oxidation state of -2. The hydrogen sulfide can then be combined with O-acetyl-serine, through the activity of cysteine synthase proteins, to form the amino acid cysteine. Interestingly, with the exception of the two genes encoding cysteine synthases, *cysK* and *cysM*, every predicted gene in this pathway was identified as essential for the growth of *A. baumannii* inside the *G. mellonella* larvae (Figure 4.1). This finding highlights the importance of the sulfur assimilation pathway for survival and/or growth of *A. baumannii* in this model system. It is likely that functional redundancy between CysK and CysM (both serve as cysteine synthase enzymes) is the reason that these genes are not required for survival in *G. mellonella*.

The GigC protein is in the LysR family of transcriptional regulators, which constitutes the most abundant category of transcriptional regulators across the bacterial kingdom (Maddocks and Oyston 2008). As shown in Figure 4.2, the GigC protein contains both a DNA binding domain (HTH-1) and a substrate-binding domain (PBP2-CysL like). Consistent with studies performed on other LysR family regulators, such as the CbnR protein from *Ralstonia eutropha*

(Muraoka, Okumura, Ogawa, et al. 2003), data from size exclusion chromatography suggests that GigC forms a tetramer in solution (Figure 4.4). Additionally, using differential scanning fluorimetry, I showed that sulfate and cysteine both increase the thermal stability of the GigC protein, suggesting that these small molecules may serve as a ligand for GigC. Either of these potential ligands are plausible inducers for the GigC protein, as both molecules are components of the sulfur assimilation/cysteine biosynthetic pathway. Further biophysical experiments, such as isothermal titration calorimetry and/or surface plasmon resonance, are required to confirm if one or both of these molecules are *bona fide* ligands for the GigC protein.

I also demonstrated that GigC regulates the expression of several of the *cys* genes identified in the TnSeq screen. Interestingly, unlike other LysR regulators, which have been shown to act as transcriptional activators for target genes and negatively regulate their own promoters, the data presented in Figure 4.3 suggests that GigC is not involved in autoregulation. The promoter activity studies and the EMSA experiments demonstrating DNA binding of GigC to the *cysI* promoter support a model where GigC functions as a transcriptional activator for the *cysI* gene. An important question raised by these experiments is whether the GigC-dependent activity is a direct result of GigC binding to these promoters or if the results are due to an indirect affect caused by the lack of *gigC* itself. One way to answer this question is to determine if GigC directly binds to these other promoters, including that of the *cysDN* operon, which requires GigC for activity, and the *cysH* promoter, which appears to be negatively regulated by GigC.

In addition to determining if the GigC protein is directly responsible for the regulation of these promoters, the information gathered by these experiments would be useful in determining the DNA sequences recognized by GigC. An alternative approach to identify the GigC

recognition sequence would be to empirically determine the nucleotides required for GigC binding to the *cysI* promoter region using the EMSA assay. The ultimate goal of determining the GigC binding sequence is to identify additional genes of the GigC regulon. This information could then be used to determine if GigC regulates genes outside of those described in the cysteine biosynthetic pathway, such as genes required to resist oxidative stress, which has been shown for other transcriptional regulators that control *cys* gene expression (Alvarez et al. 2015). Indeed, one model for the requirement of GigC for survival in the *Galleria* larval cavity goes beyond the cysteine auxotrophy of the Δ*gigC* strain. In this model, the strain lacking GigC is unable to adequately respond to the oxidative burst generated by *G. mellonella*, leading to loss of bacterial viability. The finding that the Δ*gigC* strain shows increased sensitivity to paraquat and N-ethylmaleimide (NEM) does lend support to this model. However, as NEM is a thiol-reducing agent, and the Δ*gigC* strain likely has a reduced thiol pool from the decreased expression of cysteine biosynthetic genes, the increase in NEM sensitivity should be interpreted with caution.

Finally, a careful analysis of the genes identified in the TnSeq experiment detailed in Chapter II also reveals several additional genes that could also be involved with sulfur metabolism (Table 2.5). These genes include several genes predicted to be involved with the molybdopterin biosynthesis pathway (ABUW_1710 – 1713) and also lipoic acid synthesis (ABUW_1228 and ABUW_2132). Both molybdopterin and lipoic acid are sulfur-containing enzyme cofactors required for a variety of processes in bacteria (Filiatrault et al. 2013, Tombline et al. 2013, Morris, Reed, and Cronan 1995, Sokatch et al. 1981). Given the requirements for sulfur ions in both of these cofactors, it would be interesting to determine if the expression of these genes are also under control of the GigC protein.

To conclude, the experiments described above have enhanced our understanding of the GigC protein, a LysR family transcriptional regulator identified by its requirement for growth of *A. baumannii* in the *G. mellonella* model. I have shown that this protein is required for growth of *A. baumannii* in media lacking cysteine and that GigC regulates the expression of a subset of the genes involved with the sulfur assimilation and cysteine biosynthetic pathways. Further investigation into both GigC and the cysteine biosynthetic pathway may lead to the discovery of novel therapeutic avenues to treat infections caused by *A. baumannii*.

CHAPTER V

Conclusions

The emergence of *Acinetobacter baumannii* as a human pathogen should be met with concern. This organism, while not an exceptionally virulent pathogen, has rapidly developed extensive resistance to many, and in some cases, all of the routinely used antimicrobial therapeutic options (Gottig et al. 2014). When coupled with the recalcitrance of certain *A. baumannii* isolates to antibiotics, however, infections arising from pathogens that are not exceptionally virulent can nevertheless be life threatening given the lack of treatment options.

That *A. baumannii* is not considered a highly virulent pathogen is reflected by results from infection models, where many animal models require either (or both) a non-physiological inoculum (i.e. high bacterial burden) in order to cause disease and/or direct immune suppression of the host's immune system in order to cause disease (Jacobs, Thompson, Black, et al. 2014). Additionally, as mentioned previously, *A. baumannii* largely only afflicts people with underlying health issues; primarily infecting patients hospitalized for an unrelated condition or causing disease in the greater community in people with poor health. These observations are suggestive of a typical opportunistic pathogen and that *A. baumannii* is not necessarily a specific human pathogen, but rather an organism that is capable of infecting compromised individuals when afforded the opportunity.

A slightly alternative hypothesis to explain the emergence of *A. baumannii* as a human pathogen was presented in Chapter I. Recent comparative genomics studies have shown that *A. baumannii*, as a species, recently diverged from many closely related *Acinetobacter* species

(largely those comprising the *A. baumannii/calcoaceticus* complex) (Touchon et al. 2014, Wright et al. 2014). The authors of these reports speculate that the underlying driver of *A. baumannii* speciation was the emergence of what is now *A. baumannii* from a significant genetic bottleneck. In the terms of population genetics, a bottleneck is typically defined as an event that greatly restricts the population size, such that only a limited number of organisms survive the particular event, resulting in a relatively low level of genetic diversity amongst the survivors (reviewed in Achtman 2004). While the direct identification a specific population bottleneck in terms of an organism's evolutionary history is usually not possible, it is intriguing, nonetheless, to consider that the population bottleneck leading to the *A. baumannii* speciation event was the adaptation of an ancestral *Acinetobacter* for survival within the clinical environment. In this scenario, the recent reports that describe highly virulent *A. baumannii* isolates could be interpreted as the sequential result of *A. baumannii* evolving to this new environmental niche as a hospital dwelling organism that routinely encounters the human host (Jacobs, Thompson, Black, et al. 2014, Jones et al. 2015).

The work presented in the preceding chapters fits well with this model of *A. baumannii* evolution and leads to a new picture of *A. baumannii* as a pathogen. The pathogenic life cycle of *A. baumannii* includes many potential barriers to its survival, including the clinical healthcare setting where the organism faces harsh environmental conditions including desiccation, nutrient limitation and the ability to survive the routine decontamination efforts. Additionally, successful contemporary *A. baumannii* isolates must further resist the action of the antibiotics used as therapeutic agents. A third facet of the *A. baumannii* life cycle, survival within the human host, also requires robust environmental stress resistance, as well as nutritional versatility. Indeed, one

hallmark feature of *A. baumannii* (and the entire *Acinetobacter* genus, for that matter) is the ability to utilize a wide variety of molecules as potential carbon and nitrogen sources.

At the onset of the studies presented herein, my main goals were to begin answering questions pertaining to the emergent properties that endow *A. baumannii* with the ability to cause human disease. Particularly, I hoped to uncover the regulatory networks that underlie *A. baumannii* pathogenesis. Towards this end, I performed a transposon insertion sequencing (TnSeq) experiment with the goal of identifying genetic determinants required for survival of *A. baumannii* strain AB5075, a contemporary, multi-drug resistant clinical isolate (Zurawski et al. 2012, Jacobs, Thompson, Black, et al. 2014) within the larvae of the insect *Galleria mellonella*. The TnSeq experiment led to the identification of 300 genes as being required for the survival and/or growth of AB5075 in the *Galleria mellonella* larvae. Many of the genes identified in this experiment had been previously characterized as *A. baumannii* virulence genes. Indeed, the TnSeq study described herein represents the first large-scale experiment to determine the genetic requirements for survival of *A. baumannii* in the *Galleria* model. While other researchers had published findings describing methods with which to employ the *G. mellonella* model as a means to study *A. baumannii* pathogenesis (Peleg et al. 2009, Jacobs, Thompson, Black, et al. 2014, Wand et al. 2012), a thorough investigation of how well the model recapitulates the disease setting had not been performed. The results presented in Chapter II directly describe such an investigation and provided strong evidence to support the utility of the *G. mellonella* model for the study of *A. baumannii* pathogenesis. In addition, the finding of known virulence factors in the TnSeq screen also increases confidence that the novel genes which had previously not been assigned a role in virulence are also important for the pathogenesis of *A. baumannii.*

As described above, one explanation for the recent emergence of *A. baumannii* is that the species itself is relatively young. This hypothesis serves to explain not only the apparent genetic isolation of *A. baumannii* from other closely related *Acinetobacter* species, but also the diversity across contemporary isolates of *A. baumannii*, which may represent an exploration of new sequence space for *A. baumannii* isolates (Diancourt et al. 2010, Touchon et al. 2014). Looking at the results presented in Chapter II through this intellectual framework explains some of the findings that at first glance are hard to reconcile with previous reports. Importantly, the TnSeq experiment presented herein highlights key strain-to-strain differences across two of the more commonly used strains for studying *A. baumannii*.

One such example of these differences pertains to the observation that many of the genes identified as required by *A. baumannii* for growth/survival in the *G. mellonella* model include those required for the synthesis and secretion of capsular polysaccharides. In the type strain of *A. baumannii*, ATCC 17978, which has been one of the more widely studied *A. baumannii* strains in the literature, several recent reports suggest that the capsule locus is essential for viability of this particular strain; including both a TnSeq-like experiment investigating the genetic requirements of *A. baumannii* persistence in the mouse lung (Wang et al. 2014), and a second paper that specifically investigated the capsule locus in this strain (Geisinger and Isberg 2015). Indeed, both of these reports hint at the notion of the essentiality of capsule biosynthesis in strain 17978. In the work presented by Wang and colleagues, the transposon library used for the study, when sequenced, contained very few strains harboring interruptions within the capsule locus, suggesting that such strains incur a significant fitness cost and are lost from the population. The second report specifically attempted to create mutations within the 17978 capsule locus and discovered that strains harboring capsule gene deletions also acquired suppressing mutations,

again supporting the conclusion that in the 17978 strain background, the capsule is relatively essential for viability.

These findings are in stark contrast to the AB5075 strain background, in which individual capsule genes, including the structural proteins required for secretion of the capsule, were readily mutated in my hands. Furthermore, the capsule deletion mutants acquire a characteristic 'rough' colony morphology that is easily distinguished from the 'smooth' morphology of wild type AB5075. Interestingly, several recent reports using the AB5075 strain background have described a similar plate morphology, although these papers refer to the capsule minus strains as having a 'translucent' phenotype (Tipton, Dimitrova, and Rather 2015, Tipton and Rather 2016). The dispensability of capsular polysaccharide biosynthesis suggests the AB5075 strain has undergone evolutionary events that allow for strains to lose the ability to produce capsule. Given the well-documented requirements of capsule for the virulence of *A. baumannii* in several infection models (Russo et al. 2010, Gebhardt et al. 2015), an alternative pressure driving this evolutionary development may be predation by bacteriophage. Indeed, a recent study reports the isolation of an AB5075-specific bacteriophage that specifically uses the expolysaccharide capsule as its receptor and phage resistant clones present with the rough or translucent plate morphology (Regeimbal et al. 2016).

In addition to uncovering factors that highlight strain-to-strain variation across *A. baumannii* isolates, I propose that the results of the TnSeq experiment presented in Chapter II provide additional insights into how *A. baumannii* has evolved into a serious human pathogen, as well as serving as the starting point for many of the other lines of experimentation described herein. The key finding that supports this proposal is the discovery of a previously unappreciated connection between virulence, environmental stress resistance and antibiotic resistance in *A.*

baumannii. Indeed, several genes identified in the TnSeq experiment are required for the full multi-drug resistant phenotype of the parental AB5075 strain (Table 2.4).

Two of the genes found to be required for both antibiotic resistance and growth in the *Galleria* model, *gigA* and *gigB*, were of particular interest due to both the genetic context and the predicted domains encoded within the predicted proteins encoded by these two genes. The annotations indicated that these two proteins likely comprise components of a signal transduction pathway. GigA is a non-canonical two-component system response regulator and harbors a protein phosphatase domain (PP2C) instead of the more commonly found DNA binding domain. The GigB protein consists of a STAS domain, which is a domain commonly found in bacterial anti-sigma factor antagonists. Proteins containing these domains have been shown to function together in a variety of signaling modules across many bacterial species (Bouillet et al. 2016, Pane-Farre, Lewis, and Stulke 2005, Thompson et al. 2015, Morris and Visick 2013). The widespread co-occurrence of PP2C and STAS domain proteins across diverse bacterial species and the overall lack of knowledge regarding signal transduction pathways in *A. baumannii* made a further characterization of the GigA and GigB proteins an attractive avenue of investigation.

The characterization of the GigA/B signaling axis established that these two proteins are an integral part of a global stress response program in *A. baumannii* and likely comprise an upstream signaling platform that ultimately directs the transcriptional response to adapt to the changing environment. Many similarities exist between the GigA/B signaling axis and similar signaling modules found in other bacterial species, such as the Rsb regulatory network in *Bacillus subtilis* (Kuo et al. 2004) or the CsrRA proteins found in *Shewanella oneidensis* (Bouillet et al. 2016). A key difference, however, between the GigA/B axis and these other networks is the presence of an anti-sigma factor that also serves as a kinase that phosphorylates

the corresponding STAS domain protein. Examples of this dual anti-sigma factor/kinase protein can be found in other systems either as an independent protein, such as the RsbW protein in the *B. subtilis* Rsb system, or as an additional domain within the two-component regulator protein, such as the CsrR regulatory protein from *S. oneidensis*, which contains both an RswB domain and a PP2C domain. In the later case, the multi-domain protein functions as an anti-sigma factor and serves both as a phosphatase and a kinase towards the STAS domain anti-anti-sigma factor (Bouillet et al. 2016).

Unlike these systems, an RsbW-like kinase is absent from the *A. baumannii* genome, which strongly suggests that the GigA/B signaling axis contains a novel mechanism for transmitting signals to the downstream components. Indeed, the genetic and biochemical experiments discussed in Chapter III indicate that the nitrogen phosphotransferase system (PTS^{Ntr}) likely fills the role of both an anti-sigma factor and a kinase for the STAS domain of the GigB protein. Since its discovery in the 1990's, the PTS^{Ntr} has largely been considered as a regulatory system that, in conjunction with the carbohydrate PTS system, coordinates central metabolism in terms of carbon and nitrogen availability (Rabus et al. 1999, Pfluger and de Lorenzo 2008, Goodwin and Gage 2014). More recent reports, however, indicate an expanding role for the PTS^{Ntr} that extends beyond regulating central metabolism. These reports have identified a role for the PTS^{Ntr} in biofilm formation in *Pseudomonas aeruginosa*, encystation in *Azotobacter vinelandii* and a membrane stress response in *E. coli* (Cabeen, Leiman, and Losick 2016, Muriel-Millan et al. 2015, Lee et al. 2015). Interestingly, the *A. baumannii* PTS^{Ntr} is incomplete and lacks the third and terminal phosphate-accepting protein, Enzyme IIA ($EIIA^{Ntr}$). Much like the case of the GigA/GigB module, where an RsbW-like kinase domain is missing, the absence of the $EIIA^{Ntr}$ protein suggests that the *A. baumannii* PTS^{Ntr} utilizes a novel

mechanism to mediate regulatory control. Indeed, the data presented in Chapter III strongly suggest that one of the key functions of the PTS^{Ntr} in *A. baumannii* is to oppose the activity of the GigA/GigB signaling axis.

The intersection of the GigA/GigB signaling axis with the PTS^{Ntr} leads to a model where *A. baumannii* finely regulates cellular activities using mechanisms that coordinate a balance between intrinsic antibiotic resistance, nutritional status (as measured by the PTS^{Ntr}) and environmental stress responses. Indeed, the lifestyle of *A. baumannii* requires the ability to thrive under the stresses imposed under a variety of environmental conditions and insults. As such, I propose that the coordination of environmental stress resistance, intrinsic antibiotic resistance and nutritional robustness represents a key feature of *A. baumannii* – and other opportunistic pathogens for that matter – that allows this organism to survive inside of the human host and cause disease.

In addition to the work described above to characterize GigA and GigB, I also conducted studies to explore another gene identified by the TnSeq experiment, *gigC*. In addition to a requirement for survival and/or growth of *A. baumannii* in the *Galleria* larvae, I demonstrated that the *gigC* gene product is required for expression of multiple genes involved with the cysteine biosynthetic pathway. The expression of one of these genes, *cysI*, is likely directly controlled by GigC binding to the promoter *in vivo*, as I was able to recapitulate binding of GigC to the *cyI* promoter using purified components *in vitro*. In addition to the control of cysteine gene expression, biochemical and biophysical analyses of recombinant GigC protein revealed that GigC likely exists as a tetramer in solution. Additionally, using differential scanning fluorimetry, I identified two small molecules, L-cysteine and sulfate ions, which increase the thermal stability

of GigC, suggesting that these two molecules may function as ligands that impact protein activity.

The importance of cysteine biosynthesis and sulfur assimilation extends beyond the requirement of cysteine as an amino acid utilized for protein translation. In other bacterial species, including both gram-negative and gram-positive organisms, the importance of sulfur metabolism is demonstrated by the findings that inhibition of proteins of the sulfur assimilation pathway lead to increased antibiotic sensitivity (Shatalin et al. 2011). Similarly, work in *Salmonella* species has uncovered that the proteins involved with the sulfur assimilation and cysteine biosynthetic pathways are required for oxidative stress resistance in this gram-negative pathogen (Alvarez et al. 2015, Turnbull and Surette 2010). While I was able to demonstrate that a strain lacking the *gigC* gene was more sensitive to N-ethyl maleimide and paraquat, a more detailed investigation of oxidative stress sensitivity in this strain is warranted before we can conclude that the GigC regulon also responds to oxidative stressors.

The aforementioned necessity of the sulfur assimilation pathway and cysteine biosynthesis for antibiotic and oxidative stress resistance likely served as the impetus for researchers to examine proteins involved in the cysteine biosynthetic pathway as potential targets for novel antibiotics (Campanini et al. 2015). As bacteria utilize a different biosynthetic pathway for cysteine than that employed by humans - bacteria combine activated sulfur (generally in the form of H_2S) with acetylated serine while humans generate cysteine from methionine – the enzymes involved in this pathway represent attractive targets for novel antibiotics since host cells do not encode similar enzymes (Griffith 1987). One important follow-up experiment to my work to characterizing the GigC protein is to determine the requirements of not only GigC for survival in more stringent mammalian models, but also to examine what role(s) are played by the

other genes in the sulfur assimilation pathway. These studies would provide valuable information regarding the utility of the previous studies on inhibitors of bacterial cysteine biosynthetic proteins to those harbored by *A. baumannii*.

As mentioned in Chapter IV, I favor the hypothesis that the attenuation of *A. baumannii* mutants lacking genes in the sulfur assimilation/cysteine biosynthetic pathway or the *gigC* gene arises not only from the inability of these strains to synthesize the amino acid cysteine, but also from an impaired ability to tolerate the oxidative stress encountered upon infection of host tissues. Interestingly, results from a similar TnSeq-like experiment that sought to identify genes required for persistence in a murine pneumonia model (Wang et al. 2014), provide some support for this hypothesis. The results presented by Wang and colleagues indicate that both the *cysD* and *cysN* genes are required for survival of *A. baumannii* in the mouse lung. Given that human serum contains ~100 μM cysteine in the mouse (Granholm, Neil Reese, and Granholm 1996), the requirement for *cysD* and *cysN* may indicate that these genes do, in fact, play an additional role beyond that of sulfur assimilation/cysteine biosynthesis.

As an opportunistic pathogen, *A. baumannii* encounters a wide variety of environmental conditions throughout the infectious cycle, ranging from surviving on surfaces in the clinical setting to colonizing indwelling medical devices and surviving inside of host tissues. Indeed, contemporary strains of *A. baumannii* have become well adapted to surviving and thriving in these various environmental niches. To do so requires the ability to coordinately regulate gene expression in order to adapt to rapidly changing conditions. The experiments discussed in the preceding chapters highlight how *A. baumannii* achieves this adaptation through the use of signal transduction networks and metabolic surveillance programs. Collectively, the work presented herein provides a solid foundation for understanding the emergence of *A. baumannii* as a

significant human pathogen and serves as a platform for future endeavors aimed at enhancing our understanding of this and other opportunistic pathogen.

CHAPTER VI

Materials and Methods

Bacterial strains and culture techniques

The bacterial strains used in these studies are listed in Table 6.1. Routine cultivation of *E. coli* and *Acinetobacter* occurred in Lysogeny Broth (LB) (10 g/L tryptone, 10 g/L NaCl, 5 g/L yeast extract) at 37 ˚C unless indicated otherwise. Solid media was prepared by the addition of 15 g/L agar prior to autoclaving. Except when noted otherwise, antibiotics were routinely added to solid and liquid medium as follows: ampicillin: 100 µg/mL (solid) and 50 µg/mL (liquid); apramycin: 50 µg/mL (solid) and 25 µg/mL (liquid); chloramphenicol: 30 µg/mL (solid) and 20 µg/mL (liquid); kanamycin, 50 µg/mL (solid & liquid); gentamicin: 10 µg/mL (solid); hygromycin: 500 µg/mL (solid) and 250 µg/mL (liquid); tetracycline: 10 µg/mL (solid) and 5 µg/mL (liquid). As needed, sterile sucrose was added solid medium to 10% (w/v) after autoclaving. Minimal medium M63 (13.6 g/L KH_2PO_4, 2 g/L $(NH_4)_2SO_4$, 0.5 mg/L $FeSO_4$–$7H_2O$, 0.02% (weight/volume, w/v) $MgSO_4$) was used for growth of bacteria on a defined medium with the sole carbon source supplied as 10 mM succinate. When needed, casamino acids or cysteine were added to the M63-Succinate medium at 0.02% (w/v) and 20 µg/mL, respectively. Strains were stored at -80 ˚C by mixing overnight cultures in LB medium 1:1 with sterile 60% (volume/volume, v/v) glycerol.

General cloning procedures

Plasmid cloning was performed according to standard practices. Plasmid purifications were conducted according to the manufacturer's recommendations using the Qiagen Mini or Maxi Prep systems with 5 or 250 mL LB cultures, respectively. For the best yield, cultures for plasmid extraction were typically grown at 37 ˚C for ~16-18 hours. Restriction enzyme digests were performed using enzymes purchased from New England Biolabs (NEB, Ipswitch, MA) in 50-µL reactions using the appropriate reaction buffer as recommended by the supplier. Best results for plasmid digestions were achieved by digestion of 2 - 3 µg of plasmid DNA in a 50-µL reaction containing 10 - 20 units of enzyme. Plasmid digestions were allowed to proceed for one hour at 37 ˚C, at which time 10 units of calf intestine alkaline phosphatase (CIP) was added to dephosphorylate the digested DNA for an additional 30 minutes at 37 ˚C. Digested plasmid DNA was resolved by agarose gel electrophoresis and the appropriate band was excised from the gel and purified using the Qiagen QIAquick gel extraction system.

The DNA to be introduced into the plasmid was routinely prepared by PCR using PrimeStar Max High Fidelity polymerase (Takara Bio) with 500 nM oligonucleotide primers (ordered from Integrated DNA Technologies, Coralville, IA) and template DNA. For PCR templates, genomic DNA was used at 50 - 150 ng per reaction, plasmid DNA was used at 5 - 10 ng per reaction, and, in the case of strand overlap extension PCR (described below), approximately 100 ng of each fragment to be combined was used. PCR products were purified following gel electrophoresis and subjected to restriction enzyme digestion as described above, with the exception that insert DNA was not treated with CIP. When necessary, oligonucleotide primers contained the desired restriction enzyme recognition sites appended to the 5' terminus of the primer to facilitate cloning. In the case when blunt-end ligations were performed, the primers

were either synthesized with a 5' phosphate group to facilitate cloning, or the PCR product was treated with 10 units of T4 Polynucleotide Kinase (NEB) for 30 minutes at 37 ˚C.

Ligation of plasmid DNA and insert DNA was performed using T4 DNA Ligase (NEB) in a 20-µL reaction according to the manufacturer's recommendations. For cohesive (sticky) end ligations, ligation reactions were incubated at room temperature for 15 minutes. For blunt-end ligations, best results were obtained when the ligation reaction was incubated overnight at 16 ˚C. Ligations reactions were subsequently transformed into chemically competent DH5α *E. coli* as described below.

Recombineering / SLiCE Cloning

In a few cases, alternative cloning methods were used for plasmid construction, including recombineering (Datsenko and Wanner 2000) and the SLiCE (Seamless Ligation in Cell Extracts) cloning method (Zhang, Werling, and Edelmann 2014). Recombineering occurred in *E. coli* strain EL350, which encodes the λRED recombinase genes under control of the λcI857 repressor. Electroporation was used to introduce DNA into the EL350 cells. Cultures were prepared for electroporation as follows. Briefly, overnight cultures of EL350 were back-diluted 1:50 into fresh LB and grown to exponential phase at 30 ˚C (to prevent expression of the recombinase genes). Upon entry into the exponential growth phase, the cultures were switched to growth at 42 ˚C for 15 minutes to induce expression of the recombinase genes. Immediately following this heat shock, cultures were placed on ice for 20 minutes. The cells were pelleted in a pre-chilled centrifuge (5500 x g for 5 min). The spent medium was removed and the cells were resuspended in ~ 0.1 volumes of ice cold deionized-distilled H_2O (ddH_2O) and centrifuged as before. A total of 4 washes were performed. Following the final wash, cells were either

resuspended in ddH_2O for immediate use or in10% glycerol, frozen in liquid nitrogen and stored at -80 ˚C for future use. Generally, recombineering was used to modify the drug resistance marker encoded by a particular plasmid (described below) and for this procedure, both plasmid DNA (approximately 100 ng) and the template DNA (approximately 100 ng) to be recombined in to the plasmid were electroporated concurrently. DNA (plasmid & insert) was mixed with 50 µL electrocompetent EL350 cells and incubated on ice for 1 minute. The cell/DNA mixture was transferred to a 2 mm gap electroporation cuvette and electroporated using a BioRad Gene Pulser with the following settings: 1.75 kV, 200 Ω, 25 µFaradays (µF). Immediately following electroporation, 900 µL SOC medium (0.5% (w/v) yeast extract, 2% (w/v) tryptone, 10 mM NaCl, 2.5 mM KCl, 10 mM $MgCl_2$, 10 mM $MgSO_4$, 20 mM glucose) was added to the electroporation cuvette and the culture was transferred to a 1.5 mL microcentrifuge tube. The cells were allowed to recover for 90 minutes at 30 ˚C prior to plating on the appropriate selective growth medium. The plates were incubated at 30 ˚C for 1 - 2 days and controls included cells transformed with no DNA, plasmid DNA alone and template DNA alone.

The SLiCE cloning method was used when the desired restriction enzymes would recognize internal sites, and thus digest, a given DNA insert to be cloned. For SLiCE cloning, plasmid DNA was digested and prepared as described above while the template DNA was amplified using primers that incorporate ≥ 15 bp of DNA homologous to the plasmid insertion site at their 5' termini. The ligation of insert and plasmid DNA in the SLiCE reaction utilizes the homologous recombination functions present in a bacterial cell extract from *E. coli* strain PPY, which encodes the λRED recombinase genes under control of an arabinose inducible promoter (P_{BAD}). To prepare the SLiCE extract, a single colony of strain PPY was inoculated into 4 mL 2XYT medium (16 g/L tryptone, 10 g/L yeast extract, 5 g/L NaCl, pH 7.2) and grown for 8 hours

at 37 ˚C. At this time, 2 mL of the starter culture was inoculated into 100 mL of fresh 2XYT broth and grown overnight at 37 ˚C. The following day, expression of the λRED recombinase genes was induced by addition of L-arabinose to a final concentration of 0.2% (w/v). The culture was induced for 2 hours at 37 ˚C and then cells were pelleted by centrifugation at 5,000 x g for 20 minutes at 4 ˚C. The spent medium was removed and cell pellet was suspended in 1 mL of ice-cold ddH_2O and transferred to 2 pre-weighed 1.5 mL LoBind Eppendorf tubes (500 µL cells per tube). The cells were pelleted by centrifugation at 10,000 x g for 5 minutes at 4 ˚C. The supernatant was removed from the cell pellets and the mass of cells (wet weight) was determined. Cell lysis was achieved by resuspending the cell pellet in CellLytic™ B Cell Lysis Reagent (Sigma product # B7435) at 1.3 mL CellLytic solution per gram of cells. Lysis was allowed to proceed for 10 minutes at room temperature with occasional mixing. Following lysis, cell debris was pelleted by centrifugation at maximum speed for 3 minutes in a table top microcentrifuge. The supernatant was then transferred to a fresh LoBind Eppendorf tube, mixed in an equal volume of sterile glycerol (i.e. a final glycerol concentration of 50% v/v) and aliquoted in 50-µL volumes into fresh LoBind Eppendorf tubes and stored at -80 ˚C.

For SLiCE cloning reactions, a 10-µL reaction was assembled on ice and contained 1 µL of 10X SLiCE Buffer (0.5 M Tris, pH 7.5, 100 mM $MgCl_2$, 10 mM dithiothreitol (DTT), 10 mM ATP), 1 µL of SLiCE extract as prepared above, digested plasmid DNA (25 - 50 ng) and insert DNA (supplied at a 10 fold molar excess to the plasmid DNA) containing ≥15 bp of homology to the desired insertion site on the target plasmid. The mixture was mixed gently and incubated at 37 ˚C for one hour before standard heat shock transformation as described below.

Colony PCR

To screen plasmids for the insertion of target DNA, colony PCRs were performed. Briefly, individual colonies were resuspended in 50 µL of sterile ddH_2O and 1 µL of this suspension was used as the template DNA for a 20-µL PCR reaction. Colony PCRs were performed with 200 nM oligonucleotide primers using the Standard Taq Polymerase (NEB). For the PCR reaction, an initial 2-minute incubation step at 95 ˚C served to lyse bacterial cells. This lysis presumably releases adequate amounts of DNA to serve as a suitable template for the PCR reaction. Standard gel electrophoresis was used to identify clones containing the desired plasmid construct or chromosomal integration.

Construction of pMJG plasmids

Vector maps for the pMJG plasmids described below can be found in Figures 6.1 and 6.2. Plasmids pMJG42, pMJG70, pMJG111 and pMJG118 do not replicate in *Acintobacter* spp. and are used for integrating DNA into the *Acinetobacter* chromosome, with the exception of plasmid pMJG111, which is a delivery plasmid for the Tn7 cassette (Figure 6.1). Maps for the freely replicating plasmids pMJG114, pMJG116, pMJG120 and pMJG126 are shown in Figure 6.2, while a map of plasmid pMJG129 can be found in Figure 3.8.

Plasmids pMJG42 (tetracycline resistance) and pMJG70 (hygromycin resistance) were both derived from plasmid pLAW344. To generate these plasmids, an inverse PCR (iPCR) reaction was performed using pLAW344 as the template DNA with primers MJG263 and MJG264. The resulting PCR product no longer contains the *cat* gene conferring chloramphenicol resistance. This PCR product was ligated to either the tetracycline resistance cassette from pXDC77 (amplified with primers MJG228 and MJG229) or the hygromycin resistance cassette

from pGEM-T-Easy.Hygro (amplified with primers MJG410 and MJG428) to generate plasmids pMJG42 and pMJG70, respectively.

The Tn7-delivery plasmid, pMJG111, was constructed by digesting plasmid pUC18T-Tn7.*hph-lux* with the restriction enzymes BamHI and HindIII to remove the luciferase cassette (*lux* genes). The resulting DNA fragment was treated with Klenow DNA polymerase to fill in the restriction sites and self-ligated to yield pMJG111. The pMJG111 plasmid has unique restriction sites KpnI and StuI in the multiple cloning site (MCS) for insertion of DNA.

Plasmid pMJG118 is a derivative of plasmid pMJG70 in which the *trpW205lacZ* cassette from plasmid pRS415 was ligated to an iPCR product generated from pMJG70 amplified with primers MJG581 and MJG582, which removes the *ampR* and *sacB* genes. The *trpW205lacZ* cassette was amplified with primers MJG338 and MJG548 and digested with ScaI prior to the ligation reaction. This plasmid is used for the generation of chromosomally integrated *lacZ* operon/promoter fusions.

The freely replicating plasmids pMJG116, pMJG120, pMJG126 and pMJG129 are apramycin-resistant derivatives of plasmid pMMB207 (pMJG116 and pMJG120) and plasmid pMMB207c (pMJG126 and pMJG129). The only difference between pMMB207 and pMMB207c is that pMMB207c contains an interruption of the *mobA* gene responsible for the mobility functions of plasmid pMMB207. For construction of plasmid pMJG116, the mCherry gene located on plasmid pXDC50 (IncQ, Cm^R, $mobA^-$) was amplified using primers MJG35 and MJG36. The resulting PCR product was digested with EcoRI and XbaI and cloned in to the same sites on plasmid pMMB207, resulting in plasmid pMJG60 (IncQ, Cm^R, $mobA^+$). Plasmids pMJG60 and pMMB207 were digested with DraI, which release a 339 base pair internal fragment from the *cat* gene. The apramycin cassette from plasmid pLLAB13B was amplified

with primers MJG733 and MJG734 and ligated into the DraI-digested parental plasmids to yield plasmids pMJG116 and pMJG120. PCR was used to identify clones in which the apramycin resistance cassette was orientated in the same direction between the two plasmids to maintain uniformity.

Plasmids pMJG114 (chloramphenicol resistant) and pMJG126 (apramycin resistant) are used for assessing promoter activity and are derived from plasmid pMMB207c. The *trpW205lacZ* cassette from plasmid pRS415 was amplified with primers MJG338 and MJG584, digested with ScaI and blunt-cloned into pMMB207c that had been digested with the enzymes HpaI and XmnI to remove the bulk of the *lacI*^{q} coding sequence, the P_{tac} promoter, and the MCS. This ligation resulted in plasmid pMJG114.

Plasmids pMJG126 and pMJG129 confer apramycin resistance and were derived from plasmid pMJG114 and the LacZ-translational fusion vector, pGS-*lac*-02, respectively. The plasmids were generated by recombineering as described above. The apramycin resistance gene used for the recombineering reaction was amplified from plasmid pMJG120 using primers MJG437 and MJG438.

Preparation of transformation-competent *E. coli*

E. coli strain DH5α was used for general cloning and routine plasmid propagation. For introduction of plasmid DNA into DH5α, cells were made chemically competent using the rubidium chloride method. Briefly, an overnight culture of DH5α was back-diluted 1:100 into 1 L of fresh LB supplemented with 20 mM $MgSO_4$ and allowed to grow until the exponential growth phase was reached (an OD_{600} of 0.4 - 0.6). Upon entry into exponential phase, the cells were chilled on ice for 20 minutes prior to centrifugation in a pre-chilled (4 ˚C) Sorval centrifuge

using an SLA-3000 rotor for 5 minutes at 4,500 x g. The supernatant was removed and the cell pellets were carefully suspended 250 mL in ice-cold transformation buffer 1 (TFB-1) (30 mM potassium acetate, 10 mM $CaCl_2$, 50 mM $MnCl_2$, 100 mM RbCl, 15% (v/v) glycerol). The resuspended cells were incubated on ice for 5 minutes and centrifuged again at 4,500 x g at 4 ˚C for 5 minutes. The TFB-1 buffer was decanted and the cell pellet was gently resuspended in 20 mL of transformation buffer 2 (TFB-2; 10 mM MOPS, 75 mM $CaCl_2$, 10 mM RbCl, 15% (v/v) glycerol pH 5.4 (adjusted with 1 M KOH)) and incubated on ice for 15 - 60 minutes. Aliquots (200 µL) of the cells were then prepared and frozen in liquid nitrogen and stored at -80 ˚C. For best results, it is imperative that all reagents, pipettes, and tubes used for this procedure be pre-chilled to ≤ 4 ˚C before coming in contact with the cells.

For introduction of DNA into these cells, a heat shock protocol was performed. Briefly, vials of frozen cells were allowed to thaw on ice (~10 minutes). The DNA to be transformed was carefully mixed with 50 µL of competent cells and incubated on ice for 30 minutes. After this incubation, the cell/DNA mixture was subjected to a heat shock in a 42 ˚C heat block for 1 minute and returned to ice for 2 minutes. After the 2-minute incubation on ice, 950 µL of SOC medium was added to the cells, which were then incubated at 37 ˚C with gentle agitation for 1 hour prior to plating onto the appropriate selective growth medium.

Electroporation of plasmids into *Acinetobacter* strains

In order to introduce plasmid DNA into *A. baumannii*, approximately 1.5 mL of an overnight culture was centrifuged in a 2.0 mL microcentrifuge tube at full speed for 1 minute. The resulting cell pellet was subjected to 3 washes with 1.5 mL of sterile, room temperature 300 mM sucrose. Centrifugation (3 minutes at full speed) followed each wash and the cell pellet

following the final wash was resuspended in 300 µL of 300 mM sucrose. At this point, the cells were electrocompetent and plasmid DNA (0.1 - 1.0 µg) was mixed with 100 µL of competent cells. The plasmid-cell mixture was allowed to incubate for ~ 1 minute at room temperature prior to electroporation using a BioRad Gene Pulser with settings of 1.8 V, 200 Ohms, and 25 µF. Immediately following electroporation, 900 µL of SOC medium was added to the electroporation cuvette and the cells were transferred to a 1.5 mL microcentrifuge tube and incubated with gentle agitation for 60 minutes at 37 ˚C prior to plating on the appropriate selective media.

Conjugation of plasmids into *Acinetobacter baumannii* AB5075

Conjugal transfer of plasmid DNA into strain AB5075 was mediated by the *E. coli* strain LW264. Strain LW264 possesses the ability to mobilize plasmids containing the origin of transfer (*oriT*) from the pRK2/pRP4 plasmids (Hmelo et al. 2015). To conjugate plasmid DNA from LW264 (donor) to AB5075 and its derivatives (recipient), a fresh colony of each strain (donor and recipient) were resuspended in 100 µL of LB medium and incubated at 37 ˚C for 30 minutes. Following this incubation, 50 µL of each donor and recipient were spotted onto the surface of a fresh, pre-warmed LB plate. As control, 50 µL of each strain alone was also spotted onto the surface of the LB plate. The plates were incubated overnight at 37 ˚C for 12-14 hours, after which time growth from each of the spots (donor alone, recipient alone, donor + recipient) was scraped and suspended in sterile PBS. Aliquots (typically 100 µL) of each bacterial suspension was then plated onto media that specifically selected for the transconjugant and contained the antibiotic marker contained on the plasmid being transferred (to select for recipient clones that acquired the plasmid) and also a second antibiotic that prevented growth of the recipient; in the case LW264, chloramphenicol (5 µg/mL) was routinely used for this purpose.

Following overnight incubation at 37 ˚C, colony PCR was performed as described above to confirm that the transconjugants had acquired the desired plasmid.

Generation of mutant strains

Gene deletions were performed using an allelic exchange plasmid (pMJG42 or pMJG70) that contains a *sacB* gene for counter-selection via growth on media containing 10% (w/v) sucrose. The desired gene knockout cassette was prepared using strand overlap extension (SOE) PCR. Primers for gene deletions are listed in Table 6.3 and knockout cassettes were constructed in two stages. Stage 1 generated two PCR products: an approximately 1 kb fragment of the 5' region of the targeted gene was amplified with primers P1 and P2 and a second ~ 1 kb fragment consisting of the 3' region of the targeted gene was amplified with primers P3 and P4. Importantly, the primer-binding regions for P2 and P3 stopped at the bases immediately preceding (P2) or following (P3) the start and stop codon of the targeted gene, respectively. Additionally the P2 and P3 primers were designed to be complementary to each other, such that each primer contains a 5' extension matching the binding region of the opposing primer. The second PCR (stage 2) was performed using the PCR products generated in stage 1 as template DNA (~100 ng each fragment) with primers P1 and P4. Generally, with the exception of the *kefF, kef, mscS, otsB* and *trkH* gene deletion cassettes, which were cloned into the unique EcoRV (blunt-end cloning) restriction site of plasmid pMJG70, primers P1 and P4 included additional bases that introduced a NotI restriction site to facilitate cloning into the unique NotI restriction site on plasmid pMJG42.

After cloning the gene deletion cassette into pMJG42 and DNA sequencing to confirm the gene knock-out cassette was designed as intended, the resulting plasmid was transformed into

E. coli strain LW264 and conjugated into *A. baumannii* strain AB5075 as described above. Selection for plasmid integration occurred on LB plates containing 10 μg/mL tetracycline and 5 μg/mL to select for transconjugants and against the donor, respectively. Transconjugants were screened by colony PCR to identify clones harboring the desired integration event. For *A. baumannii* strain 17978, the Δ*bfmS* deletion plasmid was introduced by electroporation. Once the integration of the pMJG42 derivative plasmids were confirmed by colony PCR, loss of the plasmid was achieved by the counter-selection against the plasmid using the *sacB* gene, which confers sucrose toxicity in gram-negative bacteria. Counter-selection occurred on LB plates containing 10% (w/v) sucrose and colony PCR was used to identify clones that had lost the wild type gene. Gene deletions were confirmed by sequencing.

Complementation of gene deletion strains

Two modes of complementation were generally employed: expressing a wild type copy of the gene from a plasmid or introduction of a wild type copy of the gene at the Tn7 attachment site. For plasmid-based complementation, the coding sequence of the gene in question was amplified using the primers described in Table 6.3 and cloned into the EcoRI/XbaI restriction site of plasmid pMJG120 or into the NdeI/SphI site of plasmid pMJG116 (the mCherry gene located on pMJG116 is removed by digestion with NdeI and SphI). The resulting plasmids were introduced into *A. baumannii* by electroporation as described above.

For construction of plasmids harboring the point mutant alleles of *gigA* and *gigB*, SOE PCR was used to generate the desired mutation in a similar fashion to the generation of gene deletion constructs. However, in this case the P2 and P3 primers were complementary to each

other and the requisite nucleotide changes for generating the specific amino acid changes were incorporated into these primers.

For complementation at the Tn7 site, DNA containing the entire open reading frame of the deleted gene, including approximately 200 nucleotides 5' to the annotated start codon was amplified using PCR and cloned into pMJG111 at the KpnI site, with the exception of the *ptk* complementation construct, which was blunt-cloned into pMJG111 at the StuI site. Introduction of Tn7 elements, including pMJG111 and its derivatives, was performed using a four-parental mating, including three *E. coli* strains, DH5α pMJG111 +/- gene complementation constructs, DH5α(λpir) pTNS3, and HB101 pRK600 and the recipient *A. baumannii* strain. 100-µL volumes of overnight cultures from each of the parental strains were combined in a 1.5 mL microcentrifuge tube and centrifuged at 5,000 x g for 1 minute. The supernatant was removed and the cell pellet was washed with 0.5 mL fresh LB medium and pelleted again. Following this wash, the cell pellet was resuspended in 50 µL fresh LB medium and spotted onto a plain LB plate. For transfer of Tn7 elements into *A. baumannii* strains, conjugation was allowed to occur for approximately 10 hours at 37 ˚C before the conjugation mixture was scraped from the LB plate into 1 mL sterile PBS. Approximately 100 µL of the cell suspension was plated onto LB plates containing hygromycin (500 µg/mL) and kanamycin (50 µg/mL) to select for *A. baumannii* strains containing the hygromycin resistance gene included in the Tn7 cassette. Proper integration was confirmed using colony PCR and DNA sequencing.

Bacterial Growth Curves

Growth curves were performed in a Tecan M200 microtiter plate reader. Overnight cultures of the indicated strains were back-diluted 1:100 into fresh LB (100 µL final volume)

with or without kanamycin (500 μg/mL). The optical density at 600 nm (OD_{600}) was recorded every 15 minutes for 24 hours. For each strain/condition, triplicate wells were used and data is presented as the mean value of the three wells. Lag time increase was calculated as previously described (Grosser et al. 2016). Briefly, lag time, τ, was defined as the time required to reach exponential phase, which I define as an OD_{600} of ≥ 0.02. Lag time increase was calculated for each strain by dividing the increase in lag time in LB + kanamycin relative to the lag time in plain LB medium for the mutant strain by that for WT AB5075 as follows: $(\tau_{Km} - \tau_{LB})_{mutant} / (\tau_{Km} - \tau_{LB})_{WT}$. Data presented represents the mean lag time increase from one of three independent experiments with error bars representing one standard deviation.

***Dictyostelium discoideum* culturing and infection techniques**

Dictyostelium discoideum strain AX3 was grown axenically in in HL5 medium (5 g/L proteose peptone, 5 g/L thiotone E peptone, 5 g/L yeast extract, 10 g/L glucose, 0.35 g/L $Na_2HPO_4 \cdot 7\ H_2O$, 0.35 g/L KH_2PO_4, pH 6.4-6.7) at room temperature without shaking. For the *Dictyostelium* plate test (DPT), amoebae were resuspended and centrifuged in a 50 mL centrifuge tube at 1000 x g for 5 minutes. Spent medium was aspirated by vacuum and the cell pellet was resuspended in 1 volume of SorC buffer (0.2% w/v KH_2PO_4, 0.055% w/v $Na_2HPO_4 \cdot 7\ H_2O$, 50 μM $CaCl_2$, pH 6.0). Cells were counted using a hemacytometer and set to a density of 10^5 cells/mL in SorC buffer. For preparation of bacterial cultures for the DPT, the OD_{600} of overnight cultures of bacteria were recorded and the equivalent of 5.5 OD units were centrifuged at full speed for 1 minute in a 1.5 mL microcentrifuge tube. The supernatant was removed and the cell pellet was washed with 1 mL SorC buffer. Following centrifugation (1 minute at full speed), the supernatant was removed and the resulting cell pellet was suspended in 1 mL fresh

SorC buffer. To each bacterial suspension, *D. discoideum* cells were added to a final density of 500 cells/mL. 200 µL of the resulting mixture were spread onto SM/5 plates (2% (w/v) agar, 0.2% (w/v) peptone, 0.2% (w/v) yeast extract, 0.19% (w/v) KH_2PO_4, 0.1% (w/v) K_2HPO_4, 0.02% (w/v) $MgSO_4 \cdot 7\ H_2O$, 0.2% (w/v) glucose). The 'ethanol stimulated virulence' phenotype was assessed on SM/5 plates containing 1% (v/v) ethanol. Plates were incubated at room temperature for 5 days and photographed. The ImageJ program was used to measure the area (in pixels) of plaque sizes formed on the plates containing *E. coli* strain MC4100.

Galleria mellonella infection

Final instar stage larvae of *G. mellonella* were purchased from Knutson's Live Bait (www.knutsonlivebait.com, Brooklyn, MI). Infection of *G. mellonella* was performed as previously described (Jacobs, Thompson, Black, et al. 2014) using a Hamilton syringe outfitted with a repeat dispensing unit to deliver 10 µL of inoculum into one of the terminal prolegs. Bacterial suspensions were prepared from overnight cultures. Briefly, the OD_{600} was recorded and the equivalent of 10^8 CFU of each strain was added to a 1.5 microcentrifuge tube using a conversion factor of 1 OD = 2.42 x 10^8 CFU. The aliquots were pelleted at full speed for 1 minute in a table top centrifuge, the supernatant was removed and the cell pellet was resuspended in 1 mL of sterile phosphate buffered saline (PBS).

For larval survival experiments, larvae were inoculated with either 10^6 or 10^5 CFU of the indicated strain and maintained in the dark at 37 ˚C and assessed for survival daily for 6 days. Larvae that were non-responsive to gentle prodding were considered dead and were removed from the experiment. All larval survival included two control groups: larvae that were not injected and larvae that were injected with sterile PBS. In the event that more than 2 larvae from

either control group died during the course of the experiment, the entire experiment was considered invalid and results were not used. Significance of survival differences was assessed using the log rank test.

For bacterial growth/recovery experiments, larvae were infected with ~10^6 colony forming units (CFU) of the indicated strains. Larvae (n = 2 per time point) were homogenized with a Benchtop D1000 homogenizer in 2 mL of PBS immediately following infection (t = 0) and after 4 hours (t = 4) incubation at 37 ˚C. Homogenates were diluted and plated onto LB agar with 5 μg/mL chloramphenicol to eliminate the growth of the normal flora of *G. mellonella* without impacting the growth of *Acinetobacter* spp. Bacterial growth is represented as the ratio of CFU per larvae at t = 4 divided by the CFU at t = 0.

For assessing bacterial growth in hemolymph, 10 μL of the indicated strains of bacteria (10^4 CFU) were mixed with 90 μL freshly collected hemolymph. Larvae were lanced and the hemolymph was collected and pooled from several larvae prior to bacterial inoculation. Bacteria-hemolymph mixtures were incubated at 37 ˚C and bacteria were enumerated at the indicated times. Hemolymph experiments were repeated three times and the results of a single experiment are shown.

Transposon mutant library and TnSeq experiment

The *A. baumannii* AB5075 transposon mutant library used in these studies was kindly provided by the Manoil lab at the University of Washington (Gallagher, Shendure, and Manoil 2011, Gallagher et al. 2015). Aliquots of the transposon library (maintained at -80 ˚C) were thawed on ice for 30 minutes, diluted in PBS and ~10^6 CFU were inoculated into either 5 mL of LB or into *G. mellonella* larvae. The LB and *G. mellonella* pools were grown at 37 ˚C for 4

hours, at which time larvae were homogenized as described above and aliquots of the LB cultures or larval homogenates were plated onto LB agar with tetracycline (10 μg/mL) to eliminate the normal bacterial flora of *G. mellonella*. The plates were incubated at 37 ˚C for 4 hr. Bacteria were carefully scraped from the plates into 1.5 mL sterile PBS and genomic DNA was prepared from using the QIAGEN DNEasy kit according to the manufacturer's recommendation.

Preparation of the TnSeq sequencing library was performed and sequenced as previously described (Gallagher, Shendure, and Manoil 2011). Following the mapping of reads to the AB5075 genome, genes with less than five unique insertions mapped in the LB sample were omitted from further analysis. To identify underrepresented genes following growth in *G. mellonella*, the number of reads per gene from the *G. mellonella* sample was divided by the number of reads per gene from the LB sample to generate a read ratio (RR). A RR of 0 is reported for cases when no reads mapped to a given gene in the *G. mellonella* sample. A hit was defined as a gene with a RR less than 0.1; i.e. a 1 – log reduction in the number reads following passage through *G. mellonella*. The library preparation, sequencing and initial bioinformatic processing was performed by Larry Gallagher at the University of Washington

Biofilm attachment assays

Biofilm formation was assessed using the crystal violet attachment method essentially as previously described (Djordjevic, Wiedmann, and McLandsborough 2002). Briefly, overnight cultures of bacteria were diluted 1:100 into fresh LB medium in a 96 well microtiter plate in a volume of 100 μL/well. Each strain was added to triplicate wells and the plate was incubated at 37 ˚C with out shaking for 24 hours. Following this growth period, the OD_{600} was recorded using a Tecan M200 plate reader and non-adherent material was removed from the plate by shaking.

The wells were carefully washed 4 times with deionized H_2O and allowed to dry on absorbent paper towels for ~15 minutes at room temperature. Once dry, 100 µL of crystal violet solution (0.1% w/v in 0.25% (v/v) acetic acid) was added to each well and incubated on a rotating shaker for 15 minutes at room temperature. Following this incubation, the staining solution was removed and the plate was again washed 4 times with deionized H_2O and allowed to dry. Upon drying, the remaining crystal violet was dissolved in 100 µL of 70% (v/v) ethanol and the absorbance was read at 595 nm. Biofilm formation was calculated as the ratio between the crystal violet (OD_{595}) and bacterial density (OD_{600}) in order to account for any growth differences between strains.

Antibiotic susceptibility testing

The antibiotic sensitivity testing presented in Table 2.4 was performed at the NorthShore University Hospital in accordance with CLSI guidelines (CLSI). For this particular experiment, Disc Diffusion Assay (DDA) and E-test experiments were repeated 5 times and the data is reported as the mean zone of inhibition (DDA)/minimal inhibitory concentration (E-test) +/- standard deviation.

Efficiency of Plating Experiments

Overnight cultures of the indicated strains were back-diluted 1:100 into fresh LB to a final volume of 3 mL. After 2 hours of out-growth at 37 ˚C, aliquots of the cultures were serially diluted in sterile ddH_2O and 10-µL volumes of the dilution series were spotted onto LB agar plates containing the indicated stressors as follows: for acidic pH, LB medium adjusted to pH 5.5 with HCl prior to autoclaving; kanamycin and gentamicin were added at 500 µg/mL and 10

μg/mL, respectively; zinc chloride ($ZnCl_2$) was added to 1.25 mM. The plates were incubated in a biological safety cabinet until the spots were dry. When necessary, apramycin (10 μg/mL) and IPTG (0.1 mM) were added for plasmid maintenance and expression of complementing plasmids, respectively. Efficiency of plating (EOP) was calculated by dividing the CFU recovered on stress medium by the CFU recovered on plain LB grown at 37 ˚C. EOP experiments were repeated at least three times and data presented represent the mean EOP from a representative experiment with error bars representing one standard deviation.

Analysis of proteins

For analysis of bacterial whole cell extracts, cell lysates were prepared as follows. The OD_{600} of bacterial cultures were determined and the equivalent of 1 OD_{600} unit of the culture was pelleted in a 1.5 mL microcentrifuge tube. The spent medium was removed and the cell pellet was dissolved in 100 μL of 1X SDS-PAGE sample buffer (50 mM Tris-HCl, pH 8.0, 2% (w/v) SDS, 10% (v/v) glycerol, 1% β-mercaptoethanol (β-ME), 12.5 mM EDTA, 0.02% (w/v) bromophenol blue). Prior to electrophoresis, cell lysates were boiled for 5 minutes and centrifuged at maximum speed for 1 minute at room temperature. For electrophoresis, 10 μL or 7.5 μL of the whole cell lysates were resolved through gels containing 10 or 15 wells, respectively. For visualization of purified proteins, gel lanes were routinely loaded with 0.5 - 5 μg of protein.

For the separation of phosphorylated proteins, SDS-PAGE gels were prepared with 50 μM Phos-tag™ acrylamide (Wako-Chem product AAL-107) and 100 μM $MnCl_2$ according to the manufacturer's recommendations. The Phos-tag™ molecule specifically binds to the phosphate moiety in the presence of divalent cations, such as Zn^{2+} and Mn^{2+}, leading to a

reduced migration of phosphorylated proteins through the gel (Kinoshita et al. 2006). On several occasions, preparation of gels containing the Phos-tag™ moiety produced gels with an uneven interface between the resolving and stacking gels. This phenomenon was attributed to poor polymerization of the resolving gel containing the Phos-tag™/$MnCl_2$, and was alleviated when the resolving gels were overlaid with isopropanol (~ 1 mL) that had been degassed for 10 minutes by bubbling compressed nitrogen through the isopropanol.

Staining of protein gels

Routine staining of protein gels was performed with Coomassie Blue R-250. Gels were removed from the electrophoresis cassette and fixed in a solution of 25% isopropanol, 10% acetic acid in ddH_2O for 30 - 60 minutes. Gels were then stained in a solution of 60 mg/L Coomassie Blue R-250 in 10% acetic acid in ddH_2O. Bands typically appeared within 30 - 60 minutes; however adequate staining occasionally required longer incubation periods, particularly for gels containing Phos-tag™ acrylamide. Once the desired level of intensity was achieved, the gel was destained in a solution of 10% acetic acid for a minimum of 2 hours.

When required, a more sensitive detection technique, silver staining, was performed essentially as described previously (Shevchenko et al. 1996). Briefly, the gel was fixed in a solution of 50% (v/v) methanol in 5% (v/v) acetic acid for 20 minutes followed by successive 10-minutes washes in 50% methanol and ddH_2O. The gel was sensitized for silver staining by a 1-minute incubation in 0.02% sodium thiosulfate. Following two 1-minute washes with ddH_2O, the gel was submerged in chilled 0.1% silver nitrate solution (4 ˚C) and incubated for 20 minutes at 4 ˚C. Following this incubation, the gel was washed twice for 1 minute each with ddH_2O. Bands were visualized using a developing solution (0.04% formaldehyde in 2% sodium

carbonate) with intense shaking. In order to achieve a clear background staining of the gel, the developing solution was discarded upon the formation of a yellow color and replaced with a fresh portion. Once the desired intensity of staining was achieved, development was stopped by discarding the reagent and placing the gel in a solution of 5% acetic acid.

Protein Immunoblotting/Western Blotting

For immune detection of proteins following SDS-PAGE, proteins were transferred to nitrocellulose membranes (Amersham Protran NC Membrane, GE Healthcare product 84-875) using a BioRad SemiDry transfer apparatus. Prior to transfer, the gel, membrane and 2 pieces of filter paper were soaked in 1X transfer buffer (39 mM glycine, 48 mM Tris base, 0.0375% (w/v) SDS, 20% (v/v) methanol) for ~5 minutes prior to assembly. The order of assembly (starting from the bottom) was as follows: filter paper - membrane - gel - filter paper. Transfer was performed at 8 V for 30 minutes and then 15 V for 60 minutes. Membranes were subsequently blocked in 5% (w/v) powdered milk in 1X TTBS (20 mM Tris-HCl, pH 7.6, 137 mM NaCl, 0.05% (v/v) Tween 20) for 2 hours at room temperature or overnight at 4 ˚C. Following blocking, membranes were washed twice with 1X TTBS for 5 minutes. Antibodies were diluted to the appropriate concentration in 2% (w/v) powdered milk in 1X TTBS; the affinity purified anti-GigB antibodies (described below) were used at a 1:10,000 dilution and the secondary antibody, goat anti-rabbit IgG, was used at a 1:1000 dilution. Primary antibodies were incubated with the membranes for 2 hours at room temperature or overnight at 4 ˚C. Following primary antibody exposure, membranes were washed twice for 5 minutes and once for 15 minutes in 1X TTBS at room temperature. HRP-conjugated secondary antibody exposure occurred for one hour at room temperature. The membranes were subsequently washed once for 15 minutes and 4

times for 5 minutes each in 1X TTBS. The SuperSignal West Pico Chemiluminescent Substrate (ThermoFisher Scientific) was used for visualization using a LAS-3000 Imaging System (Fujifilm).

When immunoblots were performed on samples separated by Phos-tag^{TM} SDS-PAGE, gels were soaked for 10 minutes with gentle agitation at room temperature in 50 mL of transfer buffer containing 1 mM EDTA followed by a second wash in 1X transfer buffer with out EDTA prior to transfer. The EDTA wash facilitates transfer of phosphorylated proteins from the gel as the Phos-tag^{TM} molecule only binds phosphate groups in the presence of divalent cations such as Zn^{2+} or Mn^{2+}.

Antibodies

Recombinant GigB protein was used to generate polyclonal antibodies raised in rabbits. Briefly, the purified proteins were separated via SDS-PAGE and recovered from the gel as described previously (Burgess 2009). Briefly, proteins were visualized by submerging the gel in a solution of 0.25 M KCl containing 1 mM DTT for 5 minutes at room temperature followed by destaining in cold (4 ˚C) ddH_2O. The KCl solution causes SDS precipitation, and yields white bands corresponding to proteins following destaining. The appropriate band was excised from the gel and placed into 2.0 mL microcentrifuge tubes. The gel slices were crushed using a Teflon pestle and mixed with protein elution buffer (50 mM Tris, pH 8.0, 0.1 M EDTA, 1 mM DTT, 0.15 M NaCl, 0.1% (w/v) SDS) and incubated at room temperature with gentle agitation overnight.

The following day, samples were centrifuged for 5 minutes at room temperature in a tabletop microcentrifuge. The supernatants were transferred to fresh microcentrifuge tubes and

centrifuged again to remove residual acrylamide. Four volumes of cold acetone (-20 ˚C) was added in order to precipitate the protein and the tubes were incubated in a dry ice/ethanol bath for 20 minutes. The samples were allowed to thaw in an ice water bath for approximately 5 minutes prior to centrifugation at full speed for 5 minutes at room temperature. The resulting protein pellet was washed with 1 mL of 80% (v/v) acetone in water to remove residual SDS from the sample. The tubes were air-dried on an adsorbent paper towel for 10 minutes at room temperature. Proteins were re-folded in 20 μL refolding buffer (50 mM Tris, pH 7.9, 20% (v/v) glycerol, 0.1 mM EDTA, 1 mM DTT, 0.15 M NaCl, 0.1% (v/v) SDS) containing 6 M guanidium hydrochloride for 20 minutes at room temperature, at which time 1 mL of refolding buffer lacking guanidium hydrochloride was added. The refolded protein was used as the antigen for immunization of one rabbit at the Pocono Rabbit Farm and Laboratory (Canadensis, PA).

Affinity purification of anti-GigB antibodies

The rabbit serum containing polyclonal antibodies recognizing GigB were subjected affinity purification prior to their use as a reagent for western blot analysis. Briefly, a HiTrap NHS-activated column (1 mL resin volume, GE Healthcare) was prepared for protein conjugation as recommended by the manufacturer. A peristaltic pump set to a flow rate of ~1 mL/min was used for all steps. A 6 mL wash with cold 1 mM HCl was followed with a 6 mL wash with conjugation buffer (0.2 M $NaHCO_3$, 0.5 M NaCl, pH 8.3). Recombinant protein (1-2 mg) was diluted into 11 mL of conjugation buffer and circulated through the column for ~2 hours at room temperature. After conjugation of the protein, the column was inactivated with alternating washes (6 mL each) with buffer A (0.5 M ethanolamine, 0.5 M NaCl, pH 83) and buffer B (0.1 M NaOAc, 0.5 M NaCl, pH 4.0). A total of three cycles (6 total washes) was

performed. After the second wash with buffer A, the flow was stopped and incubated at room temperature for 15 minutes prior to continuing the wash cycles. After the third and final wash with buffer B, the column was washed with 6 mL of PBS.

For affinity purification of antibodies, 13.5 mL of antiserum was mixed with 1.5 mL 10X PBS and circulated through the column for 1.5 hours. The column was then washed twice with 50 mL of PBS. The PBS washes were recirculated for one hour each. Captured antibodies were eluted from the column with elution buffer (1 M Glycine, 0.5 M NaCl, pH 2.5). 10 elution fractions were collected (6 drops each) and were immediately neutralized with 300 µL 1 M Tris, pH 8.5. The fractions were analyzed by SDS-PAGE and fractions containing antibodies were purified and desalted into PBS using PD-10 columns (Pharmacia). Briefly, the PD-10 column (5 mL bed volume) was equilibrated with five 5-mL washes of PBS, the pooled antibody fractions were added to the column in a 2.5-mL volume and eluted with 3.5 mL PBS. Antibodies were aliquoted into ~350-µL volumes and stored at -20 ˚C.

Purification of Recombinant Proteins

The coding sequences of the proteins to be purified were cloned in to pET24b at the NdeI and XhoI sites using the oligonucleotide primers as listed in Table 6.3. Recombinant GigB, GigC and EI^{Ntr} were purified using nickel-affinity chromatography using the 6X-Histidine tag encoded by the pET24b vector backbone while recombinant NPr protein was purified using Streptactin Sepharose Resin (Iba Lifesciences). For generating the Strep-tag sequence at the C-Terminus of NPr, the *ptsO* gene was amplified with primers MJG997 and MJG998. Primer MJG998 contains additional nucleotides to incorporate the 8-amino acid strep-tag sequence, WSHPQFEK, and a stop codon at the end of the NPr coding sequence. PCR products were digested with NdeI and

XhoI and cloned into pET24b cut with the same enzymes, with the exception of the *ptsP* gene (EI^{Ntr} protein), which was cloned via the SLiCE method (Zhang, Werling, and Edelmann 2014) as described above. Plasmid constructs were confirmed via DNA Sequencing and introduced into chemically-competent *E. coli* BL21(DE) by heat shock transformation. Overnight cultures grown at room temperature were back-diluted 1:100 into 1 L of LB broth. Following nine hours of outgrowth at room temperature, protein expression was induced by the addition of IPTG to 25 μM and grown overnight.

Following induction, cells were harvested by centrifugation at 6,000 x g for 10 minutes at 4 ˚C. The resulting cell pellet was resuspended in 20 mL metal chelate affinity chromatography (MCAC) buffer (50 mM Tris-HCl pH 8.0, 150 mM NaCl, 5 mM $MgCl_2$, 1 mM DTT) and incubated on ice for 30 - 60 minutes with lysozyme (1 mg/mL), DNAse I (10 μg/mL) and Protease Inhibitor Cocktail (Pierce). Cells were lysed by three passages through a French Press Pressure Cell at ~20,000 PSI. The resulting lysate was cleared by centrifugation at 25,000 x g for 30 minutes at 4 ˚C in a Sorval SS-34 rotor to separate the soluble and insoluble protein fractions. The supernatant (i.e. the soluble protein fraction) was filtered through a 0.45 μm syringe filter. The cleared lysate was then subjected to affinity purification using Nickel-NTA resin (Qiagen) or Streptactin resin (IBA Lifesciences) as described below.

For the purification of 6XHistidine-Tagged (His-tagged) proteins (GigB, GigC and EI^{Ntr}), cell lysates were mixed with 1 mL of pre-equilibrated Nickel-NTA resin and incubated at 4 ˚C with gentle end-over-end mixing for 60 minutes to allow for adsorption of His-tagged proteins to the resin. At this stage, imidazole was added to a final concentration of 20 mM to reduce non-specific binding of proteins to the resin. The mixture was applied to a chromatography column and allowed to enter by gravity flow. The column was subsequently washed with 50 mL of

MCAC buffer containing 20 mM imidazole. Aliquots of the flow-through and wash samples were retained for SDS-PAGE analysis. His-tagged proteins were eluted by addition of increasing concentrations of imidazole in MCAC buffer. Concentrations of 50, 100, 200 and 500 mM imidazole were used for protein elution and 5 x 1-mL fractions of each concentration were collected.

For purification of NPr-strep, the cleared lysate was added directly to a chromatography column containing 8 mL pre-equilibrated Streptactin resin and allowed to enter the column by gravity flow. The column was then washed with 5 column volumes of MCAC buffer. Bound proteins were eluted with 3 column volumes of MCAC buffer containing 2.5 mM desthiobiotin. For elution of NPr-Strep, 6 fractions of 4 mL each were collected.

Aliquots of each elution fraction were assessed by SDS-PAGE and fractions containing the target protein were pooled and concentrated using ultrafiltration centrifugation (Amicon Ultra). Concentrated protein fractions were desalted into MCAC buffer using PD-10 desalting columns as described above. Recombinant EI^{Ntr} protein was stored in MCAC buffer lacking $MgCl_2$, as previous reports have shown that EI^{Ntr} requires Mg^{2+} ions for activity and dimerization (Rabus et al. 1999). For GigB::His, the 200 mM imidazole elution fraction was used, while for GigC::His and EI^{Ntr} proteins, the 100 mM imidazole elution fractions were used.

Protein concentration was measured via the Bradford Assay as recommended by the manufacturer (BioRad). Briefly, a standard curve of bovine serum albumin (BSA) was prepared in MCAC buffer with concentrations ranging from 25 to 500 µg/mL. 10 µL of each standard and purified protein were added to triplicate wells of a 96 well microtiter plate and mixed with 200 µL of Bradford reagent. The plate was incubated at room temperature for 5 minutes prior to reading the absorbance at 595 nm in a Tecan microtiter plate reader. Protein concentrations were

determined by generating a standard curve based on the values recorded for the BSA standards. Aliquots of the purified proteins were flash frozen in liquid nitrogen and stored at -80 ˚C for further use.

Mass Spectroscopy analysis of GigB::His purified from AB5075

A 6xHistidine tag was added to the coding sequence of the WT *A. baumannii gigB* coding sequence using primers MJG768 and MJG750 and cloned into the NdeI/SphI restriction sites of plasmid pMJG116. The resulting *gigB::His* plasmid was introduced into AB5075 via electroporation. Expression of the GigB::His allele was induced by the addition of 0.1 mM IPTG. Exponentially growing cells (1 L) were collected by centrifugation at 6,000 x g for 10 minutes and processed for nickel-ion affinity column chromatography as described above. GigB::His was eluted with MCAC buffer containing 200 mM Imidazole. Aliquots of the elution fractions were resolved by SDS-PAGE, silver stained as described above and the band corresponding to GigB was excised and subjected to Mass Spectroscopic Analysis at the Taplin Lab at Harvard Medical School.

***In vitro* Phospho-transfer Assays**

Phospho-transfer assays were performed in 20-µL reactions containing 5 µg of the indicated proteins in reaction buffer (50 mM Tris, 5 mM $MgCl_2$, 2 mM DTT). As previous reports have shown that the *E. coli* EI^{Ntr} protein requires Mg^{2+} ions for activity and dimerization, and the recombinant EI^{Ntr} protein used in these studies were stored in the absence of Mg^{2+}, each reaction component was prepared in the Mg^{2+}-replete reaction buffer separately and incubated for 15 minutes at 30 ˚C prior to reaction assembly to allow for activation of EI^{Ntr} (Rabus et al.

1999). Where indicated, phosphoenolpyruvate (Sigma) was added at the indicated concentrations. Reactions progressed for 30 min at 30 ˚C, at which time reactions were terminated by addition of 10 µL 3X-concentrated SDS-PAGE Sample Buffer. Samples were resolved through SDS-PAGE gels polymerized with 50 µM Phos-tag™ acrylamide and 100 µM $MnCl_2$ and stained with Coomassie Blue as described above. For these experiments, samples were not boiled prior to SDS-PAGE, as the phosphorylation of NPr was found to be heat-labile.

Construction of pRK75 plasmid library

The genomic fragment library plasmid pool, pRK75, was derived from the broad host range plasmid pRK415 (Keen et al. 1988). For library preparation, *A. baumannii* AB5075 genomic DNA was partially digested with Sau3AI. Briefly, five 50-µL reactions were prepared with each reaction containing ~5 µg of AB5075 gDNA in reaction buffer (New England Biolabs Buffer 1). A serial dilution of Sau3AI enzyme was performed and added to the reaction tubes. The enzyme concentrations used ranged from 1 unit to 0.0625 units of enzyme. Upon enzyme addition, the tubes were carefully mixed and incubated at 37 ˚C for 30 minutes, at which time 5 µL of 0.5 M EDTA (pH 8.0) was added to terminate the digestion reaction. The digested DNA was separated by agarose gel electrophoresis, fragments ranging in size from ~5 – 10 kb were excised from the gel and cloned into the unique BamHI site of pRK415. Following transformation into *E. coli* DH5α, recombinants were pooled and plasmid DNA was extracted via miniprep. Approximately 1 µg of the resulting plasmid pool, named pRK75, was used for introduction into *A. baumannii* as described below.

NPr-over expression experiment

A. baumannii AB5075 harboring pMJG120.*ptsO* was electroporated with the pRK75 library (~1 μg of plasmid DNA) and cells containing both plasmids were selected on LB plates with apramycin (50 μg/mL) and tetracycline (10 μg/mL). The resulting colonies (~8,000 clones) were carefully scraped from the plates into fresh LB medium and aliquots were mixed 1:1 with 60% (v/v) glycerol and frozen at -80 ˚C. For the NPr-over expression experiment, an aliquot of this pRK75 library was thawed on ice for 30 minutes and 10 LB plates containing apramycin (50 μg/mL), tetracycline (10 μg/mL), kanamycin (500 μg/mL) and 50 μM IPTG were spread with 100 μL a 10^{-4} dilution to select for clones harboring DNA fragments that suppressed the NPr-induced toxicity. As a control, the library was also spread onto LB plates containing only 50 μg/mL apramycin and 10 μg/mL tetracycline. Following overnight growth, colonies were either isolated for standard DNA sequencing or, alternatively, for high-throughput (Illumina) DNA sequencing, the growth from the entire plate was carefully scraped from the two groups of plates (with and without kanamycin) and plasmid DNA was collected via miniprep.

For standard sequencing, plasmid DNA from the purified clones was prepared by miniprep and the resulting pRK75 plasmid was transformed into DH5α via heat shock as described above. Plasmid DNA was subsequently purified from the DH5α clone and subjected to standard dideoxy-sequencing by the DNA Sequencing Core facility at the University of Chicago.

For high-throughput sequencing analysis, a PCR was performed using primers MJG485 and MJG487 to amplify the insert region of the pRK75 clones to enrich the samples for the insertions of the pRK75 library. Illumina library preparation and sequencing was performed by the University of Chicago Functional Genomics Core Facility. Results were analyzed using the Geneious program. The reads from each sample (control/no kanamycin and kanamycin-selected)

were assembled to the AB5075 genome and plasmid sequences using the default setting in Geneious version 10.08. Areas of enrichment were visualized using the coverage graph tool of Geneious.

RNASeq Experiment

Following a 1:100 back dilution of overnight cultures into 30 mL of fresh LB medium, exponentially growing bacteria (OD ~ 0.6) were exposed to kanamycin (500 µg/mL) or left untreated for 30 minutes. After this treatment, 1/10 volume (3 mL) of ice-cold 10% phenol in ethanol was added to each culture to stabilize cellular RNA. Cells were collected by centrifugation, the supernatant was removed and the cell pellet was frozen in liquid nitrogen. The frozen cell pellets were stored at -80 ˚C until RNA extraction. To extract total RNA, 500 µL of ice cold Solution I (10 mM EDTA, 0.05 M Sodium Acetate (NaOAc), pH 4.5) was added to the thawed cell pellets and quickly mixed. 300 µL of the resulting mixture was combined with 300 µL pre-warmed (65 ˚C) Solution II (2% (w/v) SDS, 0.01M NaOAc, pH 4.5). This solution was inverted 5 times and 500 µL was added to 600 µL of hot (65 ˚C) buffer-saturated acid phenol (pH 4.5). The phenol/cell lysate mixture was mixed by inversion several times and incubated for 5 minutes at 65 ˚C. Phase separation was achieved by a 5-minute centrifugation at full speed in a tabletop microcentrifuge at 4 ˚C. The upper, aqueous phase containing total RNA was extracted a second time with an additional 600-µL volume of hot acid phenol. The samples were again mixed and incubated at 65 ˚C for 5 minutes prior to centrifugation. Following the second centrifugation, the aqueous phase was extracted with 500 µL ice-cold phenol/chloroform/isoamyl alcohol (25:24:1), pH 4.5. After another 5-minute centrifugation, the aqueous phase was transferred to microcentrifuge tube containing 500 µL chloroform/isoamyl alcohol (24:1) and

centrifuged again. The aqueous phase was subsequently precipitated in an ice-cold NaOAc/Ethanol mixture (40 µL 3 M NaOAc, pH 4.5 + 900 µL absolute ethanol) and incubated at -20 ˚C for ≥ 30 minutes, after which time the nucleic acid was pelleted by centrifugation at maximum speed for 20 minutes at 4 ˚C. The resulting RNA pellet was washed two times with 1 mL ice-cold 75% ethanol. Following the final wash, the tube containing the RNA pellet was inverted onto absorbent filter paper and allowed to dry for 15 minutes at room temperature. Once dried of residual ethanol, the sample was dissolved in 100 µL of molecular biology grade H_2O.

Contaminating DNA was removed with the TURBO DNAse kit according to the manufacturer's recommendations (Ambion). Briefly, 10 µg of RNA was mixed with 5 µL 10X buffer and 1 µL of TURBO DNAse was added. The samples were mixed and incubated at 37 ˚C for 30 minutes. The DNAse was inactivated by the addition of 5 µL of DNAse Inactivation reagent and incubated with occasional mixing for 5 minutes at room temperature. The samples were centrifuged at 10,000 x g for 1.5 minutes to pellet the DNAse Inactivation reagent and the supernatant, containing DNA-free RNA was retained and subjected to a second round of DNAse treatment.

cDNA library preparation and Illumina sequencing were performed on biological triplicate samples for each strain/condition by the Functional Genomics Core Facility at the University of Chicago. In order to assess gene expression, the Rockhopper program (McClure et al. 2013) was used to map reads to the AB5075 genome. The individual read counts per gene from each of the biological triplicate samples were exported from the Rockhopper program and subsequently used as input for differential gene expression analysis using the Degust program to assess gene expression values across the various samples and conditions. Venn Diagrams of differentially expressed genes were generated using the VennT program. The Degust and VennT

programs are curated by the Victorian Bionformatics Consortium and are maintained at http://www.vicbioinformatics.com/software.shtml.

Measurement of β-galactosidase levels (Miller Assays)

The standard Miller assay was used to assess levels of β-galactosidase (β-gal) in strains harboring *lacZ*-fusions (Miller 1972). Briefly, exponentially growing cultures (OD_{600} between 0.4 - 0.8) were incubated on ice for 20 minutes to halt cellular activity. Following this incubation, the OD_{600} of each culture was recorded and 100 µL of culture was combined with 900 µL Z-buffer (60 mM Na_2HPO_4, 40 mM NaH_2PO_4, 10 mM KCl, 1 mM $MgSO_4$, 38.3 mM β-ME). The β-ME was added to the Z-buffer just prior to use. Cells were permeabilized by the addition of 2 drops of chloroform and 1 drop of 0.1% SDS, vortexed vigorously for 10 seconds and incubated at 28 ˚C for 5 minutes. Following permeabilization, 200 µL *o*-nitrophenyl-β-D-galactopyranoside (ONPG) solution (4 mg/mL in 0.1 M phosphate buffer, pH 7.0) was added to each tube and mixed briefly by vortexing and incubated at 28 ˚C as the reaction progressed. The time of ONPG addition was recorded. Tubes were monitored for development of yellow color and when adequate color had developed (an OD_{420} value between 0.5 – 1.2 is ideal), the time was recorded and reactions were stopped by the addition of 500 µL of 1 M sodium carbonate (Na_2CO_3). The absorbance of each reaction was then determined at 420 nm and 550 nm. β-gal levels were then calculated in Miller units according to equation 1.

Equation 1: $$Miller\ Units = 1000 \times \frac{A_{420} - (1.75 \times A_{550})}{t \times 0.1 \times A_{600}}$$

where *t* = reaction time in minutes. For each condition tested, triplicate samples from each culture were prepared and data is presented as the mean value from these triplicate measurements.

FPLC analysis of recombinant GigC protein

For determination of the molecular weight of recombinant GigC::His protein, the purified protein was subjected to size exclusion chromatography (SEC) using an AKTA Purifier Fast Performance Liquid Chromatography (FPLC) instrument (GE Lifesciences). A Superose 12 10/30 SEC column (GE Lifesciences) was used. The mobile phase consisted of MCAC buffer lacking glycerol. The column void volume (V_0) and total column volume (V_C) were determined by measuring the elution volumes of blue dextran and acetone, respectively. The column was equilibrated by determining the elution volume (V_E) for proteins of known molecular weight (MW) (BioRad Gel Filtration Standard, BioRad product number 151-1901). The column affinity for a given protein (K_{av}) was determined using equation 2.

Equation 2: $$K_{av} = \frac{(V_E - V_O)}{(V_C - V_O)}$$

A standard curve was generated using the $\log_{10}$ MW of the proteins in the equilibration standards and the empirically determined K_{av} values. This standard curve was then used to determine the molecular weight of GigC::His using equation 3.

Equation 3: $$MW\ in\ kilodaltons = 10^{\left(\frac{Kav - \text{slope}}{y\ intercept}\right)} \div 1000$$

Electrophoretic Mobility Shift Assays of GigC and the *cysI* promoter region

For determination of GigC binding to *cysI* promoter DNA, an electrophoretic mobility shift assay (EMSA) was performed. The *cysI* promoter region was amplified using primers MJG896 and MJG897, both of which contain the infrared dye, IRD700, appended to the 5' terminal nucleotide for infrared visualization. EMSA reactions were prepared in reaction buffer (20 mM HEPES, 100 mM KCl, 4 mM $MgCl_2$, 0.2 mM EDTA, 0.5 mM DTT, 6% (v/v) glycerol, 20 µg/mL salmon sperm DNA, 0.1 mg/mL BSA). The EMSA Reaction buffer was prepared as a 5X concentrate and aliquots were stored at -20 ˚C. Reactions were prepared with 100 fmole labeled DNA probe and the indicated amounts (in pmole) of recombinant GigC::His protein and incubated in the dark for 30 minutes at room temperature. Following this incubation, 2 µL of 10X loading buffer (10 mM Tris-HCl, 10 mM EDTA, 65% (w/v) sucrose, 0.3% (w/v) Orange G Dye, pH 7.4) was added and samples were resolved through a 6% Tris-Acetate-EDTA (TAE) polyacrylamide gel at a constant 100 volts for 60 minutes. Gels were imaged using a Li-Cor Odyssey imaging system.

Differential Scanning Fluorimetry of GigC

Differential scanning fluorimetry (DFS) experiments were performed essentially as previously described (Vivoli et al. 2014). Briefly, 20-µL reactions were prepared in optically clear 96-well microtiter plates (Applied Biosystems) in DFS buffer (9.25 mM HEPES, 140 mM NaCl, 7.5X SYPRO Orange, pH 7.0). SYPRO Orange dye was purchased as a 5000X concentrate from Sigma (Product number S5692). Recombinant GigC::His protein was added to a concentration of 0.1 mg/mL. The indicated protein ligands were prepared in ddH_2O and added

to the reactions at the concentrations shown in Figure 4.6. Once assembled, the plates were sealed with optically clear caps and subjected to a thermal denaturation curve using an Applied Biosystems StepOne Real Time PCR machine. The temperature incline started at 25 ˚C and ramped to 95 ˚C in 0.3 ˚C increments. Each temperature was maintained for 60 seconds prior to reading the absorbance of the SYPRO Orange dye. Thermal denaturation analysis was conducted using Microsoft Excel by plotting the first derivative of the change in SYPRO orange fluorescence over change in temperature. The melting temperature was defined as the temperature at which the derivative reached the maximum value.

Bibliography

Abraham, E. P., and E. Chain. 1940. "An enzyme from bacteria able to destroy penicillin." *Nature* 146:837.

Achtman, M. 2004. "Population structure of pathogenic bacteria revisited." *Int J Med Microbiol* 294 (2-3):67-73. doi: 10.1016/j.ijmm.2004.06.028.

Adams, M. D., K. Goglin, N. Molyneaux, K. M. Hujer, H. Lavender, J. J. Jamison, I. J. MacDonald, K. M. Martin, T. Russo, A. A. Campagnari, A. M. Hujer, R. A. Bonomo, and S. R. Gill. 2008. "Comparative genome sequence analysis of multidrug-resistant *Acinetobacter baumannii*." *J Bacteriol* 190 (24):8053-64. doi: 10.1128/jb.00834-08.

Agarwal, Subhash M., Ruchi Jain, Alok Bhattacharya, and Amir Azam. 2008. "Inhibitors of *Escherichia coli* serine acetyltransferase block proliferation of *Entamoeba histolytica* trophozoites." *International journal for parasitology* 38 (2):137-141. doi: 10.1016/j.ijpara.2007.09.009.

Alba, B. M., and C. A. Gross. 2004. "Regulation of the *Escherichia coli* sigma-dependent envelope stress response." *Mol Microbiol* 52 (3):613-9. doi: 10.1111/j.1365-2958.2003.03982.x.

Alvarez, R., G. Neumann, J. Fravega, F. Diaz, C. Tejias, B. Collao, J. A. Fuentes, D. Paredes-Sabja, I. L. Calderon, and F. Gil. 2015. "CysB-dependent upregulation of the *Salmonella typhimurium cysJIH* operon in response to antimicrobial compounds that induce oxidative stress." *Biochem Biophys Res Commun*. doi: 10.1016/j.bbrc.2015.01.058.

Antonios Markogiannakis, M. P. H., M. D. George Fildisis, M. D. Sofia Tsiplakou, PhD Alexandros Ikonomidis, M. D. Alexandra Koutsoukou, M. D. Spyros Pournaras, M. D. Evangelos N. Manolis, M. D. George Baltopoulos, and M. D. Athanassios Tsakris. 2008. "Cross‐Transmission of Multidrug‐Resistant *Acinetobacter baumannii* Clonal Strains Causing Episodes of Sepsis in a Trauma Intensive Care Unit •." *Infection Control and Hospital Epidemiology* 29 (5):410-417. doi: 10.1086/533545.

Antunes, L. C., P. Visca, and K. J. Towner. 2014. "*Acinetobacter baumannii*: evolution of a global pathogen." *Pathog Dis* 71 (3):292-301. doi: 10.1111/2049-632x.12125.

Baumann, P., M. Doudoroff, and R. Y. Stanier. 1968. "A study of the *Moraxella* group. II. Oxidative-negative species (genus *Acinetobacter*)." *J Bacteriol* 95 (5):1520-41.

Beceiro, A., E. Llobet, J. Aranda, J. A. Bengoechea, M. Doumith, M. Hornsey, H. Dhanji, H. Chart, G. Bou, D. M. Livermore, and N. Woodford. 2011. "Phosphoethanolamine

modification of lipid A in colistin-resistant variants of *Acinetobacter baumannii* mediated by the *pmrAB* two-component regulatory system." *Antimicrob Agents Chemother* 55 (7):3370-9. doi: 10.1128/aac.00079-11.

Becker, R. E., and J. Bubeck Wardenburg. 2015. "*Staphylococcus aureus* and the skin: a longstanding and complex interaction." *Skinmed* 13 (2):111-9; quiz 120.

Blattner, F. R., G. Plunkett, 3rd, C. A. Bloch, N. T. Perna, V. Burland, M. Riley, J. Collado-Vides, J. D. Glasner, C. K. Rode, G. F. Mayhew, J. Gregor, N. W. Davis, H. A. Kirkpatrick, M. A. Goeden, D. J. Rose, B. Mau, and Y. Shao. 1997. "The complete genome sequence of *Escherichia coli* K-12." *Science* 277 (5331):1453-62.

Bos, Martine P., and Jan Tommassen. 2011. "The LptD Chaperone LptE Is Not Directly Involved in Lipopolysaccharide Transport in *Neisseria meningitidis*." *Journal of Biological Chemistry* 286 (33):28688-28696. doi: 10.1074/jbc.M111.239673.

Boucher, H. W., G. H. Talbot, J. S. Bradley, J. E. Edwards, D. Gilbert, L. B. Rice, M. Scheld, B. Spellberg, and J. Bartlett. 2009. "Bad bugs, no drugs: no ESKAPE! An update from the Infectious Diseases Society of America." *Clin Infect Dis* 48 (1):1-12. doi: 10.1086/595011.

Bouillet, S., O. Genest, C. Jourlin-Castelli, M. Fons, V. Mejean, and C. Iobbi-Nivol. 2016. "The General Stress Response sigmaS is Regulated by a Partner-Switch in the Gram-Negative Bacterium *Shewanella oneidensis*." *J Biol Chem*. doi: 10.1074/jbc.M116.751933.

Brisou, J., and A. R. Prevot. 1954. "[Studies on bacterial taxonomy. X. The revision of species under Acromobacter group]." *Ann Inst Pasteur (Paris)* 86 (6):722-8.

Burgess, R. R. 2009. "Elution of proteins from gels." *Methods Enzymol* 463:565-72. doi: 10.1016/s0076-6879(09)63032-9.

Button, J. E., T. J. Silhavy, and N. Ruiz. 2007. "A suppressor of cell death caused by the loss of sigmaE downregulates extracytoplasmic stress responses and outer membrane vesicle production in *Escherichia coli*." *J Bacteriol* 189 (5):1523-30. doi: 10.1128/jb.01534-06.

Cabeen, M. T., S. A. Leiman, and R. Losick. 2016. "Colony-morphology screening uncovers a role for the *Pseudomonas aeruginosa* nitrogen-related phosphotransferase system in biofilm formation." *Mol Microbiol* 99 (3):557-70. doi: 10.1111/mmi.13250.

Camarena, L., V. Bruno, G. Euskirchen, S. Poggio, and M. Snyder. 2010. "Molecular mechanisms of ethanol-induced pathogenesis revealed by RNA-sequencing." *PLoS Pathog* 6 (4):e1000834. doi: 10.1371/journal.ppat.1000834.

Campanini, B., M. Pieroni, S. Raboni, S. Bettati, R. Benoni, C. Pecchini, G. Costantino, and A. Mozzarelli. 2015. "Inhibitors of the sulfur assimilation pathway in bacterial pathogens as enhancers of antibiotic therapy." *Curr Med Chem* 22 (2):187-213.

Catel-Ferreira, M., G. Coadou, V. Molle, P. Mugnier, P. Nordmann, A. Siroy, T. Jouenne, and E. De. 2011. "Structure-function relationships of CarO, the carbapenem resistance-associated outer membrane protein of *Acinetobacter baumannii*." *J Antimicrob Chemother* 66 (9):2053-6. doi: 10.1093/jac/dkr267.

Cerqueira, G. M., X. Kostoulias, C. Khoo, I. Aibinu, Y. Qu, A. Traven, and A. Y. Peleg. 2014. "A global virulence regulator in *Acinetobacter baumannii* and its control of the phenylacetic acid catabolic pathway." *J Infect Dis* 210 (1):46-55. doi: 10.1093/infdis/jiu024.

Choi, A. H., L. Slamti, F. Y. Avci, G. B. Pier, and T. Maira-Litran. 2009. "The *pgaABCD* locus of *Acinetobacter baumannii* encodes the production of poly-beta-1-6-N-acetylglucosamine, which is critical for biofilm formation." *J Bacteriol* 191 (19):5953-63. doi: 10.1128/jb.00647-09.

Choi, C. H., J. S. Lee, Y. C. Lee, T. I. Park, and J. C. Lee. 2008. "*Acinetobacter baumannii* invades epithelial cells and outer membrane protein A mediates interactions with epithelial cells." *BMC Microbiology* 8:11. doi: Http://biomedcentral.com/1471-2180/8/216.

CLSI. Performance Standards for Antimicrobial Susceptibility Testing; Twenty-Fourth Informational
Supplement. CLSI document M100-S24. Wayne, PA: Clinical and Laboratory Standards Institute; 2014.

Cosconati, S., J. A. Hong, E. Novellino, K. S. Carroll, D. S. Goodsell, and A. J. Olson. 2008. "Structure-based virtual screening and biological evaluation of *Mycobacterium tuberculosis* adenosine 5'-phosphosulfate reductase inhibitors." *J Med Chem* 51 (21):6627-30. doi: 10.1021/jm800571m.

Cox, J. S., B. Chen, M. McNeil, and W. R. Jacobs, Jr. 1999. "Complex lipid determines tissue-specific replication of *Mycobacterium tuberculosis* in mice." *Nature* 402 (6757):79-83. doi: 10.1038/47042.

D'Argenio, David A., Ana Segura, Wayne M. Coco, Patricia V. Bünz, and L. Nicholas Ornston. 1999. "The Physiological Contribution of *Acinetobacter* PcaK, a Transport System That Acts upon Protocatechuate, Can Be Masked by the Overlapping Specificity of VanK." *Journal of Bacteriology* 181 (11):3505-3515.

Da Silva, G. J., and S. Domingues. 2016. "Insights on the Horizontal Gene Transfer of Carbapenemase Determinants in the Opportunistic Pathogen *Acinetobacter baumannii*." *Microorganisms* 4 (3). doi: 10.3390/microorganisms4030029.

Damier-Piolle, L., S. Magnet, S. Bremont, T. Lambert, and P. Courvalin. 2008. "AdeIJK, a resistance-nodulation-cell division pump effluxing multiple antibiotics in *Acinetobacter baumannii*." *Antimicrob Agents Chemother* 52 (2):557-62. doi: 10.1128/aac.00732-07.

Datsenko, K. A., and B. L. Wanner. 2000. "One-step inactivation of chromosomal genes in *Escherichia coli* K-12 using PCR products." *Proc Natl Acad Sci U S A* 97 (12):6640-5. doi: 10.1073/pnas.120163297.

Diancourt, L., V. Passet, A. Nemec, L. Dijkshoorn, and S. Brisse. 2010. "The population structure of *Acinetobacter baumannii*: expanding multiresistant clones from an ancestral susceptible genetic pool." *PLoS One* 5 (4):e10034. doi: 10.1371/journal.pone.0010034.

Dietsche, T., M. Tesfazgi Mebrhatu, M. J. Brunner, P. Abrusci, J. Yan, M. Franz-Wachtel, C. Scharfe, S. Zilkenat, I. Grin, J. E. Galan, O. Kohlbacher, S. Lea, B. Macek, T. C. Marlovits, C. V. Robinson, and S. Wagner. 2016. "Structural and Functional Characterization of the Bacterial Type III Secretion Export Apparatus." *PLoS Pathog* 12 (12):e1006071. doi: 10.1371/journal.ppat.1006071.

Dijkshoorn, L., A. Nemec, and H. Seifert. 2007. "An increasing threat in hospitals: multidrug-resistant *Acinetobacter baumannii*." *Nat Rev Microbiol* 5 (12):939-51. doi: 10.1038/nrmicro1789.

Djordjevic, D., M. Wiedmann, and L. A. McLandsborough. 2002. "Microtiter Plate Assay for Assessment of *Listeria monocytogenes* Biofilm Formation." *Applied and Environmental Microbiology* 68 (6):2950-2958. doi: 10.1128/aem.68.6.2950-2958.2002.

Enoch, D. A., C. Summers, N. M. Brown, L. Moore, M. I. Gillham, R. M. Burnstein, R. Thaxter, L. M. Enoch, B. Matta, and O. Sule. 2008. "Investigation and management of an outbreak of multidrug-carbapenem-resistant *Acinetobacter baumannii* in Cambridge, UK." *J Hosp Infect* 70 (2):109-18. doi: 10.1016/j.jhin.2008.05.015.

Erhardt, M., and P. Dersch. 2015. "Regulatory principles governing *Salmonella* and *Yersinia* virulence." *Front Microbiol* 6:949. doi: 10.3389/fmicb.2015.00949.

Erridge, C., O. L. Moncayo-Nieto, R. Morgan, M. Young, and I. R. Poxton. 2007. "*Acinetobacter baumannii* lipopolysaccharides are potent stimulators of human monocyte activation via Toll-like receptor 4 signalling." *J Med Microbiol* 56 (Pt 2):165-71. doi: 10.1099/jmm.0.46823-0.

Falagas, M. E., E. A. Karveli, I. Kelesidis, and T. Kelesidis. 2007. "Community-acquired *Acinetobacter* infections." *European Journal of Clinical Microbiology & Infectious Diseases* 26 (12):857-868. doi: 10.1007/s10096-007-0365-6.

Fiester, S. E., B. A. Arivett, R. E. Schmidt, A. C. Beckett, T. Ticak, M. V. Carrier, R. Ghosh, E. J. Ohneck, M. L. Metz, M. K. Sellin Jeffries, and L. A. Actis. 2016. "Iron-Regulated Phospholipase C Activity Contributes to the Cytolytic Activity and Virulence of *Acinetobacter baumannii*." *PLoS One* 11 (11):e0167068. doi: 10.1371/journal.pone.0167068.

Filiatrault, M. J., G. Tombline, V. E. Wagner, N. Van Alst, K. Rumbaugh, P. Sokol, J. Schwingel, and B. H. Iglewski. 2013. "*Pseudomonas aeruginosa* PA1006, which plays a

role in molybdenum homeostasis, is required for nitrate utilization, biofilm formation, and virulence." *PLoS One* 8 (2):e55594. doi: 10.1371/journal.pone.0055594.

Fuchs, Beth Burgwyn, Elizabeth O'Brien, Joseph B. El Khoury, and Eleftherios Mylonakis. 2010. "Methods for using *Galleria mellonella* as a model host to study fungal pathogenesis." *Virulence* 1 (6):475-482. doi: 10.4161/viru.1.6.12985.

Gaddy, J. A., B. A. Arivett, M. J. McConnell, R. Lopez-Rojas, J. Pachon, and L. A. Actis. 2012. "Role of acinetobactin-mediated iron acquisition functions in the interaction of *Acinetobacter baumannii* strain ATCC 19606T with human lung epithelial cells, *Galleria mellonella* caterpillars, and mice." *Infect Immun* 80 (3):1015-24. doi: 10.1128/iai.06279-11.

Gal-Mor, O., T. Zusman, and G. Segal. 2002. "Analysis of DNA Regulatory Elements Required for Expression of the *Legionella pneumophila icm* and *dot* Virulence Genes." *J Bacteriol* 184 (14):3823-33. doi: 10.1128/jb.184.14.3823-3833.2002.

Gallagher, L. A., E. Ramage, E. J. Weiss, M. Radey, H. S. Hayden, K. G. Held, H. K. Huse, D. V. Zurawski, M. J. Brittnacher, and C. Manoil. 2015. "Resources for Genetic and Genomic Analysis of Emerging Pathogen *Acinetobacter baumannii*." *J Bacteriol* 197 (12):2027-35. doi: 10.1128/JB.00131-15.

Gallagher, L. A., J. Shendure, and C. Manoil. 2011. "Genome-scale identification of resistance functions in *Pseudomonas aeruginosa* using Tn-seq." *MBio* 2 (1):e00315-10. doi: 10.1128/mBio.00315-10.

Gebhardt, Michael J., Larry A. Gallagher, Rachael K. Jacobson, Elena A. Usacheva, Lance R. Peterson, Daniel V. Zurawski, and Howard A. Shuman. 2015. "Joint Transcriptional Control of Virulence and Resistance to Antibiotic and Environmental Stress in *Acinetobacter baumannii*." *mBio* 6 (6). doi: 10.1128/mBio.01660-15.

Geisinger, E., and R. R. Isberg. 2015. "Antibiotic modulation of capsular exopolysaccharide and virulence in *Acinetobacter baumannii*." *PLoS Pathog* 11 (2):e1004691. doi: 10.1371/journal.ppat.1004691.

Gellatly, S. L., and R. E. Hancock. 2013. "*Pseudomonas aeruginosa*: new insights into pathogenesis and host defenses." *Pathog Dis* 67 (3):159-73. doi: 10.1111/2049-632x.12033.

Gibson, D. L., A. P. White, S. D. Snyder, S. Martin, C. Heiss, P. Azadi, M. Surette, and W. W. Kay. 2006. "*Salmonella* produces an O-antigen capsule regulated by AgfD and important for environmental persistence." *J Bacteriol* 188 (22):7722-30. doi: 10.1128/jb.00809-06.

Godino, Agustina, Analía Príncipe, and Sonia Fischer. 2016. "A *ptsP* deficiency in PGPR *Pseudomonas fluorescens* SF39a affects bacteriocin production and bacterial fitness in the wheat rhizosphere." *Research in Microbiology* 167 (3):178-189. doi: http://dx.doi.org/10.1016/j.resmic.2015.12.003.

Goodwin, Reed A., and Daniel J. Gage. 2014. "Biochemical Characterization of a Nitrogen-Type Phosphotransferase System Reveals that Enzyme EI(Ntr) Integrates Carbon and Nitrogen Signaling in *Sinorhizobium meliloti*." *Journal of Bacteriology* 196 (10):1901-1907. doi: 10.1128/JB.01489-14.

Gottig, S., T. M. Gruber, P. G. Higgins, M. Wachsmuth, H. Seifert, and V. A. Kempf. 2014. "Detection of pan drug-resistant *Acinetobacter baumannii* in Germany." *J Antimicrob Chemother* 69 (9):2578-9. doi: 10.1093/jac/dku170.

Granholm, David E., R. Neil Reese, and Nels H. Granholm. 1996. "Agouti Alleles Alter Cysteine and Glutathione Concentrations in Hair Follicles and Serum of Mice (Ay/a, AwJ/AwJ, and a/a)." *Journal of Investigative Dermatology* 106 (3):559-563. doi: http://dx.doi.org/10.1111/1523-1747.ep12344031.

Griffith, O. W. 1987. "Mammalian sulfur amino acid metabolism: an overview." *Methods Enzymol* 143:366-76.

Grizanova, E. V., I. M. Dubovskiy, M. M. Whitten, and V. V. Glupov. 2014. "Contributions of cellular and humoral immunity of *Galleria mellonella* larvae in defence against oral infection by *Bacillus thuringiensis*." *J Invertebr Pathol* 119:40-6. doi: 10.1016/j.jip.2014.04.003.

Grosser, Melinda R., Andy Weiss, Lindsey N. Shaw, and Anthony R. Richardson. 2016. "Regulatory Requirements for *Staphylococcus aureus* Nitric Oxide Resistance." *Journal of Bacteriology*. doi: 10.1128/jb.00229-16.

Guillouard, I., S. Auger, M. F. Hullo, F. Chetouani, A. Danchin, and I. Martin-Verstraete. 2002. "Identification of *Bacillus subtilis* CysL, a regulator of the *cysJI* operon, which encodes sulfite reductase." *J Bacteriol* 184 (17):4681-9.

Harding, C. R., G. N. Schroeder, S. Reynolds, A. Kosta, J. W. Collins, A. Mousnier, and G. Frankel. 2012. "*Legionella pneumophila* pathogenesis in the *Galleria mellonella* infection model." *Infect Immun* 80 (8):2780-90. doi: 10.1128/IAI.00510-12.

Harris, G., R. Kuo Lee, C. K. Lam, G. Kanzaki, G. B. Patel, H. H. Xu, and W. Chen. 2013. "A mouse model of *Acinetobacter baumannii*-associated pneumonia using a clinically isolated hypervirulent strain." *Antimicrob Agents Chemother* 57 (8):3601-13. doi: 10.1128/aac.00944-13.

Hassan, Karl A., Qi Liu, Peter J. F. Henderson, and Ian T. Paulsen. 2015. "Homologs of the *Acinetobacter baumannii* AceI Transporter Represent a New Family of Bacterial Multidrug Efflux Systems." *mBio* 6 (1). doi: 10.1128/mBio.01982-14.

Heeb, S., and D. Haas. 2001. "Regulatory roles of the GacS/GacA two-component system in plant-associated and other gram-negative bacteria." *Mol Plant Microbe Interact* 14 (12):1351-63. doi: 10.1094/mpmi.2001.14.12.1351.

Henriksen, S. D. 1973. "*Moraxella*, *Acinetobacter*, and the *Mimeae*." *Bacteriol Rev* 37 (4):522-61.

Henry, R., B. Crane, D. Powell, D. Deveson Lucas, Z. Li, J. Aranda, P. Harrison, R. L. Nation, B. Adler, M. Harper, J. D. Boyce, and J. Li. 2015. "The transcriptomic response of *Acinetobacter baumannii* to colistin and doripenem alone and in combination in an in vitro pharmacokinetics/pharmacodynamics model." *J Antimicrob Chemother* 70 (5):1303-13. doi: 10.1093/jac/dku536.

Hmelo, Laura R., Bradley R. Borlee, Henrik Almblad, Michelle E. Love, Trevor E. Randall, Boo Shan Tseng, Chuyang Lin, Yasuhiko Irie, Kelly M. Storek, Jaeun Jane Yang, Richard J. Siehnel, P. Lynne Howell, Pradeep K. Singh, Tim Tolker-Nielsen, Matthew R. Parsek, Herbert P. Schweizer, and Joe J. Harrison. 2015. "Precision-engineering the *Pseudomonas aeruginosa* genome with two-step allelic exchange." *Nat. Protocols* 10 (11):1820-1841. doi: 10.1038/nprot.2015.115
http://www.nature.com/nprot/journal/v10/n11/abs/nprot.2015.115.html - supplementary-information.

Hong, J. A., D. P. Bhave, and K. S. Carroll. 2009. "Identification of critical ligand binding determinants in *Mycobacterium tuberculosis* adenosine-5'-phosphosulfate reductase." *J Med Chem* 52 (17):5485-95. doi: 10.1021/jm900728u.

Hood, M. I., and E. P. Skaar. 2012. "Nutritional immunity: transition metals at the pathogen-host interface." *Nat Rev Microbiol* 10 (8):525-37. doi: 10.1038/nrmicro2836.

Hood, M. Indriati, Brittany L. Mortensen, Jessica L. Moore, Yaofang Zhang, Thomas E. Kehl-Fie, Norie Sugitani, Walter J. Chazin, Richard M. Caprioli, and Eric P. Skaar. 2012. "Identification of an *Acinetobacter baumannii* Zinc Acquisition System that Facilitates Resistance to Calprotectin-mediated Zinc Sequestration." *PLoS Pathog* 8 (12):e1003068. doi: 10.1371/journal.ppat.1003068.

Hraiech, S., A. Roch, H. Lepidi, T. Atieh, G. Audoly, J. M. Rolain, D. Raoult, J. M. Brunel, L. Papazian, and F. Bregeon. 2013. "Impaired virulence and fitness of a colistin-resistant clinical isolate of *Acinetobacter baumannii* in a rat model of pneumonia." *Antimicrob Agents Chemother* 57 (10):5120-1. doi: 10.1128/aac.00700-13.

Hryniewicz, M. M., and N. M. Kredich. 1991. "The *cysP* promoter of *Salmonella typhimurium*: characterization of two binding sites for CysB protein, studies of in vivo transcription initiation, and demonstration of the anti-inducer effects of thiosulfate." *J Bacteriol* 173 (18):5876-86.

Huttner, A., S. Harbarth, J. Carlet, S. Cosgrove, H. Goossens, A. Holmes, V. Jarlier, A. Voss, and D. Pittet. 2013. "Antimicrobial resistance: a global view from the 2013 World Healthcare-Associated Infections Forum." *Antimicrob Resist Infect Control* 2:31. doi: 10.1186/2047-2994-2-31.

Hwang, A. Y., and J. G. Gums. 2016. "The emergence and evolution of antimicrobial resistance: Impact on a global scale." *Bioorg Med Chem* 24 (24):6440-6445. doi: 10.1016/j.bmc.2016.04.027.

Imperi, F., L. C. Antunes, J. Blom, L. Villa, M. Iacono, P. Visca, and A. Carattoli. 2011. "The genomics of *Acinetobacter baumannii*: insights into genome plasticity, antimicrobial resistance and pathogenicity." *IUBMB Life* 63 (12):1068-74. doi: 10.1002/iub.531.

Jacobs, A. C., M. G. Thompson, C. C. Black, J. L. Kessler, L. P. Clark, C. N. McQueary, H. Y. Gancz, B. W. Corey, J. K. Moon, Y. Si, M. T. Owen, J. D. Hallock, Y. I. Kwak, A. Summers, C. Z. Li, D. A. Rasko, W. F. Penwell, C. L. Honnold, M. C. Wise, P. E. Waterman, E. P. Lesho, R. L. Stewart, L. A. Actis, T. J. Palys, D. W. Craft, and D. V. Zurawski. 2014. "AB5075, a Highly Virulent Isolate of *Acinetobacter baumannii*, as a Model Strain for the Evaluation of Pathogenesis and Antimicrobial Treatments." *MBio* 5 (3):e01076-14. doi: 10.1128/mBio.01076-14.

Jacobs, A. C., M. G. Thompson, M. Gebhardt, B. W. Corey, S. Yildirim, H. A. Shuman, and D. V. Zurawski. 2014. "Genetic Manipulation of *Acinetobacter baumannii*." *Curr Protoc Microbiol* 35:6g.2.1-6g.2.11. doi: 10.1002/9780471729259.mc06g02s35.

Jahn, S., B. R. Haverkorn van Rijsewijk, U. Sauer, and K. Bettenbrock. 2013. "A role for EIIA(Ntr) in controlling fluxes in the central metabolism of *E. coli* K12." *Biochim Biophys Acta* 1833 (12):2879-89. doi: 10.1016/j.bbamcr.2013.07.011.

Jander, G., L. G. Rahme, and F. M. Ausubel. 2000. "Positive correlation between virulence of *Pseudomonas aeruginosa* mutants in mice and insects." *J Bacteriol* 182 (13):3843-5.

Jawad, A., H. Seifert, A. M. Snelling, J. Heritage, and P. M. Hawkey. 1998. "Survival of *Acinetobacter baumannii* on dry surfaces: comparison of outbreak and sporadic isolates." *J Clin Microbiol* 36 (7):1938-41.

Jin, J. S., S. O. Kwon, D. C. Moon, M. Gurung, J. H. Lee, S. I. Kim, and J. C. Lee. 2011. "*Acinetobacter baumannii* secretes cytotoxic outer membrane protein A via outer membrane vesicles." *PLoS One* 6 (2):e17027. doi: 10.1371/journal.pone.0017027.

Johnson, Tanya L., Ursula Waack, Sara Smith, Harry Mobley, and Maria Sandkvist. 2016. "*Acinetobacter baumannii* Is Dependent on the Type II Secretion System and Its Substrate LipA for Lipid Utilization and *In Vivo* Fitness." *Journal of Bacteriology* 198 (4):711-719. doi: 10.1128/jb.00622-15.

Jones, C. L., M. Clancy, C. Honnold, S. Singh, E. Snesrud, F. Onmus-Leone, P. McGann, A. C. Ong, Y. Kwak, P. Waterman, D. V. Zurawski, R. J. Clifford, and E. Lesho. 2015. "Fatal Outbreak of an Emerging Clone of Extensively Drug-Resistant *Acinetobacter baumannii* With Enhanced Virulence." *Clin Infect Dis* 61 (2):145-54. doi: 10.1093/cid/civ225.

Juni, E. 1972. "Interspecies transformation of *Acinetobacter*: genetic evidence for a ubiquitous genus." *J Bacteriol* 112 (2):917-31.

Kavanagh, K., and E. P. Reeves. 2004. "Exploiting the potential of insects for *in vivo* pathogenicity testing of microbial pathogens." *FEMS Microbiol Rev* 28 (1):101-12. doi: 10.1016/j.femsre.2003.09.002.

Kawamura-Sato, K., J. Wachino, T. Kondo, H. Ito, and Y. Arakawa. 2010. "Correlation between reduced susceptibility to disinfectants and multidrug resistance among clinical isolates of *Acinetobacter* species." *J Antimicrob Chemother* 65 (9):1975-83. doi: 10.1093/jac/dkq227.

Keen, N. T., S. Tamaki, D. Kobayashi, and D. Trollinger. 1988. "Improved broad-host-range plasmids for DNA cloning in gram-negative bacteria." *Gene* 70 (1):191-7.

Kelley, Lawrence A., Stefans Mezulis, Christopher M. Yates, Mark N. Wass, and Michael J. E. Sternberg. 2015. "The Phyre2 web portal for protein modeling, prediction and analysis." *Nat. Protocols* 10 (6):845-858. doi: 10.1038/nprot.2015.053.

Kenyon, J. J., and R. M. Hall. 2013. "Variation in the complex carbohydrate biosynthesis loci of *Acinetobacter baumannii* genomes." *PLoS One* 8 (4):e62160. doi: 10.1371/journal.pone.0062160.

Kessler, D. 2006. "Enzymatic activation of sulfur for incorporation into biomolecules in prokaryotes." *FEMS Microbiol Rev* 30 (6):825-40. doi: 10.1111/j.1574-6976.2006.00036.x.

Khan, B. A., A. J. Yeh, G. Y. Cheung, and M. Otto. 2015. "Investigational therapies targeting quorum-sensing for the treatment of *Staphylococcus aureus* infections." *Expert Opin Investig Drugs* 24 (5):689-704. doi: 10.1517/13543784.2015.1019062.

Kim, B., S. M. Richards, J. S. Gunn, and J. M. Slauch. 2010. "Protecting against antimicrobial effectors in the phagosome allows SodCII to contribute to virulence in *Salmonella enterica* serovar Typhimurium." *J Bacteriol* 192 (8):2140-9. doi: 10.1128/jb.00016-10.

Kim, M. S., M. Y. Hahn, Y. Cho, S. N. Cho, and J. H. Roe. 2009. "Positive and negative feedback regulatory loops of thiol-oxidative stress response mediated by an unstable isoform of sigmaR in actinomycetes." *Mol Microbiol* 73 (5):815-25. doi: 10.1111/j.1365-2958.2009.06824.x.

Kinoshita, E., E. Kinoshita-Kikuta, K. Takiyama, and T. Koike. 2006. "Phosphate-binding tag, a new tool to visualize phosphorylated proteins." *Mol Cell Proteomics* 5 (4):749-57. doi: 10.1074/mcp.T500024-MCP200.

Kobayashi, K., M. Fujikawa, and T. Kozawa. 2014. "Oxidative stress sensing by the iron-sulfur cluster in the transcription factor, SoxR." *J Inorg Biochem* 133:87-91. doi: 10.1016/j.jinorgbio.2013.11.008.

Korotkov, K. V., M. Sandkvist, and W. G. Hol. 2012. "The type II secretion system: biogenesis, molecular architecture and mechanism." *Nat Rev Microbiol* 10 (5):336-51. doi: 10.1038/nrmicro2762.

Krahn, T., C. Gilmour, J. Tilak, S. Fraud, N. Kerr, C. H. Lau, and K. Poole. 2012. "Determinants of intrinsic aminoglycoside resistance in *Pseudomonas aeruginosa*." *Antimicrob Agents Chemother* 56 (11):5591-602. doi: 10.1128/aac.01446-12.

Kredich, N. M. 1992. "The molecular basis for positive regulation of cys promoters in *Salmonella typhimurium* and *Escherichia coli*." *Mol Microbiol* 6 (19):2747-53.

Krishnan, N., P. Hyrsl, and V. Simek. 2006. "Nitric oxide production by hemocytes of larva and pharate prepupa of *Galleria mellonella* in response to bacterial lipopolysaccharide: Cytoprotective or cytotoxic?" *Comp Biochem Physiol C Toxicol Pharmacol* 142 (1-2):103-10. doi: 10.1016/j.cbpc.2005.10.016.

Krzywinski, Martin I, Jacqueline E Schein, Inanc Birol, Joseph Connors, Randy Gascoyne, Doug Horsman, Steven J Jones, and Marco A Marra. 2009. "Circos: An information aesthetic for comparative genomics." *Genome Research*. doi: 10.1101/gr.092759.109.

Kuo, Shrin, Shuyu Zhang, Robyn L. Woodbury, and W. G. Haldenwang. 2004. "Associations between *Bacillus subtilis* σB regulators in cell extracts." *Microbiology* 150 (12):4125-4136. doi: 10.1099/mic.0.27421-0.

Kvint, K., L. Nachin, A. Diez, and T. Nystrom. 2003. "The bacterial universal stress protein: function and regulation." *Curr Opin Microbiol* 6 (2):140-5.

La Forgia, C., J. Franke, D. M. Hacek, R. B. Thomson, Jr., A. Robicsek, and L. R. Peterson. 2010. "Management of a multidrug-resistant *Acinetobacter baumannii* outbreak in an intensive care unit using novel environmental disinfection: a 38-month report." *Am J Infect Control* 38 (4):259-63. doi: 10.1016/j.ajic.2009.07.012.

Langridge, G. C., M. D. Phan, D. J. Turner, T. T. Perkins, L. Parts, J. Haase, I. Charles, D. J. Maskell, S. E. Peters, G. Dougan, J. Wain, J. Parkhill, and A. K. Turner. 2009. "Simultaneous assay of every *Salmonella typhi* gene using one million transposon mutants." *Genome Res* 19 (12):2308-16. doi: 10.1101/gr.097097.109.

Lee, Jaeseop, Young-Ha Park, Yeon-Ran Kim, Yeong-Jae Seok, and Chang-Ro Lee. 2015. "Dephosphorylated NPr is involved in an envelope stress response of *Escherichia coli*." *Microbiology* 161 (Pt 5):1113-1123. doi: 10.1099/mic.0.000056.

Leite, G. C., M. S. Oliveira, L. V. Perdigao-Neto, C. K. Rocha, T. Guimaraes, C. Rizek, A. S. Levin, and S. F. Costa. 2016. "Antimicrobial Combinations against Pan-Resistant *Acinetobacter baumannii* Isolates with Different Resistance Mechanisms." *PLoS One* 11 (3):e0151270. doi: 10.1371/journal.pone.0151270.

Lin, M. F., Y. Y. Lin, and C. Y. Lan. 2015. "The Role of the Two-Component System BaeSR in Disposing Chemicals through Regulating Transporter Systems in *Acinetobacter baumannii*." *PLoS One* 10 (7):e0132843. doi: 10.1371/journal.pone.0132843.

Lin, M. F., Y. Y. Lin, H. W. Yeh, and C. Y. Lan. 2014. "Role of the BaeSR two-component system in the regulation of *Acinetobacter baumannii adeAB* genes and its correlation with tigecycline susceptibility." *BMC Microbiol* 14:119. doi: 10.1186/1471-2180-14-119.

Lionakis, M. S. 2011. "*Drosophila* and *Galleria* insect model hosts: new tools for the study of fungal virulence, pharmacology and immunology." *Virulence* 2 (6):521-7. doi: 10.4161/viru.2.6.18520.

Liou, Ming-Li, Po-Chi Soo, Siao-Ru Ling, Han-Yueh Kuo, Chuan Yi Tang, and Kai-Chih Chang. 2013. "The sensor kinase BfmS mediates virulence in *Acinetobacter baumannii*." *Journal of Microbiology, Immunology, and Infection*

Liu, L., Y. Cui, B. Zheng, S. Jiang, W. Yu, P. Shen, J. Ji, L. Li, N. Qin, and Y. Xiao. 2016. "Analysis of tigecycline resistance development in clinical *Acinetobacter baumannii* isolates through a combined genomic and transcriptomic approach." *Sci Rep* 6:26930. doi: 10.1038/srep26930.

Maddocks, S. E., and P. C. Oyston. 2008. "Structure and function of the LysR-type transcriptional regulator (LTTR) family proteins." *Microbiology* 154 (Pt 12):3609-23. doi: 10.1099/mic.0.2008/022772-0.

Makinoshima, H., and M. S. Glickman. 2006. "Site-2 proteases in prokaryotes: regulated intramembrane proteolysis expands to microbial pathogenesis." *Microbes Infect* 8 (7):1882-8. doi: 10.1016/j.micinf.2006.02.021.

Malinverni, Juliana C., and Thomas J. Silhavy. 2009. "An ABC transport system that maintains lipid asymmetry in the Gram-negative outer membrane." *Proceedings of the National Academy of Sciences of the United States of America* 106 (19):8009-8014. doi: 10.1073/pnas.0903229106.

Martin, P., E. Jullien, and P. Courvalin. 1988. "Nucleotide sequence of *Acinetobacter baumannii aphA-6* gene: evolutionary and functional implications of sequence homologies with nucleotide-binding proteins, kinases and other aminoglycoside-modifying enzymes." *Mol Microbiol* 2 (5):615-25.

May, J. M., D. J. Sherman, B. W. Simpson, N. Ruiz, and D. Kahne. 2015. "Lipopolysaccharide transport to the cell surface: periplasmic transport and assembly into the outer membrane." *Philos Trans R Soc Lond B Biol Sci* 370 (1679). doi: 10.1098/rstb.2015.0027.

McClure, R., D. Balasubramanian, Y. Sun, M. Bobrovskyy, P. Sumby, C. A. Genco, C. K. Vanderpool, and B. Tjaden. 2013. "Computational analysis of bacterial RNA-Seq data." *Nucleic Acids Res* 41 (14):e140. doi: 10.1093/nar/gkt444.

Micklinghoff, J. C., M. Schmidt, R. Geffers, W. Tegge, and F. C. Bange. 2010. "Analysis of expression and regulatory functions of the ribosome-binding protein TypA in *Mycobacterium tuberculosis* under stress conditions." *Arch Microbiol* 192 (6):499-504. doi: 10.1007/s00203-010-0571-y.

Mihara, K., T. Tanabe, Y. Yamakawa, T. Funahashi, H. Nakao, S. Narimatsu, and S. Yamamoto. 2004. "Identification and transcriptional organization of a gene cluster involved in biosynthesis and transport of acinetobactin, a siderophore produced by *Acinetobacter baumannii* ATCC 19606T." *Microbiology* 150 (Pt 8):2587-97. doi: 10.1099/mic.0.27141-0.

Miller, Jeffrey H. 1972. *Experiments in Molecular Genetics*. Cold Spring Harbor Laboratory: Cold Spring Harbor, New York.

Morris, A. R., and K. L. Visick. 2013. "The response regulator SypE controls biofilm formation and colonization through phosphorylation of the syp-encoded regulator SypA in *Vibrio fischeri*." *Mol Microbiol* 87 (3):509-25. doi: 10.1111/mmi.12109.

Morris, T. W., K. E. Reed, and J. E. Cronan, Jr. 1995. "Lipoic acid metabolism in *Escherichia coli*: the lplA and lipB genes define redundant pathways for ligation of lipoyl groups to apoprotein." *J Bacteriol* 177 (1):1-10.

Mortensen, Brittany L., Subodh Rathi, Walter J. Chazin, and Eric P. Skaar. 2014. "*Acinetobacter baumannii* Response to Host-Mediated Zinc Limitation Requires the Transcriptional Regulator Zur." *Journal of Bacteriology* 196 (14):2616-2626. doi: 10.1128/jb.01650-14.

Mukherjee, K., B. Altincicek, T. Hain, E. Domann, A. Vilcinskas, and T. Chakraborty. 2010. "*Galleria mellonella* as a model system for studying *Listeria* pathogenesis." *Appl Environ Microbiol* 76 (1):310-7. doi: 10.1128/AEM.01301-09.

Muraoka, S., R. Okumura, N. Ogawa, T. Nonaka, K. Miyashita, and T. Senda. 2003. "Crystal structure of a full-length LysR-type transcriptional regulator, CbnR: unusual combination of two subunit forms and molecular bases for causing and changing DNA bend." *J Mol Biol* 328 (3):555-66.

Muraoka, S., R. Okumura, Y. Uragami, T. Nonaka, N. Ogawa, K. Miyashita, and T. Senda. 2003. "Purification and crystallization of a LysR-type transcriptional regulator CbnR from *Ralstonia eutropha* NH9." *Protein Pept Lett* 10 (3):325-9.

Muriel-Millan, L. F., S. Moreno, Y. Romero, L. P. Bedoya-Perez, M. Castaneda, D. Segura, and G. Espin. 2015. "The unphosphorylated EIIA(Ntr) protein represses the synthesis of alkylresorcinols in *Azotobacter vinelandii*." *PLoS One* 10 (2):e0117184. doi: 10.1371/journal.pone.0117184.

Neidig, A., A. T. Yeung, T. Rosay, B. Tettmann, N. Strempel, M. Rueger, O. Lesouhaitier, and J. Overhage. 2013. "TypA is involved in virulence, antimicrobial resistance and biofilm

formation in *Pseudomonas aeruginosa*." *BMC Microbiol* 13:77. doi: 10.1186/1471-2180-13-77.

Nolan, Richard A. 1971. "Amino Acids and Growth Factors in Vitamin-Free Casamino Acids." *Mycologia* 63 (6):1231-1234. doi: 10.2307/3757997.

Noor, Rashed. 2015. "Mechanism to control the cell lysis and the cell survival strategy in stationary phase under heat stress." *SpringerPlus* 4:599. doi: 10.1186/s40064-015-1415-7.

Nowak, Jennifer, Thamarai Schneiders, Harald Seifert, and Paul G. Higgins. 2016. "The Asp20-to-Asn Substitution in the Response Regulator AdeR Leads to Enhanced Efflux Activity of AdeB in *Acinetobacter baumannii*." *Antimicrobial Agents and Chemotherapy* 60 (2):1085-1090. doi: 10.1128/aac.02413-15.

Pane-Farre, J., R. J. Lewis, and J. Stulke. 2005. "The RsbRST stress module in bacteria: a signalling system that may interact with different output modules." *J Mol Microbiol Biotechnol* 9 (2):65-76. doi: 10.1159/000088837.

Park, Y. H., C. R. Lee, M. Choe, and Y. J. Seok. 2013. "HPr antagonizes the anti-sigma70 activity of Rsd in *Escherichia coli*." *Proc Natl Acad Sci U S A* 110 (52):21142-7. doi: 10.1073/pnas.1316629111.

Park, Y. H., S. H. Um, S. Song, Y. J. Seok, and N. C. Ha. 2015. "Structural basis for the sequestration of the anti-sigma(70) factor Rsd from sigma(70) by the histidine-containing phosphocarrier protein HPr." *Acta Crystallogr D Biol Crystallogr* 71 (Pt 10):1998-2008. doi: 10.1107/s1399004715013759.

Peleg, A. Y., A. de Breij, M. D. Adams, G. M. Cerqueira, S. Mocali, M. Galardini, P. H. Nibbering, A. M. Earl, D. V. Ward, D. L. Paterson, H. Seifert, and L. Dijkshoorn. 2012. "The success of *Acinetobacter* species; genetic, metabolic and virulence attributes." *PLoS One* 7 (10):e46984. doi: 10.1371/journal.pone.0046984.

Peleg, A. Y., S. Jara, D. Monga, G. M. Eliopoulos, R. C. Moellering, Jr., and E. Mylonakis. 2009. "*Galleria mellonella* as a model system to study *Acinetobacter baumannii* pathogenesis and therapeutics." *Antimicrob Agents Chemother* 53 (6):2605-9. doi: 10.1128/AAC.01533-08.

Peterson, Celeste N., Natividad Ruiz, and Thomas J. Silhavy. 2004. "RpoS Proteolysis Is Regulated by a Mechanism That Does Not Require the SprE (RssB) Response Regulator Phosphorylation Site." *Journal of Bacteriology* 186 (21):7403-7410. doi: 10.1128/JB.186.21.7403-7410.2004.

Pfluger, K., and V. de Lorenzo. 2008. "Evidence of *in vivo* cross talk between the nitrogen-related and fructose-related branches of the carbohydrate phosphotransferase system of *Pseudomonas putida*." *J Bacteriol* 190 (9):3374-80. doi: 10.1128/jb.02002-07.

Pour, N. K., D. H. Dusane, P. K. Dhakephalkar, F. R. Zamin, S. S. Zinjarde, and B. A. Chopade. 2011. "Biofilm formation by *Acinetobacter baumannii* strains isolated from urinary tract infection and urinary catheters." *FEMS Immunol Med Microbiol* 62 (3):328-38. doi: 10.1111/j.1574-695X.2011.00818.x.

Powell, B. S., D. L. Court, T. Inada, Y. Nakamura, V. Michotey, X. Cui, A. Reizer, M. H. Saier, Jr., and J. Reizer. 1995. "Novel proteins of the phosphotransferase system encoded within the *rpoN* operon of *Escherichia coli.* Enzyme IIANtr affects growth on organic nitrogen and the conditional lethality of an *era*ts mutant." *J Biol Chem* 270 (9):4822-39.

Prevention, Centers for Disease Control and. 2016. "Antibiotic / Antimicrobial Resistance: Biggest Threats." Last Modified September 8, 2016 Accessed December 20. https://www.cdc.gov/drugresistance/biggest_threats.html.

Pukatzki, S., R. H. Kessin, and J. J. Mekalanos. 2002. "The human pathogen *Pseudomonas aeruginosa* utilizes conserved virulence pathways to infect the social amoeba *Dictyostelium discoideum*." *Proc Natl Acad Sci U S A* 99 (5):3159-64. doi: 10.1073/pnas.052704399.

Puza, V., and Z. Mracek. 2009. "Mixed infection of *Galleria mellonella* with two entomopathogenic nematode (Nematoda: Rhabditida) species: *Steinernema affine* benefits from the presence of *Steinernema kraussei*." *J Invertebr Pathol* 102 (1):40-3. doi: 10.1016/j.jip.2009.06.005.

Qiu, H., R. KuoLee, G. Harris, and W. Chen. 2009. "High susceptibility to respiratory *Acinetobacter baumannii* infection in A/J mice is associated with a delay in early pulmonary recruitment of neutrophils." *Microbes Infect* 11 (12):946-55. doi: 10.1016/j.micinf.2009.06.003.

Rabus, R., J. Reizer, I. Paulsen, and M. H. Saier, Jr. 1999. "Enzyme I(Ntr) from *Escherichia coli*. A novel enzyme of the phosphoenolpyruvate-dependent phosphotransferase system exhibiting strict specificity for its phosphoryl acceptor, NPr." *J Biol Chem* 274 (37):26185-91.

Rasko, David A., M. J. Rosovitz, Garry S. A. Myers, Emmanuel F. Mongodin, W. Florian Fricke, Pawel Gajer, Jonathan Crabtree, Mohammed Sebaihia, Nicholas R. Thomson, Roy Chaudhuri, Ian R. Henderson, Vanessa Sperandio, and Jacques Ravel. 2008. "The Pangenome Structure of *Escherichia coli*: Comparative Genomic Analysis of *E. coli* Commensal and Pathogenic Isolates." *Journal of Bacteriology* 190 (20):6881-6893. doi: 10.1128/jb.00619-08.

Ratajczak, A., W. Geissdorfer, and W. Hillen. 1998. "Expression of alkane hydroxylase from *Acinetobacter* sp. Strain ADP1 is induced by a broad range of n-alkanes and requires the transcriptional activator AlkR." *J Bacteriol* 180 (22):5822-7.

Reddy, P., A. Peterkofsky, and K. McKenney. 1985. "Translational efficiency of the *Escherichia coli* adenylate cyclase gene: mutating the UUG initiation codon to GUG or AUG results

in increased gene expression." *Proceedings of the National Academy of Sciences of the United States of America* 82 (17):5656-5660.

Regeimbal, J. M., A. C. Jacobs, B. W. Corey, M. S. Henry, M. G. Thompson, R. L. Pavlicek, J. Quinones, R. M. Hannah, M. Ghebremedhin, N. J. Crane, D. V. Zurawski, N. C. Teneza-Mora, B. Biswas, and E. R. Hall. 2016. "Personalized Therapeutic Cocktail of Wild Environmental Phages Rescues Mice from *Acinetobacter baumannii* Wound Infections." *Antimicrob Agents Chemother* 60 (10):5806-16. doi: 10.1128/aac.02877-15.

Roca, I., P. Espinal, X. Vila-Farres, and J. Vila. 2012. "The *Acinetobacter baumannii* Oxymoron: Commensal Hospital Dweller Turned Pan-Drug-Resistant Menace." *Front Microbiol* 3:148. doi: 10.3389/fmicb.2012.00148.

Rodriguez-Martinez, J. M., L. Poirel, and P. Nordmann. 2010. "Genetic and functional variability of AmpC-type beta-lactamases from *Acinetobacter baumannii*." *Antimicrob Agents Chemother* 54 (11):4930-3. doi: 10.1128/aac.00427-10.

Roux, D., O. Danilchanka, T. Guillard, V. Cattoir, H. Aschard, Y. Fu, F. Angoulvant, J. Messika, J. D. Ricard, J. J. Mekalanos, S. Lory, G. B. Pier, and D. Skurnik. 2015. "Fitness cost of antibiotic susceptibility during bacterial infection." *Sci Transl Med* 7 (297):297ra114. doi: 10.1126/scitranslmed.aab1621.

Rumbo-Feal, Soraya, Manuel J. Gómez, Carmen Gayoso, Laura Álvarez-Fraga, María P. Cabral, Ana M. Aransay, Naiara Rodríguez-Ezpeleta, Ane Fullaondo, Jaione Valle, María Tomás, Germán Bou, and Margarita Poza. 2013. "Whole Transcriptome Analysis of *Acinetobacter baumannii* Assessed by RNA-Sequencing Reveals Different mRNA Expression Profiles in Biofilm Compared to Planktonic Cells." *PLoS ONE* 8 (8):e72968. doi: 10.1371/journal.pone.0072968.

Russo, T. A., N. R. Luke, J. M. Beanan, R. Olson, S. L. Sauberan, U. MacDonald, L. W. Schultz, T. C. Umland, and A. A. Campagnari. 2010. "The K1 capsular polysaccharide of *Acinetobacter baumannii* strain 307-0294 is a major virulence factor." *Infect Immun* 78 (9):3993-4000. doi: 10.1128/iai.00366-10.

Russo, T. A., U. MacDonald, J. M. Beanan, R. Olson, I. J. MacDonald, S. L. Sauberan, N. R. Luke, L. W. Schultz, and T. C. Umland. 2009. "Penicillin-binding protein 7/8 contributes to the survival of *Acinetobacter baumannii* in vitro and in vivo." *J Infect Dis* 199 (4):513-21. doi: 10.1086/596317.

Salsi, Enea, Alexander S. Bayden, Francesca Spyrakis, Alessio Amadasi, Barbara Campanini, Stefano Bettati, Tetyana Dodatko, Pietro Cozzini, Glen E. Kellogg, Paul F. Cook, Steven L. Roderick, and Andrea Mozzarelli. 2010. "Design of O-acetylserine sulfhydrylase inhibitors by mimicking Nature." *Journal of medicinal chemistry* 53 (1):345-356. doi: 10.1021/jm901325e.

Sampedro, G. R., A. C. Dedent, R. E. Becker, B. J. Berube, M. Gebhardt, H. Cao, and J. Bubeck Wardenburg. 2014. "Targeting *Staphylococcus aureus* alpha-toxin as a novel approach to

reduce severity of recurrent skin and soft tissue infections." *J Infect Dis*. doi: 10.1093/infdis/jiu223.

Schwartz, Drew J., Vasilios Kalas, Jerome S. Pinkner, Swaine L. Chen, Caitlin N. Spaulding, Karen W. Dodson, and Scott J. Hultgren. 2013. "Positively selected FimH residues enhance virulence during urinary tract infection by altering FimH conformation." *Proceedings of the National Academy of Sciences* 110 (39):15530-15537. doi: 10.1073/pnas.1315203110.

Scott, N. E., R. L. Kinsella, A. V. Edwards, M. R. Larsen, S. Dutta, J. Saba, L. J. Foster, and M. F. Feldman. 2014. "Diversity within the O-linked protein glycosylation systems of *Acinetobacter* species." *Mol Cell Proteomics* 13 (9):2354-70. doi: 10.1074/mcp.M114.038315.

Scott, P., G. Deye, A. Srinivasan, C. Murray, K. Moran, E. Hulten, J. Fishbain, D. Craft, S. Riddell, L. Lindler, J. Mancuso, E. Milstrey, C. T. Bautista, J. Patel, A. Ewell, T. Hamilton, C. Gaddy, M. Tenney, G. Christopher, K. Petersen, T. Endy, and B. Petruccelli. 2007. "An outbreak of multidrug-resistant *Acinetobacter baumannii-calcoaceticus* complex infection in the US military health care system associated with military operations in Iraq." *Clin Infect Dis* 44 (12):1577-84. doi: 10.1086/518170.

Segal, G., M. Purcell, and H. A. Shuman. 1998. "Host cell killing and bacterial conjugation require overlapping sets of genes within a 22-kb region of the *Legionella pneumophila* genome." *Proc Natl Acad Sci U S A* 95 (4):1669-74.

Sharma, A. K., A. C. Rigby, and S. L. Alper. 2011. "STAS domain structure and function." *Cell Physiol Biochem* 28 (3):407-22. doi: 10.1159/000335104.

Shatalin, K., E. Shatalina, A. Mironov, and E. Nudler. 2011. "H2S: a universal defense against antibiotics in bacteria." *Science* 334 (6058):986-90. doi: 10.1126/science.1209855.

Shaw, K. J., and C. M. Berg. 1979. "*Escherichia coli* K-12 auxotrophs induced by insertion of the transposable element Tn5." *Genetics* 92 (3):741-7.

Shevchenko, A., M. Wilm, O. Vorm, and M. Mann. 1996. "Mass spectrometric sequencing of proteins silver-stained polyacrylamide gels." *Anal Chem* 68 (5):850-8.

Sievers, F., and D. G. Higgins. 2014. "Clustal omega." *Curr Protoc Bioinformatics* 48:3.13.1-16. doi: 10.1002/0471250953.bi0313s48.

Simpson, R. J. 2010. "SYPRO Orange fluorescent staining of protein gels." *Cold Spring Harb Protoc* 2010 (4):pdb.prot5414. doi: 10.1101/pdb.prot5414.

Slauch, J. M., and A. Camilli. 2000. "IVET and RIVET: use of gene fusions to identify bacterial virulence factors specifically induced in host tissues." *Methods Enzymol* 326:73-96.

Smith, M. G., S. G. Des Etages, and M. Snyder. 2004. "Microbial Synergy via an Ethanol-Triggered Pathway." *Molecular and Cellular Biology* 24 (9):3874-3884. doi: 10.1128/mcb.24.9.3874-3884.2004.

Smith, M. G., T. A. Gianoulis, S. Pukatzki, J. J. Mekalanos, L. N. Ornston, M. Gerstein, and M. Snyder. 2007. "New insights into *Acinetobacter baumannii* pathogenesis revealed by high-density pyrosequencing and transposon mutagenesis." *Genes Dev* 21 (5):601-14. doi: 10.1101/gad.1510307.

Sokatch, J. R., V. McCully, J. Gebrosky, and D. J. Sokatch. 1981. "Isolation of a specific lipoamide dehydrogenase for a branched-chain keto acid dehydrogenase from *Pseudomonas putida*." *J Bacteriol* 148 (2):639-46.

Spellberg, Brad, and John H. Rex. 2013. "The value of single-pathogen antibacterial agents." *Nature reviews. Drug discovery* 12 (12):963-963. doi: 10.1038/nrd3957-c1.

Spencer, J. B., N. J. Stolowich, C. A. Roessner, and A. I. Scott. 1993. "The *Escherichia coli cysG* gene encodes the multifunctional protein, siroheme synthase." *FEBS Lett* 335 (1):57-60.

Subashchandrabose, Sargurunathan, Sara Smith, Valerie DeOrnellas, Sebastien Crepin, Monica Kole, Carina Zahdeh, and Harry L. T. Mobley. 2016. "*Acinetobacter baumannii* Genes Required for Bacterial Survival during Bloodstream Infection." *mSphere* 1 (1). doi: 10.1128/mSphere.00013-15.

Sugawara, Etsuko, and Hiroshi Nikaido. 2012. "OmpA Is the Principal Nonspecific Slow Porin of *Acinetobacter baumannii*." *Journal of Bacteriology* 194 (15):4089-4096. doi: 10.1128/JB.00435-12.

Taylor, Jennifer L., Rukman S. De Silva, Gabriela Kovacikova, Wei Lin, Ronald K. Taylor, Karen Skorupski, and F. Jon Kull. 2012. "The crystal structure of AphB, a virulence gene activator from *Vibrio cholerae*, reveals residues that influence its response to oxygen and pH." *Molecular Microbiology* 83 (3):457-470. doi: 10.1111/j.1365-2958.2011.07919.x.

Thompson, C. C., C. Griffiths, S. S. Nicod, N. M. Lowden, S. Wigneshweraraj, D. J. Fisher, and M. O. McClure. 2015. "The Rsb Phosphoregulatory Network Controls Availability of the Primary Sigma Factor in *Chlamydia trachomatis* and Influences the Kinetics of Growth and Development." *PLoS Pathog* 11 (8):e1005125. doi: 10.1371/journal.ppat.1005125.

Thompson, C. M., and K. L. Visick. 2015. "Assessing the function of STAS domain protein SypA in *Vibrio fischeri* using a comparative analysis." *Front Microbiol* 6:760. doi: 10.3389/fmicb.2015.00760.

Thompson, R. J., B. G. Bobay, S. D. Stowe, A. L. Olson, L. Peng, Z. Su, L. A. Actis, C. Melander, and J. Cavanagh. 2012. "Identification of BfmR, a response regulator involved in biofilm development, as a target for a 2-Aminoimidazole-based antibiofilm agent." *Biochemistry* 51 (49):9776-8. doi: 10.1021/bi3015289.

Thong, Shuhua, Bilge Ercan, Federico Torta, Zhen Yang Fong, Hui Yi Alvina Wong, Markus R. Wenk, and Shu-Sin Chng. 2016. "Defining key roles for auxiliary proteins in an ABC transporter that maintains bacterial outer membrane lipid asymmetry." *eLife* 5:e19042. doi: 10.7554/eLife.19042.

Tipton, K. A., D. Dimitrova, and P. N. Rather. 2015. "Phase variable control of multiple phenotypes in *Acinetobacter baumannii* strain AB5075." *J Bacteriol*. doi: 10.1128/jb.00188-15.

Tipton, K. A., and P. N. Rather. 2016. "An *ompR/envZ* Two-Component System Ortholog Regulates Phase Variation, Osmotic Tolerance, Motility, and Virulence in *Acinetobacter baumannii* strain AB5075." *J Bacteriol*. doi: 10.1128/jb.00705-16.

Tomaras, A. P., C. W. Dorsey, R. E. Edelmann, and L. A. Actis. 2003. "Attachment to and biofilm formation on abiotic surfaces by *Acinetobacter baumannii*: involvement of a novel chaperone-usher pili assembly system." *Microbiology* 149 (Pt 12):3473-84.

Tomaras, A. P., M. J. Flagler, C. W. Dorsey, J. A. Gaddy, and L. A. Actis. 2008. "Characterization of a two-component regulatory system from *Acinetobacter baumannii* that controls biofilm formation and cellular morphology." *Microbiology* 154 (Pt 11):3398-409. doi: 10.1099/mic.0.2008/019471-0.

Tombline, G., J. M. Schwingel, J. D. Lapek, Jr., A. E. Friedman, T. Darrah, M. Maguire, N. E. Van Alst, M. J. Filiatrault, and B. H. Iglewski. 2013. "*Pseudomonas aeruginosa* PA1006 is a persulfide-modified protein that is critical for molybdenum homeostasis." *PLoS One* 8 (2):e55593. doi: 10.1371/journal.pone.0055593.

Touchon, M., J. Cury, E. J. Yoon, L. Krizova, G. C. Cerqueira, C. Murphy, M. Feldgarden, J. Wortman, D. Clermont, T. Lambert, C. Grillot-Courvalin, A. Nemec, P. Courvalin, and E. P. Rocha. 2014. "The genomic diversification of the whole *Acinetobacter* genus: origins, mechanisms, and consequences." *Genome Biol Evol* 6 (10):2866-82. doi: 10.1093/gbe/evu225.

Turnbull, A. L., and M. G. Surette. 2010. "Cysteine biosynthesis, oxidative stress and antibiotic resistance in *Salmonella typhimurium*." *Res Microbiol* 161 (8):643-50. doi: 10.1016/j.resmic.2010.06.004.

van der Ploeg, J. R., E. Eichhorn, and T. Leisinger. 2001. "Sulfonate-sulfur metabolism and its regulation in *Escherichia coli*." *Arch Microbiol* 176 (1-2):1-8.

van der Ploeg, J. R., R. Iwanicka-Nowicka, M. A. Kertesz, T. Leisinger, and M. M. Hryniewicz. 1997. "Involvement of CysB and Cbl regulatory proteins in expression of the *tauABCD* operon and other sulfate starvation-inducible genes in *Escherichia coli*." *Journal of Bacteriology* 179 (24):7671-7678.

van Faassen, Henk, Rhonda KuoLee, Greg Harris, Xigeng Zhao, J. Wayne Conlan, and Wangxue Chen. 2007. "Neutrophils Play an Important Role in Host Resistance to Respiratory

Infection with *Acinetobacter baumannii* in Mice." *Infection and Immunity* 75 (12):5597-5608. doi: 10.1128/iai.00762-07.

van Opijnen, T., K. L. Bodi, and A. Camilli. 2009. "Tn-seq: high-throughput parallel sequencing for fitness and genetic interaction studies in microorganisms." *Nat Methods* 6 (10):767-72. doi: 10.1038/nmeth.1377.

van Opijnen, T., and A. Camilli. 2013. "Transposon insertion sequencing: a new tool for systems-level analysis of microorganisms." *Nat Rev Microbiol* 11 (7):435-42. doi: 10.1038/nrmicro3033.

Visca, P., H. Seifert, and K. J. Towner. 2011. "*Acinetobacter* infection--an emerging threat to human health." *IUBMB Life* 63 (12):1048-54. doi: 10.1002/iub.534.

Vivoli, Mirella, Halina R. Novak, Jennifer A. Littlechild, and Nicholas J. Harmer. 2014. "Determination of Protein-ligand Interactions Using Differential Scanning Fluorimetry." *Journal of Visualized Experiments : JoVE* (91):51809. doi: 10.3791/51809.

Vogel, J. P., H. L. Andrews, S. K. Wong, and R. R. Isberg. 1998. "Conjugative transfer by the virulence system of *Legionella pneumophila*." *Science* 279 (5352):873-6.

Wand, M. E., L. J. Bock, J. F. Turton, P. G. Nugent, and J. M. Sutton. 2012. "*Acinetobacter baumannii* virulence is enhanced in *Galleria mellonella* following biofilm adaptation." *J Med Microbiol* 61 (Pt 4):470-7. doi: 10.1099/jmm.0.037523-0.

Wang, N., E. A. Ozer, M. J. Mandel, and A. R. Hauser. 2014. "Genome-wide identification of *Acinetobacter baumannii* genes necessary for persistence in the lung." *MBio* 5 (3):e01163-14. doi: 10.1128/mBio.01163-14.

Wilharm, G., J. Piesker, M. Laue, and E. Skiebe. 2013. "DNA uptake by the nosocomial pathogen *Acinetobacter baumannii* occurs during movement along wet surfaces." *J Bacteriol* 195 (18):4146-53. doi: 10.1128/jb.00754-13.

Withman, B., T. S. Gunasekera, P. Beesetty, R. Agans, and O. Paliy. 2013. "Transcriptional responses of uropathogenic *Escherichia coli* to increased environmental osmolality caused by salt or urea." *Infect Immun* 81 (1):80-9. doi: 10.1128/iai.01049-12.

Wong, D., T. B. Nielsen, R. A. Bonomo, P. Pantapalangkoor, B. Luna, and B. Spellberg. 2017. "Clinical and Pathophysiological Overview of *Acinetobacter* Infections: a Century of Challenges." *Clin Microbiol Rev* 30 (1):409-447. doi: 10.1128/cmr.00058-16.

Wright, M. S., D. H. Haft, D. M. Harkins, F. Perez, K. M. Hujer, S. Bajaksouzian, M. F. Benard, M. R. Jacobs, R. A. Bonomo, and M. D. Adams. 2014. "New insights into dissemination and variation of the health care-associated pathogen *Acinetobacter baumannii* from genomic analysis." *MBio* 5 (1):e00963-13. doi: 10.1128/mBio.00963-13.

Wroblewska, M. M., A. Sawicka-Grzelak, H. Marchel, M. Luczak, and A. Sivan. 2008. "Biofilm production by clinical strains of *Acinetobacter baumannii* isolated from patients hospitalized in two tertiary care hospitals." *FEMS Immunol Med Microbiol* 53 (1):140-4. doi: 10.1111/j.1574-695X.2008.00403.x.

Wu, C. C., C. K. Wang, Y. C. Chen, T. H. Lin, T. R. Jinn, and C. T. Lin. 2014. "IscR regulation of capsular polysaccharide biosynthesis and iron-acquisition systems in *Klebsiella pneumoniae* CG43." *PLoS One* 9 (9):e107812. doi: 10.1371/journal.pone.0107812.

Wyatt, G. R., T. C. Loughheed, and S. S. Wyatt. 1956. "The chemistry of insect hemolymph; organic components of the hemolymph of the silkworm, *Bombyx mori*, and two other species." *J Gen Physiol* 39 (6):853-68.

Xayarath, B., and N. E. Freitag. 2012. "Optimizing the balance between host and environmental survival skills: lessons learned from *Listeria monocytogenes*." *Future Microbiol* 7 (7):839-52. doi: 10.2217/fmb.12.57.

Xodo, L. E., G. Manzini, F. Quadrifoglio, G. van der Marel, and J. van Boom. 1991. "DNA hairpin loops in solution. Correlation between primary structure, thermostability and reactivity with single-strand-specific nuclease from mung bean." *Nucleic Acids Research* 19 (7):1505-1511.

Yang, X, C M Kang, M S Brody, and C W Price. 1996. "Opposing pairs of serine protein kinases and phosphatases transmit signals of environmental stress to activate a bacterial transcription factor." *Genes & Development* 10 (18):2265-2275. doi: 10.1101/gad.10.18.2265.

Yoon, E. J., P. Courvalin, and C. Grillot-Courvalin. 2013. "RND-type efflux pumps in multidrug-resistant clinical isolates of *Acinetobacter baumannii*: major role for AdeABC overexpression and AdeRS mutations." *Antimicrob Agents Chemother* 57 (7):2989-95. doi: 10.1128/aac.02556-12.

Yoon, E. J., Y. Nait Chabane, S. Goussard, E. Snesrud, P. Courvalin, E. De, and C. Grillot-Courvalin. 2015. "Contribution of Resistance-Nodulation-Cell Division Efflux Systems to Antibiotic Resistance and Biofilm Formation in *Acinetobacter baumannii*." *MBio* 6 (2). doi: 10.1128/mBio.00309-15.

Zhang, Y., U. Werling, and W. Edelmann. 2014. "Seamless Ligation Cloning Extract (SLiCE) cloning method." *Methods Mol Biol* 1116:235-44. doi: 10.1007/978-1-62703-764-8_16.

Zimbler, D. L., W. F. Penwell, J. A. Gaddy, S. M. Menke, A. P. Tomaras, P. L. Connerly, and L. A. Actis. 2009. "Iron acquisition functions expressed by the human pathogen *Acinetobacter baumannii*." *Biometals* 22 (1):23-32. doi: 10.1007/s10534-008-9202-3.

Zschiedrich, C. P., V. Keidel, and H. Szurmant. 2016. "Molecular Mechanisms of Two-Component Signal Transduction." *J Mol Biol* 428 (19):3752-75. doi: 10.1016/j.jmb.2016.08.003.

Zurawski, D. V., M. G. Thompson, C. N. McQueary, M. N. Matalka, J. W. Sahl, D. W. Craft, and D. A. Rasko. 2012. "Genome sequences of four divergent multidrug-resistant *Acinetobacter baumannii* strains isolated from patients with sepsis or osteomyelitis." *J Bacteriol* 194 (6):1619-20. doi: 10.1128/JB.06749-11.

Appendix A

Figures

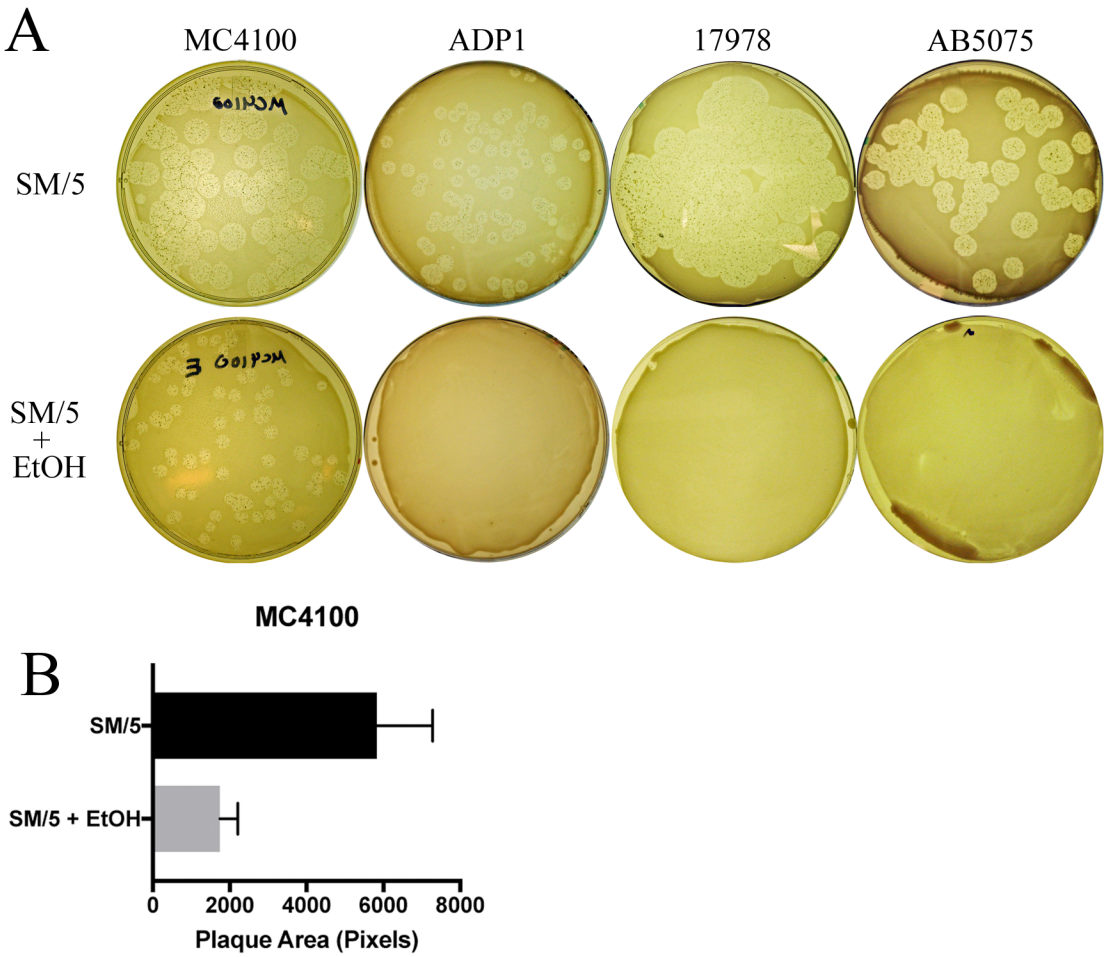

Figure 2.1. *Dictyostelium* Plate Test. (A) Photographs depicting the results of the *Dictystelium* Plate Test. The equivalent of 5.5 OD units of the indicated bacterial strains were suspended in 1 mL SorC buffer and mixed with approximately 500 *Dictyostelium discoideum* cells. 200 µL of the resulting mixture was spread onto SM/5 agar plates with and without the addition of 1% ethanol (SM/5 + EtOH). The plates were incubated at room temperature for 5 days. **(B)** Bars represent the mean area (in pixels) from 20 plaques formed on the lawn of MC4100 grown on the indicated plates. Measurements were performed using ImageJ.

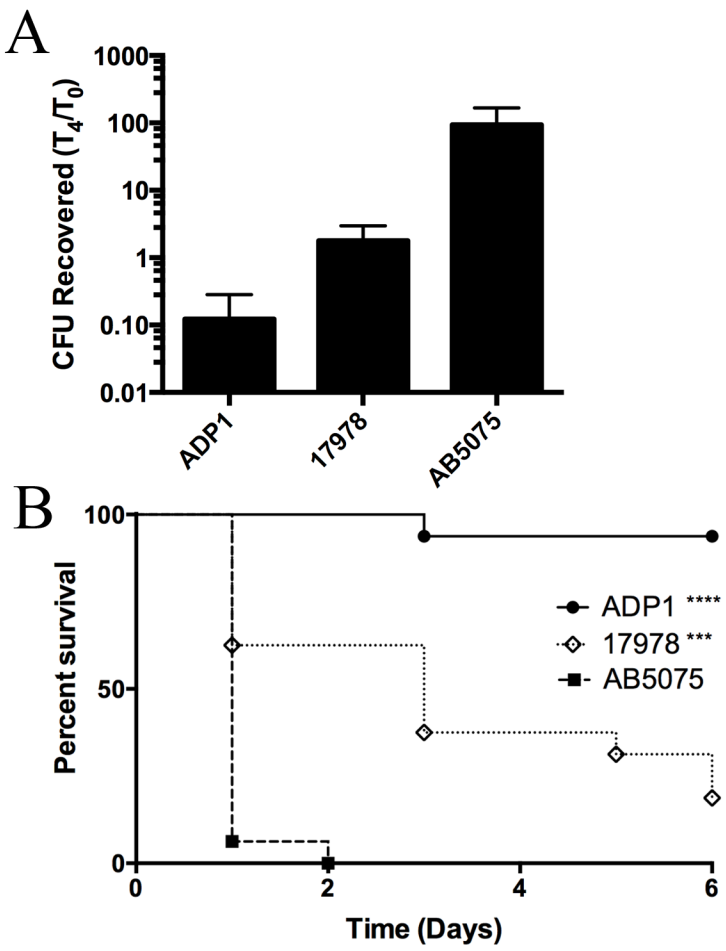

Figure 2.2 *Galleria mellonella* differentiates pathogenic and non-pathogenic *Acinetobacter* strains. (A) *G. mellonella* larvae were inoculated with 10^6 CFU of the indicated strains. Larvae were homogenized and bacteria were quantified immediately following infection (t = 0) and after 4 hr at 37 ˚C (t = 4). Data from a representative experiment are presented as the ratio between CFU recovered at t = 4 and at t = 0 (error bars, 1 SD). **(B)** *G. mellonella* larvae were inoculated with 10^6 CFU of the indicated strains. Survival was monitored daily for 6 days. **** $p < 0.0001$, *** $p < 0.001$, ADP1, *A. baylyi* strain ADP1; 17978, *A. baumannii* ATCC 17978; AB5075, *A. baumannii* str. AB5075.

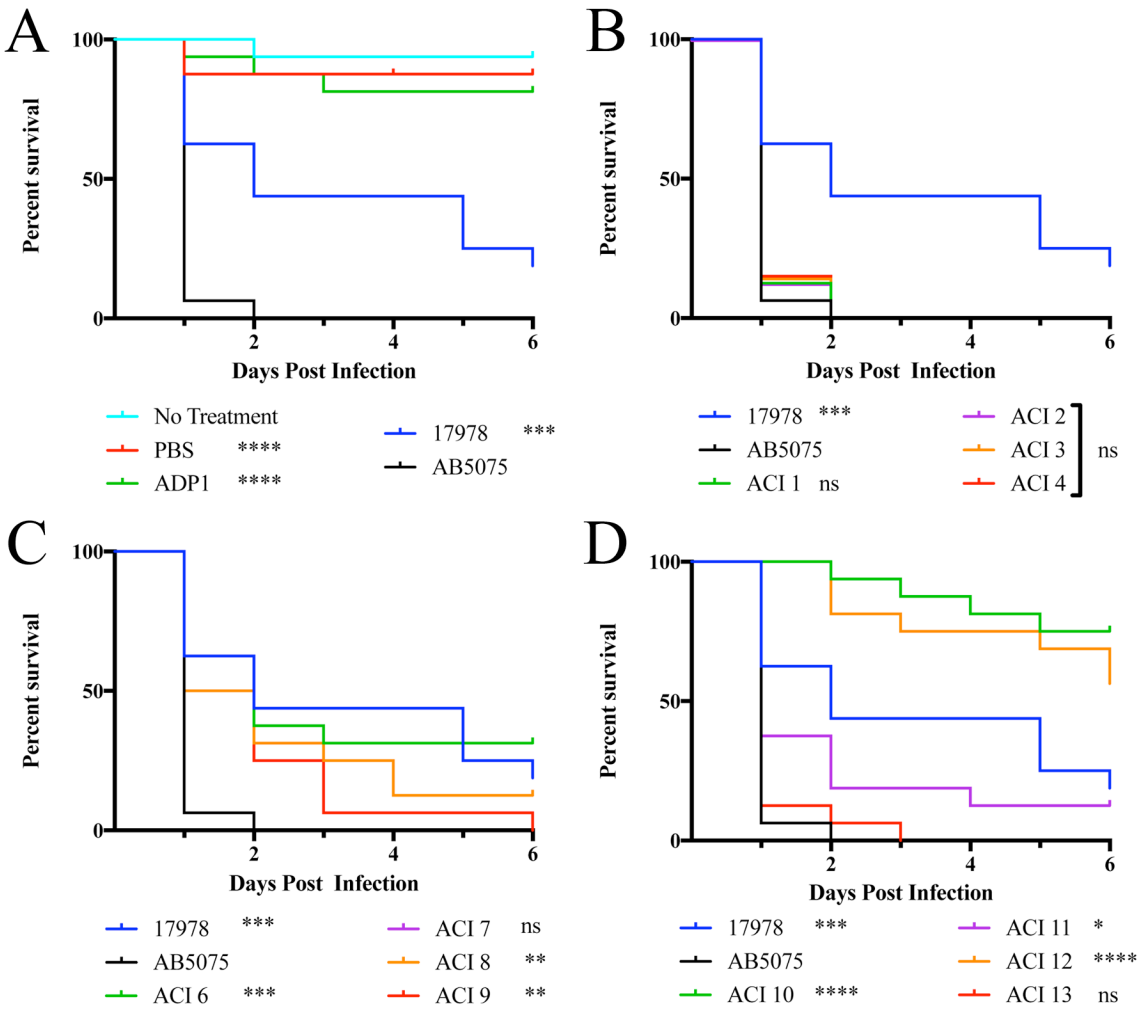

Figure 2.3 Characterization of *Acinetobacter* Clinical Isolates. The indicated strains of bacteria were inoculated (10^6 CFU/larvae) into *Galleria mellonella* larvae (n = 16 larvae per strain) and monitored for survival for 6 days. Each panel includes the *A. baumannii* strains 17978 and AB5075 as a reference in blue and black, respectively. The panels depict **(A)** controls; **(B)** ACI strains 1-4; **(C)** ACI strain 6-9; **(D)** ACI strains 10-13. Table 2.2 contains a more detailed description of each strain. Survival differences were analyzed and compared to AB5075 using the log-rank test; asterisks indicate the degree of significance as follows: **** $p < 0.0001$, *** $p < 0.001$, ** $p < 0.01$, * $p < 0.05$, ns, not significant.

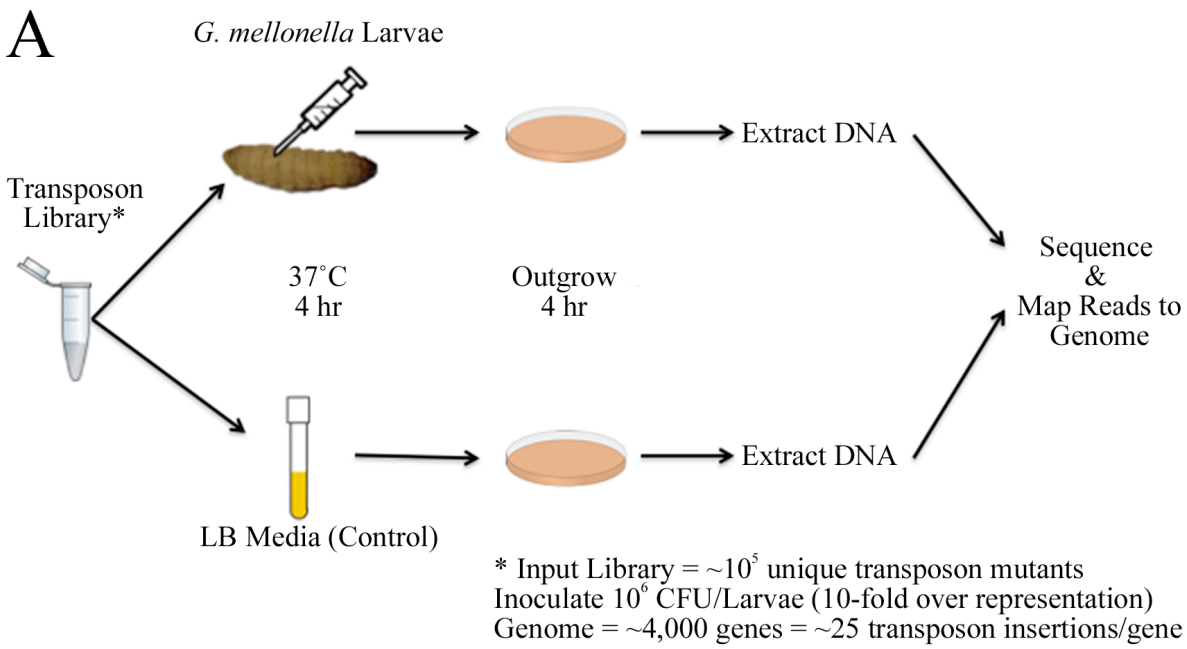

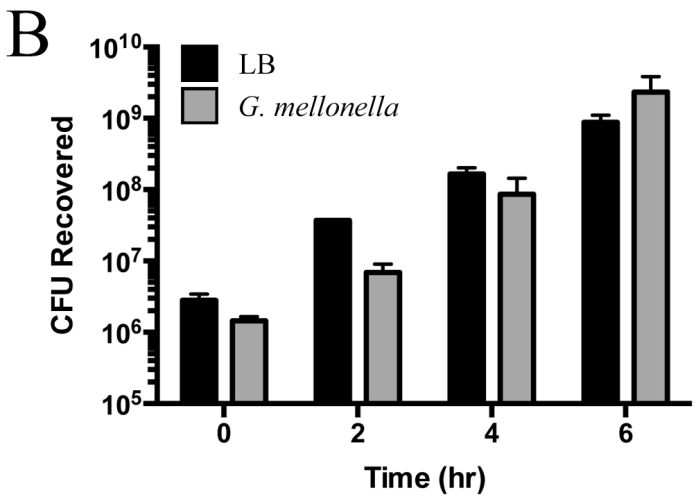

Figure 2.4 Schematic of TnSeq experiment. **(A)** Diagram of the TnSeq experiment. Briefly, 10 µL of the AB5075 transposon mutant library (adjusted to ~10^8 CFU/mL in sterile PBS) was inoculated into either LB medium (growth control) or into *G. mellonella* larvae and incubated for 4 hours at 37 ˚C. Following this incubation, bacteria were collected by homogenization (Gm pool) or centrifugation (LB Pool) and plated onto LB agar plates containing 10 µg/mL tetracycline for an additional 4 hours to eliminate the endogenous bacterial flora present in *G. mellonella* and to increase biomass. Following out-growth, bacteria were collected from the plates by gentle scraping and DNA was extracted and used for preparation of TnSeq libraries using the TnSeq-Circle Method (Gallagher, Shendure, and Manoil 2011). **(B)** Graph depicts CFU recovery following growth of the Tn mutant pool over time in LB (black bars) and *G. mellonella* larvae (grey bars).

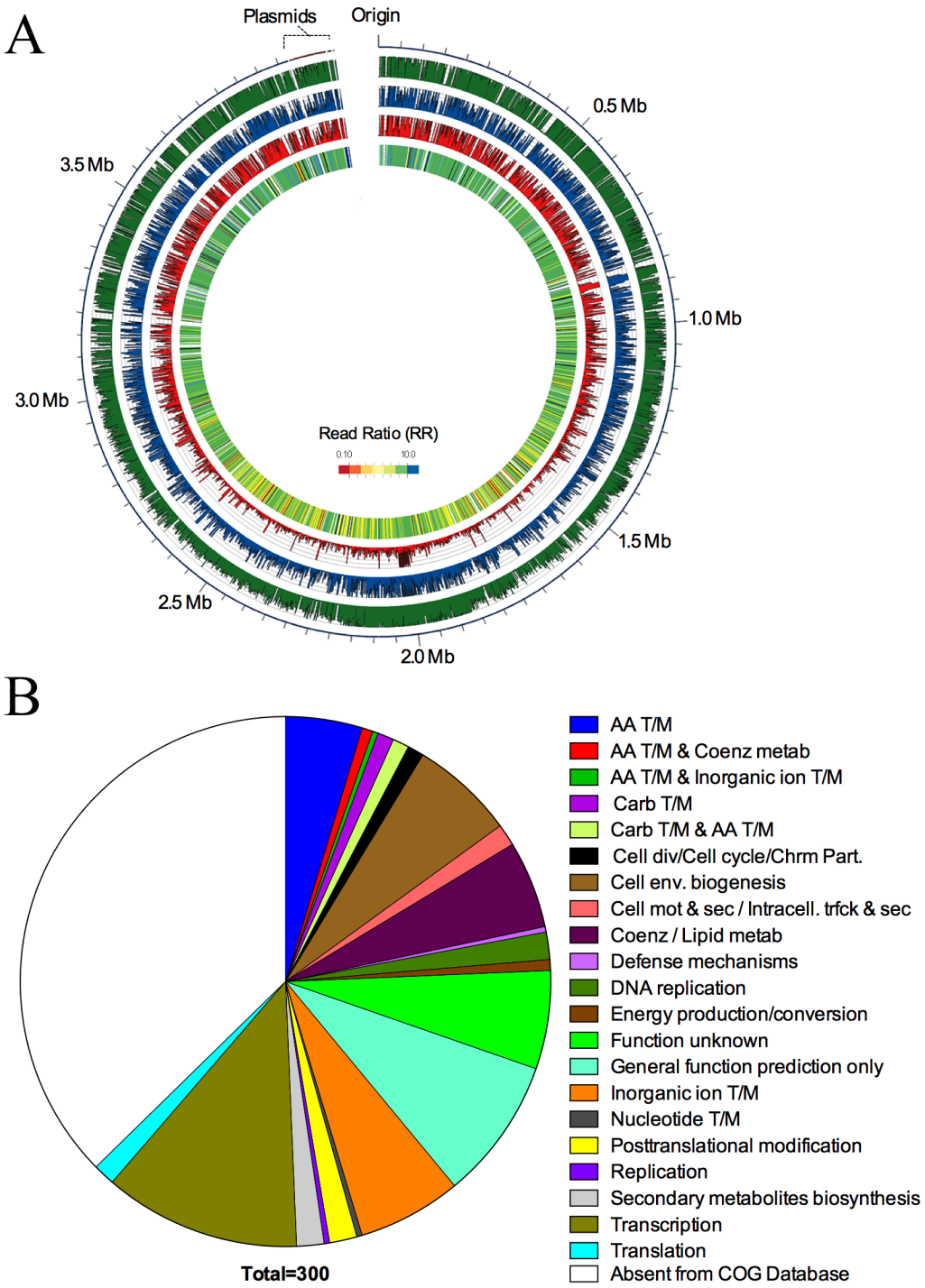

Figure 2.5 Results from the TnSeq Experiment. (A) Graphical representation of the TnSeq data. The outermost ring depicts the AB5075 chromosome and plasmids. The 3 middle rings depict hits per gene in the Pre-Growth, LB-Growth and *Galleria*-Growth samples (green, blue, and red, respectively). The innermost ring displays a heat map of the read ratio (RR) between the Gm and LB samples (Gm-essential genes are colored red). Essential genes are colored white;

Figure 2.5 (continued)
genes displaying a general growth defect are colored black. This image created using Circos (Krzywinski et al. 2009). **(B)** Pie chart depicting Gm-essential hits grouped by COG categories. Abbreviations: AA, Amino Acid; T/M, Transport and Metabolism; Coenz, Coenzyme; metab, Metabolism; Chrm Part., Chromosome Partitioning; mot & sec, Motility and Secretion, trfck & sec, Trafficking and Secretion.

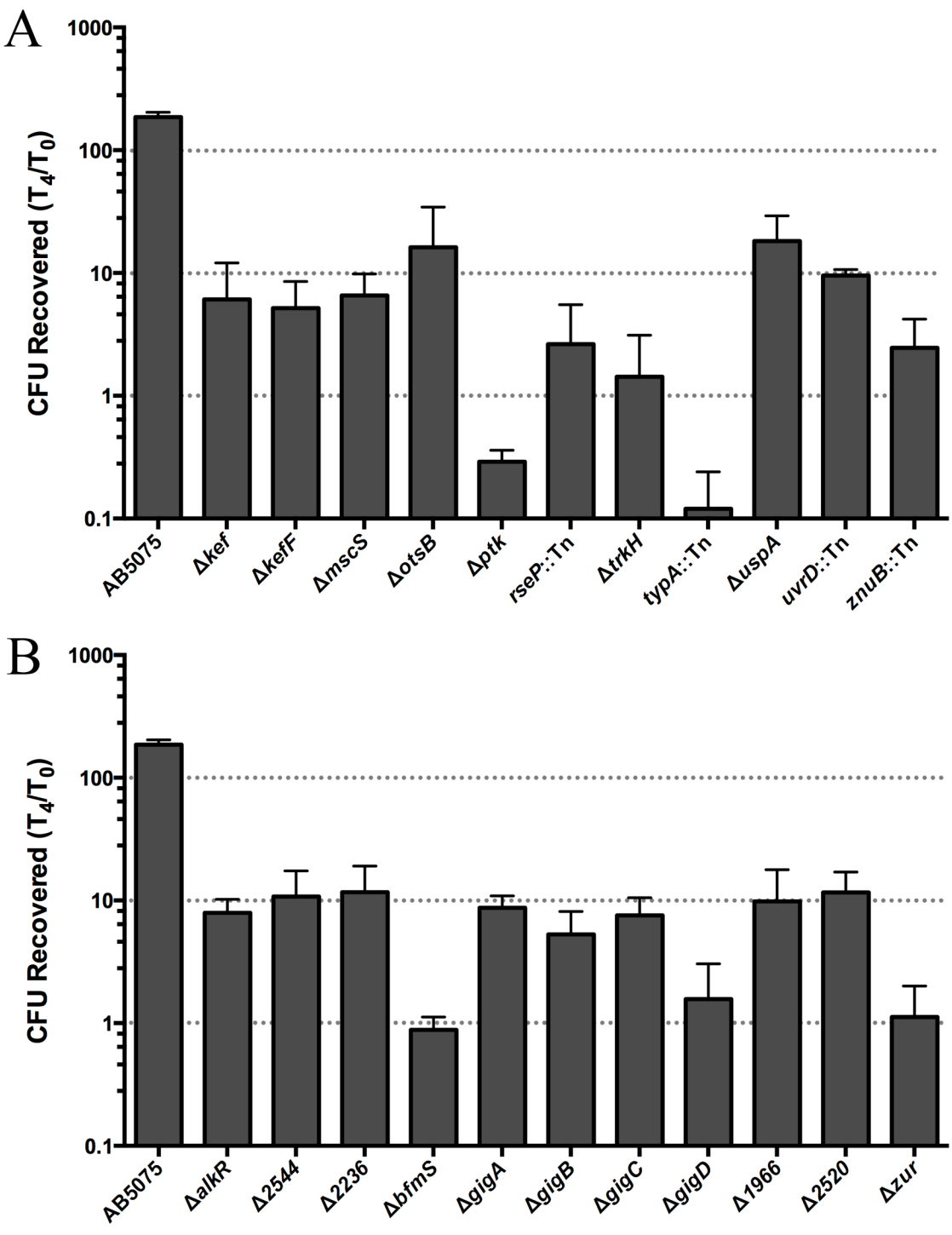

Fig. 2.6 Growth of selected mutants in *G. mellonella* larvae. The indicated mutants strains were inoculated into *G. mellonella* larvae. Data is presented as described in the legend for Figure 2.2. **(A)** Stress response genes; **(B)** Transcriptional regulators.

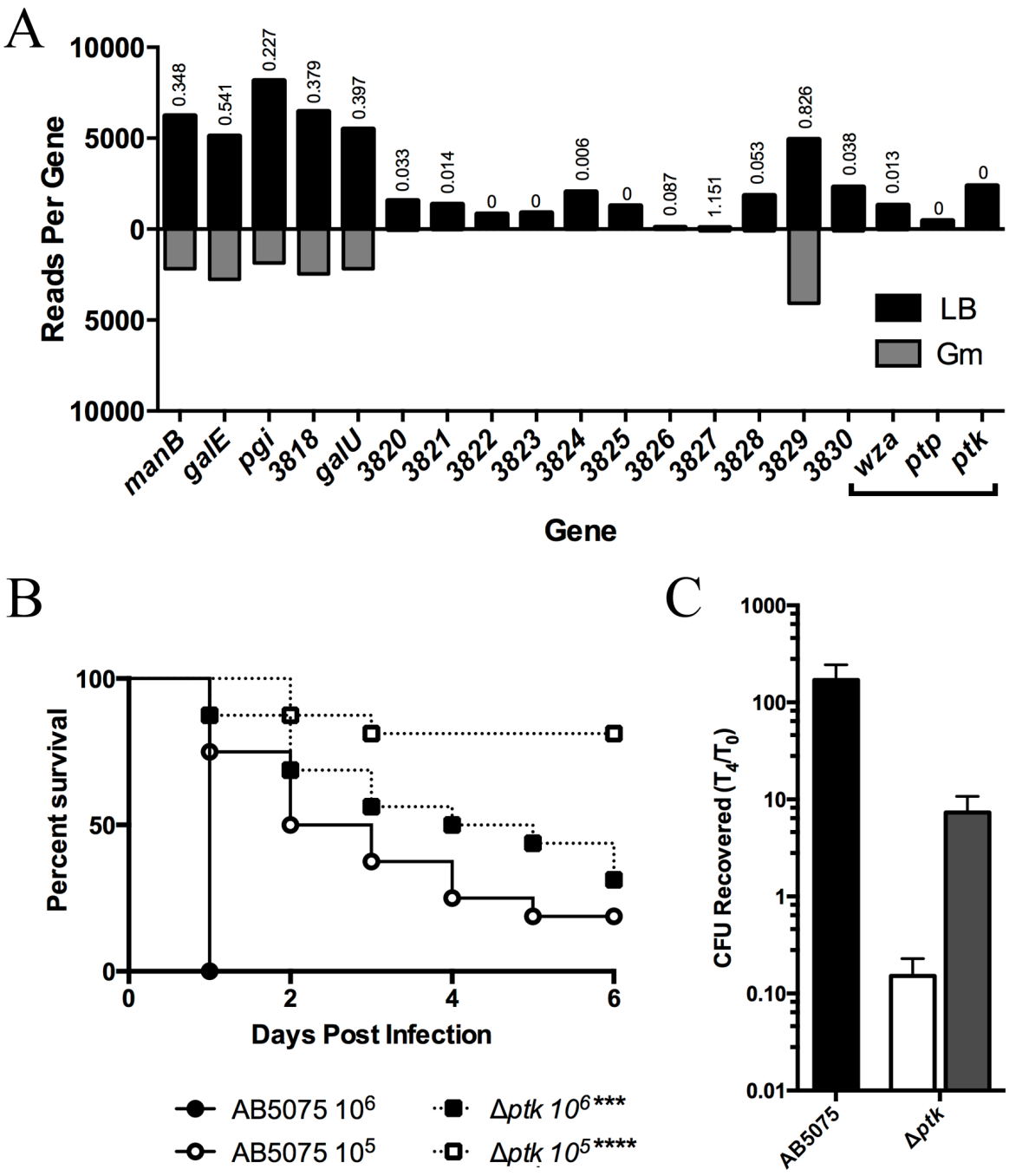

Figure 2.7 Capsule production is required for virulence in *G. mellonella*. (A) TnSeq data for capsule biosynthetic operon depicted as total transposon reads per gene mapped to the capsule operon from the LB growth sample (top, black) and from the *G. mellonella* growth samples (bottom, grey). The gene read ratio, RR, (Gm/LB) is shown above each bar (significant reductions are defined as a RR ≤ 0.10 as described in the main text). Genes labeled with numbers indicate gene annotations for unnamed genes in the format (ABUW_####). The bracketed genes indicate the structural genes required for capsular polysaccharide export to the outer membrane.

Figure 2.7 (continued)
(B) *G. mellonella* (n = 16) larvae were infected with either wild type or *ptk* deficient bacteria as indicated. Survival was monitored for 6 days. **(C)** Growth of wild type AB5075 carrying a hygromycin resistance cassette at the Tn7 locus (black) or a *ptk* deletion strain harboring either a hygromycin cassette at the Tn7 attachment site (white) or a wild type copy of the *ptk* gene (grey) after injection into *G. mellonella* larvae. Larval survival and bacterial growth assays are presented as described in the legend for Figure 2.2. For (B), survival differences were assessed by the log rank test of significance with significant differences indicated as follows: ***, $p \leq 0.001$; ****, $p \leq 0.0001$.

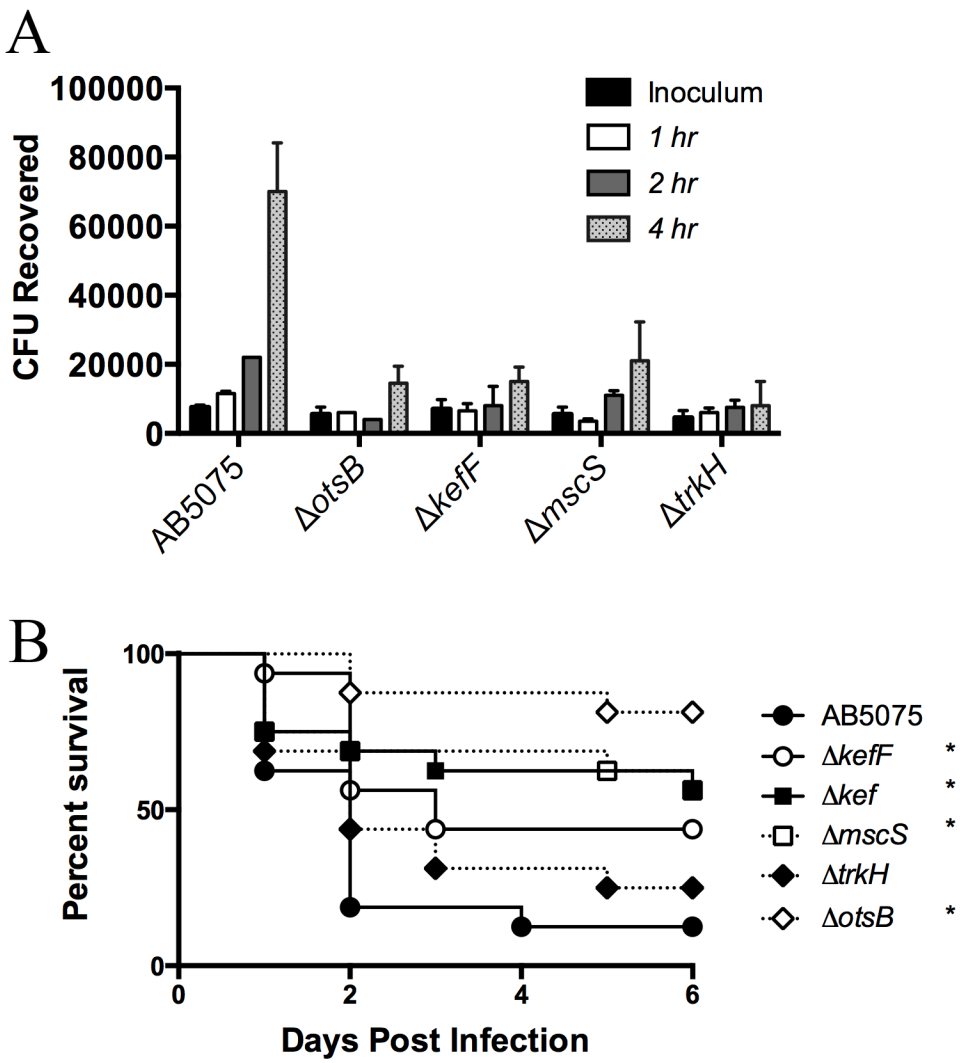

Figure 2.8 Osmotic stress genes are required for virulence in *G. mellonella*. (A) Growth of osmotic stress mutants in freshly collected hemolymph monitored over time. The indicated strains (10^4 CFU) were added to hemolymph and quantified over time as indicated. **(B)** *G. mellonella* larvae (n = 16) were infected with 10^5 CFU of wild type AB5075 or isogenic mutants. Larval survival was monitored daily for 6 days and analyzed as described in the legend of Figure 2.2. *, $p \leq 0.05$.

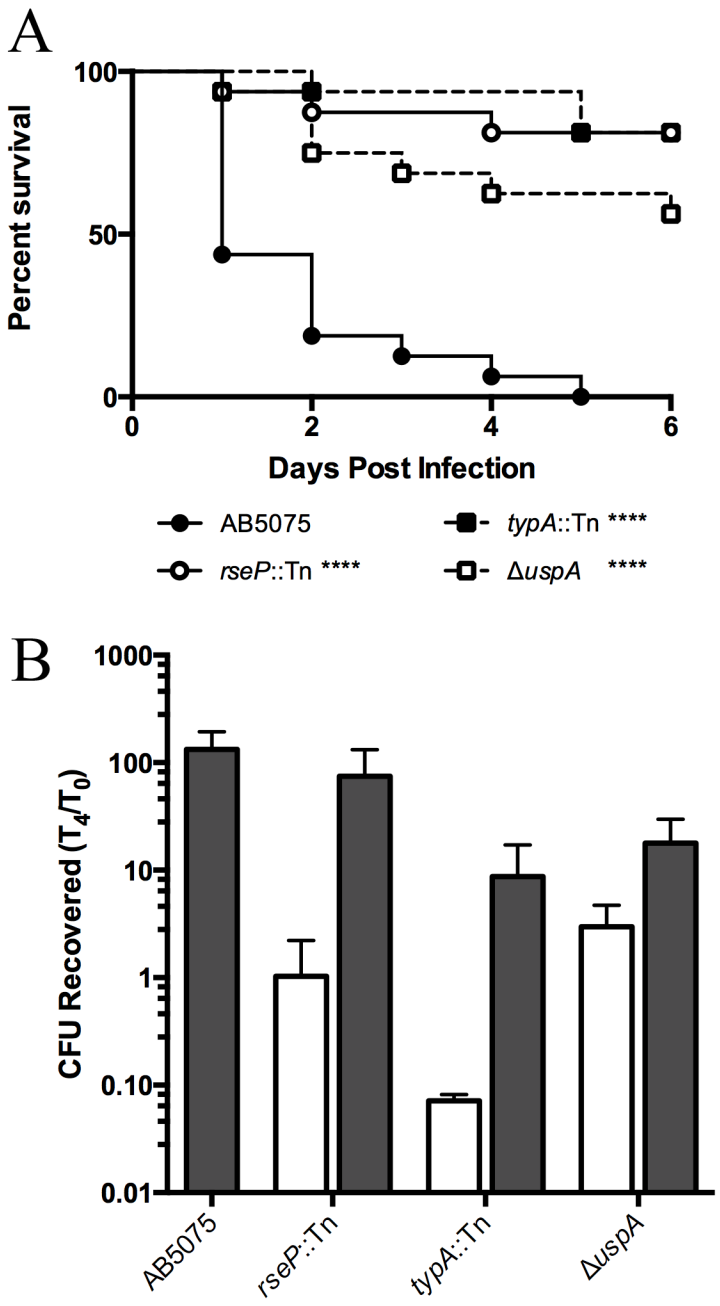

Figure 2.9 Stress response genes are required for *G. mellonella* killing and growth in *Galleria*. (A) *G. mellonella* larvae were infected with the indicated strains and monitored for survival as described in the legend for Figure 2.2. **(B)** Growth of wild type AB5075 (grey bar) or the indicated strains harboring a hygromycin gene (white bars) or a wild type copy of deleted gene at the Tn7 locus (grey bars) following inoculation of *G. mellonella* larvae as described in the legend of Figure 2.2. ****, $p \leq 0.0001$.

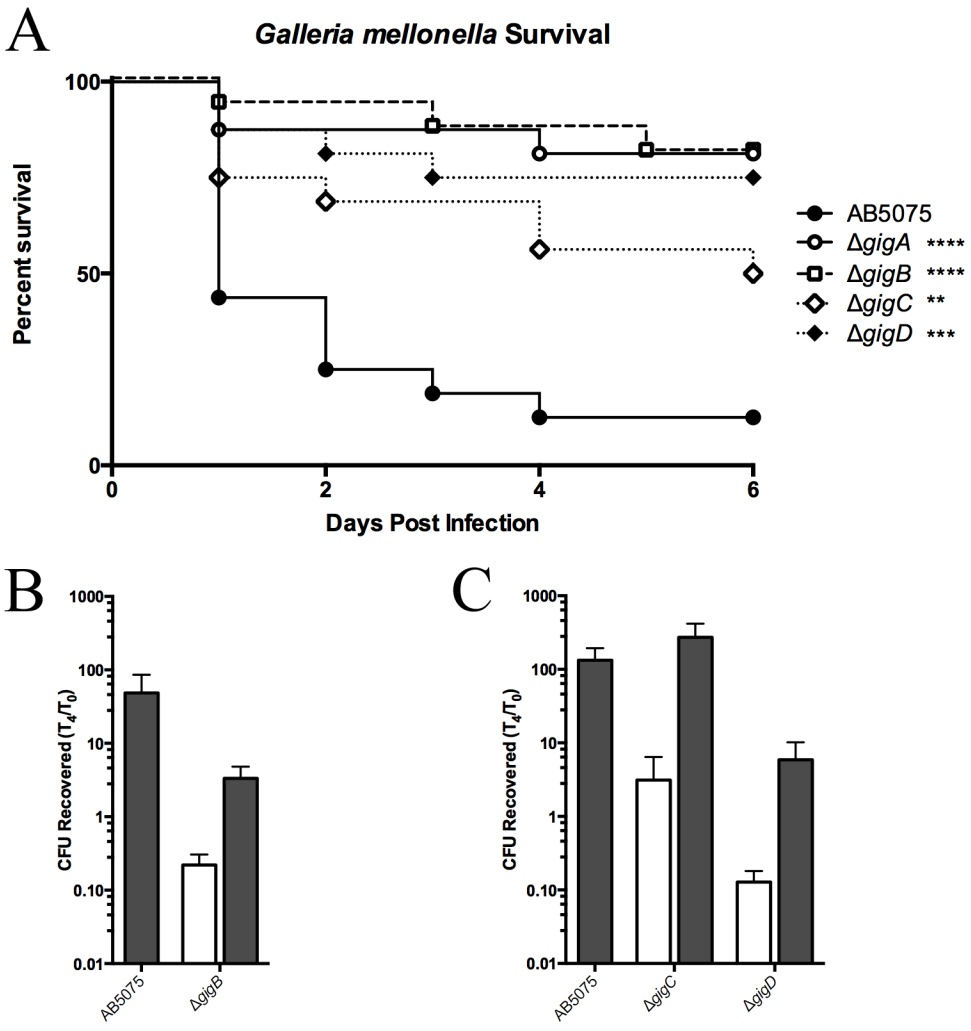

Figure 2.10 Growth in *Galleria* (*gig*) genes are required for virulence in *G. mellonella.* (A) *G. mellonella* larvae were infected with the indicated strains and monitored for survival as described in the legend of Figure 2.2. **(B)** Growth of AB5075 with empty vector (grey bar) or the *gigB* mutant harboring empty vector (white) or a complementing clone of *gigB* (grey bar). **(C)** Growth of wild type AB5075 (grey bar) or the indicated strains harboring a hygromycin gene (white bars) or a wild type copy of deleted gene at the Tn7 locus (grey bars). For B, and C, growth is depicted as described in the legend of Figure 2.2. ****, $p \leq 0.0001$; **, $p \leq 0.01$.

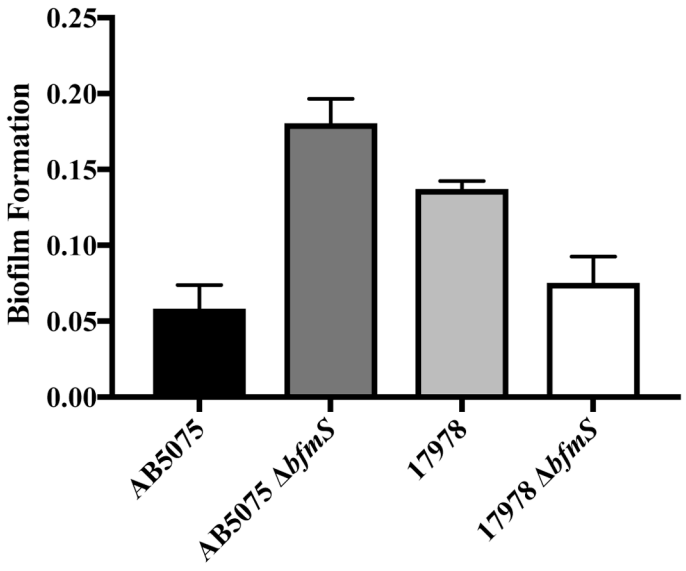

Figure 2.11 The role of the *bfmS* gene in biofilm differs across *A. baumannii* strains. Graph depicts biofilm production as measured by the crystal violet staining method (Djordjevic, Wiedmann, and McLandsborough 2002). Briefly, overnight cultures of the indicated strains were diluted 1:100 into fresh media in triplicate wells of a 96-well microtiter plate and incubated for 24 hours without shaking at 37 ˚C in LB medium. After 24 hours of incubation, the optical density of each well was measured at 600 nm. The medium and non-adherent cells were removed and the plate was washed with sterile ddH_2O four times prior to staining with crystal violet for 15 minutes under gentle agitation. The wells were washed again with ddH_2O and residual crystal violet was dissolved in 70% ethanol and measured at 595 nm in the microtiter plate reader. Biofilm formation is plotted as the amount of crystal violet staining normalized for cell density (OD_{595} / OD_{600}) from triplicate wells and is plotted as the mean values with error bars representing one standard deviation.

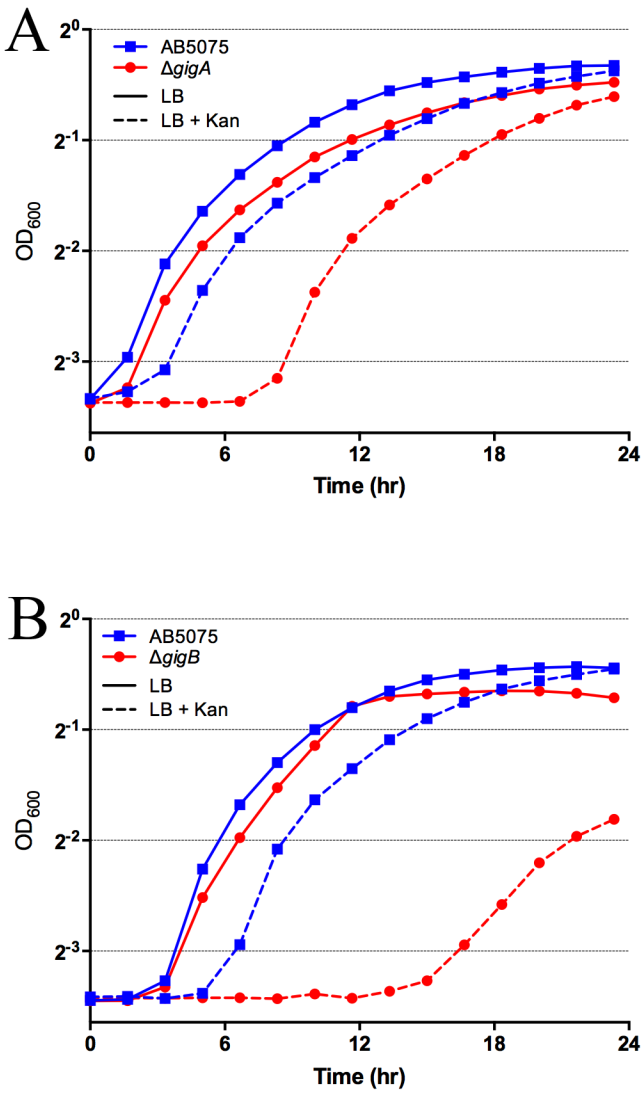

Figure 2.12 Genes required for growth in *Galleria* are also required for growth in sub-inhibitory antibacterials. The indicated strains were grown for 24 hr at 37 ˚C in LB with or without 625 µg/mL kanamycin. Growth was measured by OD_{600} every 10 minutes in a Tecan 96 well Plate reader.

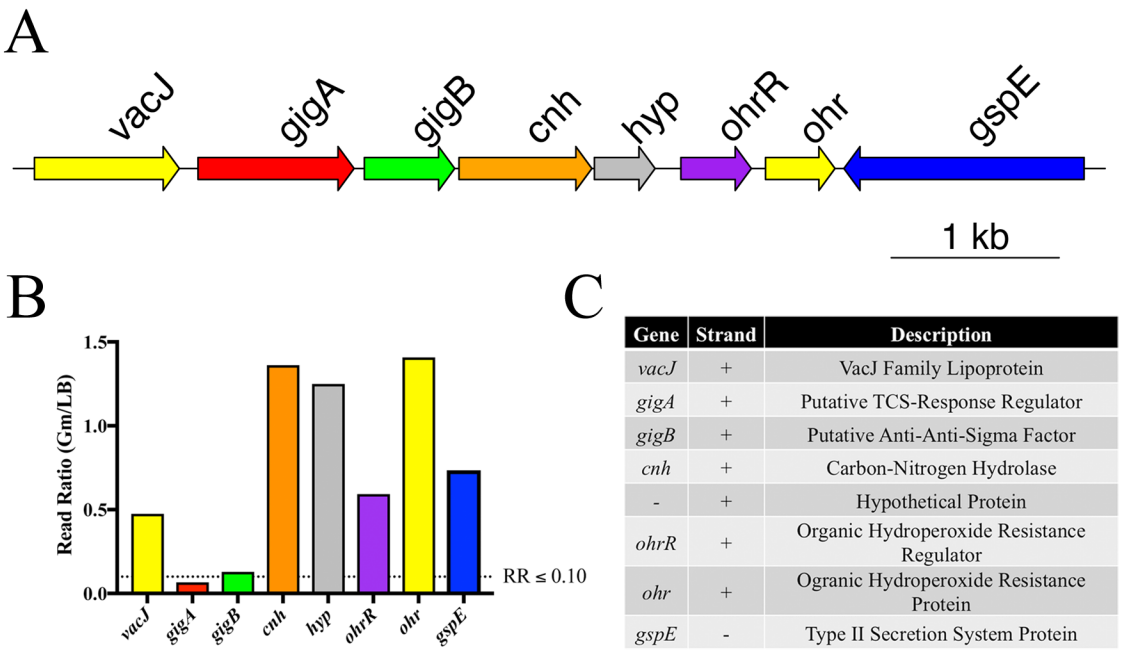

Gene	Strand	Description
vacJ	+	VacJ Family Lipoprotein
gigA	+	Putative TCS-Response Regulator
gigB	+	Putative Anti-Anti-Sigma Factor
cnh	+	Carbon-Nitrogen Hydrolase
-	+	Hypothetical Protein
ohrR	+	Organic Hydroperoxide Resistance Regulator
ohr	+	Ogranic Hydroperoxide Resistance Protein
gspE	-	Type II Secretion System Protein

Figure 3.1 The *gigA*/*gigB* locus (A) Schematic diagram of the *gigAB* locus in *A. baumannii* AB5075. Drawn to scale as indicated. **(B)** TnSeq Read Ratios for the genes in the *gigAB* locus. Read Ratio calculated from the TnSeq experiment described in Chapter II. The threshold for significance was a RR ≤ 0.10. **(C)** Gene descriptions for the genes located in the *gigAB* locus.

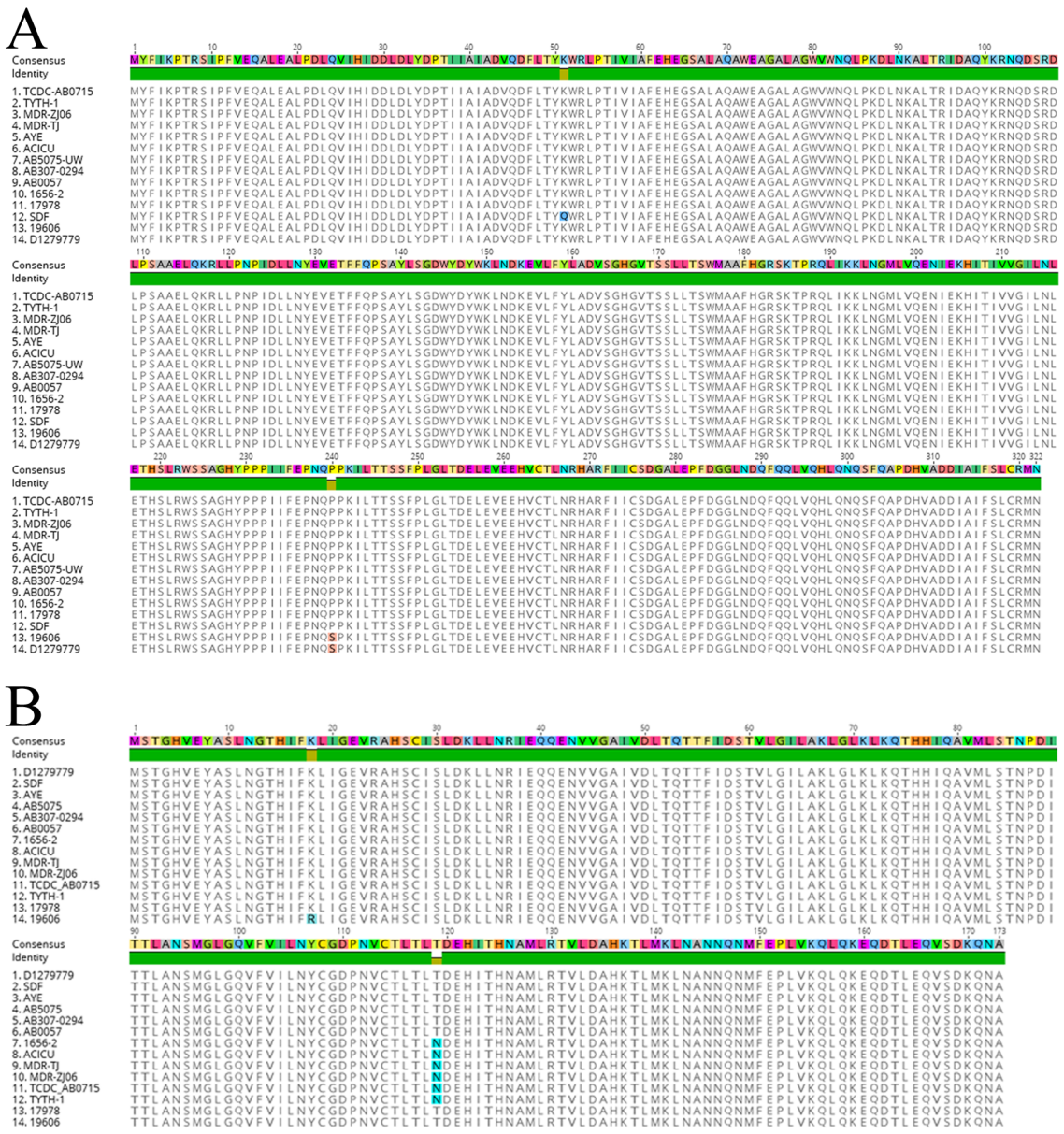

Figure 3.2 GigA and GigB are highly conserved across *A. baumannii* isolates. Clustal-Omega alignments for GigA (A) and GigB (B) from 14 *A. baumannii* isolates. Amino Acid differences are highlighted.

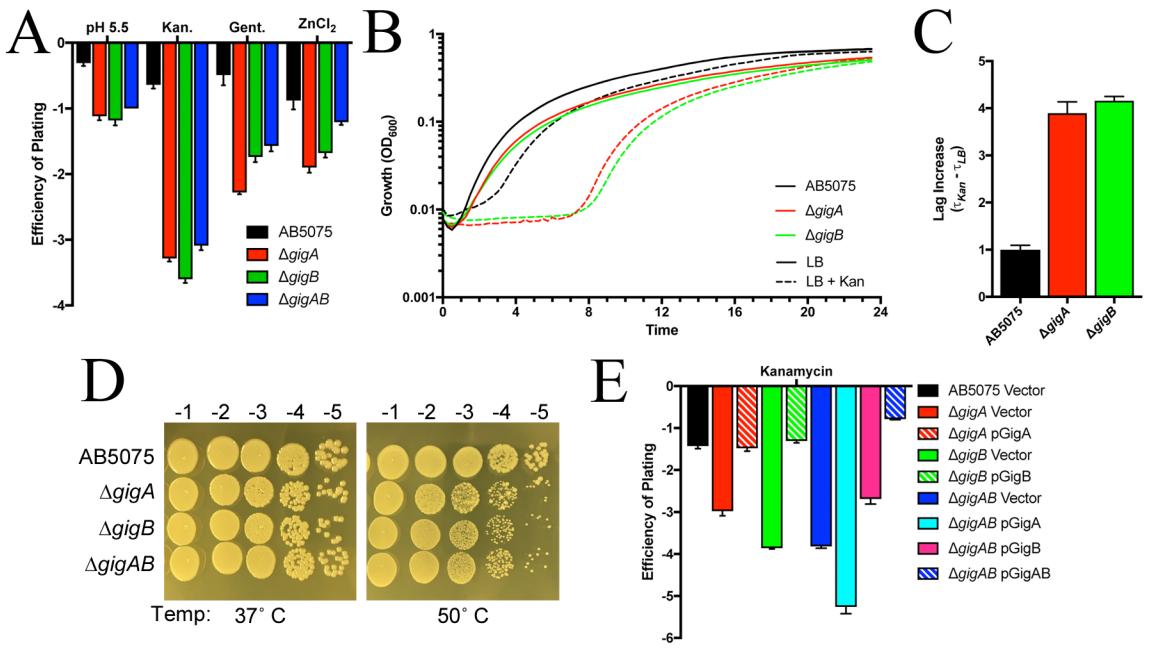

Figure 3.3 *gigA* and *gigB* are required for *in vitro* stress resistance. (A) Plating efficiency experiment. Data represents the mean $\log_{10}$ value of CFUs recovered on LB plates containing the indicated stressors divided by the CFUs recovered on plain LB plates. Data from a representative experiment is shown with error bars representing one standard deviation. Medium conditions are as follows: pH 5.5, LB medium adjusted to pH 5.5 with HCl; Kan., kanamycin added to 500 µg/mL; Gent., gentamicin added to 10 µg/mL; $ZnCl_2$, $ZnCl_2$ added to 1.25 mM. **(B)** Growth curve of the indicated strains grown with (dotted lines) and without (solid lines) the addition of kanamycin (500 µg/mL). Mean OD_{600} readings from triplicate wells for each strain/medium condition are shown from a representative experiment. **(C)** Plot depicts the relative increase in the time required to enter exponential phase defined follows: $(\tau_{Kan} - \tau_{LB})_{mutant} / (\tau_{Kan} - \tau_{LB})_{WT}$, where τ = the time required to reach an OD of 0.02. **(D)** Photograph of the indicated strains grown on LB at either 37 ˚C (left panel) or 50 ˚C (right panel). Numbers above the image represent the dilution factor ($\log_{10}$) of the given spots. **(E)** Plating efficiency experiment for the indicated strains on LB + 500 µg/mL kanamycin.

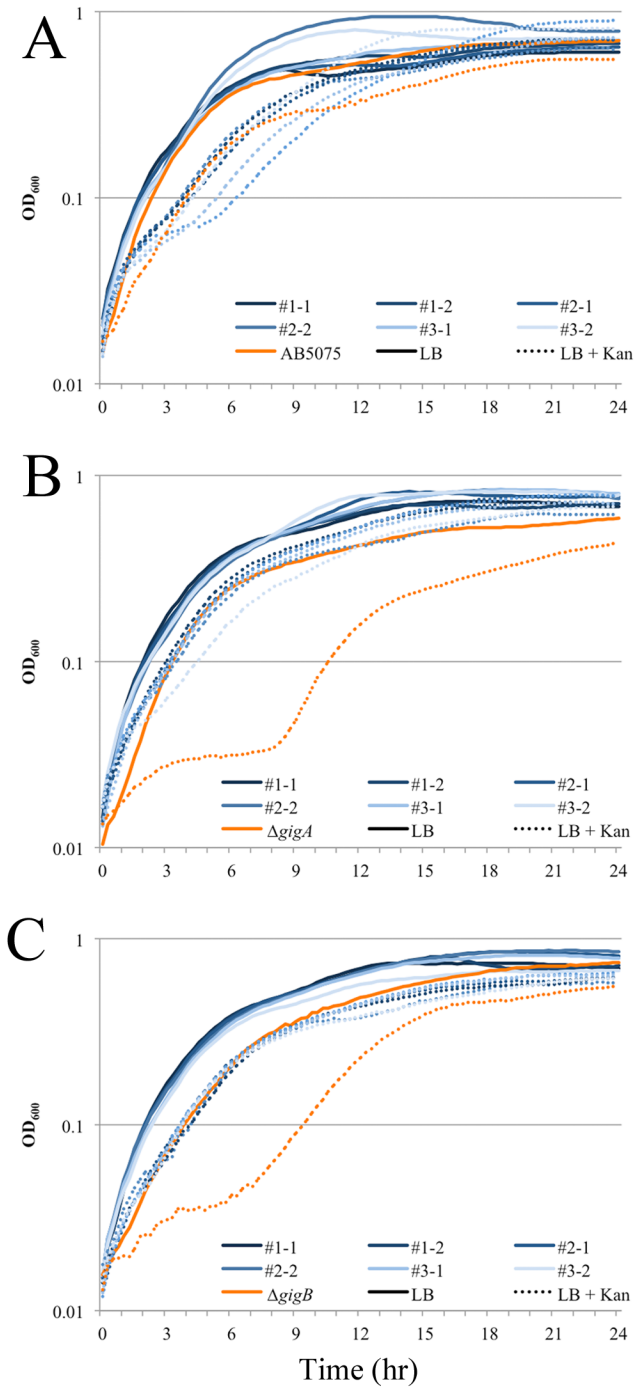

Figure 3.4 Growth in Kanamycin selects for suppressors in the Δ*gigA*/Δ*gigB* backgrounds. Growth curves of AB5075 **(A)**, Δ*gigA* **(B)** and Δ*gigB* **(C)** strains and derivatives thereof in the presence (dotted lines) or absence of 500 µg/mL kanamycin (solid lines). For each strain, two colonies from three independent cultures grown overnight in LB + 500 µg/mL kanamycin (a total of six colonies per strain) were retested for the characteristic lag-time increase observed for *gig* mutant strains. The growth of the re-tested strains are plotted in shades of blue, while the parental strain is plotted in orange.

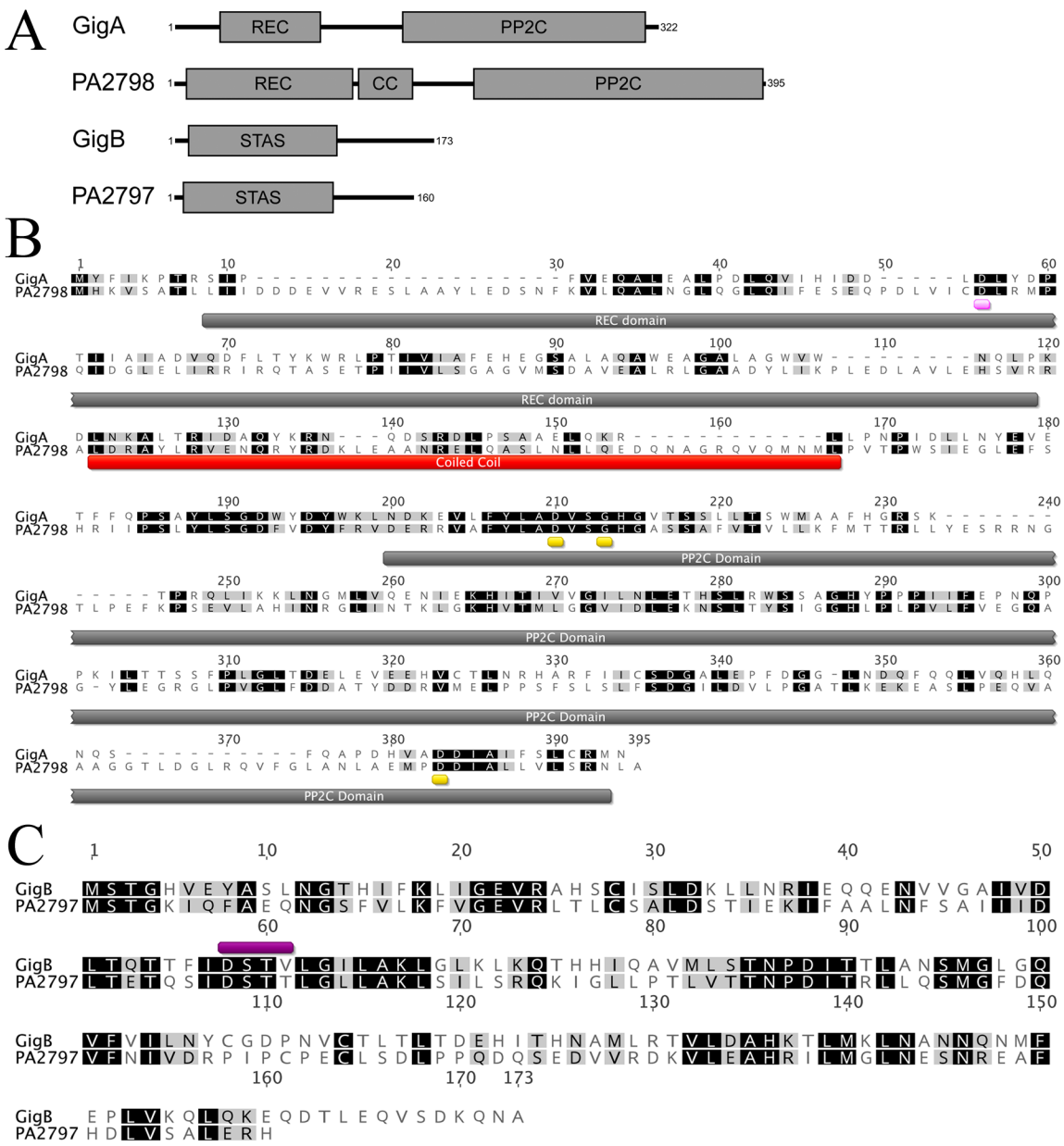

Figure 3.5 *P. aeruginosa* proteins PA2798 and PA2797 are homologous to GigA and GigB. **(A)** Domain organization of GigA, GigB, and the corresponding homologs found in *Pseudomonas aeruginosa,* PA2798 and PA2797. REC, Two-Component Receiver Domain; PP2C, protein phosphatase domain; CC, Coiled-coil domain; STAS, Sulfate Transport and Anti-Sigma Factor Antagonist. **(B)** and **(C)** Clustal-Omega alignments for GigA/PA2798 and GigB/PA2797, respectively. Black shading indicates conserved residues; grey shading indicates similar residues. For (B), domain boundaries are shown below the alignment. Yellow bars, Mg^{2+} binding site from the 3D structure of PA2798 (3EQ2); Magenta, predicted phosphoryl-acceptor aspartate residue (Asp-32 in GigA, Asp-56 in PA2798); Red, coiled-coil region. For (C), the purple box identifies the "DSSG" motif region containing the serine targeted for phosphorylation (Ser-59 in both GigA and PA2797).

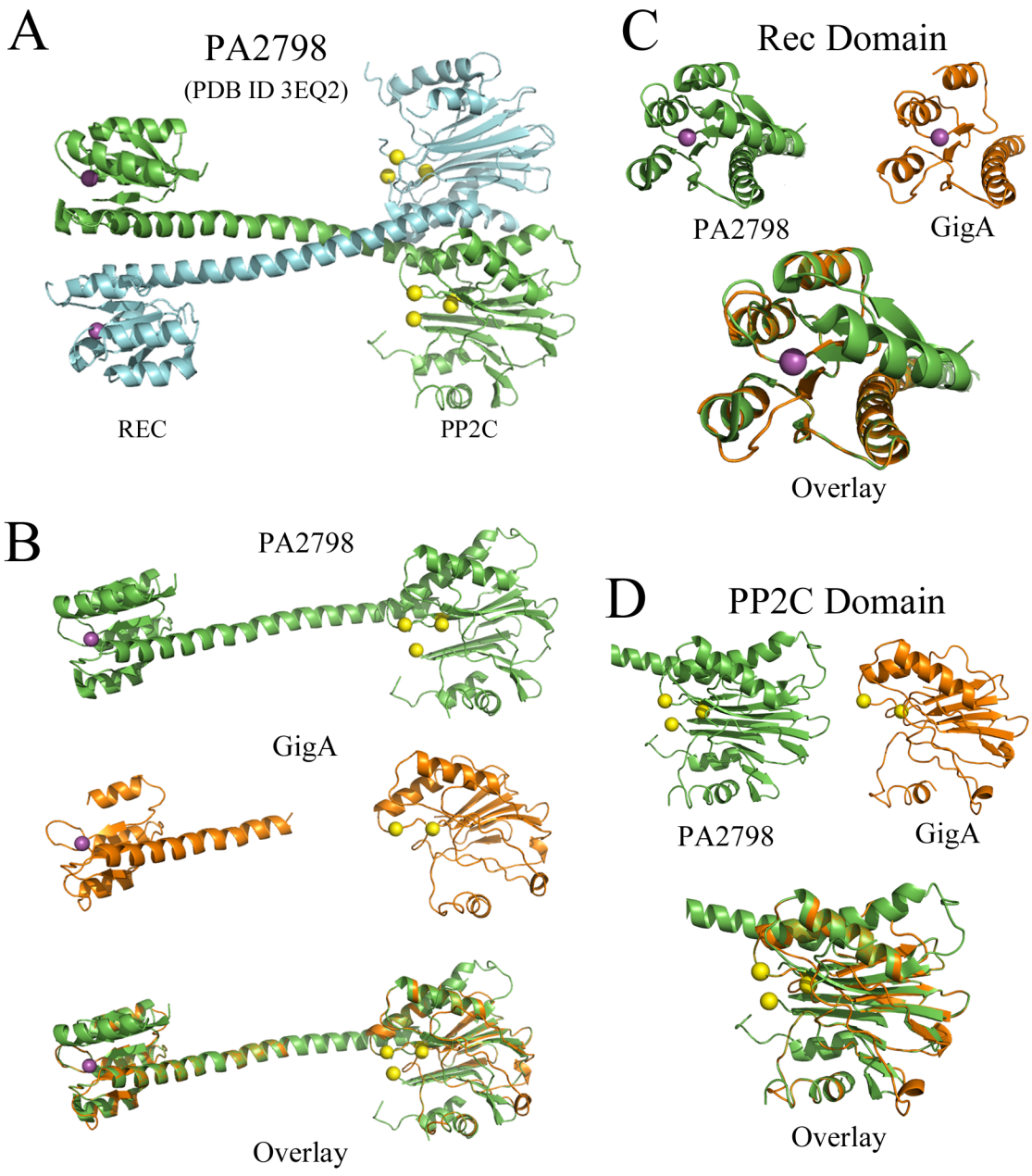

Figure 3.6 Structural modeling of GigA. (A) Three-dimensional structure of PA2798 (PDB ID 3EQ2). PA2798 crystalized as a dimer and the monomers are colored green and cyan. **(B – D)** The Phyre2 Server (Kelley et al. 2015) was used to generate a three-dimensional model of GigA. Panel B depicts the entire structural prediction for a single promoter of PA2798 (top, green), GigA (middle, orange) and an overlay between PA2798 and GigA (bottom). Panels C and D depict the structural alignments between the REC and PP2C domains, respectively. Spheres indicate the location of the predicted phosphoryl-acceptor aspartate residue (magenta) and the residues predicted to coordinate an Mg^{2+} ion required for PP2C activity (yellow). The third Mg^{2+} binding residue (Asp-311) in the GigA PP2C domain was not modeled by the Phyre2 program.

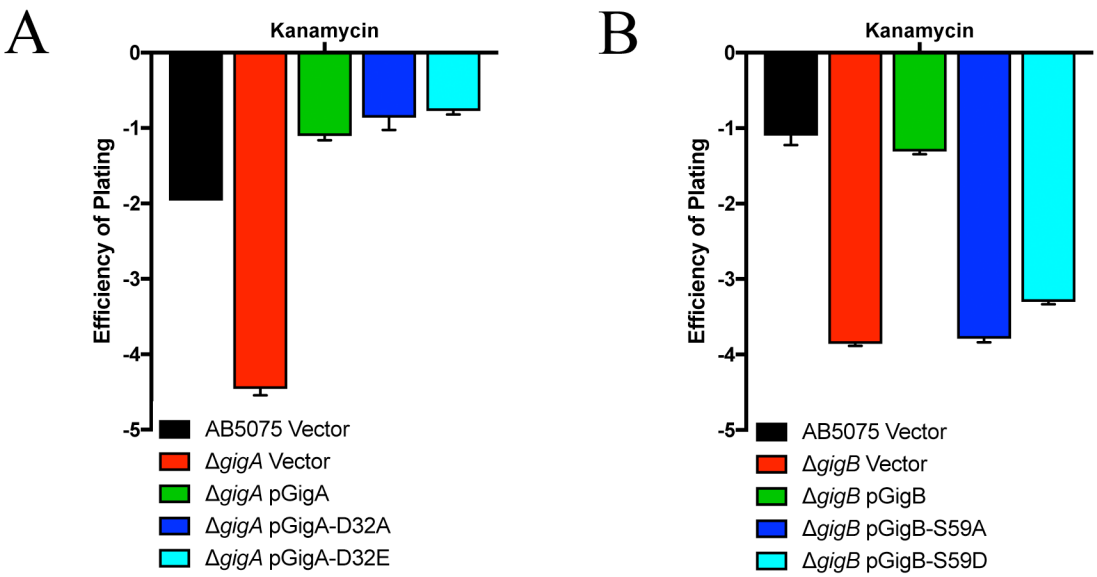

Figure 3.7 Mutational Analysis of the GigA and GigB proteins. Plating efficiency experiments for LB + 500 µg/mL Kanamycin for the indicated strains in the Δ*gigA* background **(A)** and Δ*gigB* background **(B).** Experiments were performed as described in Figure 3.3.

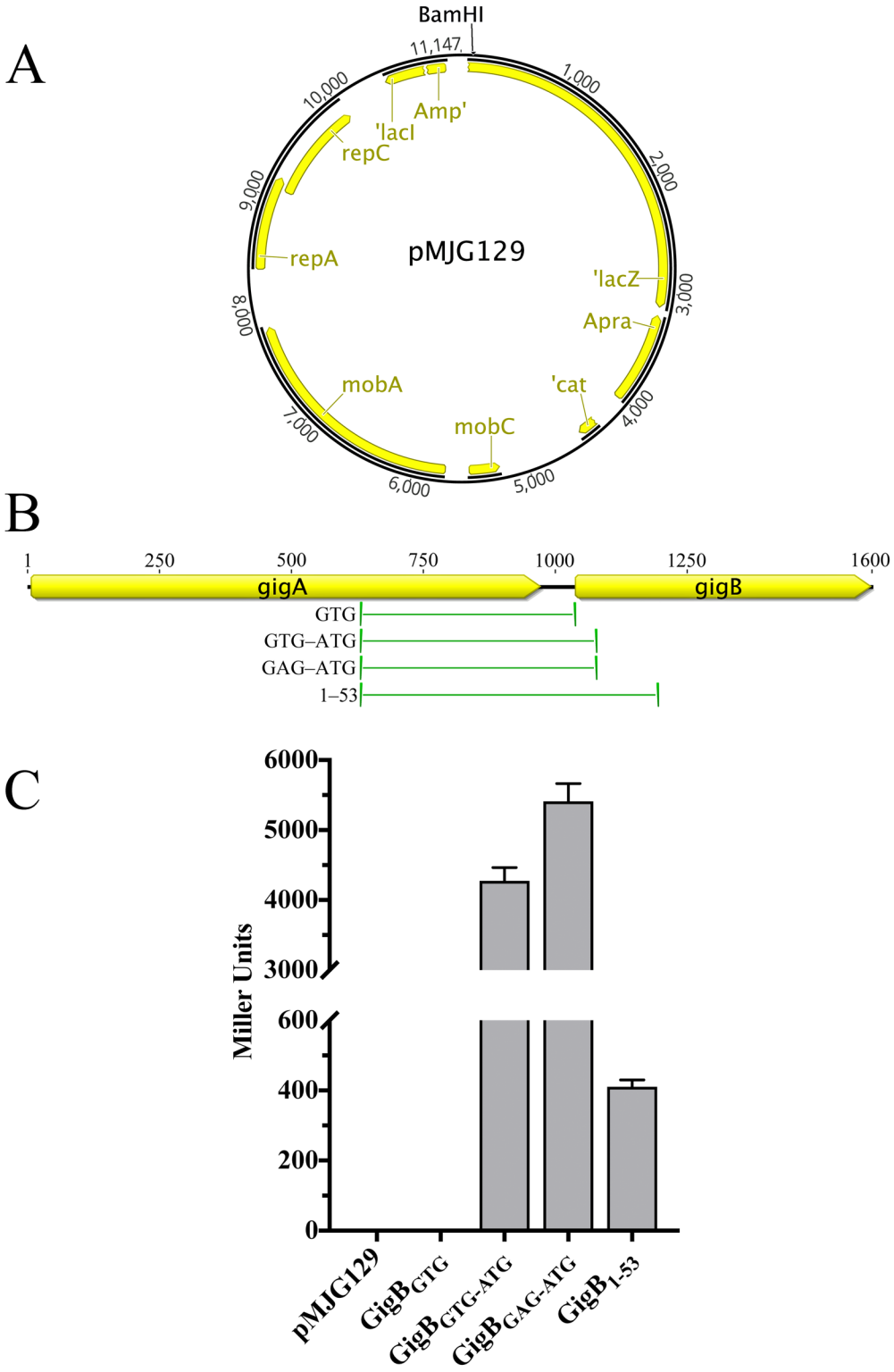

Figure 3.8 Translation start site analysis of GigB. (A) Map of plasmid pMJG129 used for translation start site analysis. pMJG129 is a derivative of pGS-*lac*-02 (Gal-Mor, Zusman, and Segal 2002). Annotations are as follows: BamHI, restriction site used for intorduction of test

Figure 3.8 (continued)
DNA; '*lacZ*, promoterless *lacZ* gene; Apra, apramycin resistance gene; *'cat*, chloramphenicol resistance gene (interrupted); *mobA/mobC*, genes for mobility functions of the plasmid (interrupted); *repA/repC*, genes for plasmid replication; *'lacI*, interrupted *lacI*^{q} repressor gene; *Amp'*, interrupted ampicillin resistance gene. **(B)** Schematic representation of the four constructs used to assess the translation start of GigB. All constructs share a common 5' start site located within the 3' region of *gigA*. The GTG represents the annotated start codon of the *gigB* gene; ATG represents the second potential start codon located 39 bases downstream of the GTG. The 1-53 constructs contains the first 53 codons of *gigB* prior to fusion with the *lacZ* coding sequence. Additional details can be found in the main text of Chapter III. **(C)** Results of Miller assays conducted with AB5075 harboring the empty vector (pMJG129) or the indicated test constructs.

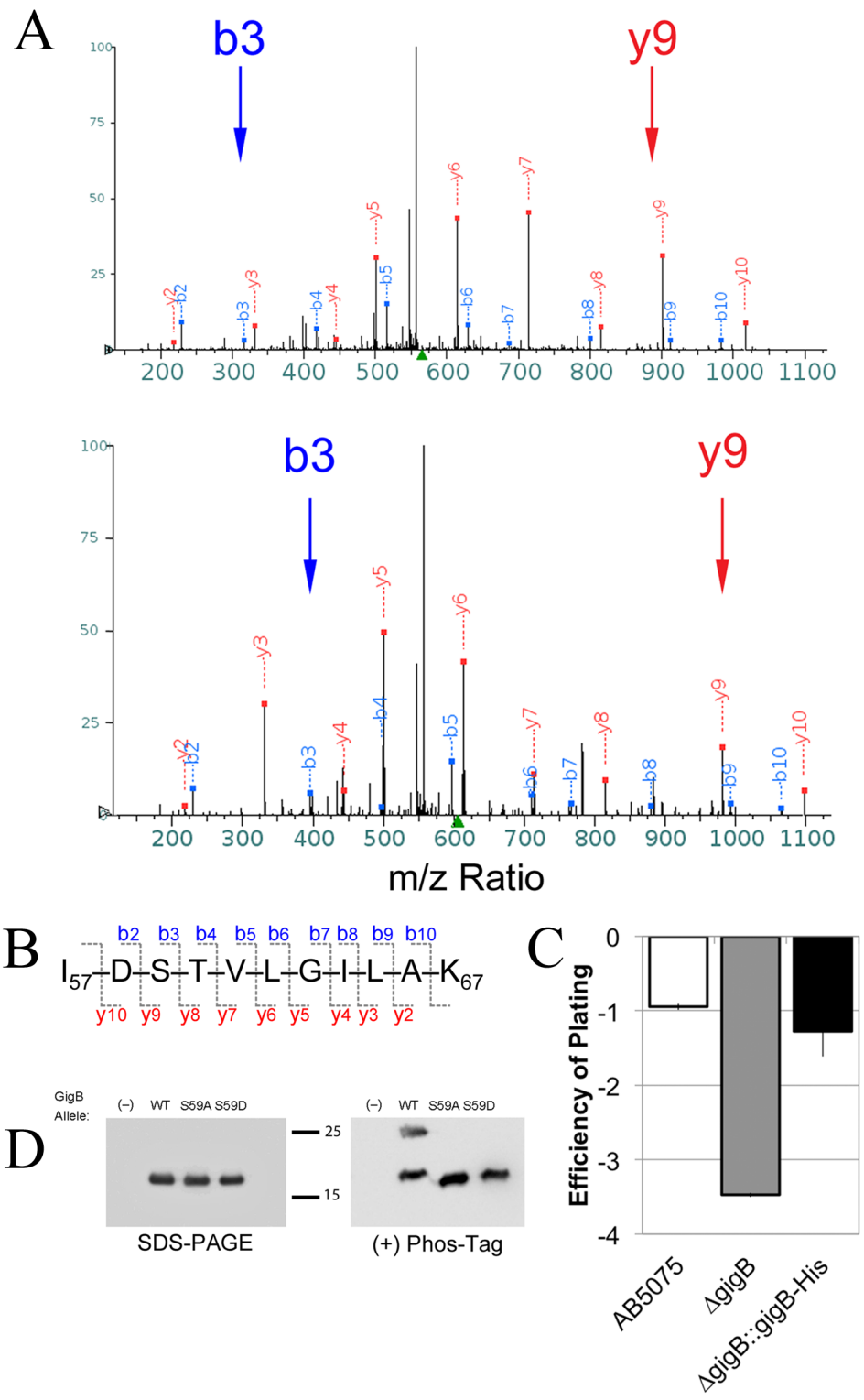

Figure 3.9 GigB is phosphorylated *in vivo*. (A) Mass Spectrometry ionization fragments identified from *in vivo* purified GigB showing GigB (top panel) and GigB–P (bottom panel). Arrows indicate the ion fragments supporting the existence of GigB–P, which are shifted by the

Figure 3.9 (continued)
size of a phosphate group (~80 mass units) in the phosphorylated specie. **(B)** Peptide fragment, including the *b* (top, blue) and *y* (bottom, red) ions shown in the spectra presented in panel A. **(C)** Plating efficiency experiment for the indicated strains for LB + 500 µg/L kanamycin as described in the legend for Figure 3.3. **(D)** Western blot analysis of whole cell lysates separated by standard SDS-PAGE (right) and Phos-tag™ SDS-PAGE (left) as described in the Material & Methods. Cell lysates were prepared from exponentially growing cultures of the Δ*gigAB* strain harboring the empty vector, "(–)", or the indicated GigB allele following induction with 0.1 mM IPTG for 2 hours.

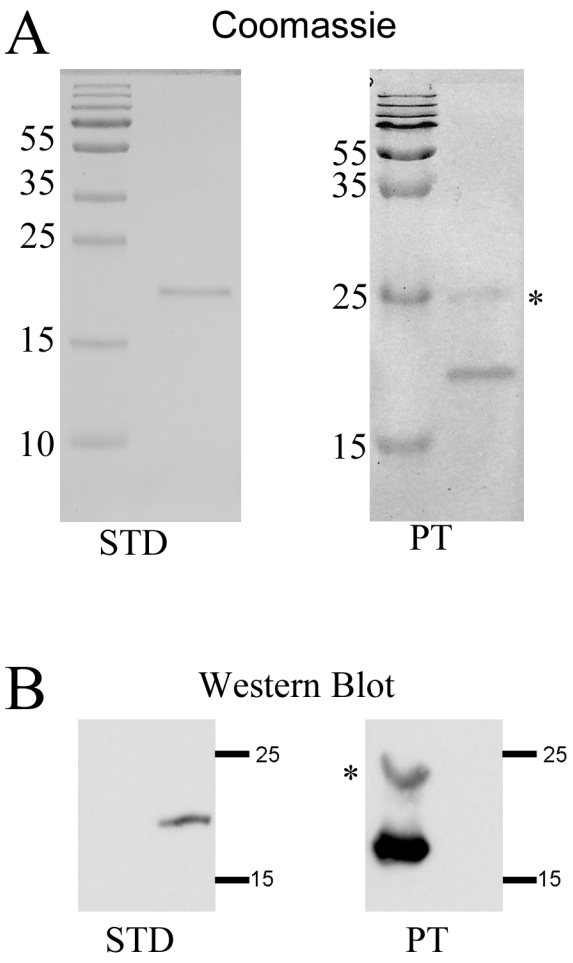

Figure 3.10 GigB is phosphorylated in *E. coli*. **(A)** and **(B)** show Coomassie-Blue stained gel and western blot analysis, respectively, of recombinant GigB-6xHis purified from *E. coli*. STD, standard 12% SDS-PAGE; PT, 12% SDS-PAGE gels polymerized with 50 µM Phos-tag™ acrylamide and 100 µM $MnCl_2$. Asterisks indicate the differential migration of GigB–P. Numbers adjacent to the gels/blots represent the migration of size standards (in kDa).

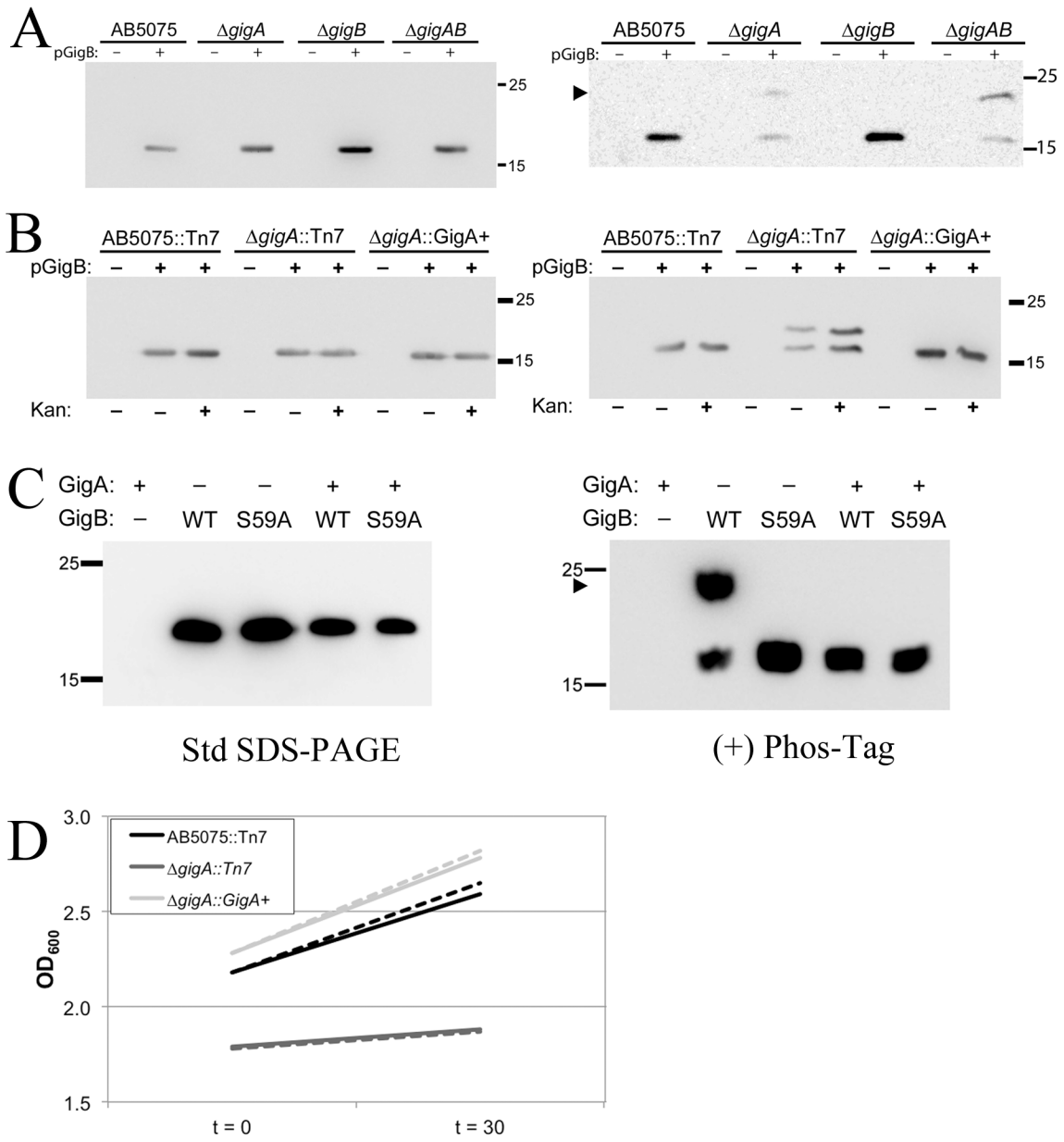

Figure 3.11 GigA functions as a GigB – Phosphatase *in vivo*. (A) Western Blot analysis of whole cell lysates from the indicated strains separated by standard SDS-PAGE (left) and Phos-tag™ SDS-PAGE (right). **(B)** As in (A), except that the indicated lysates (marked with a '+') were exposed to 500 µg/mL kanamycin prior to lysate preparation. **(C)** Western blot analysis of whole cell lysates from *E. coli* BL21(DE) harboring plasmids containing GigA and/or the indicated GigB allele. **(D)** Growth of the indicated strains in presence of kanamycin. Exponentially growing cultures of the indicated strains were split into fresh medium without (solid lines) and with (dashed lines) 500 µg/mL kanamycin for 30 minutes. OD_{600} values were recorded prior to and following 30 minutes of exposure to kanamycin. The lysates in panel B correspond with the growth data presented in panel D. Arrowheads in panels A, B and C indicate the band corresponding to GigB–P.

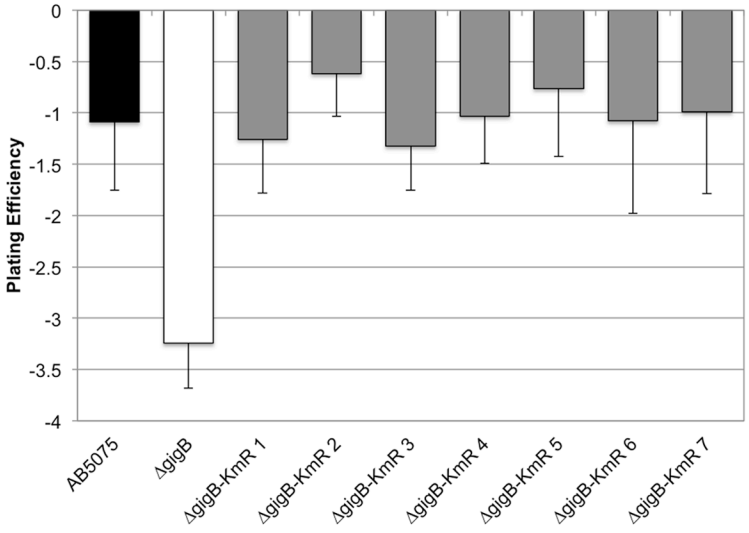

Figure 3.12 Kanamycin resistant suppressors of Δ*gigB*. Plating efficiency experiment performed as described in Figure 3.3 for the seven kanamycin resistant suppressor strains of the Δ*gigB* deletion strain. Results represent the average plating efficiency from 3 independent experiments with error bars representing one standard deviation.

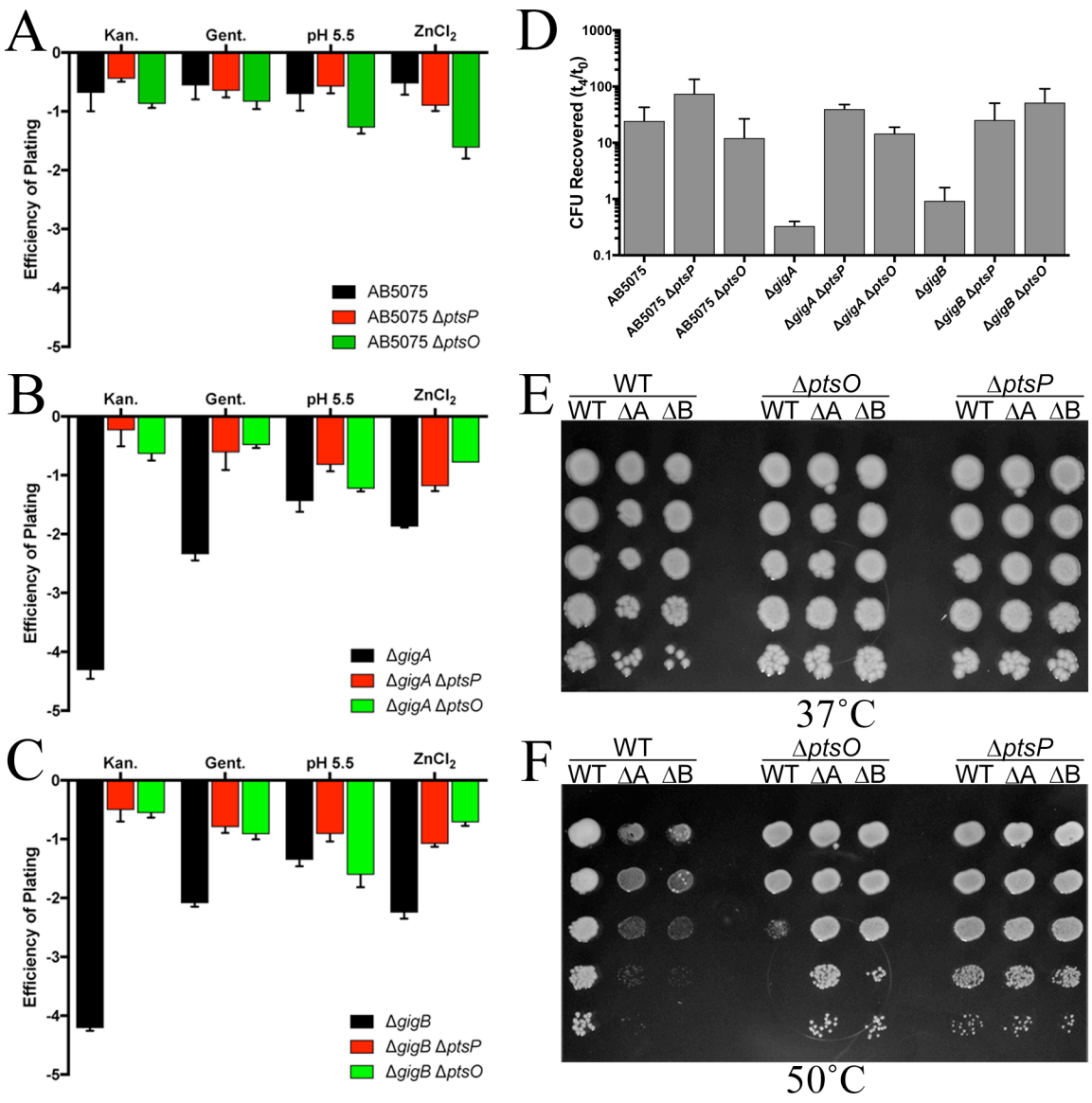

Figure 3.13 The Nitrogen Phosphotransfer system (PTS^{Ntr}) suppresses the *gig* phenotype. **(A, B, C)** Plating efficiency experiments conducted as described in Figure 3.3 for AB5075 **(A)**, Δ*gigA* **(B),** and Δ*gigB* **(C)** lacking PTS^{Ntr} genes. **(D)** Growth of the indicated strains in *G. mellonella* larvae. Data is depicted as the number of CFU recovered following 4 hours post infection divided by the CFU recovered immediately following infection (t = 0). Mean recovery values from three independent experiments are show with error bars representing 1 standard deviation. **(E)** and **(F)** Growth of the indicated strains following overnight incubation at 37 ˚C (E) or 50 ˚C (F).

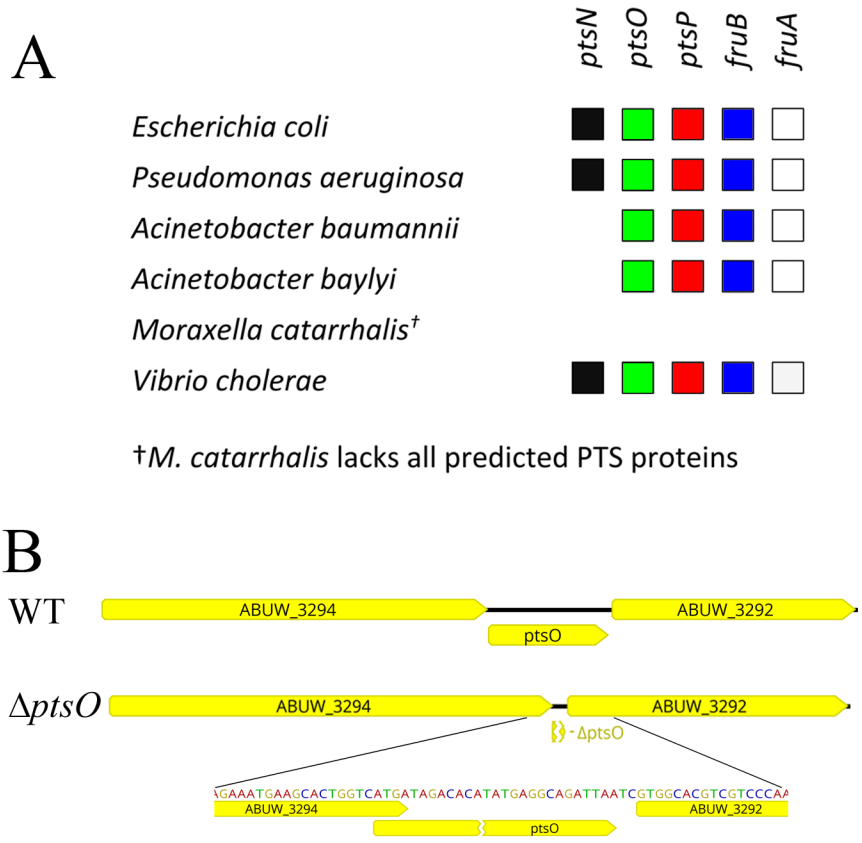

Figure 3.14 The PTS^{Ntr} is incomplete in *A. baumannii*. (A) Presence/absence plot for predicted PTS genes as assessed by the STRING database (www.string-db.org). **(B)** Mutagenesis scheme for generating the Δ*ptsO* mutation. A detailed description for the construction of the Δ*ptsO* strains can be found in Chapter III.

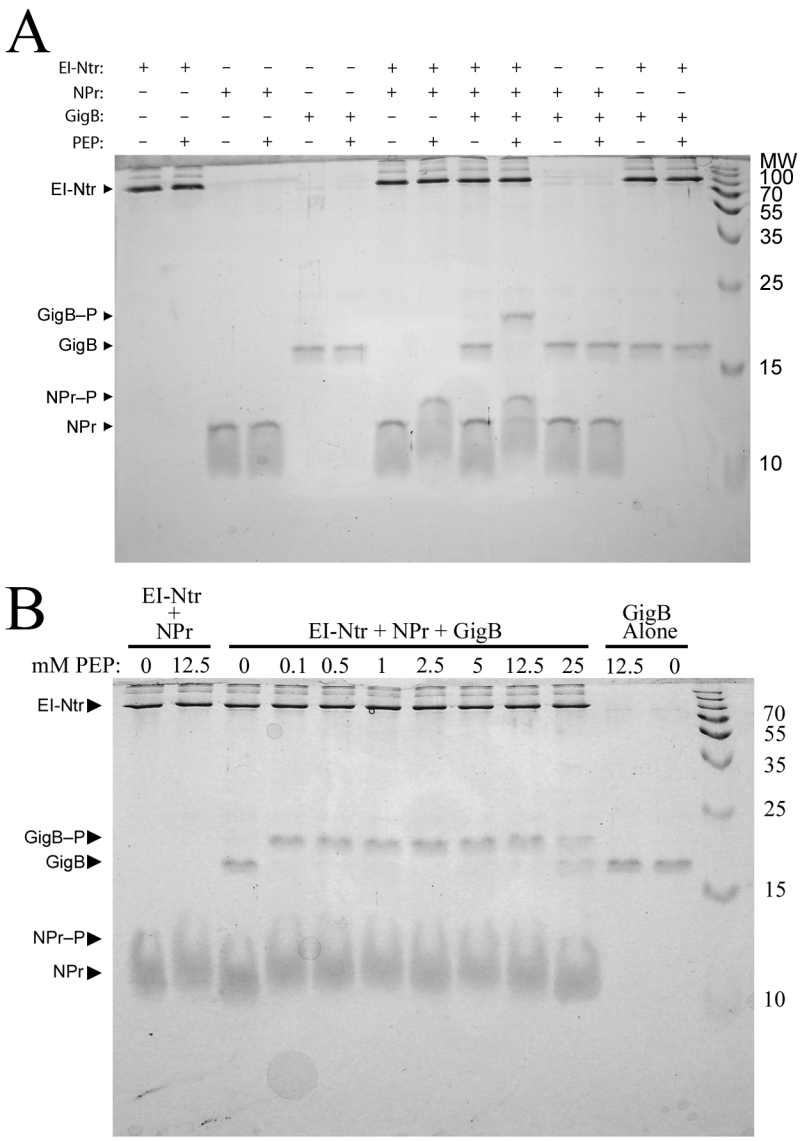

Figure 3.15 PTS^{Ntr} proteins mediate phospho-transfer to GigB *in vitro*. (A) The indicated components (5 µg of each protein) were combined in 20 µL reactions and incubated for 30 minutes at 30 ˚C and resolved through 15% acrylamide SDS-PAGE gels containing 50 µM Phos-tag^{TM} and 100 µM $MnCl_2$. Where indicated, phosphoenolpyruvate (PEP, 12.5 mM) was added to the reaction mixtures. **(B)** Phospho-transfer assays as performed in (A) with the exception of the PEP concentrations were added as indicated. In these gels, phosphorylated proteins are revealed by a reduced migration rate through the gel. Protein identities are indicated to the left of the gel. Numbers to the right of the gels indicate the migration of Molecular weight standards in kDa (MW).

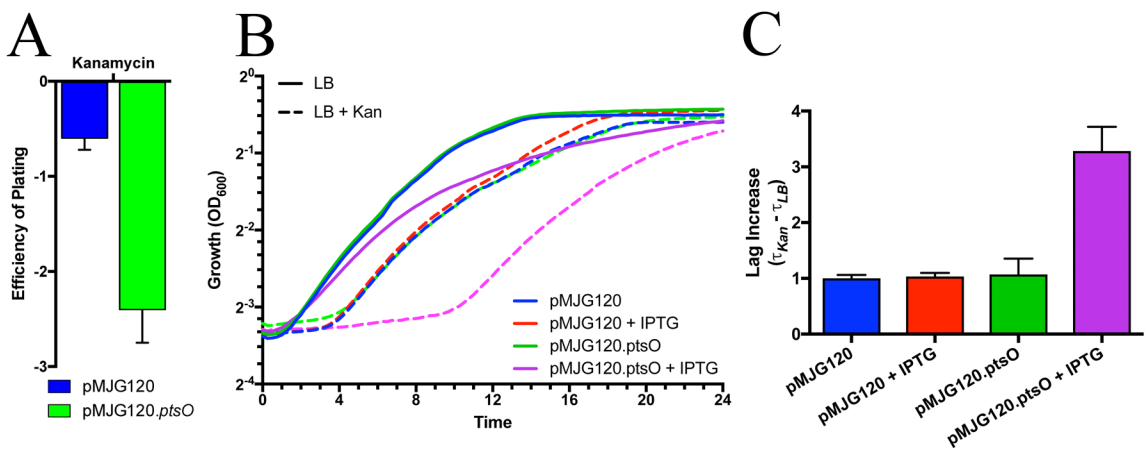

Figure 3.16 Over expression of *ptsO* (NPr) induces a *gig*⁻ phenotype in WT AB5075. (A) Plating efficiency experiment performed as described in the legend of Figure 3.3 and compares the CFU recovery on LB + Apramycin with CFU recovery on LB + Apramycin + 500 µg/mL kanamycin and 50 µM IPTG. **(B)** and **(C)** Kanamycin-induced lag time increase for growth of the indicated strains as described in the legend for Figure 3.3. For (B) and (C), IPTG indicates that 0.5 mM IPTG was included in the growth medium.

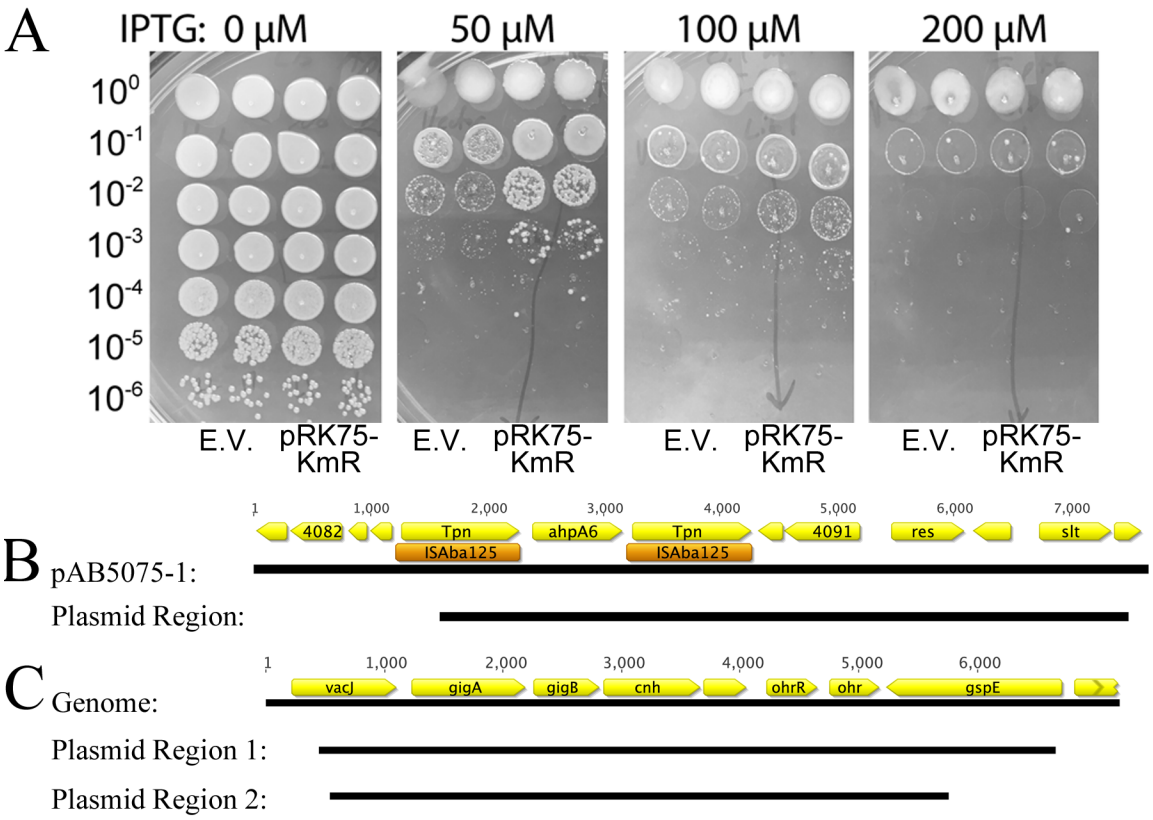

Figure 3.17 Genetic screen for suppressors of the NPr-induced *gig*⁻ phenotype. (A) Photographs from plating efficiency experiments on LB + 500 µg/mL kanamycin plates with the indicated amount of IPTG. E.V., AB5075 pMJG120.*ptsO* pRK415; pRK75KmR, a representative kanamycin resistant clone isolated from the pRK75 library. **(B)** and **(C)** Schematic of the kanamycin resistant plasmids recovered from the pRK75 screen. (B) depicts the *aphA6*-gene containing fragment mapping to plasmid pAB5075-1 and (C) depicts the two independent plasmids containing the *gigAB* locus. Gene maps constructed using Geneious. Orange boxes depict the ISAba125 insertion site sequences while yellow arrows depict gene annotations. Numbers within the gene annotations represent the locus tag (ABUW_####). When known, gene names are used. *Tpn*, transposase; *res*, resolvase gene; *slt*, soluble lytic murien transglycosylase; *cnh*, carbon-nitrogen hydrolase; *ohrR*, organic hydroperoxide resistance regulator; *ohr*, organic hydroperoxide resistance protein; *gspE*, general secretion pathway protein E.

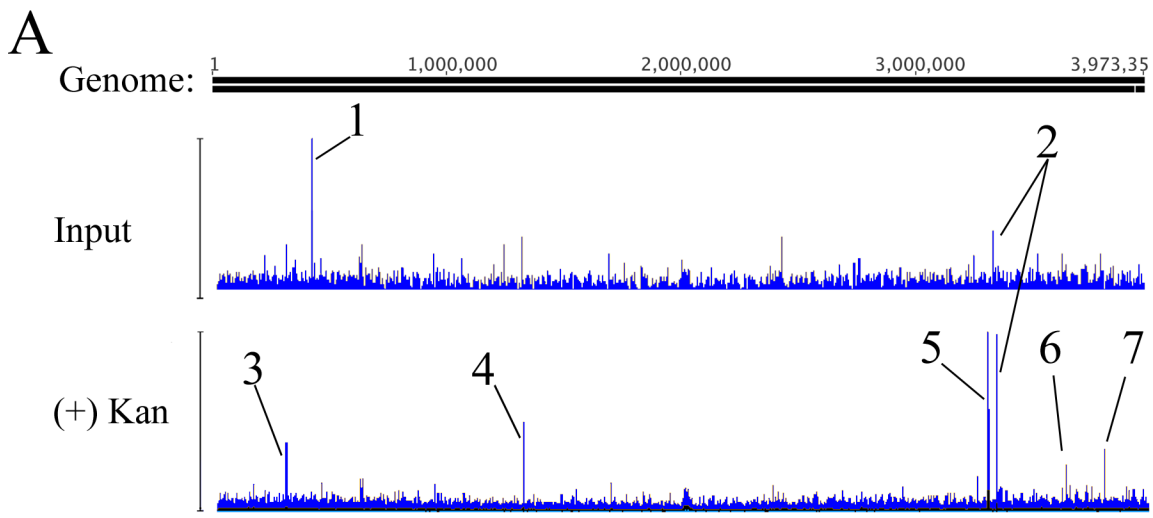

B

DNA	Reads Mapped	
	Input	(+) Kan
Genome	1.4 x 10^6	2.4 x 10^6
p1AB5075	16,500	53,000
p2AB5075	212,000	329,000
p3AB5075	193,00	234,000

C

Peak	Gene/Region
1	*mlaF**
2	*ptsO*
3	*gltX**
4	hypothetical protein*
5	*gigAB* locus
6	*uvrC**
7	glutathione peroxidase*

* Only one read mapped to these genes, suggesting they are artefacts.

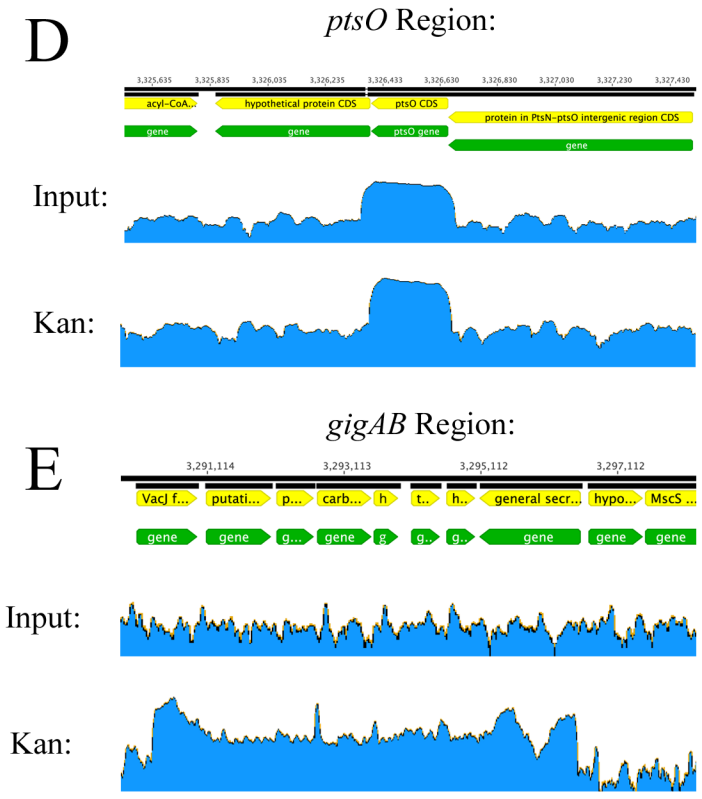

Figure 3.18 Deep sequencing results from NPr over expression Screen for the AB5075 chromosome. (A) Read coverage density for the AB5075 chromosome. Numbered peaks indicate regions of increased coverage for either the input sample (top, input) or kanamycin-selected sample (bottom, (+) Kan). **(B)** Table depicts the number of reads mapping to either the AB5075 chromosome or the indicated plasmids. **(C)** Table identifies the genes and/or regions identified in panel A. Asterisks indicate genes where only a single read mapped to that particular gene, suggesting the increased coverage is due to a sequencing artefact rather than actual over-representation in the library. **(D)** and **(E)** Coverage of the *ptsO* region (D) and *gigAB* locus (E).

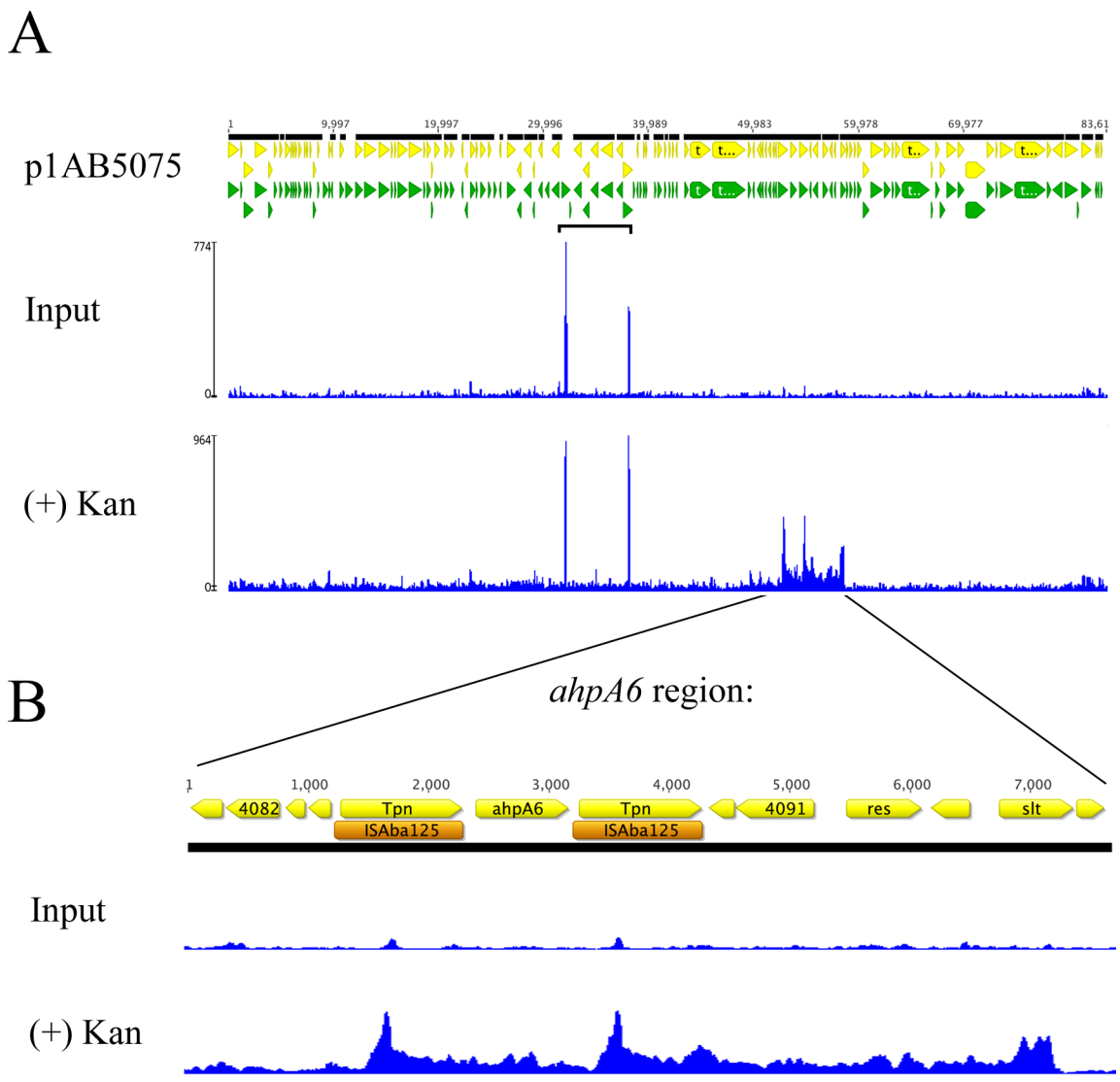

Figure 3.19 Deep sequencing results from NPr over expression screen for plasmid p1AB5075. (A) Read coverage density for the p1AB5075 plasmid. The bracketed peaks present in both the input and kanamycin-selected pools map to two identical copies of an integrase gene, *intI*, (locus tags ABUW_4053 and ABUW_4061). **(B)** Read coverage of the *ahpA6* region. Input, coverage plot from the unselected pRK75 library; (+) Kan, coverage plot from the kanamycin-selected pRK75 library.

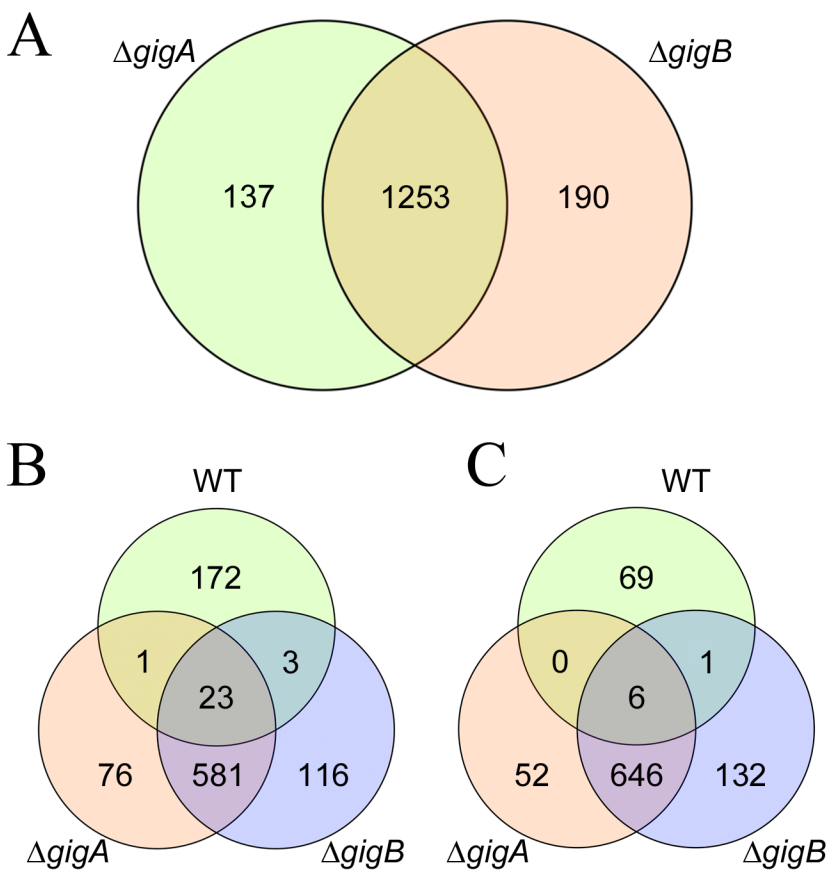

Figure 3.20 RNASeq analysis of Δ*gigA* and Δ*gigB*. **(A)** Venn Diagram showing differentially expressed genes in the Δ*gigA* and Δ*gigB* mutant strains relative to wild type AB5075. Gene expression was determined using RockHopper and Degust analysis tools as described in the Materials and Methods Chapter. **(B)** and **(C)** Venn Diagrams showing differentially expressed genes in response to kanamycin compared to wild type AB5075 exponential phase. B indicates genes with increased expression following kanamycin treatment and C indicates genes showing decreased expression following kanamycin exposure. All data are presented as the number of genes with a *q* value ≤ 0.01 and an absolute $\log_2$ fold change ≥ 2. Venn Diagrams were developed using the VennT program.

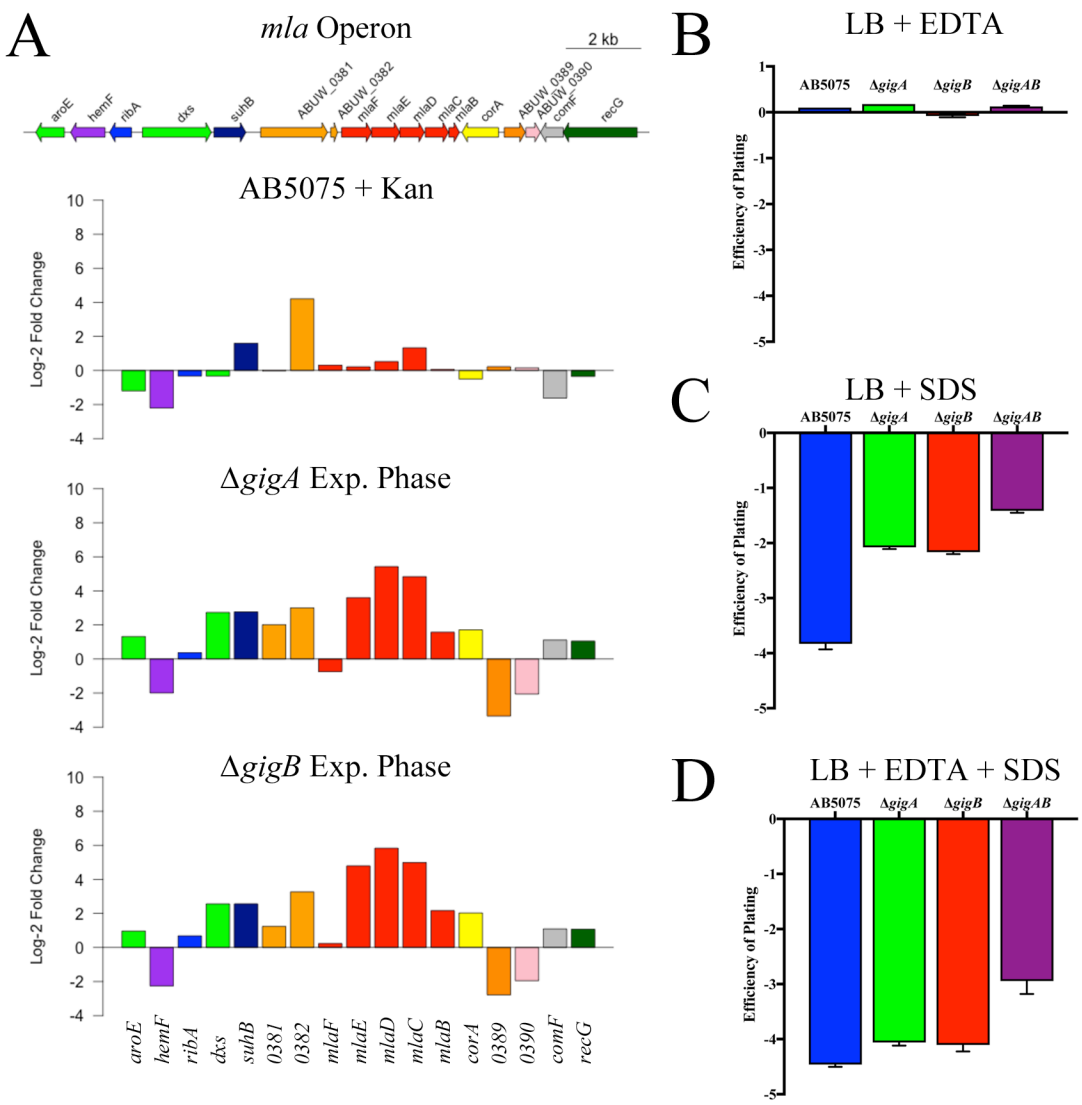

Figure 3.21 Increased expression of the *mla* operon correlates with SDS resistance in the Δ*gigA/B* mutants. (A) RNASeq expression analysis of the *mlaFEDCB* operon region. Top panel depicts the genes within and around the *mla* operon (drawn to scale). The three panels below show the RNASeq-derived expression data for each of the genes from the indicated strains/culture conditions. **(B), (C), (D)** Plating efficiency experiments for the indicated strains on LB media containing 100 µM EDTA (B), 0.5% SDS (C), and a combination of 100 µM EDTA and 0.5% SDS (D).

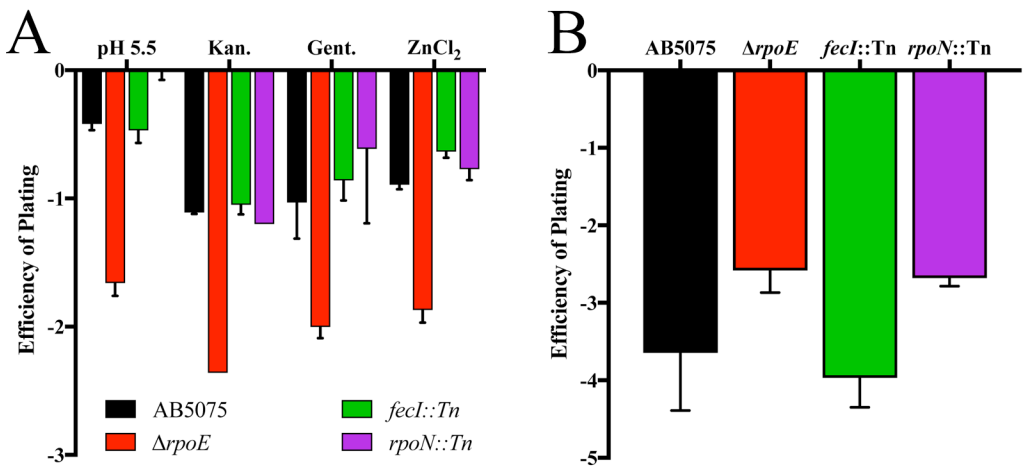

Figure 3.22 A strain lacking the *rpoE* gene phenocopies Δ*gigA*/Δ*gigB*. Plating efficiency experiments for the indicated strains performed as described in the legend for Figure 3.3 for the indicated stressors (panel A) or 0.5% SDS (panel B). For comparison, the data for SDS Plating efficiency of the Δ*gigA*/Δ*gigB* mutant strains can be found in Figure 3.21 panel C.

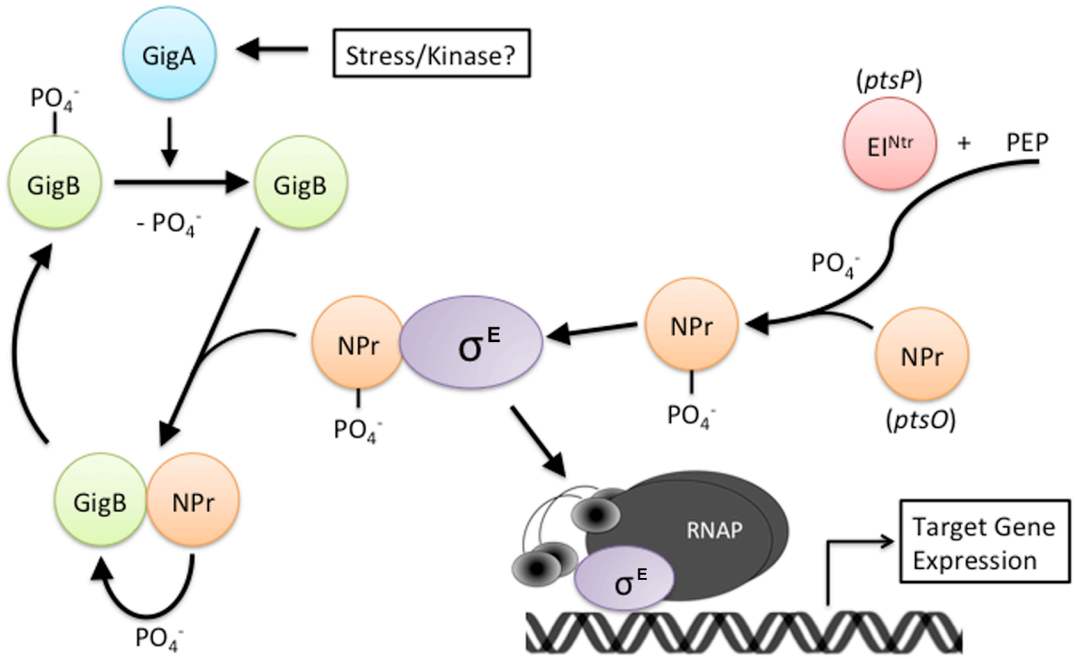

Figure 3.23 Current working model for GigA/B and PTS^{Ntr} regulatory pathway. Stress is perceived and/or transmitted to GigA, which then removes a phosphate group from phosphorylated GigB (GigB–P). Unphosphorylated GigB functions as an anti-anti-sigma factor and sequesters NPr–P from RpoE (σ^E). σ^E then directs the transcription of genes required for stress resistance. Additionally, upon GigB binding NPr–P, the phosphate group of NPr is transferred to GigB, regenerating GigB–P and eliminating the GigB-NPr interaction. Unphospohrylated NPr then acquires a new phosphate group, which is mediated by phosphoryl transfer through EI^{Ntr} from PEP. Additional details can be found in the text of Chapter III.

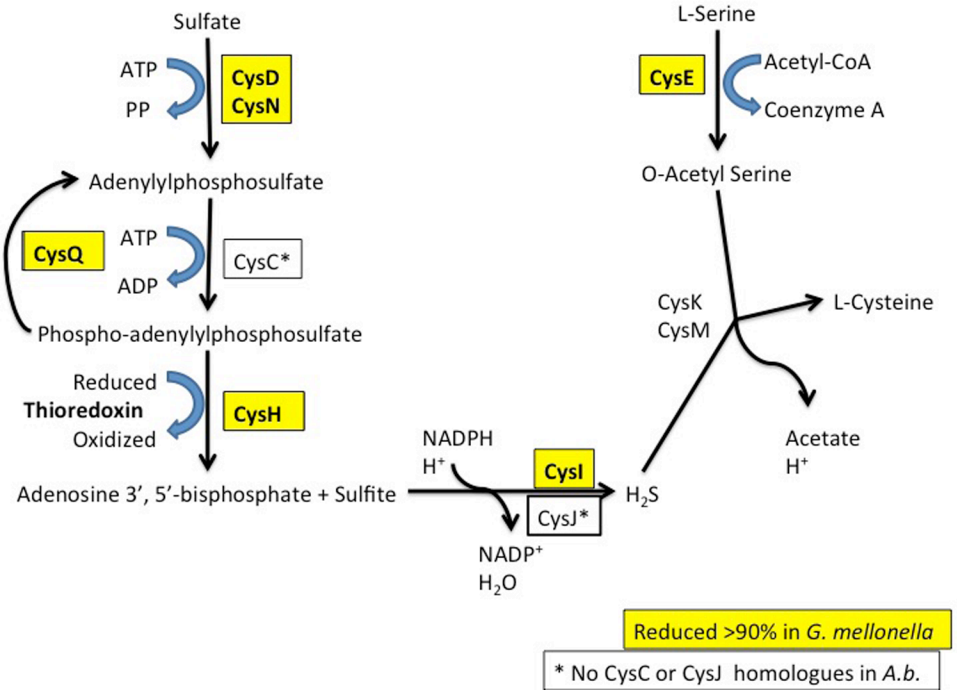

Figure 4.1 Sulfur activation/assimilation pathway of *A. baumannii*. Depicted are the major steps involved in the reductive sulfur assimilation pathway. Sulfate is imported into the cell and combined with adenosine triphosphate to generate adenylylphosphosulfate. A phosphate group is subsequently added to form the intermediate molecule phospho-adenylylphosphosulfate, which is then converted to sulfite and adenosine 3', 5-biphosphate. The sulfite is reduced into sulfide, in the form of Hydrogen Sulfide, which can then be combined with O-Acetyl Serine to yield acetate and cysteine. Yellow boxes indicate genes that were identified as being required for proper growth of *A. baumannii* inside the *G. mellonella* larvae. The white boxes indicate genes absent from the genome of *A. baumannii* AB5075.

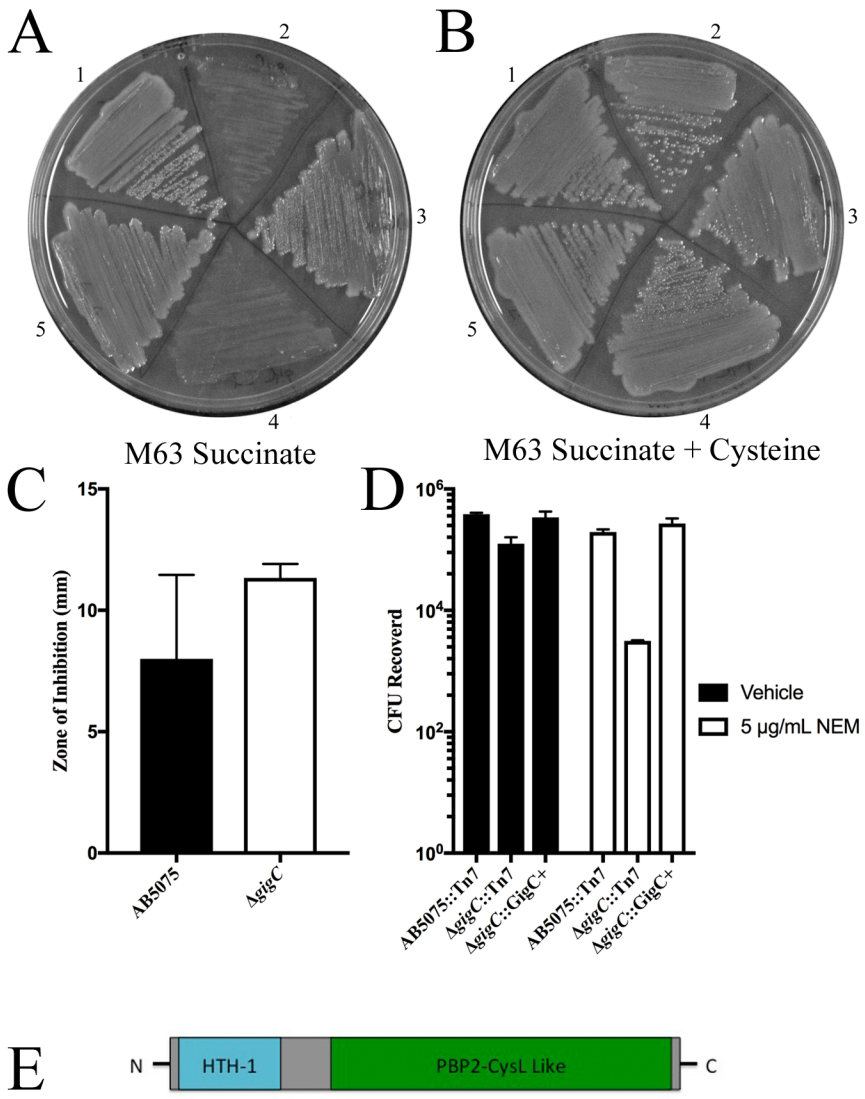

Figure 4.2 Phenotypes of the Δ*gigC* mutant. Bacterial were inoculated on either **(A)** M63-Succinate or **(B)** M63-Succinate + 20 µg/mL L-Cysteine and incubated overnight at 37˚C. Numbers indicates strains as follows: (1) WT AB5075, (2) Δ*gigC* mutant, (3) Δ*gigC*-Complement, (4) Δ*gigC*-Vector, (5) AB5075-Vector **(C)** Disc diffusion assays for paraquat. Overnight cultures of the indicated strains were spread onto LB plates and 6 µL of paraquat (10 mg/mL) was added to sterile filter paper disks. Following overnight growth, zones of inhibition were measured. Data is presented as the average zone of inhibition measured from 3 plates. Error bars represent one standard deviation. **(D)** Survival of the indicated strains following 2 hours incubation with either vehicle (% Ethanol) or 5 µg/mL N-Ethyl Maleimide (NEM). **(E)** Domain organization of the GigC protein. HTH-1, Helix-Turn-Helix Domian; PBP2, Penicillin Binding Protein 2 Domain.

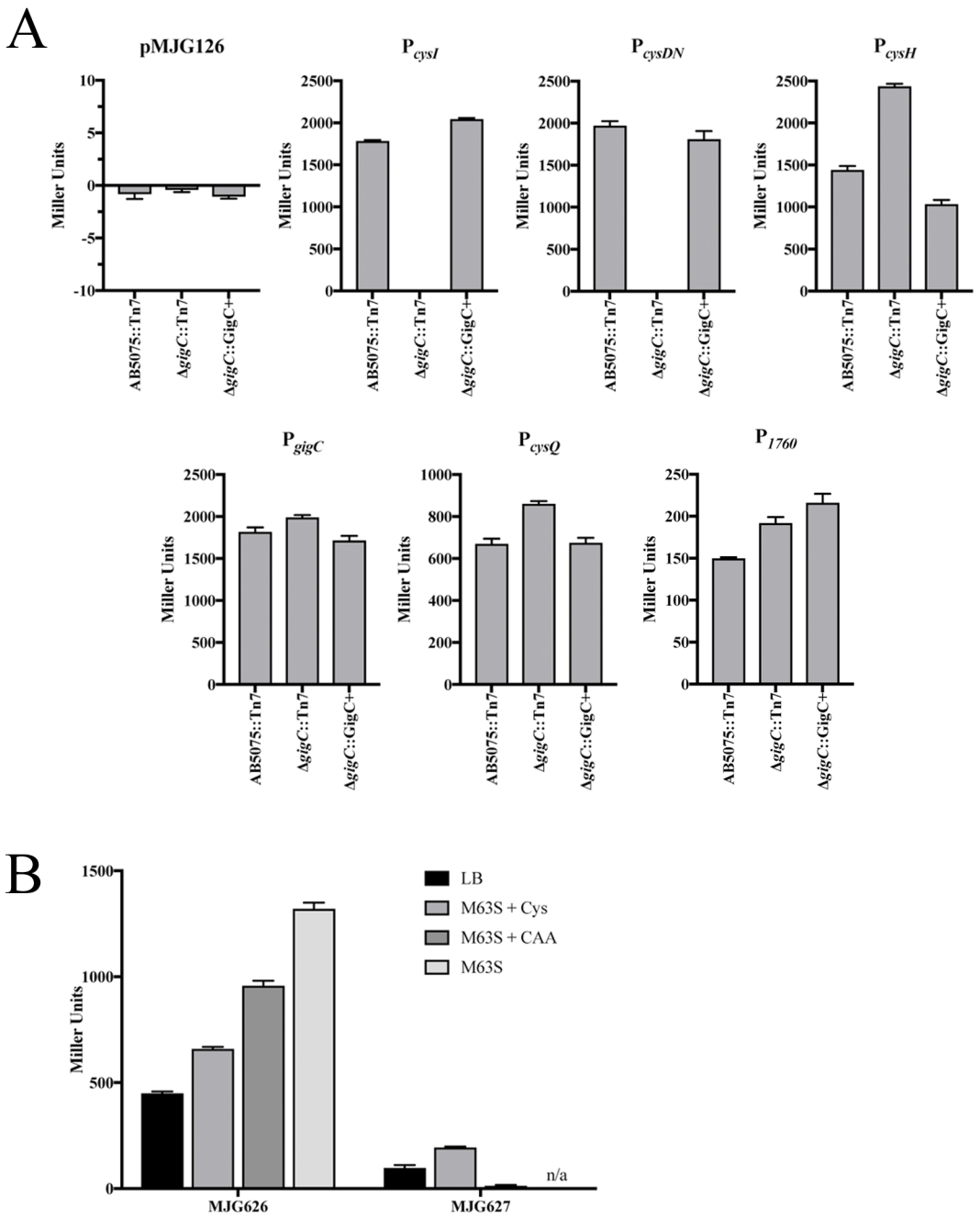

Figure 4.3 GigC is required for expression of *cysI* and *cysDN*. Miller assay results for the indicated strains and promoter constructs in plasmid pMJG126 **(A)** or from strains harboring plasmid pMJG118.*cysI* integrated at the *cysI* locus **(B)**. Experiments were performed on exponentially growing cultures (typical OD_{600} ~0.5 – 0.7) as described in Chapter VI. For (B), strains MG626 (AB5075::pMJG118.*cysI*) and MG627 (Δ*gigC*::pMJG118.*cysI*) were grown in the indicated media. M63S + Cys, M63 succinate medium with 20 μg/mL L-cysteine; M63S + CAA, M63 succinate medium with 0.2% casamino acids; M63S, M63 succinate medium; n/a, strain MG627 cannot grow in the absence of cysteine and was not tested in M63S medium.

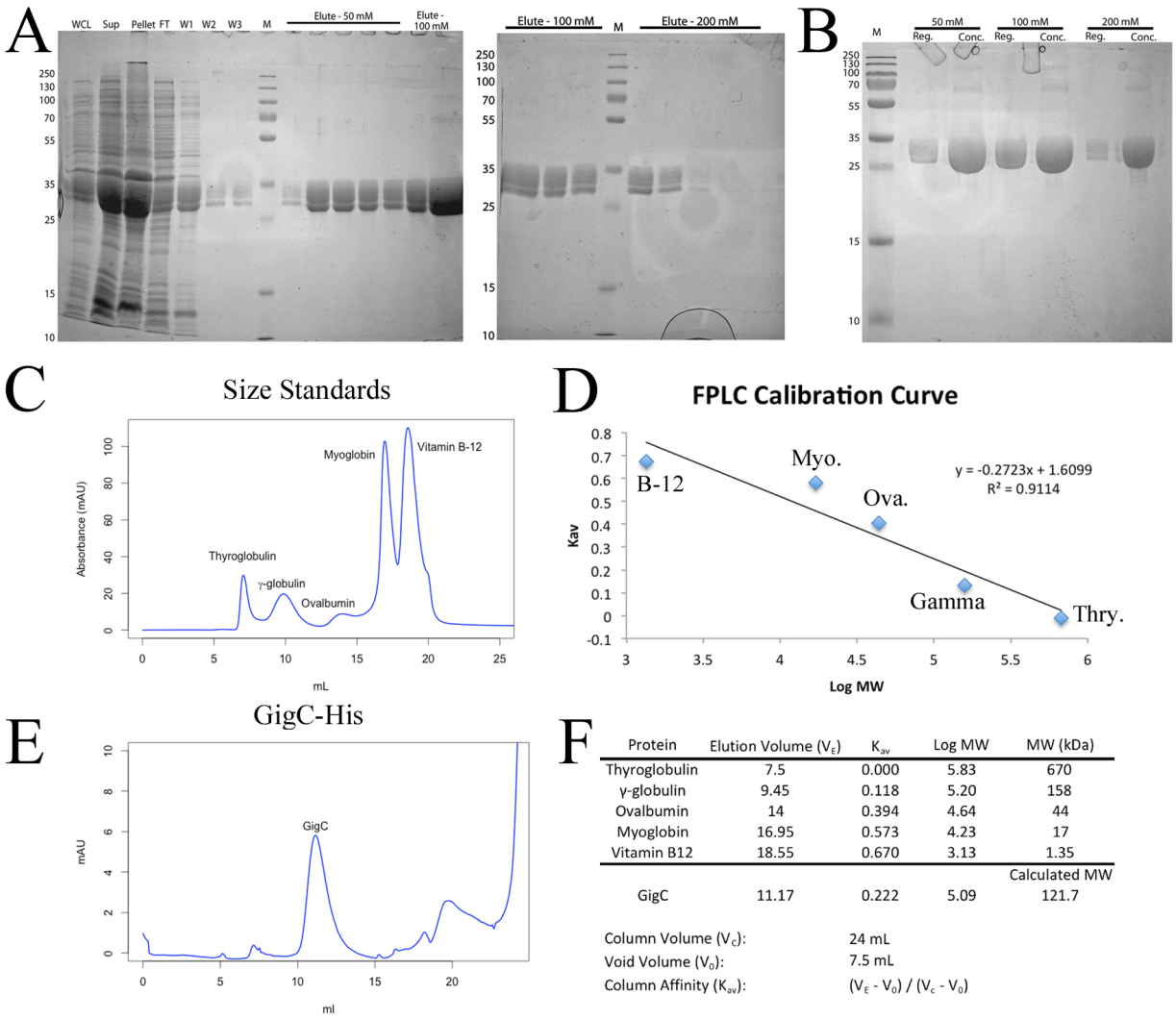

Protein	Elution Volume (V_E)	K_{av}	Log MW	MW (kDa)
Thyroglobulin	7.5	0.000	5.83	670
γ-globulin	9.45	0.118	5.20	158
Ovalbumin	14	0.394	4.64	44
Myoglobin	16.95	0.573	4.23	17
Vitamin B12	18.55	0.670	3.13	1.35
				Calculated MW
GigC	11.17	0.222	5.09	121.7

Column Volume (V_c): 24 mL
Void Volume (V_0): 7.5 mL
Column Affinity (K_{av}): $(V_E - V_0) / (V_c - V_0)$

Figure 4.4 Purification of recombinant GigC. (A) and **(B)** SDS-PAGE gels showing purification of recombinant GigC for preliminary purification (A) and following concentration of the elution fractions containing the GigC protein (B). Abbreviations: WCL, Whole Cell Lysate; Sup., Supernatant/Soluble protein fraction; Pellet, Insoluble protein fraction; FT, Column Flow Through fraction (i.e. proteins not bound by column); W1, W2, & W3, Wash fractions; M, Molecular Weight Markers (sizes in kDa indicated to left of gels). For (B) Reg., Pre-concentration sample; Conc., Post-Concentration Sample. **(C)** FPLC trace recording the absorbance at 280 nm for a mixture of the indicated proteins used for size exclusion chromatography (SEC) column calibration. **(D)** Plot shows the correlation between the molecular weight (log_{10}) and column affinity (K_{av}) for the protein standards from (C). **(E)** FPLC trace for the concentrated 100 mM fraction of GigC protein. **(F)** Protein size calculations derived from the correlation of column affinity (K_{av}) and known molecular weights of the protein size standards used in (C).

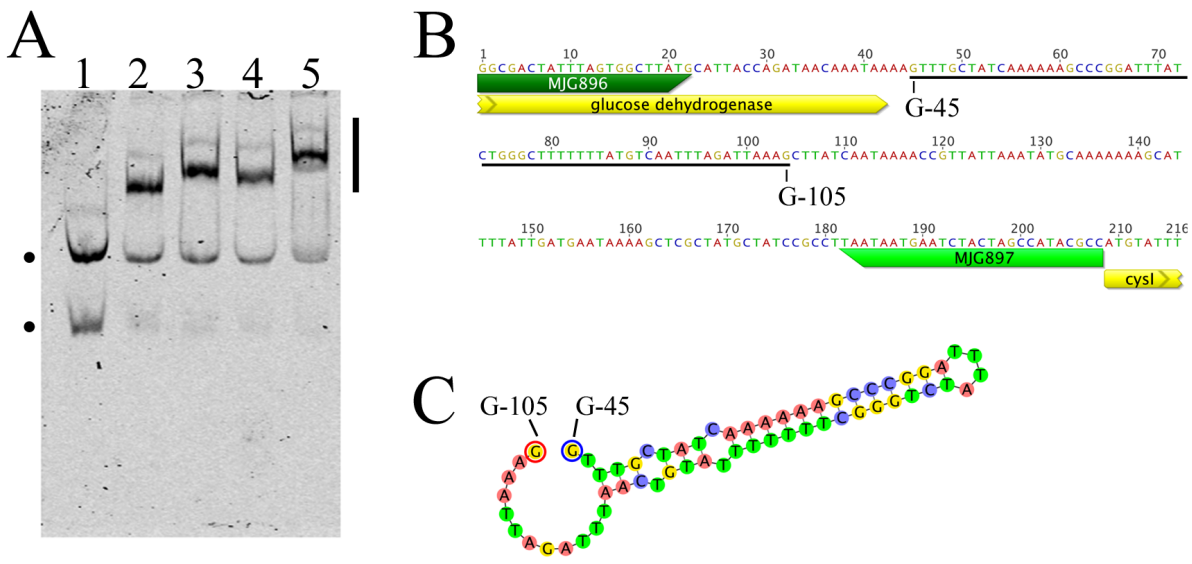

Figure 4.5 GigC binds to *cysI* promoter DNA. (A) Electrophoretic Mobility Shift Assay (EMSA) with recombinant GigC protein and a PCR-derived, IRDye 700 labeled DNA fragment consisting of the 208 nucleotides immediately 5' to the *cysI* start codon. Each lane contains 100 fmole of the labeled P*cysI* probe and the following amounts of GigC: Lane 1, no GigC; Lane 2, 1.25 pmole; Lane 3, 2.5 pmole; Lane 4, 5 pmole; Lane 5, 10 pmole. Gel was resolved through 6% TAE-Acrylamide gels at a constant 100 V for one hour. Black bar indicates the shifted migration of the probe in the presence of GigC; Black dots represent the two discrete bands as described in the main text (Chapter IV). **(B)** DNA sequence of the probe used for the EMSA experiments. The underlined region indicates the potential hairpin structure. **(C)** Representative model of the potential hairpin formed by the underlined nucleotides in (B). The hairpin model was generated using the program Geneious version 10.08

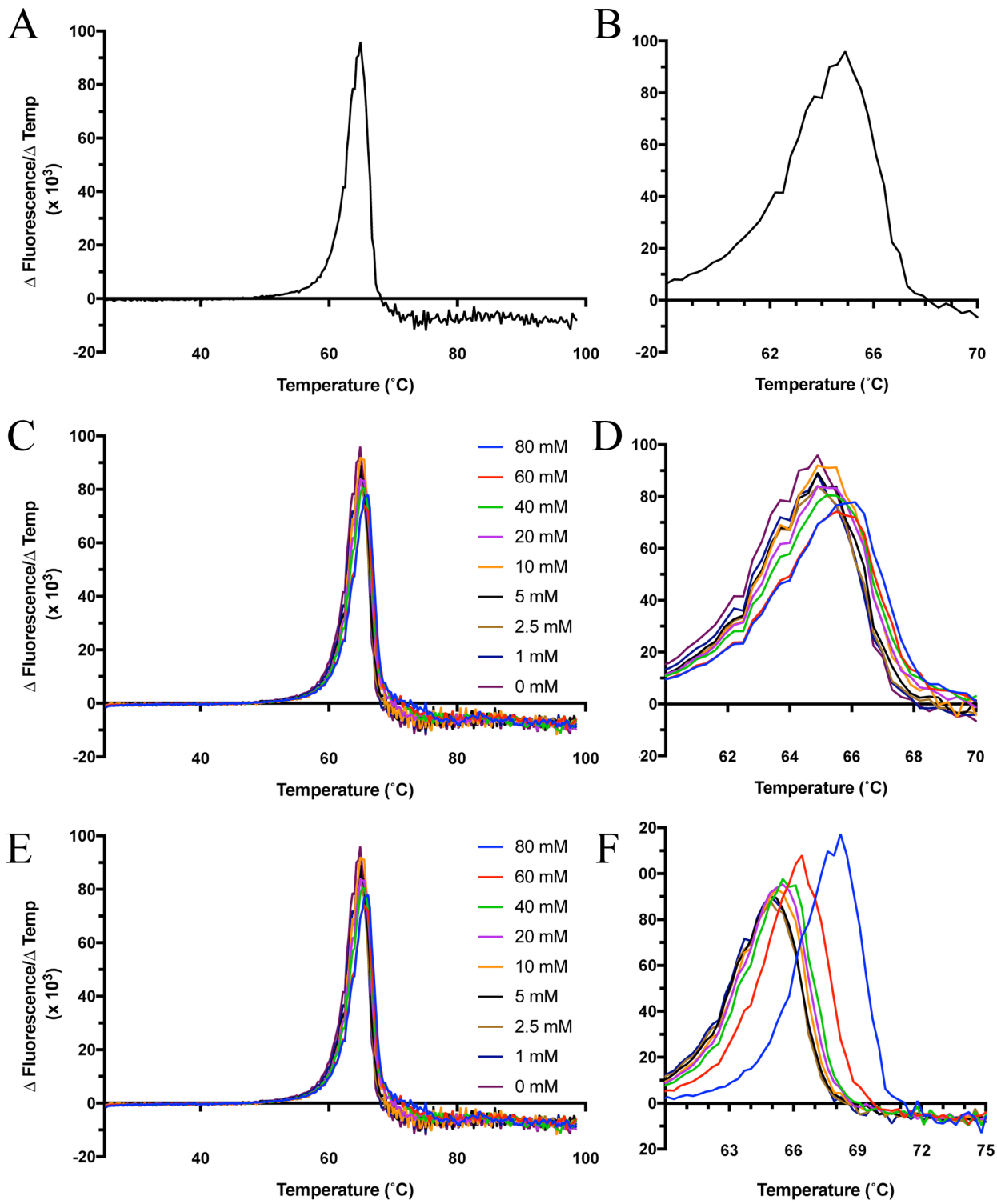

Figure 4.6 Differential Scanning Fluorimetry analysis of GigC. Plots depict Differential Scanning Fluorimetry analysis of GigC Alone **(A & B)**, GigC + $MgSO_4$ **(C & D)**, and GigC + Cysteine **(E & F)**. Reactions (20 µL) contained GigC (0.2 µg), 9.25 mM HEPES, pH 7.0, 140 mM NaCl and 7.5X concentration of SYPRO Orange dye (diluted from 5000X stock as supplied by Sigma). For panels C/D and E/F, $MgSO_4$ or Cysteine were added at the indicated

Figure 4.6 (continued)
concentrations, respectively. Data is plotted as the mean first derivative (calculated by dividing the change in fluorescence by the change in temperature) from triplicate wells. Temperature curve and fluorescence intensity were conducted using an Applied Biosystems Step One Plus Real Time PCR instrument.

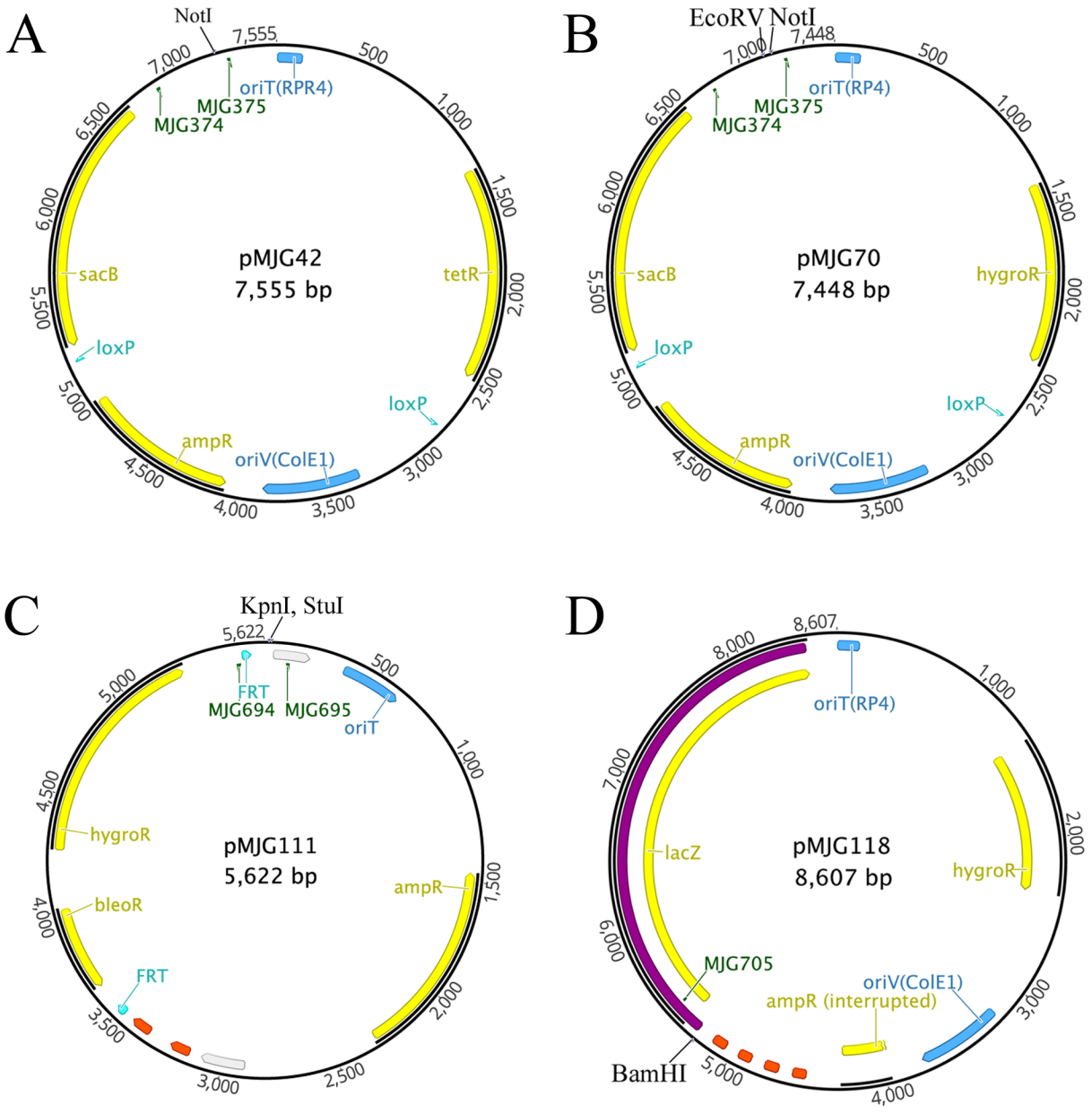

Figure 6.1 Integrating pMJG plasmids. (A), (B) Allele exchange vectors pMJG42 (tetracycline resistance) and pMJG70 (hygromycin resistance). **(C)** Tn7-delivery plasmid pMJG111. Grey bars indicate the boundaries of the Tn7 cassette. The *bleoR* gene encodes resistance to bleomycin. **(D)** Plasmid pMJG118 contains the *trpW205lacZ* cassette (purple bar) for generating chromosomally integrated *lacZ* promoter fusions. Orange bars represent transcriptional terminators. Unique restriction sites used for insertion of homologous DNA for gene deletion/integration cassettes are shown. Cyan arrows labeled *loxP* and *FRT* indicate recombinase targets for *cre* and *Flp* recombinases, respectively. Blue arrows/bars indicate origins of replication (*oriV*) and transfer (*oriT*). Green arrows indicate binding sites for MJG primers used for insertion screening/sequencing purposes. Yellow arrows indicate gene-coding sequences. Further details can be found in the Materials and Methods chapter.

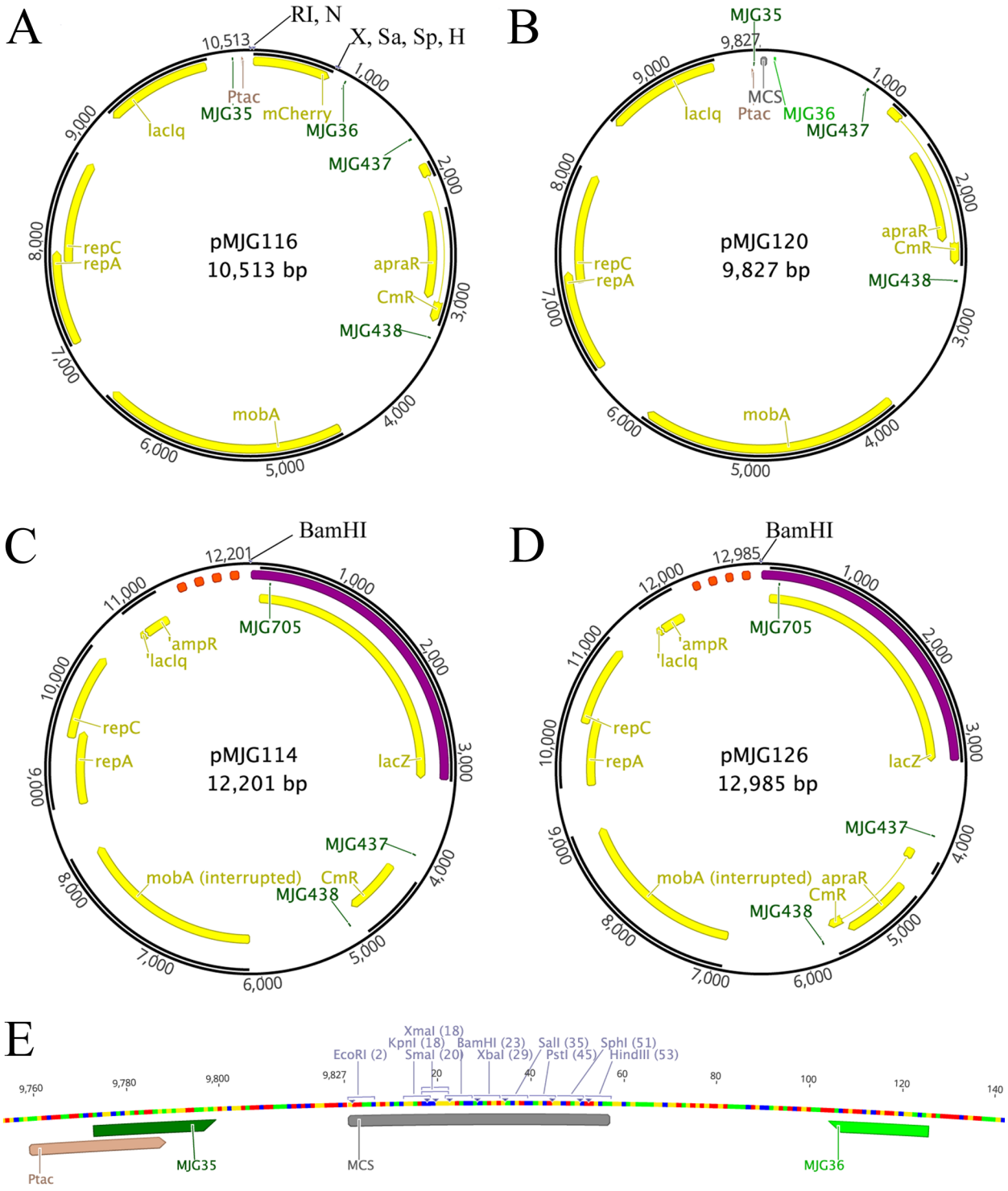

Figure 6.2. Replicating pMJG vectors. **(A), (B)** Plasmids pMJG116 (A) and pMJG120 (B) were used for genetic complementation of mutant strains. These plasmids utilize P_{tac}/IPTG for expression control. **(C), (D)** Plasmids pMJG114 (C, chloramphenicol resistance) and pMJG126

Figure 6.2 (continued)
(D, apramycin resistance) contain the *trpW205lacZ* cassette (purple bar) for generating *lacZ*-promoter fusions. **(E)** The P_{tac} promoter and Multiple Cloning Site (MCS) of plasmid pMJG120 are shown. The positions of primers MJG35/MJG36 are indicated, as well as unique restriction enzyme sites to facilitate cloning. Relevant restriction sites are shown and abbreviated as follows: RI, EcoRI; N, NdeI; X, XbaI, Sa, SalI; Sp, SphI, H, HindIII. See Materials & Methods for further details. The remaining annotations are colored/labeled as described in the legend for Figure 6.1.

Appendix B

Tables

Table 2.1 Antibiotic Resistance Profile of *A. baumannii* strains AB5075 and 17978

Antibiotic	Minimum Inhibitory Concentration (µg/mL)	
	17978	**AB5075**
Apramycin	n/d	4
Carbenicillin	8	≥ 256
Chloramphenicol	32	64
Gentamicin	1	128
Hygromycin	80	160
Kanamycin	4	≥256
Polymyxin B	2	2
Rifampicin	2	≤ 0.5
Streptomycin	32	≥256
Tetracylcine	1	2

Abbreviations: n/d, Not determined

Table 2.2 Acinetobacter Clinical Isolates

Strain	Species	MDR	Site of Isolation	Notes[a]
ACI 1	*A. baumannii*	Yes	Bloodstream Infection	Outbreak
ACI 2	*A. baumannii*	Yes	Bloodstream infection	Outbreak
ACI 3	*A. baumannii*	Yes	Environmental - Drain	Outbreak
ACI 4	*A. baumannii*	Yes	Unknown	
ACI 6	*A. baumannii*	Yes	Bloodstream infection	
ACI 7	*A. baumannii*	Yes	Urine	
ACI 8	*A. baumannii*	No	Urine	
ACI 9	*A. baumannii*	No	Blood venipuncture	
ACI 10	*A. pitti*	No	Surveillance Swab	
ACI 11	*A. pitti*	No	Bloodstream Infection	
ACI 12	*A. pitti*	No	Urine	
ACI 13	*A. baumannii*	No	Ventilation Tubing	Outbreak

a – Outbreak indicates these strains have identical multi-locus sequence tag (MLST) patterns and were isolated during a series of infections of ICU Patients (La Forgia et al. 2010).

Table 2.3. Genes required for growth of *A. baumannii* in *G. mellonella*[a]

Annotation	Gene	Description	Read Ratio
Micronutrient Acquisition			
ABUW_1173	*bauD*	Acinetobactin permease	0.0119
ABUW_1174	*bauC*	Acinetobactin permease	0.0976
ABUW_1176	*bauB*	Acinetobactin periplasmic binding protein	0.0472
ABUW_1177	*bauA*	Acinetobactin receptor	0.0111
ABUW_3740	*znuA*	High affinity Zn transport protein	0.0312
ABUW_3741	*zur*	Fur family transcriptional regulator	0.0730
ABUW_3742	*znuC*	Zinc import ATP-binding protein	0.0685
ABUW_3743	*znuB*	High affinity Zn transport protein	0.0449
Cysteine Metabolism/Sulfur Assimilation			
ABUW_0643	*cysI*	Sulfite reductase	0.0217
ABUW_0722	*cysH*	Phosphoadenosine phosphosulfate reductase	0
ABUW_0853	*cysG*	Uroporphyrin-III C-methyltransferase	0
ABUW_1760	-	Sulfate permease	0.0959
ABUW_2218	*cysQ*	3'(2'),5'-bisphosphate nucleotidase	0.0503
ABUW_2362	*cysE*	Serine acetyltransferase	0.0361
ABUW_2895	*cysN*	Sulfate adenylyltransferase subunit 1	0
ABUW_2896	*cysD*	Sulfate adenylyltransferase subunit 2	0
Aromatic Hydrocarbon Metabolism			
ABUW_1835	*pcaD*	3-oxoadipate enol-lactonase	0.0469
ABUW_1837	*pcaC*	4-carboxymuconolactone decarboxylase	0.0652
ABUW_1848	*pcaU*	*pca* operon regulatory protein	0.0852
ABUW_1854	*benP*	Benzoate transport porin	0.0305
ABUW_2090	-	4-hydroxybenzoate transporter	0.0909
ABUW_2349	-	4-oxalocrotonate tautomerase	0.0086
ABUW_2374	-	Isochorismatase hydrolase	0.0631
ABUW_2523	*paaI1*	Thioesterase domain protein	0.0069
ABUW_2524	*paaY*	Phenylacetic acid degradation protein	0.0934
Cell Envelope/Membrane/Wall			
ABUW_3360	*lptE*	Lipopolysaccharide assembly IptE	0
ABUW_3447	*lpxL*	Lipid A biosynthesis acyltransferase	0
ABUW_3448	*lptB*	Glycosyl transferase, group 1	0.0248
ABUW_3638	*pbpG*	D-alanyl-D-alanyl carboxypeptidase	0
ABUW_3831	*wza*	Polysaccharide export protein	0.0133
ABUW_3832	*ptp*	Protein-tyrosine-phosphatase	0
ABUW_3833	*ptk*	Tyrosine-protein kinase	0
Stress Response			
ABUW_0655	*typA*	GTP-binding protein TypA/BipA	0.0223
ABUW_1595	*kef*	Ion transport protein	0.0666
ABUW_1648	*mscS*	Mechanosensitive ion channel	0.0658
ABUW_1740	*rseP*	Intramembrane metallopeptidase	0.0279
ABUW_1763	*uspA*	UspA domain protein	0
ABUW_1804	*trkH*	K^+ uptake system component	0.0639

Table 2.3. Genes required for growth of *A. baumannii* in *G. mellonella* (continued)

Annotation	Gene	Description	Read Ratio
ABUW_2521	*uvrD*	UvrD/REP helicase	0.0460
ABUW_2590	*kefF*	NADPH oxidoreductase	0.0405
ABUW_3122	*otsB*	Trehalose-phosphatase	0.0859
Antibiotic Resistance			
ABUW_0842	*adeK*	Multidrug efflux protein	0
ABUW_0843	*adeJ*	Multidrug efflux protein	0.0157
ABUW_0844	*adeI*	Multidrug efflux protein	0.0154
ABUW_1156	-	Drug/metabolite exporter	0.0442
ABUW_1499	-	EamA-like transporter	0.0619
ABUW_1520	-	EamA-like transporter	0.0635
ABUW_1673	-	Bacterial trans-membrane pair family protein	0.0458
ABUW_1851	-	Aminoglycoside phosphotransferase	0.0912
ABUW_2123	-	Metallo-β-lactamase family protein	0.0828
ABUW_2550	-	EamA-like transporter	0.0584
Transcriptional Regulation			
ABUW_1645	-	TetR family transcriptional regulator	0.0437
ABUW_1672	-	LysR family transcriptional regulator	0.0676
ABUW_1692	-	TetR family transcriptional regulator	0.0493
ABUW_1755	*gigD*	AsnC family transcriptional regulator	0
ABUW_1768	-	MarR family transcriptional regulator	0.0272
ABUW_1849	-	LysR family transcriptional regulator	0.0547
ABUW_1966	-	LysR family transcriptional regulator	0.0556
ABUW_2074	-	Fur family transcriptional regulator	0.0495
ABUW_2196	*alkR*	AraC family transcriptional regulator	0.0516
ABUW_2236	-	AraC family transcriptional regulator	0.0550
ABUW_2370	*arsR*	ArsR family transcriptional regulator	0
ABUW_2520	-	TetR family transcriptional regulator	0.0666
ABUW_2544	-	AraC family transcriptional regulator	0.0373
ABUW_2555	*soxR*	Redox-sensitive transcriptional regulator	0.0934
ABUW_3161	*gigC*	LysR family transcriptional regulator	0.0007
ABUW_3180	*bfmS*	TCS Sensor Kinase protein	0
ABUW_3260	*gigA*	Putative TCS Response Regulator	0.0671

a – This table lists a subset of genes identified in the TnSeq screen and mentioned specifically in the text of Chapter II. The complete set of genes (n = 300) can be found in Table 2.5.

Abbreviations: TCS, two-component system.

Table 2.4 Antibiotic Susceptibility of Selected TnSeq Hits

Strain[c,d]	Antibiotic[a,b]									
	Amp/ Sulb	Pip/ Tazo	Merop	Amik	Tobra	Livofl	Col	Minocyc	Gent	Tigecyc (μg/mL)[e]
17978	29	23	27	25	24	26	14	28	25	0.13
AB5075	6	6	8.2	8.4	10	11.2	12.7	24	6	1.5
Δ*alkR*	6	6	7	9	10.5	11	12	23	6	1
Δ*2544*	6	6	8	8	10	11	13	25	6	1
Δ*2236*	6	6	7	9	10	11	13	24	6	1
Δ*arsR*	6	6	8	8	10	12	12	21	6	2
bfmR::Tn	6	6	8	9	10.5	12	14	25	6	1
Δ*bfmS*	8	6	9	6	8	8	12	21	6	2
Δ*gigA*	6	6	**9.2**	**14.6**	**17.8**	12.1	13.5	24	**13**	**0.75**
Δ*gigB*	**8.4**	**7.5**	**10.8**	**18.2**	**20.7**	**13**	**14.7**	**27.5**	**16**	**0.125**
Δ*gigC*	6	6	8	6	9	12	14	27	6	***0.5***
Δ*gigD*	9	6	9	6	10	11	14	27	6	0.75
Δ*fur*	6	6	8	9	10	10	14	25	6	1.5
Δ*1849*	6	6	8	7	10	11	12	22	6	1
Δ*1966*	**9**	6.5	**9.8**	7.1	8.7	10.7	13.1	25	6	1.5
Δ*1672*	6	6	8	7.5	10	11	14	27	6	0.75
Δ*1768*	6	6	8	9	9	11.5	13	25	6	1
Δ*ptk*	**10**	**7.8**	**10.5**	7.4	10	9.3	**14.5**	**27.5**	6	**0.75**
Δ*1645*	6	6	8	9	11	11	13	24	6	0.75
Δ*1692*	6	6	8	6	10	11	12	20	6	2
Δ*2520*	6	6	8	9	9	11	14	25	6	1
typA::Tn	6	6	9	**15**	11	10	15	**28**	6	1.0
Δ*uspA*	8	6	9	6	9	9	12	22	6	2
Δ*zur*	**12.5**	**10**	**11**	9	11.5	11.4	12	26	6	2.0

a – Sensitivity is represented as the zone of growth inhibition (in mm) surrounding a filter disc impregnated with the indicated antibiotic.

b – Bold text indicates statistically significant differences from WT AB5075.

c – Numbers indicate strains harboring a deletion/interruption of the annotation number (ABUW_####).

d – Mutant strains listed in this table are all in the AB5075 background.

e – Tigecycline is reported as the Minimum Inhibitory Concentration as determined by E-Test.

Abbreviations: Amp/Sulb, Ampicillin + Sulbactam; Pip/Tazo, Piperacillin + Tazobactam; Merop, Meropenem; Amik, Amikacin; Tobra, Tobramycin; Col, Colistin; Mino, Minocycline; Gent, Gentamicin; Tigecyc, Tigecycline.

Table 2.5. Full Set of Genes required for growth in *G. mellonella* larvae (continued)

Locus Tag	Gene	Description	Read Ratio (Gm/LB)
ABUW_0091	*pgpA*	phosphatidylglycerophosphatase A	0.0514
ABUW_0379	*dxs*	1-deoxy-D-xylulose-5-phosphate synthase	0.0992
ABUW_0460	-	hypothetical protein	0
ABUW_0590	-	putative polysaccharide deacetylase	0
ABUW_0593	-	glycosyl hydrolase family 43 domain-containing protein	0.0287
ABUW_0643	*cysI*	sulfite reductase	0.0217
ABUW_0655	*typA*	GTP-binding protein TypA/BipA	0.0223
ABUW_0719	*cafA*	ribonuclease G	0
ABUW_0722	*cysH*	phosphoadenosine phosphosulfate reductase	0
ABUW_0779	-	hypothetical protein	0.0705
ABUW_0842	*adeK*	multidrug efflux protein AdeK	0
ABUW_0843	*adeJ*	multidrug efflux protein AdeJ	0.0157
ABUW_0844	*adeI*	multidrug efflux protein AdeI	0.0154
ABUW_0853	*cysG*	uroporphyrin-III C-methyltransferase	0
ABUW_0933	-	hypothetical protein	0.0923
ABUW_0934	-	hypothetical protein	0.0733
ABUW_0935	-	hypothetical protein	0.0628
ABUW_0936	-	hypothetical protein	0
ABUW_1094	-	hypothetical protein	0.0249
ABUW_1095	-	hypothetical protein	0.0825
ABUW_1096	-	hypothetical protein	0.0576
ABUW_1121	-	hypothetical protein	0.0531
ABUW_1156	-	transporter, drug/metabolite exporter family	0.0442
ABUW_1160	-	hypothetical protein	0
ABUW_1173	*bauD*	ferric acinetobactin transport system permease	0.0119
ABUW_1174	*bauC*	ferric acinetobactin transport system permease	0.0976
ABUW_1176	*bauB*	ferric acinetobactin transport system periplasmic binding protein	0.0472
ABUW_1177	*bauA*	ferric acinetobactin receptor	0.0111
ABUW_1212	-	hypothetical protein	0.0900
ABUW_1228	*lipA1*	lipoic acid synthetase	0
ABUW_1239	-	branched-chain amino acid permease	0.0985
ABUW_1240	-	hypothetical protein	0.0924
ABUW_1284	-	hypothetical protein	0.0578
ABUW_1285	-	hypothetical protein	0.0457
ABUW_1287	-	hypothetical protein	0.0648
ABUW_1330	-	hypothetical protein	0.0691
ABUW_1341	*hisM*	histidine transport system permease protein HisM	0.0947

Table 2.5. Full Set of Genes required for growth in *G. mellonella* larvae (continued)

Locus Tag	Gene	Description	Read Ratio (Gm/LB)
ABUW_1388	-	hypothetical protein	0.0749
ABUW_1390	-	hypothetical protein	0.0558
ABUW_1396	-	hypothetical protein	0.0019
ABUW_1417	-	hypothetical protein	0.0850
ABUW_1438	-	acyltransferase 3 domain-containing protein	0.0588
ABUW_1439	-	hypothetical protein	0.0696
ABUW_1447	-	M48 family peptidase	0.0042
ABUW_1466	-	hypothetical protein	0.0545
ABUW_1475	-	transcriptional regulator, AraC family	0.0757
ABUW_1497	-	ADP-ribose pyrophosphatase (pseudogene)	0.0703
ABUW_1499	-	EamA-like transporter family protein	0.0619
ABUW_1501	*pqiA-2*	paraquat-inducible protein A	0.0768
ABUW_1504	*uraH2*	transthyretin	0.0615
ABUW_1509	*desC*	delta-9 acyl-lipid desaturase 1	0.0826
ABUW_1512	*cfa*	cyclopropane-fatty-acyl-phospholipid synthase	0.0761
ABUW_1515	-	two-component system response regulator protein	0.0909
ABUW_1516	-	hypothetical protein	0
ABUW_1520	-	EamA-like transporter family protein	0.0635
ABUW_1537	*gidA*	glucose inhibited division protein A	0.0357
ABUW_1571	-	transcriptional regulator, AraC family	0.0756
ABUW_1587	-	hypothetical protein	0
ABUW_1594	-	hypothetical protein	0
ABUW_1595	*kef*	ion transport protein	0.0666
ABUW_1603	-	putative acetyltransferase	0.0819
ABUW_1625	-	putative helicase	0.0743
ABUW_1628	-	hypothetical protein	0.0659
ABUW_1629	-	hypothetical protein	0.0988
ABUW_1632	-	PapD-like P pilus assembly protein	0.0530
ABUW_1636	-	short chain dehydrogenase	0.0770
ABUW_1637	-	oxidoreductase short-chain dehydrogenase/reductase family	0.0971
ABUW_1643	-	hypothetical protein	0.0262
ABUW_1644	-	hypothetical protein	0.0617
ABUW_1645	-	transcriptional regulator, TetR family	0.0437
ABUW_1648	-	mechanosensitive ion channel family protein	0.0658
ABUW_1651	-	hypothetical protein	0
ABUW_1652	-	hypothetical protein	0.0418
ABUW_1654	-	acetyltransferase, gnat family	0.0479
ABUW_1655	-	TonB-dependent siderophore receptor	0.0727

Table 2.5. Full Set of Genes required for growth in *G. mellonella* larvae (continued)

Locus Tag	Gene	Description	Read Ratio (Gm/LB)
ABUW_1658	-	hypothetical protein	0
ABUW_1662	-	hypothetical protein	0
ABUW_1672	-	transcriptional regulator, LysR family	0.0676
ABUW_1673	-	bacterial transmembrane pair family protein	0.0458
ABUW_1681	-	hypothetical protein	0
ABUW_1684	-	iron-containing alcohol dehydrogenase	0.0866
ABUW_1691	-	PepSY-associated TM helix domain-containing protein	0.0937
ABUW_1692	-	transcriptional regulator, TetR family	0.0493
ABUW_1710	-	molybdopterin converting factor subunit 1	0
ABUW_1711	*moaE*	molybdopterin converting factor, subunit 2	0.0092
ABUW_1713	-	molybdopterin biosynthesis protein	0.0857
ABUW_1724	-	hypothetical protein	0
ABUW_1726	-	D-amino acid dehydrogenase 3 small subunit	0.0741
ABUW_1727	-	hypothetical protein	0.0945
ABUW_1734	-	TRAM domain-containing protein	0.0901
ABUW_1740	*rseP*	peptidase M50, putative membrane-associated zinc metallopeptidase	0.0279
ABUW_1747	*recX*	regulatory protein RecX	0.0922
ABUW_1750	-	HAD-superfamily hydrolase	0.0969
ABUW_1753	-	hypothetical protein	0.0733
ABUW_1755	-	transcriptional regulator, AsnC family	0
ABUW_1758	-	alpha/beta hydrolase fold-3	0.0912
ABUW_1760	-	sulfate permease	0.0959
ABUW_1763	-	UspA domain protein	0
ABUW_1764	-	GGDEF family protein	0.0727
ABUW_1768	-	transcriptional regulator, MarR-family	0.0272
ABUW_1774	-	hypothetical protein	0.0440
ABUW_1788	-	hypothetical protein	0.0598
ABUW_1804	*trkH*	K+ uptake system component	0.0639
ABUW_1805	*trkAH*	K+ uptake system component	0.0822
ABUW_1816	*aro1*	3-deoxy-7-phosphoheptulonate synthase	0.0794
ABUW_1828	-	hypothetical protein	0.0546
ABUW_1835	*pcaD*	3-oxoadipate enol-lactonase	0.0469
ABUW_1837	*pcaC*	4-carboxymuconolactone decarboxylase	0.0652
ABUW_1848	*pcaU*	pca operon regulatory protein	0.0852
ABUW_1849	-	transcriptional regulator, LysR family	0.0547
ABUW_1851	-	aminoglycoside phosphotransferase	0.0912
ABUW_1854	-	benzoate transport porin BenP	0.0305

Table 2.5. Full Set of Genes required for growth in *G. mellonella* larvae (continued)

Locus Tag	Gene	Description	Read Ratio (Gm/LB)
ABUW_1857	-	Glu-tRNA amidotransferase	0.0986
ABUW_1860	-	hypothetical protein	0.0761
ABUW_1864	-	2Fe-2S iron-sulfur cluster binding domain protein	0.0783
ABUW_1879	-	hypothetical protein	0.0903
ABUW_1901	-	hypothetical protein	0.0458
ABUW_1904	-	antibiotic biosynthesis monooxygenase	0.0931
ABUW_1912	-	hypothetical protein	0.0114
ABUW_1915	-	hypothetical protein	0.0541
ABUW_1918	-	hypothetical protein	0.0670
ABUW_1941	-	TauE-like transmembrane protein (pseudogene)	0
ABUW_1960	-	hypothetical protein	0.0662
ABUW_1962	-	acetyltransferase (pseudogene)	0
ABUW_1966	-	transcriptional regulator, LysR family	0.0556
ABUW_2061	-	hypothetical protein	0.0661
ABUW_2064	-	hypothetical protein	0.0555
ABUW_2065	-	hypothetical protein	0.0688
ABUW_2066	*acdP*	dipeptidase	0.0681
ABUW_2074	-	transcriptional regulator, fur family	0.0495
ABUW_2080	-	transcriptional regulator, ModE family	0.0785
ABUW_2090	-	4-hydroxybenzoate transporter	0.0909
ABUW_2094	-	hypothetical protein	0.0255
ABUW_2103	-	hypothetical protein	0.0882
ABUW_2107	-	hypothetical protein	0.0721
ABUW_2123	-	metallo-beta-lactamase family protein	0.0828
ABUW_2132	*lipA2*	lipoic acid synthetase	0.0288
ABUW_2145	-	hypothetical protein	0.0160
ABUW_2149	-	hypothetical protein	0.0904
ABUW_2156	-	hypothetical protein	0.0784
ABUW_2167	-	hypothetical protein	0.0753
ABUW_2171	*cobS*	cobalamin 5'-phosphate synthase	0.0804
ABUW_2177	-	HAD-superfamily hydrolase	0.0959
ABUW_2179	-	hypothetical protein	0.0959
ABUW_2181	-	hypothetical protein	0.0762
ABUW_2193	-	acyl-CoA dehydrogenase	0.0793
ABUW_2196	*alkR*	transcriptional regulator, AraC family	0.0516
ABUW_2208	-	adenylate/guanylate cyclase	0.0296
ABUW_2214	*rraA*	regulator of ribonuclease activity A	0.0956
ABUW_2217	-	phosphoglycerate mutase	0.0739
ABUW_2218	*cysQ*	3'(2'),5'-bisphosphate nucleotidase	0.0503

Table 2.5. Full Set of Genes required for growth in *G. mellonella* larvae (continued)

Locus Tag	Gene	Description	Read Ratio (Gm/LB)
ABUW_2219	-	hypothetical protein	0.0692
ABUW_2221	*gsiA*	glutathione import ATP-binding protein GsiA	0.0877
ABUW_2222	-	ABC-type dipeptide/oligopeptide/nickel transport system permease component	0.0748
ABUW_2226	-	heme-binding protein A	0.0656
ABUW_2232	-	biopolymer transport protein ExbD/TolR	0.0642
ABUW_2233	-	acetyltransferase, gnat family	0
ABUW_2235	-	AFG1-family ATPase	0.0602
ABUW_2236	-	transcriptional regulator, AraC family	0.0550
ABUW_2237	-	monooxygenase, flavin-binding family	0.0838
ABUW_2238	-	hypothetical protein	0.0937
ABUW_2252	*gspG*	general secretion pathway protein G	0.0683
ABUW_2262	*spoOJ*	chromosome partitioning protein ParB	0.0535
ABUW_2268	*surA*	PpiC-type peptidyl-prolyl cis-trans isomerase	0.0405
ABUW_2291	-	hypothetical protein	0
ABUW_2298	-	hypothetical protein	0.0030
ABUW_2304	*ruvC*	crossover junction endodeoxyribonuclease RuvC	0.0930
ABUW_2308	-	hypothetical protein	0
ABUW_2309	-	hypothetical protein	0.0441
ABUW_2311	-	pili assembly chaperone	0.0403
ABUW_2313	-	fimbrial protein	0.0907
ABUW_2314	-	hypothetical protein	0
ABUW_2322	-	phage integrase	0.0798
ABUW_2328	-	transcriptional regulator, AsnC family	0.0873
ABUW_2330	*gltL*	glutamate/aspartate transport ATP-binding protein	0.0931
ABUW_2332	*gltJ*	glutamate/aspartate transport system permease protein	0.0850
ABUW_2339	*metQ2*	D-methionine transport protein	0.0977
ABUW_2342	*ychF*	GTP-binding protein YchF	0.0085
ABUW_2344	-	transcriptional regulator, Crp/Fnr family	0.0886
ABUW_2345	-	hypothetical protein	0.0641
ABUW_2349	-	4-oxalocrotonate tautomerase	0.0086
ABUW_2362	*cysE*	serine acetyltransferase	0.0361
ABUW_2363	-	hypothetical protein	0.0184
ABUW_2368	-	transcriptional regulator, LysR family	0.0817
ABUW_2370	*arsR*	transcriptional regulator, ArsR family	0
ABUW_2371	*arsC*	arsenate reductase	0.0917
ABUW_2372	-	hypothetical protein	0.0637
ABUW_2374	-	isochorismatase hydrolase	0.0631

Table 2.5. Full Set of Genes required for growth in *G. mellonella* larvae (continued)

Locus Tag	Gene	Description	Read Ratio (Gm/LB)
ABUW_2395	*madL*	malonate transporter, MadL subunit	0.0103
ABUW_2408	-	LrgA family protein	0.0849
ABUW_2416	-	hypothetical protein	0.0971
ABUW_2418	-	lysine exporter protein	0.0955
ABUW_2424	-	ABC-type amino acid transport system	0.0686
ABUW_2430	-	transporter, LysE family	0.0950
ABUW_2434	-	hypothetical protein	0
ABUW_2438	*cinA1*	competence/damage-inducible protein CinA	0
ABUW_2439	-	hypothetical protein	0.0588
ABUW_2441	-	hypothetical protein	0.0530
ABUW_2442	-	hypothetical protein	0
ABUW_2443	-	hypothetical protein	0.0762
ABUW_2444	-	hypothetical protein	0
ABUW_2449	-	putative SAM-dependent methyltransferase	0.0771
ABUW_2450	-	long-chain fatty-acid-CoA ligase	0.0933
ABUW_2454	*mgh*	3-methylglutaconyl-CoA hydratase	0.0810
ABUW_2461	-	thioesterase superfamily protein	0.0515
ABUW_2463	-	hypothetical protein	0.0845
ABUW_2509	-	hypothetical protein (pseudogene)	0.0720
ABUW_2510	-	hypothetical protein	0
ABUW_2511	-	hypothetical protein	0
ABUW_2512	-	hypothetical protein	0
ABUW_2513	*csp2*	cold-shock DNA-binding domain protein	0.0095
ABUW_2520	-	transcriptional regulator, TetR family	0.0666
ABUW_2521	-	UvrD/REP helicase	0.0460
ABUW_2523	*paaI1*	thioesterase domain protein	0.0069
ABUW_2524	*paaY*	phenylacetic acide degradation protein PaaY	0.0934
ABUW_2544	-	transcriptional regulator, AraC family	0.0373
ABUW_2550	-	EamA-like transporter family protein	0.0584
ABUW_2555	*soxR*	redox-sensitive transcriptional activator SoxR	0.0934
ABUW_2556	-	hypothetical protein	0
ABUW_2558	-	acetyltransferase, gnat family	0.0881
ABUW_2559	-	hypothetical protein	0.0822
ABUW_2563	-	regulatory protein LysR:LysR, substrate-binding	0.0798
ABUW_2590	-	NADPH oxidoreductase	0.0405
ABUW_2592	-	urea carboxylase-associated protein 1	0.0927
ABUW_2593	-	urea carboxylase-associated protein 2	0.0777
ABUW_2597	-	hypothetical protein (pseudogene)	0.0914
ABUW_2598	-	hypothetical protein	0.0702

Table 2.5. Full Set of Genes required for growth in *G. mellonella* larvae (continued)

Locus Tag	Gene	Description	Read Ratio (Gm/LB)
ABUW_2600	-	hypothetical protein	0.0351
ABUW_2609	-	transcriptional regulator, LysR-type	0.0797
ABUW_2611	-	hypothetical protein	0.0945
ABUW_2612	-	hypothetical protein	0.0839
ABUW_2613	-	RHS family protein	0.0765
ABUW_2624	-	hypothetical protein	0.0477
ABUW_2626	-	neuraminidase domain-containing protein	0.0511
ABUW_2640	-	acetyltransferase	0.0316
ABUW_2652	-	hypothetical protein	0.0845
ABUW_2657	-	hypothetical protein (pseudogene)	0.0836
ABUW_2658	-	hypothetical protein	0.0823
ABUW_2674	-	hypothetical protein	0.0788
ABUW_2678	-	17 kDa surface antigen	0.0675
ABUW_2679	-	hypothetical protein	0
ABUW_2684	-	phage putative head morphogenesis protein	0.0449
ABUW_2685	-	hypothetical protein	0.0044
ABUW_2691	-	transporter LysE family	0.0585
ABUW_2692	-	hypothetical protein (pseudogene)	0.0476
ABUW_2741	*vfr*	cyclic nucleotide-binding domain protein	0.0945
ABUW_2744	-	putative membrane protein	0.0185
ABUW_2756	-	hypothetical protein	0.0366
ABUW_2795	-	hypothetical protein	0.0152
ABUW_2796	-	hypothetical protein	0.0430
ABUW_2797	-	hypothetical protein	0.0411
ABUW_2798	-	D-serine/D-alanine/glycine transporter	0.0727
ABUW_2811	-	hypothetical protein	0.0407
ABUW_2815	-	hypothetical protein	0.0887
ABUW_2819	-	hypothetical protein	0.0987
ABUW_2826	*rnt*	ribonuclease T	0.0132
ABUW_2833	-	hypothetical protein	0.0987
ABUW_2846	-	hypothetical protein	0.0410
ABUW_2860	-	hypothetical protein	0.0980
ABUW_2895	*cysN*	sulfate adenylyltransferase subunit 1	0
ABUW_2896	*cysD*	sulfate adenylyltransferase subunit 2	0
ABUW_2898	-	hypothetical protein	0
ABUW_2917	*yhgI*	IscR-regulated protein YhgI	0
ABUW_3003	-	hypothetical protein	0.0558
ABUW_3083	*smpB*	SsrA-binding protein	0
ABUW_3122	*otsB*	trehalose-phosphatase	0.0859

Table 2.5. Full Set of Genes required for growth in *G. mellonella* larvae (continued)

Locus Tag	Gene	Description	Read Ratio (Gm/LB)
ABUW_3161	*gigC*	transcriptional regulator, LysR family	0.0007
ABUW_3180	*bfmS*	two-component system sensor kinase protein	0
ABUW_3192	-	hypothetical protein	0
ABUW_3260	*gigA*	putative two-component response regulator	0.0671
ABUW_3360	*lptE*	lipopolysaccharide assembly IptE	0
ABUW_3385	*prc*	carboxy-protease	0.0774
ABUW_3447	*lpxL*	lipid A biosynthesis acyltransferase	0
ABUW_3448	*lptB*	glycosyl transferase, group 1	0.0248
ABUW_3589	*rpoC*	DNA-directed RNA polymerase, beta' subunit	0.0315
ABUW_3638	*pbpG*	D-alanyl-D-alanine carboxypeptidase family protein	0
ABUW_3650	*ribE*	riboflavin synthase, alpha subunit	0
ABUW_3710	-	putative acetyltransferase	0.0946
ABUW_3740	*znuA*	high affinity Zn transport protein	0.0312
ABUW_3741	*zur*	transcriptional regulator, Fur family	0.0730
ABUW_3742	*znuC*	zinc import ATP-binding protein ZnuC	0.0685
ABUW_3743	*znuB*	high affinity Zn transport protein	0.0449
ABUW_3820	-	nucleotide sugar epimerase/dehydratase	0.0327
ABUW_3821	*spsC*	Spore coat polysaccharide biosynthesis protein	0.0144
ABUW_3822	-	Bacterial transferase hexapeptide (three repeats) family protein	0
ABUW_3823	*weeH*	putative UDP-galactose phosphate transferase	0
ABUW_3824	-	family 1 glycosyl transferase	0.0056
ABUW_3825	-	hypothetical protein	0
ABUW_3826	-	family 1 glycosyl transferase	0.0869
ABUW_3828	-	UDP-glucose/GDP-mannose dehydrogenase family protein	0.0535
ABUW_3830	-	UDP-glucose/GDP-mannose dehydrogenase	0.0384
ABUW_3831	*wza*	polysaccharide export protein	0.0133
ABUW_3832	*ptp*	protein-tyrosine-phosphatase ptp	0
ABUW_3833	*ptk*	tyrosine-protein kinase ptk	0
ABUW_3846	*dsbA*	thiol:disulfide interchange protein DsbA	0.0764
ABUW_4005	-	hypothetical protein	0
ABUW_4023	-	Protein incC	0
ABUW_4025	-	hypothetical protein	0.0179
ABUW_4077	-	hypothetical protein	0
ABUW_4091	-	hypothetical protein	0.0695

Table 3.1 Phosphotransferase System (PTS) Proteins in *A. baumannii* AB5075

Locus Tag	Gene	Function
ABUW_1770	*fruA*	Fused Carbohydrate-Specific PTS protein; EIIB/EIIC component
ABUW_1772	*fruB*	Fused Carbohydrate-Specific PTS protein; EI/HPr/EIIA component
ABUW_3293	*ptsO*	NPr component of the PTS^{Ntr}
ABUW_3469	*ptsP*	Enzyme I component of the PTS^{Ntr}

Table 3.2 Sigma Factors Present in *A. baumannii* AB5075

Locus Tag	Gene	Function
ABUW_0862	*rpoD*	σ^{70}; Primary/House Keeping Sigma Factor
ABUW_0988	*rpoE*	σ^{24}; Periplasm/Outer Membrane Stress Sigma Factor
ABUW_1375	*rpoH*	σ^{32}; Heat Shock Sigma Factor
ABUW_2987	*fecI*	σ^{19}; Ferric Citrate Responsive Sigma Factor
ABUW_3253	*rpoN*	σ^{54}; Nitrogen Responsive Sigma Factor

Table 4.1 Sulfur Assimilation/Cysteine Biosynthetic Genes Identified by TnSeq

Locus Tag	Gene	Description
ABUW_0643	*cysI*	Sulfite reductase
ABUW_0722	*cysH*	Phosphoadenosine phosphosulfate reductase
ABUW_0853	*cysG*	Uroporphyrin-III C-methyltransferase
ABUW_1760	-	Sulfate permease
ABUW_2218	*cysQ*	3'(2'),5'-bisphosphate nucleotidase
ABUW_2362	*cysE*	Serine acetyltransferase
ABUW_2895	*cysN*	Sulfate adenylyltransferase subunit 1
ABUW_2896	*cysD*	Sulfate adenylyltransferase subunit 2

Table 6.1. Bacterial Strains

Strain	Genotype	Description[a]
Escherichia coli		
BL21 (DE3)	F⁻ *ompT gal dcm lon hsdS$_B$*($r_B^- m_B^-$) λ(DE3 [*lacI lacUV5-T7p07 ind1 sam7 nin5*]) [*malB*$^+$]$_{K\text{-}12}$(λ^S)	
DH5α	F⁻ *endA1 glnV44 thi-1 recA1 relA1 gyrA96 deoR nupG purB20* Φ80d*lacZ*ΔM15 Δ(*lacZYA-argF*)U169, hsdR17($r_K^- m_K^+$), λ⁻	
DH5α (λpir)	DH5α (λpir)	
EL350	F⁻ *mcrA* Δ(*mrr-hsdRMS-mcrBS*) ϕ80*dlacZM15* Δ*lacX74 deoR recA1 endA1 araD139* Δ(*ara, leu*)*7649 galU galK rspL nupG* [λcI857 (*cro bio* < > *araC-P$_{BAD}$cre*)]	
HB101	F⁻ *mcrB mrr* hsdS20($r_B^- m_B^-$) *recA13 leuB6 ara-14 proA2 lacY1 galK2 xyl-5 mtl-1 rpsL20*(Sm^R) *glnV44* λ⁻	
LW264	*thi thr leu tonA lacY supE recA::RP4-2-Tc^S Tri^R* λ$_{imm434}$ *cre*⁻	
MC4100	F⁻ [*araD139*]$_{B/r}$ Δ(*argF-lac*)*169* λ⁻ *e14- flhD5301 relA1 rpsL150*(strR) *rbsR22* Δ(*fimB-fimE*)*632*(*::IS1*) *deoC1*	
PPY	F⁻ *endA1 recA1 galE15 galK16 nupG rpsL*Δ*lacX74* Φ80*lacZ*ΔM15 *araD139* Δ(*ara,leu*)*7697 mcrA* Δ(*mrr-hsd*RMS-*mcr*BC) *cynX::*[*araC* pBAD-*redα* EM7- *redß* Tn5-*gam*] λ⁻	
Acinetobacter baumannii		
17978	American Type Culture Collection Strain 17978	
MG604	17978 Δ*bfmS*	Locus tag: A1S_0749
AB5075	Wild Type Isolate	MDR Organism
5075Tn16	AB5075 *fecI*::Tn	Locus tag: ABUW_2987
5075Tn17	AB5075 *rpoN*::Tn	Locus tag: ABUW_3253
5075Tn40	AB5075 *znuB*::Tn	Locus Tag: ABUW_3743
5075Tn49	AB5075 *uvrD*::Tn	Locus Tag: ABUW_2521
5075Tn64	AB5075 *typA*::Tn	Locus tag: ABUW_0655
5075Tn69	AB5075 *bfmR*::Tn	Locus Tag: ABUW_3181
5075Tn73	AB5075 *rseP*::Tn	Locus tag: ABUW_1740
5075Tn81	AB5075 *marR*::Tn	Locus Tag: ABUW_1768
MG269	AB5075 Δ*otsB*	Locus tag: ABUW_3122
MG295	AB5075 Δ*kefF*	Locus tag: ABUW_2590
MG308	AB5075 Δ*mscS*	Locus tag: ABUW_1648

Table 6.1. Bacterial Strains (continued)

Strain	Genotype	Description[a]
MG310	AB5075 Δ*trkH*	Locus tag; ABUW_1804
MG315	AB5075 Δ*kef*	Locus tag: ABUW_1595
MG381	AB5075 Δ*ABUW_2520*	TetR family regulator
MG383	AB507 5 Δ*ABUW_1645*	TetR family regulator
MG385	AB5075 Δ*ABUW_1849*	LysR family regulator
MG388	AB5075 Δ*gigA*	Locus tag: ABUW_3260
MG389	AB5075 Δ*fur*	Locus Tag: ABUW_2074
MG392	AB5075 Δ*ABUW_2236*	AraC family regulator
MG399	AB5075 Δ*ABUW_1692*	TetR family regulator
MG407	AB5075 Δ*ABUW_2544*	AraC family regulator
MG408	AB5075 Δ*arsR*	Locus tag: ABUW_2370
MG409	AB5075 Δ*alkR*	Locus Tag: ABUW_2196
MG410	AB5075 Δ*zur*	Locus tag: ABUW_3741
MG411	AB5075 Δ*ABUW_1672*	LysR family regulator
MG422	AB5075 Δ*ptk*	Locus tag: ABUW_3833
MG423	AB5075 Δ*bfmS*	Locus tag: ABUW_3810
MG424	AB5075 Δ*gigD*	Locus tag: ABUW_1755
MG425	AB5075 Δ*ABUW_1966*	LysR family regulator
MG426	AB5075 Δ*uspA*	Locus Tag: ABUW_1763
MG450	AB5075 Δ*gigC*	Locus tag: ABUW_3161
MG511	AB5075::Tn7.hygro	
MG551	MG424::Tn7.hygro	MG424 = AB5075 Δ*gigD*
MG552	MG424::Tn7.hygro.*gigD*	MG424 = AB5075 Δ*gigD*
MG553	MG450::Tn7.hygro	MG450 = AB5075 Δ*gigC*
MG554	MG450::Tn7.hygro.*gigC*	MG450 = AB5075 Δ*gigC*
MG557	MG426::Tn7.hygro	MG426 = AB5075 Δ*uspA*
MG558	MG426::Tn7.hygro.*uspA*	MG426 = AB5075 Δ*uspA*
MG563	MG422::Tn7.hygro	MG422 = AB5075 Δ*ptk*
MG564	MG422::Tn7.hygro.*ptk*	MG422 = AB5075 Δ*ptk*
MG565	5075Tn73::Tn7.hygro	5075Tn73 = AB5075 *rseP*::Tn
MG566	5075Tn73:: Tn7.hygro.*rseP*	5075Tn73 = AB5075 *rseP*::Tn
MG567	5075Tn64::Tn7.hygro	5075Tn64 = AB5075 *typA*::Tn

Table 6.1. Bacterial Strains (continued)

Strain	Genotype	Description[a]
MG568	5075Tn64::Tn7.hygro.*typA*	5075Tn64 = AB5075 *typA*::Tn
MG629	AB5075 Δ*rpoE*	Locus tag: ABUW_0988
MG639	AB5075 Δ*gigB*	Locus tag: ABUW_3261
MG708	Δ*gigB*-Km^R Clone 1	
MG709	Δ*gigB*-Km^R Clone 2	
MG710	Δ*gigB*-Km^R Clone 3	
MG731	Δ*gigB*-Km^R Clone 4	
MG732	Δ*gigB*-Km^R Clone 5	
MG733	Δ*gigB*-Km^R Clone 6	
MG734	Δ*gigB*-Km^R Clone 7	
MG847	AB5075 Δ*ptsP*	Locus tag: ABUW_3468
MG851	Δ*gigB* Δ*ptsP*	
MG861	Δ*gigA* Δ*ptsP*	
MG880	AB5075 Δ*ptsO*	Locus tag: ABUW_3293
MG881	Δ*gigA* Δ*ptsO*	
MG883	Δ*gigB* Δ*ptsO*	
MG910	AB5075 Δ*gigAB*	
ACI-01	*A. baumannii* clinical isolate ICU Outbreak Clone	Blood Stream Isolate MDR Organism
ACI-02	*A. baumannii* clinical isolate ICU Outbreak Clone	Blood Stream Isolate MDR Organism
ACI-03	*A. baumannii* clinical isolate ICU Outbreak Clone	Blood Stream Isolate MDR Organism
ACI-04	*A. baumannii* clinical isolate	MDR Organism
ACI-06	*A. baumannii* clinical isolate	Blood Stream Isolate MDR Organism
ACI-07	*A. baumannii* clinical isolate	Urine Isolate MDR Organism
ACI-08	*A. baumannii* clinical isolate	Urine Isolate
ACI-09	*A. baumannii* clinical isolate	Blood Stream Isolate
ACI-13	*A. baumannii* clinical isolate ICU Outbreak Clone	Ventilator Tubing Isolate MDR Organism

Table 6.1. Bacterial Strains (continued)

Strain	Genotype	Description[a]
Acinetobacter baylyi		
ADP1	American Type Culture Collection Strain 33305	
Acinetobater pittii		
ACI-10	*A. pittii* clinical isolate	Surveillance Swab Isolate
ACI-11	*A. pittii* clinical isolate	Blood Stream Isolate
ACI-12	*A. pittii* clinical isolate	Urine Isolate

a **-** MDR, Multiple Drug Resistant

Table 6.2. Plasmids

Plasmid	Relevant Properties[a]
General Purpose Vectors	
pET24b	*oriR*(pBR322) Kan^R; Recombinant protein expression/purification vector
pGEM-T Easy.Hygro	*oriR*(pBR322) Amp^R $Hygro^R$; Source of $Hygro^R$ gene
pGS-*lac*-02	*incQ* Cm^R *mob*$^-$ promoter-less *lacZ* gene; for LacZ-translational fusions
pLAW344	*sacB oriT*(RK2) Cm^R *loxP oriR*(ColE1) Amp^R *loxP*; Allele exchange vector
pLLAB13B	*oriR*(pBR322) *lacZα* Amp^R $Apra^R$; Source for $Apra^R$ gene
pMMB207	*incQ lacI*^{q} P_{tac} Cm^R *mob*$^+$
pMMB207c	pMMB207 with disrupted mobility functions (*mob*$^-$)
pRK415	*incP* P_{tac} Tet^R
pRK600	Helper plasmid for Tn7 transposition, supplies mobility functions; Cm^R
pRK75	pRK415 plasmid library harboring Sau3AI DNA fragments (~5-10kb) from partially digested AB5075 genomic DNA
pRS415	*oriR*(ColE1) AmpR *trpW205lacZ*; Vector for *lacZ* operon/transcriptional fusions
pTNS3	Helper plasmid for Tn7 transposition, supplies Tn7 transposase; Amp^R
pUC18T-Tn7.*hph-lux*	*oriR*(ColE1) Amp^R Hyg^R luciferase; miniTn7 vector
pXDC50	pMMB207c.mCherry; Source of mCherry gene for pMJG60/pMJG116
pXDC77	*oriR*(ColE1) *lacI*^{q}, Amp^R, Tet^R; Source of Tet^R gene
pMJG Vectors[b]	
pMJG42	pLAW344 with the Tet^R gene from pXDC77 in place of the Cm^R gene
pMJG60	pMMB207 containing the mCherry gene under control of P_{tac} from plasmid pXDC50
pMJG70	pLAW344 with the $Hygro^R$ gene from pGEM-T-Easy.Hygro in place of the Cm^R gene
pMJG111	Vector for introduction of DNA to the Tn7 attachment site. Derived from pUC18T-Tn7.*hph-lux*
pMJG114	pMMB207c containing the *trpW205lacZ* cassette from pRS415 in place of *lacI*^{q} and P_{tac}; Cm^R
pMJG116	pMJG60 converted to $Apra^R$
pMJG118	pMJG70 with the *trpW205lacZ* cassette from pRS415 in place of the Amp^R and *sacB* genes. Used for generating chromosomal *lacZ* operon/transcriptional fusions

Table 6.2. Plasmids (continued)

Plasmid	Relevant Properties[a]
pMJG120	pMMB207 converted to Apra^R
pMJG126	pMJG114 recombineered to Apra^R
pMJG129	pGS-*lac*-02 recombineered to Apra^R; Used for construction of LacZ-translational fusions on a freely replicating vector

a - Cm^R, Chloramphenicol Resistance; Amp^R, Ampicillin Resistance, Tet^R, tetracycline resistance; Hyg^R, hygromycin resistance; Apra^R, Apramycin Resistance; Kan^R, Kanamycin Resistance; *sacB,* sucrose sensitivity gene.

b – pMJG vector construction is described in the Materials and Methods Chapter.

Table 6.3 Oligonucleotide Primers

Primer	Purpose	Sequence (5'-3')[a]
General Purpose/Plasmid Construction		
MJG035	5' primer for MCS of pM4MB207 derivatives	TCGGCTCGTATAATGTGTGGAATTGTG
MJG036	3' primer for MCS of pMMB207 derivatives	CAGACCGCTTCTGCGTTCTGAT
MJG228	5' primer for Tet^R gene from pXDC77	GCGGTACCCGGGGATCCTCTA
MJG229	3' primer for Tet^R gene from pXDC77	ATCCGTTAGCGAGGTGCCGC
MJG263	5' primer for iPCR of pLAW344 Abx Site	TTTTTTTAAGGCAGTTATTGGTGCCCTTAAACG
MJG264	3' primer for iPCR of pLAW344 Abx Site	TTTAGCTTCCTTAGCTCCTGAAAATCTCGATAAC
MJG338	5' primer for the *trpW205lacZ* cassette from pRS415	GCGGTTAGCTCCTTCGGTCC
MJG410	5' primer for $Hygro^R$ gene from pGEM-T-Easy.Hygro	AACACCAGCGACAGCCGAGC
MJG428	3' primer for $Hygro^R$ gene from pGEM-T-Easy.Hygro	GGCCTTTCGTTTTATGCCATCATGG
MJG437	5' primer for Abx region of pMMB207 derivatives	GCAGCATCACCCGACGCACT
MJG438	3' primer for Abx region of pMMB207 derivatives	CCACCGACCCGAGCAAACCC
MJG485	5' primer for MCS of pRK415 derivatives	ATCGGTGCGGGCCTCTTC
MJG487	3' primer for MCS of pRK415 derivatives	AAGCACGTCCCCATGCGCTC
MJG581	5' primer for iPCR of pMJG70 to remove Amp^R & *sacB*	TCCTGTATCACATATTCTGCTGACGCACC
MJG582	5' primer for iPCR of pMJG70 to remove Amp^R & *sacB*	GCATTGGTAACTGTCAGACCAAGTTTACTCA
MJG584	3' primer for the *trpW205lacZ* cassette from pRS415	/5Phos/TTATTTTTGACACCAGACCAACTGGTAATGGTA
MJG694	5' primer for pMJG111 MCS	CTGTTGACAAAGGGAATCAGGGGAT
MJG695	3' primer for pMJG111 MCS	GGAACTGGGTGTAGCGTCGTAA

Table 6.3. Oligonucleotide Primers (continued)

Primer	Purpose	Sequence (5'-3')[a]
MJG705	3' Primer for cloning site of pMJG118/pMJG126/pMJG129	TCTTCGCTATTACGCCAGCT
MJG733	5' primer for Apra^R gene from pLLAB13B	/5Phos/ATCAAGGCCCGATCCTTGGAG
MJG734	3' primer for Apra^R gene from pLLAB13B	/5Phos/TCATGAGCTCAGCCAATCGACTGG
Gene Deletion Primers[b]		
3260 P1	*gigA* deletion	atttatgcggccgcCTGCATATTGAATATAGCCTGGCTA
3260 P2	*gigA* deletion	taagtcgtatattatgtaattaattgattcTTAAAAGAAGATATGGTAGTCCTTTTTCAA
3260 P3	*gigA* deletion	ttgaaaaaggactaccatatcttcttttaaGAATCAATTAATTACATAATATACGACTTA
3260 P4	*gigA* deletion	atttatgcggccgcAGCATCGCCAACTTGTACAT
3261 P1	*gigB* deletion	atttatgcggccgcCATCCTCTATGATGGATAAAGTGATCTTG
3261 P2	*gigB* deletion	tcatatacacatccagattagcaataaagTATAGTGCCATCTCAGACTCAAGAGTCCTTA
3261 P3	*gigB* deletion	taaggactcttgagtctgagatggcactatACTTTATTGCTAATCTGGATGTGTATATGA
3261 P4	*gigB* deletion	atttatgcggccgcGCTGTCTGGCACCTTCTG
2544 P1	*araC* family regulator deletion	atttatgcggccgcACAGCCTAAACTTGTCTTATCG
2544 P2	*araC* family regulator deletion	aattttgggttgttttatacagcccaatttTTTATGAGCTAGAGCGGACAAAGTTATAAC
2544 P3	*araC* family regulator deletion	gttataactttgtccgctctagctcataaaAAATTGGGCTGTATAAAACAACCCAAAATT
2544 P4	*araC* family regulator deletion	atttatgcggccgcTCAAGGCTTTGCTTTTGGTGG
2520 P1	*tetR family regulator deletion*	atttatgcggccgcatacaagaatgggaggtatgtttggatc
2520 P2	*tetR family regulator deletion*	tttacatataagccgtcatagaagaacaggCTCAAGTTTGTTATTGCTGAGTTTTAAGTA
2520 P3	*tetR family regulator deletion*	tacttaaaactcagcaataacaaacttgagCCTGTTCTTCTATGACGGCTTATATGTAAA

Table 6.3. Oligonucleotide Primers (continued)

Primer	Purpose	Sequence (5'-3')[a]
2520 P4	*tetR family regulator deletion*	atttatgcggccgcTCACCAAAGATGACGACCAAC
2370 P1	*arsR* deletion	atttatgcggccgcCATGGTCGCCAGTAAAACGT
2370 P2	*arsR* deletion	ctaaattttaaagacggaaatctaggaagAATCTTCAACAAAATATATTCGTTATTGCAA
2370 P3	*arsR* deletion	ttgcaataacgaatatattttgttgaagatTCTTCCTAGATTTCCGTCTTTAAAATTTAG
2370 P4	*arsR* deletion	atttatgcggccgcCTACAGCTAAAGCCAACTCAAAGTT
2236 P1	*araC* family regulator deletion	atttatgcggccgcCACAAAGTCTGGTGTAAGTTTCTT
2236 P2	*araC* family regulator deletion	cacattagcttttagcatcaagagttacacTCTTTTATCAATTTCCCTAGACTGAAATGT
2236 P3	*araC* family regulator deletion	acatttcagtctagggaaattgataaaagaGTGTAACTCTTGATGCTAAAAGCTAATGTG
2236 P4	*araC* family regulator deletion	ATTTATGCGGCCGCGAAGTCTGTTAAGTGAGGAACATTACTG
2196 P1	*alkR* gene deletion	atttatgcggccgcAGACTAATCCCGTAAAATGCT
2196 P2	*alkR* gene deletion	gcttcggcgctttttaGTTTACGTGATCAATCATTATTTTAATAAA
2196 P3	*alkR* gene deletion	tttattaaaataatgattgatcacgtaaacTAAAAAAGCGCCGAAGC
2196 P4	*alkR* gene deletion	atttatgcggccgcGGACTGTCATTTGCTCAAGCAG
2074 P1	*fur* family regulator deletion	atttatgcggccgcTCAAAACACCAAGGCATTAATTGAT
2074 P2	*fur* family regulator deletion	cctttatttttataacagtttaaaagatttCTTACTGAACCTTAATGTCTAGAAATATAG
2074 P3	*fur* family regulator deletion	ctatatttctagacattaaggttcagtaagAAATCTTTTAAACTGTTATAAAAATAAAGG
2074 P4	*fur* family regulator deletion	atttatgcggccgcGCTTAAGTGGTCCAATTTTAGGTATT
3741 P1	*zur* gene deletion	atttatgcggccgcGCAATCTTTTCCCGACTTTAGT

Table 6.3. Oligonucleotide Primers (continued)

Primer	Purpose	Sequence (5'-3')[a]
3741 P2	*zur* gene deletion	atttaacgagctgtgcggcacAGACATAACCTCAAATTTTTAATGGAATATTAGC
3741 P3	*zur* gene deletion	gctaatattccattaaaaatttgaggttatgtctGTGCCGCACAGCTCGTTAAAT
3741 P4	*zur* gene deletion	atttatgcggccgcAAGCAAAGCATCGTTTGGTAAAC
1645 P1	*tetR* family regulator deletion	atttatgcggccgcTAACCAAAACGAGCCCATACG
1645 P2	*tetR* family regulator deletion	ccattatcggggcttttatttttaatAGTTATACCGCTTAAAATAATTTTTTGTTG
1645 P3	*tetR* family regulator deletion	caacaaaaaattattttaagcggtataactATTAAAAATAAAAGCCCCGATAATGG
1645 P4	*tetR* family regulator deletion	atttatgcggccgcAGCTCATTTATTTACCTGAACTTACCA
1672 P1	*lysR* family regulator deletion	atttatgcggccgcCTTTCTTTCTCTGAAACAGCAGCT
1672 P2	*lysR* family regulator deletion	tttaggttctgcatctaaattgaaatgattCTGTCAAAAAAATTGAAAGAACCTGATTGG
1672 P3	*lysR* family regulator deletion	ccaatcaggttctttcaatttttttgacagAATCATTTCAATTTAGATGCAGAACCTAAA
1672 P4	*lysR* family regulator deletion	atttatgcggccgcGCTGGTCTAACAATCGCTTCT
1692 P1	*tetR* family regulator deletion	atttatgcggccgcATCATCTGCTGCTTCTGAGGTT
1692 P2	*tetR* family regulator deletion	ttttagtctagtatttcaatgttattaaaCGATTTCCCCGTAGTAAATCTTTTGAAAT
1692 P3	*tetR* family regulator deletion	atttcaaaagatttactacggggaaatcgTTTAATAACATTGAAATACTAGACTAAAA
1692 P4	*tetR* family regulator deletion	atttatgcggccgcGGTAATACGCCACTGGTTCC
1755 P1	*gigC* gene deletion	atttatgcggccgcGCATATCAGCATGCAGGAAAATATC
1755 P2	*gigC* gene deletion	acgagagttttttaattttagctaaatattTTTCGAATTTCATCCATATTTTTTAATTTT
1755 P3	*gigC* gene deletion	aaaattaaaaaatatggatgaaattcgaaaAATATTTAGCTAAAATTAAAAAACTCTCGT

Table 6.3. Oligonucleotide Primers (continued)

Primer	Purpose	Sequence (5'-3')[a]
1755 P4	*gigC* gene deletion	atttatgcggccgcTTACATAGGATACGTATTGGCAAACAT
1849 P1	*lysR* family regulator deletion	atttatgcggccgcAGCAGCCATGTTTCCTAAAGTATCCATT
1849 P2	*lysR* family regulator deletion	tacgatagaagcttagtagatcaatttgctGATGCATTATTTAATAAAATCATTTCATTC
1849 P3	*lysR* family regulator deletion	gaatgaaatgattttattaaataatgcatcAGCAAATTGATCTACTAAGCTTCTATCGTA
1849 P4	*lysR* family regulator deletion	atttatgcggccgcGCAATGCCAAAATTAATTCTGCCT
1966 P1	*lysR* family regulator deletion	atttatgcggccgcTTCTAAGGCTTGAGCAACAGGT
1966 P2	*lysR* family regulator deletion	tccaaccataagtcttatgagcagtatttaTAAGTATTCAATATAAGTGCTATCTGATTA
1966 P3	*lysR* family regulator deletion	taatcagatagcacttatattgaatacttaTAAATACTGCTCATAAGACTTATGGTTGGA
1966 P4	*lysR* family regulator deletion	atttatgcggccgcGTGAATCTAAACCTGTCCAGAAATAATCC
3833 P1	*ptk* gene deletion	atttatgcggccgcTCCAGATGTAATCGTACGTGTACT
3833 P2	*ptk* gene deletion	atttgatccggtttttatgaagatttttaaATGCTTAAAAATCTATACGTTAAATATAAG
3833 P3	*ptk* gene deletion	cttatatttaacgtatagatttttaagcatTTAAAAATCTTCATAAAAACCGGATCAAAT
3833 P4	*ptk* gene deletion	atttatgcggccgcTGTTGACGCTGCAATAACCAAA
1763 P1	*uspA* gene deletion	atttatgcggccgcGAGCTTATTAAGTTGTGCCGATATGG
1763 P2	*uspA* gene deletion	tagctgggtttttatataaaggtttagatATATTGCTCCTTATTGTCTTGTGA
1763 P3	*uspA* gene deletion	tcacaagacaataaggagcaatatATCTAAACCTTTATATAAAAAACCCAGCTA
1763 P4	*uspA* gene deletion	atttatgcggccgcAGATAAAGAGCTACCTAATCAGACGAT
3161 P1	*gigC* gene deletion	atttatgcggccgcTTCGCCTAGTTGTTCCTCAAGA

Table 6.3. Oligonucleotide Primers (continued)

Primer	Purpose	Sequence (5'-3')[a]
3161 P2	*gigC* gene deletion	gcgatggcattagaaaatcaagctGTTTAAAAAGCCTTAACGTTTAAAAGTATTCATT
3161 P3	*gigC* gene deletion	aatgaatacttttaaacgttaaggctttttaaacAGCTTGATTTTCTAATGCCATCGC
3161 P4	*gigC* gene deletion	atttatgcggccgcAGGTTTAGGCGATGCTGGTG
3180 P1	*bfmS* gene deletion	atttatgcggccgcCTGTATGATTTGTCGGGAGATAGCA
3180 P2	*bfmS* gene deletion	tcagttataaatgaaccaataaaaaagcaccAACAACAAGAATTACCAGCCCCGCATA
3180 P3	*bfmS* gene deletion	tatgcggggctggtaattcttgttgttGGTGCTTTTTTATTGGTTCATTTATAACTGA
3180 P4	*bfmS* gene deletion	atttatgcggccgcTTCCAGTATTAGCGCACTCCA
MJG491	P1 for *kefF* gene deletion (ABUW_2590)	GTTGGTCGAGCTGAATATGAAGTG
MJG492	P2 for *kefF* gene deletion (ABUW_2590)	catcgatattgatgctctctttttaAATAATGCCTTGTAGCTATAAAAATCATAGTCAC
MJG493	P3 for *kefF* gene deletion (ABUW_2590)	gtgactatgatttttatagctacaaggcattattTAAAAAAGAGAGCATCAATATCGATG
MJG494	P4 for *kefF* gene deletion (ABUW_2590)	ACTTCAACAAGCAGAAGCCGAA
MJG461	P1 for *otsB* gene deletion (ABUW_3122)	CTACCTGTAAGTAGGGAAAAGCATGTG
MJG465	P2 for *otsB* gene deletion (ABUW_3122)	tcgattcgataacacgattaatttagacatATTTGCCTGCCCATATTTTTTGATC
MJG466	P3 for *otsB* gene deletion (ABUW_3122)	gatcaaaaaatatgggcaggcaaatATGTCTAAATTAATCGTGTTATCGAATCGA
3122 P4	P4 for *otsB* gene deletion (ABUW_3122)	CTGTGTCGAAGCAACAATCGA
MJG497	P1 for *kef* gene deletion (ABUW_1595)	TCTACACGTAACTTCCCTAACCGTT
MJG498	P2 for *kef* gene deletion (ABUW_1595)	tgagtatgatcaggctttcgttgaatctACGGATCTGAACCACGTTATATTGAACATA
MJG499	P3 for *kef* gene deletion (ABUW_1595)	tatgttcaatataacgtggttcagatccgtAGATTCAACGAAAGCCTGATCATACTCA

Table 6.3. Oligonucleotide Primers (continued)

Primer	Purpose	Sequence (5'-3')[a]
MJG500	P4 for *kef* gene deletion (ABUW_1595)	TACAGTACCTGAAGCAGGGCATTT
MJG503	P1 for *mscS* gene deletion (ABUW_1648)	CCAGAAGCGCCACCACCATA
MJG504	P2 for *mscS* gene deletion (ABUW_1648)	aaataaaatagatagcacgctaacagttgtTTCTAGCCA AGGATAGTTGCTTAACTCAGC
MJG505	P3 for *mscS* gene deletion (ABUW_1648)	gctgagttaagcaactatccttggctagaaACAACTGTT AGCGTGCTATCTATTTTATTT
MJG506	P4 for *mscS* gene deletion (ABUW_1648)	ACCTTCTCGGCAATTATTAGAAATTTT GGCAT
MJG509	P1 for *trkH* gene deletion (ABUW_1804)	CCAATCTGGATGACGAAAGATTGTTC
MJG510	P2 for *trkH* gene deletion (ABUW_1804)	gcttttacagcggctttttaATTTTCTGGTTCGTTT TCTTATATGAAACAA
MJG511	P3 for *trkH* gene deletion (ABUW_1804)	ttgtttcatataagaaaacgaaccagaaaatTAAAAAAG CCGCTGTAAAAGC
MJG512	P4 for *trkH* gene deletion (ABUW_1804)	CGCCTAGCTTGTTATGATGCTGTGTTTA A
MJG864	P2 for *gigAB* double deletion	tcatatacacatccagattagcaataaagtAGAAGATAT GGTAGTCCTTTTTCAA
MJG865	P3 for *gigAB* double deletion	ttgaaaaaggactaccatatcttctACTTTATTGCTAA TCTGGATGTGTATATGA
MJG855	P1 for *ptsP* gene deletion (ABUW_3468)	atttatgcggccgcACCTACAATGGTATGGCCT AAATCT
MJG856	P2 for *ptsP* gene deletion (ABUW_3468)	agagctttttcactctccttttttaaatatGGATGTATACT CCAGTATTTTTTTAGACTA
MJG857	P3 for *ptsP* gene deletion (ABUW_3468)	tagtctaaaaaaatactggagtatacatccATATTTAAA AAAGGAGAGTGAAAAAGCTCT
MJG858	P4 for *ptsP* gene deletion (ABUW_3468)	aataaagcggccgcGTTGTCTGGTTCCCAAAC ATCTTC
MJG890	P1 for *ptsO* gene deletion (ABUW_3293)	taaatagcggccgcACGCGCTTAATTGATAAT CTACAAGTTGCCT
MJG891	P2 for *ptsO* gene deletion (ABUW_3293)	gacgtgccacgattaatctgcctcataTGTGTCTATCA TGACCAGTGCTTCATTTCT
MJG892	P3 for *ptsO* gene deletion (ABUW_3293)	agaaatgaagcactggtcatgatagacacaTATGAGGC AGATTAATCGTGGCACGTC

Table 6.3. Oligonucleotide Primers (continued)

Primer	Purpose	Sequence (5'-3')[a]
MJG893	P4 for *ptsO* gene deletion (ABUW_3293)	atttaagcggccgcACAAGATAGTATGCGGGTGTTAAATCCTGA
MJG756	P1 for *rpoE* gene deletion (ABUW_0988)	attattgcggccgcCATAGTATGATGACGCCCTTTTGGA
MJG757	P2 for *rpoE* gene deletion (ABUW_0988)	tcatcatgattcattggaacctcccatTTTCGGTGCTAAATCCATGGAGATG
MJG758	P3 for *rpoE* gene deletion (ABUW_0988)	catctccatggatttagcaccgaaaATGGGAGGTTCCAATGAATCATGATGA
MJG759	P4 for *rpoE* gene deletion (ABUW_0988)	taaatagcggccgcCTTGTTATGGCGGTAATATCTATATTCAAGCTA
Gene Complementation Primers – pMJG111		
MJG716	*gigC* 5' primer	ataaat*ggtacc*TACCTTTAAACCAATACGCGCAA
MJG717	*gigC* 3' primer	ataattggtaccTTAAGCCTGATCTTCATCGCAAA
MJG720	*gigD* 5' primer	atattaggtaccCCTTCTGGCAATGCAAATTCA
MJG721	*gigD* 3' primer	attttaggtaccCTACAGCGGCTTTTGTATAATTTTCTGTAA
MJG724	*ptk* 5' primer	/5Phos/GCTCGTAAGCTAAATGCTGAACATAT
MJG725	*ptk* 3' primer	/5Phos/TTAGTCTTCTTTTTGTGCCTTATAGG
MJG726	*rseP* 5' primer	attattggtaccTAGACAAGCAATGCGTGCG
MJG727	*rseP* 3' primer	attattggtaccTTACAAACGCATAAAGTCATTAAATAAAGCTAAA
MJG728	*typA* 5' primer	attattggtaccGCCCATAAACGAGGTCAA
MJG729	*typA* 3' primer	attattggtaccTTATTTATCACGGTTACGTTTACGTTCG
MJG730	*uspA* 5' primer	attattggtaccGGATACAACATAGGGCAAGGTTT
MJG731	uspA 3' primer	aattttggtaccTTATTCAGTTACGACCAATACTGGCACA
Gene Complementation Primers – pMJG116/pMJG120		

Table 6.3. Oligonucleotide Primers (continued)

Primer	Purpose	Sequence (5'-3')[a]
MJG737	*gigAB* Region 5' primer	atattaactagtCAAGCGTACATTTTTTAGGCTTTTTGGCTA
MJG738	*gigAB* Region 3' primer	attattactagtTTTCCCCTTTTCGCTAAGCGTGAT
MJG750	*gigB* 3' primer + 6XHistidine Tag	taattgcatgcttag*tggtggtggtggtggtg*GGCATTTTGCTTATCAGATACTTGTTCA
MJG753	*gigA* 5' primer	ttatatcatATGTATTTTATTAAACCGACACGCTCTATCC
MJG955	*gigA* 3' primer	taattgcatgcTTAATTCATTCGACAAAGACTAAAGATGGCAATGTC
MJG768	*gigB* 5' primer	ttaattcatATGTCAACAGGTCATGTTGAATATGCA
MJG769	*gigB* 3' primer	taattgcatgcTTAGGCATTTTGCTTATCAGATACTTGTTCA
MJG995	*ptsO* 5' primer	attttagaattcATGATAGACACAACTGTTGATGTAATTAATAAACTCGGT
MJG996	*ptsO* 3' primer	attttatctagaTTAATCTGCCTCATAAAATTTTGCGGCGAA
GigA/GigB Point Mutation Allele Primers		
MJG776	5' primer for S59A allele	AAACAACATTTATTGAT**GC**TACTGTATTAGGTATCC
MJG777	3' primer for S59A allele	GGATACCTAATACAGTA**GC**ATCAATAAATGTTGTTT
MJG778	5' primer for S59A allele	AAACAACATTTATTGAT**GA**TACTGTATTAGGTATCC
MJG779	3' primer for S59A allele	GGATACCTAATACAGTA**TC**ATCAATAAATGTTGTTT
MJG884	5' primer for D32A allele	TTCACATAGATGATCTCG**C**TTTATACGACCCAAC
MJG885	3' primer for D32A allele	GTTGGGTCGTATAAA**G**CGAGATCATCTATGTGAA
MJG886	5' primer for D32E allele	TTCACATAGATGATCTCGA**A**TTATACGACCCAAC
MJG887	3' primer for D32E allele	GTTGGGTCGTATAA**T**TCGAGATCATCTATGTGAA

Table 6.3. Oligonucleotide Primers (continued)

Primer	Purpose	Sequence (5'-3')[a]
Expression Vector Cloning – pET24b		
MJG753	GigA 5' primer	ttatatcatATGTATTTTATTAAACCGACACG CTCTATCC
MJG754	GigA 3' primer	ataatactcgagATTCATTCGACAAAGACTAA AGATGGCAA
MJG803	GigA 3' primer; includes Strep Tag	taatctcgag*TCATTTTTCAAATTGTGGATGAG ACCAA*TTCATTCGACAAAGACTAAAGA
MJG804	GigA-PP2C domain 5' primer	ttatatcat**atg**GATTTATTAAATTATGAGGTT GAAACTTTTTTCCAAC
MJG768	GigB 5' primer	ttaattcatATGTCAACAGGTCATGTTGAAT ATGCA
MJG749	GigB 3' primer	ataattctcgagGGCATTTTGCTTATCAGATA CTTGTTCA
MJG992	EI^{Ntr} 5' primer	actttaagaaggagatatacatATGTCAAACATGCA ACTCGACACTCTAAGA
MJG993	EI^{Ntr} 3' primer	ggtggtggtggtggtgctcgagTACGCTTACAAGG CGGTTAGATTTAACCA
MJG997	NPr 5' primer	attttacatATGATAGACACAACTGTTGATG TAATTAATAAACTCGGT
MJG998	NPr 3' primer; includes Strep tag	taatctcgagTCA*TTTTTCAAATTGTGGATGAG ACCA*ATCTGCCTCATAAAATTTTGCGG
MJG800	GigC 5' primer	ttaattcatATGCGGATGACATTACGCCAG
MJG801	GigC 3' primer	ttaatactcgagAGCCTGATCTTCATCGCAAA ATT
GigB Translation Start Site Investigation – pMJG129		
MJG956	5' primer, sits in *gigA* gene	taaaatgaattcTGTGGTCGGTATTCTAAATC TTGAAACTCATAGTCT
MJG957	$GigB_{GTG}$ construct 3' primer	ttaataggatcCACATAGTGCCATCTCAGACT CAAGAGTCCTTA
MJG959	$GigB_{GTG-ATG}$ construct 3' primer	ttaataggatcCATATAAATGCCATTTTCAGA GAAGGATAGAAAAATTATCACATA
MJG960	$GigB_{GAG-ATG}$ construct 3' primer	ttaataggatcCATATAAATGCCATTTTCAGA GAAGGATAGAAAAATTATC**T**CATA

Table 6.3. Oligonucleotide Primers (continued)

Primer	Purpose	Sequence (5'-3')[a]
MJG959	$GigB_{1-53}$ construct 3' primer	ttaataggatccCTGTTCAATTCTGTTTAAAAG TTTGTCTAGACTTATACAAGAATG
cys gene Promoter Fusion Studies – pMJG118/pMJG126		
MJG751	*cysI* promoter 5' primer	attaaaggatccGGTGCGGGAACTGAGCAG
MJG752	*cysI* promoter 3' primer	ataattggatccTACGTGTGCATAGCCACGGT
MJG902	*gigC* promoter 5' primer	ataaatggatccTACGCACGGACAACCAGCT CATCTCCTACC
MJG903	*gigC* promoter 3' primer	atttaaggatccCTGCTTGTTCAAAGGCTTCA CAG
MJG1006	*cysH* promoter 5' primer	ataataggatccACTCCTTCAAGATCTAGGCA TACG
MJG1007	*cysH* promoter 3' primer	ataattggatccTTCTAGAATCTCGCGCGGAC
MJG1008	*cysG* promoter 5' primer	ataaatggatccTGGTTCAGGCCTTGCTGTAG
MJG1009	*cysG* promoter 3' primer	atttaaggatccCTCCGCCCACAATCAGACAA
MJG1010	1720 promoter 5' primer	ataaatggatccGCAAGCTTAAATGGCTCCCC
MJG1011	1720 promoter 5' primer	atttaaggatccAGACCAACAACAAGCCCAG A
MJG1012	*cysQ* promoter 5' primer	ataaatggatccGCTTTCTCTTGAGTAATAAA CGTCTGA
MJG1013	*cysQ* promoter 3' primer	atttaaggatccGCATCATTGGGGCAAGTTGT
MJG1014	*cysE* promoter 5' primer	ataaatggatccCCGTTAGTGACTCAGCAGCA
MJG1015	*cysE* promoter 3' primer	atttaaggatccAGGATCTCGCGCGAATACAG
MJG1016	*cysDN* promoter 5' primer	ataataggatccAGAAATCGAAAGCACAGAT CGT
MJG1017	*cysDN* promoter 3' primer	taaattggatccTTCAGTCATGAACACGCCCT
cysI EMSA Primers		
MJG896	5' primer for *cysI* promoter	/5IRD700/GGCGACTATTTAGTGGCTTAT G
MJG897	3' primer for *cysI* promoter	/5IRD700/GGCGTATGGCTAGTAGATTCA TTATTA

a – Primer modifications are as follows: /5Phos/, Primer contains a phosphorylation group on the 5' nucleotide to facilitate blunt-end cloning; /5IRD700/, Primer contains the IRD700 infrared dye for detection via Li-Cor Imaging system. Underlined bases indicate restriction

Table 6.3. Oligonucleotide Primers (continued)

enzyme recognition sites for cloning purposes. Lower case text indicates nucleotides that do not bind to the given region being targeted. Bold-face text indicates mutated bases to generate point mutations. Italicized text indicates the introduction of additional nucleotides to incorporate affinity purification tags.

b – See Materials and Methods for details regarding gene deletion primer utilization.

Abbreviations: MCS, Multiple Cloning Site; Abx, Antibiotic resistance gene/region; iPCR, inverse-polymerase chain reaction.